

UC Berkeley

UC Berkeley Electronic Theses and Dissertations

Title

Exploring Landscapes of Naturalness with Lifshitz Field Theories

Permalink

<https://escholarship.org/uc/item/0073j1dx>

Author

Grosvenor, Kevin Torres

Publication Date

2015

Peer reviewed|Thesis/dissertation

Exploring Landscapes of Naturalness with Lifshitz Field Theories

by

Kevin Torres Grosvenor

A dissertation submitted in partial satisfaction of the

requirements for the degree of

Doctor of Philosophy

in

Physics

in the

Graduate Division

of the

University of California, Berkeley

Committee in charge:

Professor Petr Hořava, Chair

Professor Ori J. Ganor

Professor Mariusz Wodzicki

Summer 2015

Exploring Landscapes of Naturalness with Lifshitz Field Theories

Copyright 2015

by

Kevin Torres Grosvenor

Abstract

Exploring Landscapes of Naturalness with Lifshitz Field Theories

by

Kevin Torres Grosvenor

Doctor of Philosophy in Physics

University of California, Berkeley

Professor Petr Hořava, Chair

In this thesis, we examine the question of technical naturalness from the point of view of nonrelativistic quantum field theories of Lifshitz type.

Lifshitz field theories are distinguished from standard relativistic quantum field theories by the spacetime scaling symmetries that they enjoy in the vicinity of their renormalization group fixed points. These scaling symmetries are parametrized by the dynamical critical exponent, which measures the degree of scaling of time relative to spatial coordinates. Whereas in relativistic theories, space and time scale equally with each other, in Lifshitz field theories, the dynamical critical exponent may differ from unity. Furthermore, Lifshitz field theories live in spacetimes that possess a foliation structure by spatial leaves of constant time. Therefore, in contrast to relativistic theories, Lifshitz field theories are not invariant under the full diffeomorphism group of spacetime, but rather only those diffeomorphisms that preserve the built-in foliation structure. In the flat spacetime, this would simply exclude the usual spacetime boost symmetries. Since time is treated on a fundamentally different footing as is space, these theories are often referred to as *anisotropic*. In addition, these theories often require the tuning of multiple parameters in order to approach their fixed points under renormalization group flow, and are consequently called *multicritical*.

We will explore some new and interesting lessons that nonrelativistic theories have to teach us about technical naturalness. We begin this study at the modest level of Lifshitz scalar field theories. We examine the nature of Nambu-Goldstone (NG) bosons that arise from spontaneous symmetry breaking in multicritical systems described by Lifshitz scalar field theories. The NG modes in such nonrelativistic theories were previously classified into two types: (1) Type-A, which disperses linearly, and which derives its kinetic energy from a term which is quadratic in time derivatives; and (2) Type-B, which disperses quadratically, and which is described by a pair of fields with kinetic terms linear in time derivatives. In principle, Type-A modes dispersing by a power different from unity, and Type-B modes dispersing by a power different from two, can exist. However, the naive expectation from relativistic quantum field theory is that these would require fine tuning and are therefore technically unnatural. We discover that this is not the case. Instead of fine-tuning, all one needs is a new type of symmetry by which the fields transform by a polynomial function of some appropriate degree in the spatial coordinates. This *polynomial shift symmetry*

protects the naturalness of the corresponding NG bosons. This leads to a refinement of the classification of technically natural NG modes in nonrelativistic theories.

Having discovered these polynomial shift symmetries, we turn our attention to the classification of Lagrangians that are invariant (up to total derivatives) with respect to these symmetries. We develop a novel graph-theoretical technique in order to address this problem. In this language, the invariants display beautiful patterns that otherwise remain obscured. For example, linear-shift invariants are presented as equal-weight sums over all labeled trees with some fixed number of vertices. Furthermore, we develop a graph-theoretical method for constructing invariants under polynomial shifts of high degree from invariants under polynomial shifts of lower degree. In this way, one no longer needs to repeat the entire classification process for each degree of the polynomial shift symmetry.

The third part of the thesis uses some of the theories, which are built out of invariants constructed in the second part of the thesis, to study a novel feature that these Lifshitz theories possess as one changes the energy scale at which the systems are examined. We find that these systems can flow from one fixed point described by one value of the dynamical exponent, to another fixed point described by a different value of the dynamical exponent. Furthermore, the system can explore any number of fixed points between the extreme high energy regime and the extreme low energy regime. We refer to this behavior as a *cascade*. Not only can Type-A modes cascade into other Type-A modes (or similarly for Type-B modes), but Type-A modes can flow towards Type-B at low energies as well. Both mechanisms are protected by symmetries. The purely Type-A or Type-B cascade is protected by the polynomial shift symmetries in space. The Type-A to Type-B cascade can be protected by various symmetries, including a linear shift symmetry in time. Furthermore, we re-examine the Coleman-Hohenberg-Mermin-Wagner (CHMW) theorem, which prohibits the spontaneous breaking of global internal continuous symmetries in relativistic theories in two spacetime dimensions. Naively, this theorem would prevent the existence of a Type-A mode unless its dynamical exponent is strictly less than the spatial dimension, which is when the theory is in its *lower critical dimension*. The cascade represents a mechanism by which this result can be circumvented.

Next, we examine the renormalization group flow of one particular Lifshitz scalar field theory. We perform the analysis explicitly using three different standard techniques of renormalization and show that they are all mutually consistent. Furthermore, we demonstrate that the RG flow of Lifshitz theories can be interpreted physically in many different, but consistent, ways due to the additional freedom of renormalizing the dynamical exponent.

The lessons in Lifshitz field theories discussed in this thesis are most readily applied in the area of condensed matter physics, where systems often display a richer spectrum of behavior than is described by relativistic physics. We perform a preliminary study of the effects of coupling these Lifshitz theories with other systems. In particular, we study the naturalness problem of the linear dependence on temperature of the resistivity of so-called *strange metals*, which are high-temperature superconductors above their critical temperature. We show that this behavior is reproduced by the standard electron-phonon interaction picture of superconductivity, if the phonons are allowed to be multicritical and at their lower critical dimension. We also examine the impact that this model has on the heat capacity of the system.

To my mother, Estrella, and father, John,
who have shown me unwaivering patience, support and love.

Contents

1. Introduction	1
1.1. Landscapes of Naturalness	2
1.2. Naturalness and the Polynomial Shift Symmetry	3
2. Multicritical Symmetry Breaking	6
2.1. Introduction	6
2.1.1. Geometry of the Spacetime with Lifshitz Symmetries	7
2.1.2. Effective Field Theories of Type A and B Nambu-Goldstone Bosons	8
2.2. Example of Slow Nambu-Goldstone Bosons	9
2.2.1. $z=2$ Linear and Non-linear $\mathcal{O}(\mathbf{N})$ Sigma Models	10
2.2.2. Quantum Corrections to the Speed Term	11
2.3. Naturalness	13
2.4. Nonrelativistic Refinement of Goldstone's Theorem	15
2.5. Discussion	15
Appendices	17
2.A. One-loop Correction to the Mass and Speed Parameters	17
2.B. Large- N Limit	20
3. Scalar Field Theories with Polynomial Shift Symmetries	21
3.1. Introduction	21
3.1.1. Polynomial Shift Symmetries	22
3.1.2. Polynomial Shift Symmetries as Exact Symmetries	24
3.2. Galileon Invariants	25
3.2.1. The Graphical Representation	26
3.2.2. Galileon Invariants as Equal-Weight Sums of Trees	27
3.3. Beyond the Galileons	28
3.3.1. Brute-force Examples	29
$(P, N, \Delta) = (1, 3, 2)$	29
$(P, N, \Delta) = (3, 3, 4)$	29
3.3.2. Introduction to the Graphical Representation	30
$(P, N, \Delta) = (1, 3, 2)$	31
$(P, N, \Delta) = (3, 3, 4)$	31
3.3.3. New Invariants via the Graphical Approach	32

	The Minimal Invariant: $(P, N, \Delta) = (2, 4, 5)$	33
	The Minimal Invariant: $(P, N, \Delta) = (3, 4, 6)$	34
	Medusas and Total Derivative Relations	37
3.3.4.	Superposition of Graphs	37
	Quadratic Shift ($P=2$)	38
	Cubic Shift ($P=3$)	39
	Quartic Shift ($P=4$)	41
	Quintic Shift ($P=5$)	42
3.4.	Outlook	43
Appendices		45
3.A.	Glossary of Graph Theory	45
3.B.	Theorems and Proofs	46
3.B.1.	The Graphical Representation	46
	Types of Graphs and Vector Spaces	48
	Maps	49
	Relations	50
	The Consistency Equation and Associations	50
3.B.2.	Building Blocks for Consistency Equations	52
	The Loopless Realization of \mathcal{L}/\mathcal{R}	52
	Medusas and Spiders	53
	Constructing Loopless \times -Relations	56
	A Basis for $\mathcal{R}_{\text{loopless}}^\times$	58
	Lower Bound on Vertex Degree	63
3.B.3.	Linear Shift Symmetry, Trees and Galileons	64
	Minimal Invariants	65
	Non-minimal Invariants	67
3.B.4.	Invariants from Superpositions	69
	Superposition of a P -invariant and an Exact Invariant	69
	Superposition of Minimal Loopless 1-invariants	71
3.B.5.	Unlabeled Invariants	74
3.C.	Coset Construction	75
4.	Cascading Multicriticality in Spontaneous Symmetry Breaking	78
4.1.	Introduction	78
4.2.	The Relativistic CHMW Theorem	79
4.3.	Nonrelativistic CHMW Theorem	80
4.4.	Cascading Multicriticality	81
4.5.	Examples	82
	4.5.1. Type-A Hierarchy	82
	4.5.2. Type-A Cascade	82
	4.5.3. Type-A/Type-B Hierarchy	84
4.6.	Outlook	85

Appendices	86
4.A. A Flow from Type-A to Type-B	86
5. The $z=3$ Scalar Field with a Linear-Shift Invariant Interaction	87
5.1. Introduction	87
5.2. Feynman Rules and Diagrams	88
5.3. The Renormalization Group	90
5.3.1. Renormalization Conditions	90
5.3.2. The Wilsonian Approach	91
5.3.3. The Callan-Symanzik Equation	93
5.3.4. Modified Minimal Subtraction in $3 - \epsilon$ Spatial Dimensions	95
5.3.5. Physical Interpretations of the RG Flow	98
5.4. $O(N)$ Extension and the Large N Limit	99
5.5. Outlook	101
6. Multicritical Phonon-Electron Interactions in Metals	103
6.1. Introduction	103
6.2. Polynomial Shifts, Compactifications and the Lattice	104
6.2.1. Bosons on a finite periodic lattice	104
6.3. Multicritical Phonons	107
6.3.1. Hydrodynamics with Lifshitz Symmetries	107
6.3.2. Multicriticality in the Debye model	109
6.4. Electron-Phonon Transport Properties	110
6.4.1. Minimal coupling to the Fermi surface	111
6.4.2. Generalized Bloch-Grüneisen Formula	112
6.4.3. Resistivity for Various Values of D and z	114
6.4.4. Heat Capacity for Various Values of D and z	115
6.4.5. Coupling Systems with Different Scalings	116
6.5. One Loop Effects	117
6.5.1. Feynman Rules	117
6.5.2. Phonon Propagator	119
Zero-Temperature Case	119
Finite Temperature Case	120
Real Part of \mathcal{I}	121
Imaginary Part of \mathcal{I}	121
One-Loop Correction to the Phonon Propagator	122
Small k and ω Regime	123
6.6. Discussion	124
Appendices	125
6.A. The Standard Model of Superconductivity	125
6.A.1. The Phonon-Electron Interaction	125
The Classical Theory of Phonon-Electron Interaction	125
The Bloch Representation	126
Lattice Dynamics	126

The Quantum Theory of Phonon-Electron Interaction	127
6.A.2. Nakajima Transformation and Effective Four-Electron Vertex	128
6.A.3. BCS Superconductivity Theory	130
BCS Reduced Hamiltonian	130
The Cooper Pair	133
Self-Consistent Field Approximation	134
6.A.4. Anisotropic Gap Function in High- T_c Superconductivity	137
6.A.5. Green's Function Method	138
Singularities of $G_r(\omega)$	138
Equation of Motion of the Double Time Green's Function	139
6.B. Boltzmann-Bloch Transport Theory	140
6.B.1. Variational Approach to Resistivity	140
The Collision Function	140
The Variational Method	141
Resistivity	142
Entropic Interpretation	142
6.C. Derivation of the Bloch-Grüneisen Formula	143
6.C.1. An Exact Solution to the Boltzmann Equation	144
6.C.2. Bloch-Grüneisen Formula	145
7. Conclusion	148
Bibliography	150

Acknowledgments

I wish to thank my advisor, Petr Hořava, for his support and guidance, and for teaching me to go where the physics leads, without fear, no matter how murky and uncharted the territory may be. This is an infinitely simpler matter with a light as bright as he. I also wish to thank the other members of my doctoral committee, professors Ori Ganor and Mariusz Wodzicki.

Without the help of the current and former members of the Berkeley Center for Theoretical Physics, this thesis would not have been possible. Thanks to Lawrence Hall, Petr Hořava and Ori Ganor, whose courses on the Standard Model, String Theory and Electromagnetism during my first year as a graduate student shaped the way I think about theoretical high energy physics. Thanks to Shannon McCurdy for the many helpful discussions. Thanks to the BCTP students in whose first semester quantum field theory course I served as graduate student instructor; I probably learned more from you than you did from me. I am happy and honored to have played a small role in your present and future success.

Thanks to Charles Melby-Thompson who, as the senior student in Petr's group, took this naive and largely unknowledgeable graduate student under his wing. Thanks to Tom Griffin, Christopher Mogni and Ziqi Yan for being such wonderful collaborators from whom I have learned so much.

The second, third and fourth chapters of this thesis contain published work done in collaboration with Tom Griffin, Petr Hořava and Ziqi Yan. Chapters 5, 6 and 7 are unpublished and represent work done in collaboration with Tom Griffin, Petr Hořava, Christopher Mogni and Ziqi Yan.

Special thanks go to Mr. Stephen Butler, my high school physics teacher, and Mrs. Nancy Butler, my high school Spanish teacher, who inspired me immensely all those years ago. In addition, much of this thesis was written and compiled while I was a guest at their home, a unique experience that I will cherish for the rest of my life. I thank you for your kindness and generosity.

Finally, I wish to thank my family for their love and support and for standing by me through this rather protracted student phase in my life. I love you all dearly and I hope, in a small way, this thesis makes you proud.

Chapter 1

Introduction

The study of theories that exhibit anisotropy between spatial and temporal dimensions is a well-established and developed practice in condensed matter physics, particularly in the context of dynamic critical phenomena [1, 2, 3, 4, 5]. In the vicinity of fixed points under the renormalization group (RG) flow, a system can exhibit a scaling symmetry which is anisotropic between time and space. The degree of anisotropy is measured by the *dynamical critical exponent* (denoted z), such that time scales z times as much as does space. Numerous theories with various values of z have been studied in the past. For example, the value $z = 3/2$ is found in theories of surface growth [6], spin waves in XY magnets and sound waves in superfluid Helium [7]; investigations into relaxation models with $z = 2$ include [8]; and $z = 5/2$ is found in models of ferromagnetic spin waves [9]. These systems are often called *multicritical* since they usually require the tuning of multiple parameters in order to reach a fixed point under RG flow.

In contrast, the field of high energy physics has tended to favor Lorentz invariance, which precludes such anisotropy. To a large extent, this bias remains. However, more recently, the concept of anisotropy was introduced into the field of gravitational physics by Hořava [10, 11]. This anisotropic gravity theory is power-counting renormalizable and may therefore serve as a candidate for an ultra-violet complete quantum theory of gravity. Naturally, this theory has attracted much attention not only because of its improved behavior at short distances, but also for its novel phenomenology at long distances [12], its connection to the nonperturbative Causal Dynamical Triangulations approach to quantum gravity [13, 14, 15], as well as for its applications to holography and the AdS/CFT correspondence of nonrelativistic systems [16, 17, 18]. However, the quantization and renormalization of this theory presents numerous challenges and only partial results have been achieved so far [19, 20]. These technical difficulties have spurred the investigation of some of the new conceptual features of anisotropic quantum field theories (QFTs) in simpler systems.

In this dissertation, we will describe some of the interesting and surprising new features that arise in quantum field theories exhibiting dynamical critical exponents possibly taking values different from unity, which are called Lifshitz field theories. The bulk of the work will be organized as follows:

1. We will investigate the consequences of the anisotropy in Lifshitz field theories on spontaneous symmetry breaking and the classification of Nambu-Goldstone Bosons [21];

2. In the process, we will discover new symmetries of Lifshitz scalar field theories and we will study the classification of these theories [22];
3. We will study the explicit breaking of these new symmetries and the patterns of RG flow between available fixed points [23];
4. We will perform the renormalization group (RG) analysis explicitly using a number of different standard methods and show that the RG flows of Lifshitz theories possess a continuum of distinct, but mutually consistent, physical interpretations [24];
5. Finally, we will propose a theory of superconductivity in which electrons couple to multicritical phonons and demonstrate how this theory can result in a linear temperature dependence of the resistivity as well as fractional power law dependence of the heat capacity [25];

1.1. Landscapes of Naturalness

The bulk of the present work is inspired by the principle of technical *naturalness* introduced and formalized by 't Hooft as a guideline in constructing models of elementary particles [26]. The principle is summarized by the following dogma:

A set of physical parameters can be very small at some energy scale only if the symmetry of the system would increase if these parameters were to vanish.

The principle of naturalness is rooted in the time-honored physical principle of causality, which requires that the macroscopic behavior of systems follow from more fundamental microscopic equations. This principle is the assumption, nay, the conviction, that some special properties that a system may enjoy at macroscopic scales cannot be the result of the careful adjustment of various free parameters in the microscopic equations by Nature or any other entity one might care to invoke.

Ostensible violations of this principle have become some of the most fundamental problems of modern theoretical physics. These include the *cosmological constant problem* and the *Higgs mass hierarchy problem*. The former relates to the extremely small value of the observed cosmological constant relative to the Planck scale. The latter relates to the smallness of the observed Higgs mass relative to the scale of grand unification, or some other scale of new physics beyond the Standard Model. In both cases, the symmetry of the corresponding quantum field theory does not appear to increase in the limit of vanishing cosmological constant or Higgs mass. Indeed, the expected quantum corrections estimated in the framework of relativistic effective field theory (EFT) predict natural values at a much higher scale, many orders of magnitude larger than the observed ones.

It is conceivable that some puzzles of naturalness may only have environmental explanations, based on the landscape of many vacua in the multiverse. However, before we give up naturalness as our guiding principle, it is important to investigate more systematically the “landscape of naturalness”: To map out the various quantum systems and scenarios in which technical naturalness does hold, identifying possible surprises and new pieces of the puzzle that might help restore the power of naturalness in fundamental physics.

1.2. Naturalness and the Polynomial Shift Symmetry

Here we will describe a specific example of how naturalness works. There are many examples of naturalness in play in relativistic physics. For example, the electron mass, $m_e = 0.511$ MeV, is much smaller than the electroweak symmetry breaking scale, $v = 246$ GeV. This is technically natural because, in the limit of vanishing electron mass, the system gains the extra chiral symmetry – the separate conservation of left- and right-chiral electrons. An example of the opposite scenario would be the mass of a scalar particle with a quartic self-interaction. This system does not gain an enhanced symmetry in the limit of vanishing mass, and therefore it is unnatural to neglect the mass altogether. In fact, this latter example is a stripped down and simplified version of the Higgs mass hierarchy problem.

In the absence of relativistic invariance, many more types of symmetries may be considered, which drastically broaden our view of the landscape of naturalness. The *polynomial shift symmetry* is one type of symmetry that will play a crucial role in this thesis. Thus, we will describe how naturalness works in a specific interesting example of a Lifshitz scalar field theory with polynomial shift symmetry.¹

The theory under consideration lives in flat space \mathbf{R}^{3+1} , with a foliation structure by leaves of constant preferred time, t . The spatial slices are flat Euclidean space \mathbf{R}^3 . The polynomial shift symmetry for a scalar field is defined locally, with respect to spatial coordinates near a point in the spacetime, as

$$\delta\phi(t, \mathbf{x}) = a_{i_1 \dots i_P} x^{i_1} \dots x^{i_P} + \dots + a_i x^i + a, \quad (1.1)$$

where $a, a_i, \dots, a_{i_1 \dots i_P}$ are the real coefficients of a degree- P polynomial function of the spatial coordinates. Of course, one is free to consider irreducible subgroups. For example, for the quadratic shift symmetry, one could restrict to the trace, $a_{ij} \propto \delta_{ij}$, or the traceless part of the symmetry.

Suppose the scalar field theory is in the vicinity of a fixed point characterized by Lifshitz scaling with dynamical exponent $z = 3$. In this case, since $z = D$, the spatial dimension, the theory is in its lower critical dimension, where the field ϕ is classically dimensionless. Let us impose classical scale invariance by considering only classically marginal interactions. We find that there are no classically marginal interactions which are invariant with respect to polynomial shifts of degree two or higher. There are five operators, which are invariant under the constant shift symmetry. The first two are three-point interactions and the last three are four-point interactions:

$$\mathcal{O}_1 = \partial_i \phi \partial_j \partial_k \phi \partial_i \partial_j \partial_k \phi, \quad (1.2a)$$

$$\mathcal{O}_2 = \partial_i \partial_j \phi \partial_j \partial_k \phi \partial_i \partial_k \phi, \quad (1.2b)$$

$$\mathcal{O}_3 = \partial_i \phi \partial_j \phi \partial_k \phi \partial_i \partial_j \partial_k \phi, \quad (1.2c)$$

$$\mathcal{O}_4 = \partial_i \phi \partial_i \partial_j \phi \partial_j \partial_k \phi \partial_k \phi, \quad (1.2d)$$

$$\mathcal{O}_5 = \partial_i \phi \partial_i \phi \partial_j \partial_k \phi \partial_j \partial_k \phi. \quad (1.2e)$$

Note that these are exact invariants under the constant shift symmetry.

¹The relevant calculations were performed by the author with Ziqi Yan and features in unpublished work co-authored with Petr Hořava, Christopher Mogni and Ziqi Yan [27].

The two three-point interactions, \mathcal{O}_1 and \mathcal{O}_2 , are also invariant under the linear shift symmetry. It is obvious that \mathcal{O}_2 is exactly invariant under the linear shift symmetry, but \mathcal{O}_1 is also exactly invariant since we can equally well write it as $\frac{1}{2}(\partial^2\phi)\partial_i\partial_j\phi\partial_i\partial_j\phi$. The three four-point interactions, \mathcal{O}_3 , \mathcal{O}_4 and \mathcal{O}_5 , are not invariant under the linear shift symmetry, but the combination $\mathcal{O}_3 + 3\mathcal{O}_4$ is invariant up to a total derivative. Finally, under the quadratic trace shift symmetry, the only invariant is the combination of the two three-point interactions $6\mathcal{O}_1 + 5\mathcal{O}_2$. The only invariant under the quadratic traceless shift symmetry is the combination $6\mathcal{O}_1 + 2\mathcal{O}_2$. In both of these latter cases, the corresponding invariant is an exact invariant.

Suppose we were to include only the two three-point interaction terms. That is, we set the coefficients of the three four-point interactions equal to zero. Is this technically natural? That is, do \mathcal{O}_1 and \mathcal{O}_2 by themselves generate divergent quantum corrections that contribute to \mathcal{O}_3 , \mathcal{O}_4 and \mathcal{O}_5 ? A straightforward evaluation of the one-loop contribution to the four-point interaction shows that \mathcal{O}_1 and \mathcal{O}_2 by themselves generate quantum corrections to four-point interactions with at least eight spatial derivatives. Therefore, it is natural to set the coefficients of the four-point interactions equal to zero.

A glance at the previously mentioned polynomial shift symmetries immediately explains this result. \mathcal{O}_1 and \mathcal{O}_2 are separately exact invariants under the linear shift symmetry. Therefore, it is technically natural to set to zero the coefficients of all terms which are not exactly invariant under the linear shift symmetry. There is one combination, $\mathcal{O}_3 + 3\mathcal{O}_4$, which is invariant under the linear shift, but only up to a total derivative.

One can compute the one-loop correction to the three-point interaction. The corrections to \mathcal{O}_1 and \mathcal{O}_2 are independent except when the original combination is invariant under either the quadratic trace or quadratic traceless shift. In these cases, the corrections combine into a correction only to the corresponding original invariant!

More interestingly, one can write down four exact linear-shift invariant four-point interactions with eight derivatives, which are technically irrelevant:

$$\mathcal{O}'_1 = \partial_i\partial_j\phi\partial_j\partial_k\phi\partial_k\partial_\ell\phi\partial_i\partial_\ell\phi, \quad (1.3a)$$

$$\mathcal{O}'_2 = \partial^2\phi\partial_i\partial_j\phi\partial_j\partial_k\phi\partial_i\partial_k\phi, \quad (1.3b)$$

$$\mathcal{O}'_3 = \partial_i\partial_j\phi\partial_i\partial_j\phi\partial_k\partial_\ell\phi\partial_k\partial_\ell\phi, \quad (1.3c)$$

$$\mathcal{O}'_4 = (\partial^2\phi)^2\partial_i\partial_j\phi\partial_i\partial_j\phi. \quad (1.3d)$$

One linear combination is exactly invariant under the quadratic trace, $3\mathcal{O}'_1 - 4\mathcal{O}'_2 + 3\mathcal{O}'_3$. In general, \mathcal{O}_1 and \mathcal{O}_2 give finite quantum corrections to all four operators. However, the structure of these corrections is such that, if the coefficients of \mathcal{O}_1 and \mathcal{O}_2 are tuned to the combination that is exactly quadratic trace invariant, then only the specific combination $3\mathcal{O}'_1 - 4\mathcal{O}'_2 + 3\mathcal{O}'_3$, which is also exactly quadratic trace invariant, receives quantum corrections! The same story holds for the quadratic traceless shift symmetry, for which there is also one exact invariant. The above basis is not well-suited to this case – the obvious quadratic traceless shift invariant is just $(\partial^2\phi)^4$.

Note that one could have predicted these results from the beginning. However, one might imagine possible objections to the symmetry in the first place. Is it well-defined? How does one deal with boundary terms out near spatial infinity, which technically appear

to diverge? Is one allowed to consider terms which are invariant up to total derivatives, or is one constrained to consider only exact invariants? We will touch upon these questions when we study the polynomial shift on compactified spaces and periodic lattices in §6.2. For now, we are content to observe that the theory satisfies the requirements of technical naturalness and enjoys these polynomial shift symmetries whether or not we like them.

The remainder of this thesis will explore landscapes of naturalness with the use of Lifshitz scalar field theories. The aim is to open up vistas representing new phenomena and possibilities that have heretofore remained largely unexplored. It is our hope that this work will eventually prove fruitful in the fields of high energy physics and quantum gravity, and will inspire new ways to approach such naturalness problems as those presented by the Higgs mass hierarchy and the cosmological constant.

Chapter 2

Multicritical Symmetry Breaking

We investigate spontaneous global symmetry breaking in the absence of Lorentz invariance, and study technical Naturalness of Nambu-Goldstone (NG) modes whose dispersion relation exhibits a hierarchy of multicritical phenomena with Lifshitz scaling and dynamical exponents $z > 1$. For example, we find NG modes with a technically natural quadratic dispersion relation which do not break time reversal symmetry and are associated with a single broken symmetry generator, not a pair. The mechanism is protected by an enhanced ‘polynomial shift’ symmetry in the free-field limit.

2.1. Introduction

Gapless Nambu-Goldstone (NG) modes [28, 29, 30, 31] appear prominently across an impressive array of physical phenomena, both relativistic and nonrelativistic (for reviews, see *e.g.* [32, 33, 34, 35, 36].) They are a robust consequence of spontaneous symmetry breaking. Moreover, when further combined with gauge symmetries, they lead to the Higgs phenomenon, responsible for controlling the origin of elementary particle masses.

The NG modes are controlled by Goldstone’s theorem: A spontaneously broken generator of a continuous internal rigid symmetry implies the existence of a gapless mode. With Lorentz invariance, the theorem implies a one-to-one correspondence between the generators of broken symmetry and massless NG modes, but in the nonrelativistic setting, it leaves questions [37, 38, 39]: What is the number of independent NG modes? What are their low-energy dispersion relations?

In this chapter, we study the general classification of NG modes, and their Naturalness, in nonrelativistic theories with Lifshitz symmetries. The important concept of Naturalness is behind many successes of modern physics, but it also leads to some of its most intriguing and persistent puzzles. A system is technically natural if its low-energy behavior follows from that at higher energy scales, without requiring fine tuning [26]. Perhaps the most famous “Naturalness problem” comes from the apparent smallness of the cosmological constant [40, 41, 42], suggesting that something fundamental is still missing in our understanding of gravity and cosmology. And now that the Higgs boson has been discovered, (un)naturalness at the TeV scale is again at the forefront of high-energy particle physics [43, 44, 45, 46, 47]. In the context of quantum gravity, theories with Lifshitz symmetries have been studied

at least in part because of their improved short-distance (UV) behavior [10, 11, 14]. Our study illustrates that in Lifshitz-type theories, not only the short-distance behavior but also the concept of Naturalness acquires interesting new features. This leads to a refinement in the classification of NG modes in systems with Lifshitz symmetries, characterized by a multicritical behavior which is technically natural, and protected by a symmetry.

2.1.1. Geometry of the Spacetime with Lifshitz Symmetries

For clarity and simplicity, we focus on systems on the flat spacetime with Lifshitz spacetime symmetries. We define this spacetime to be $M = \mathbf{R}^{D+1}$ with a preferred foliation \mathcal{F} by fixed spatial slices \mathbf{R}^D , and equipped with a flat metric. Such a spacetime with the preferred foliation \mathcal{F} would for example appear as a ground-state solution of nonrelativistic gravity [11] whose gauge symmetry is given by the group of foliation-preserving spacetime diffeomorphisms, $\text{Diff}(M, \mathcal{F})$ (or a nonrelativistic extension thereof [14]). It is useful to parametrize M by coordinates $(t, \mathbf{x} = \{x^i, i = 1, \dots, D\})$, such that the leaves of \mathcal{F} are the leaves of constant t , and the metric has the canonical form

$$g_{ij}(t, \mathbf{x}) = \delta_{ij}, \quad \mathcal{N}(t, \mathbf{x}) = 1, \quad \mathcal{N}_i(t, \mathbf{x}) = 0 \quad (2.1)$$

(here g_{ij} is the spatial metric on the leaves of \mathcal{F} , \mathcal{N} is the lapse function, and \mathcal{N}_i the shift vector).

The isometries of this spacetime are, by definition, those elements of $\text{Diff}(M, \mathcal{F})$ that preserve this flat metric [48]. Explicitly, the connected component of this isometry group is generated by infinitesimal spatial rotations and spacetime translations,

$$\delta t = b, \quad \delta x^i = \omega^i_j x^j + b^i, \quad \omega_{ij} = -\omega_{ji}. \quad (2.2)$$

At fixed points of the renormalization group, systems with Lifshitz isometries develop an additional scaling symmetry, generated by

$$\delta x^i = \lambda x^i, \quad \delta t = z \lambda t. \quad (2.3)$$

The dynamical critical exponent z is an important observable associated with the fixed point, and characterizes the degree of anisotropy between space and time at the fixed point.

The connected component of the group of isometries of our spacetime M with the flat metric (2.1) is generated by (2.2), and we will refer to it as the ‘‘Lifshitz symmetry’’ group.¹ The full isometry group of this spacetime has four disconnected components, which can be obtained by combining the Lifshitz symmetry group generated by (2.2) with two discrete symmetries: The time-reversal symmetry \mathcal{T} , and a discrete symmetry \mathcal{P} that reverses the orientation of space. In this paper, we shall be interested in systems that are invariant under the Lifshitz symmetry group. Note that this mandatory Lifshitz symmetry does not contain either the discrete symmetries \mathcal{T} and \mathcal{P} , or the anisotropic scaling symmetry (2.3).

¹It would be natural to refer to M with the flat metric (2.1) as the ‘‘Lifshitz spacetime’’. Unfortunately, this term already has another widely accepted meaning in the holography literature, where it denotes the curved spacetime geometry in one dimension higher, whose isometries realize the Lifshitz symmetries (2.2) plus the Lifshitz scaling symmetry (2.3) for some fixed value of z [49].

2.1.2. Effective Field Theories of Type A and B Nambu-Goldstone Bosons

We are interested in the patterns of spontaneous symmetry breaking of global continuous internal symmetries in the flat spacetime with the Lifshitz symmetries, as defined in the previous paragraph. Our analysis gives an example of phenomena that are novel to Goldstone’s theorem in nonrelativistic settings, and can in principle be generalized to non-relativistic systems with even less symmetry.

We start with the NG field components π^A , $A = 1, \dots, n$, which serve as coordinates on the space of possible vacua $M = \mathcal{G}/H$ in a system with symmetries broken spontaneously from \mathcal{G} to $H \subset \mathcal{G}$. An elegant strategy has been proposed in [50, 51]: In order to classify Nambu-Goldstone modes, we can classify the corresponding EFTs available to describe their low-energy dynamics. In this EFT approach, we organize the terms in the effective action by their increasing dimension. Such dimensions are defined close enough to the infrared fixed point. However, until we identify the infrared fixed point, we don’t a priori know the value of the dynamical critical exponent, and hence the relative dimension of the time and space derivatives – it is then natural to count the time derivatives and spatial derivatives separately. Consider first the “potential terms” in the action, i.e., terms with no time derivatives. The general statement of Goldstone’s theorem implies that non-derivative terms will be absent, and the spatial rotational symmetry further implies that (for $D > 1$) all derivatives will appear in pairs contracted with the flat spatial metric. Hence, we can write the general “potential term” in the action as

$$S_{\text{eff}, V} = \int dt d\mathbf{x} \left\{ \frac{1}{2} g_{IJ}(\pi) \partial_i \pi^I \partial_i \pi^J + \dots \right\} \quad (2.4)$$

where $g_{IJ}(\pi)$ is the most general metric on the vacuum manifold which is compatible with all the global symmetries, and \dots stand for all the terms of higher order in spatial derivatives.

If the system is also invariant under the primitive version \mathcal{T} of time reversal, defined as the transformation that acts trivially on fields,

$$\mathcal{T} : \begin{cases} t & \rightarrow -t, \\ \pi^I & \rightarrow \pi^I, \end{cases} \quad (2.5)$$

the time derivatives will similarly have to appear in pairs, and the kinetic term will be given by

$$S_{\text{eff}, K} = \int dt d\mathbf{x} \left\{ \frac{1}{2} h_{IJ}(\pi) \dot{\pi}^I \dot{\pi}^J + \dots \right\}, \quad (2.6)$$

where again h_{IJ} is a general metric on the vacuum manifold compatible with all symmetries, but not necessarily equal to the g_{IJ} that appeared in (2.4); and \dots are higher-derivative terms.

However, invariance under \mathcal{T} is not mandated by the Lifshitz symmetry. If it is absent, the Lifshitz symmetries allow a new, more relevant kinetic term,

$$\tilde{S}_{\text{eff}, K} = \int dt d\mathbf{x} \left\{ \Omega_I(\pi) \dot{\pi}^I + \dots \right\}, \quad (2.7)$$

assuming one can define the suitable object $\Omega_I(\pi)$ on the vacuum manifold so that all the symmetry requirements are satisfied, and $\Omega_I(\pi) \dot{\pi}^I$ is not a total derivative. Since $\Omega_I(\pi)$

plays the role of the canonical momentum conjugate to π^I , if such Ω -terms are present in the action, they induce a natural canonical pairing on an even-dimensional subset of the coordinates on the vacuum manifold.

In specific dimensions, new terms in the effective action that are odd under spatial parity \mathcal{P} may exist. For example, in $D = 2$ spatial dimensions, we can add new terms to the “potential” part of the action, of the form

$$\tilde{S}_{\text{eff},V} = \int dt d\mathbf{x} \left\{ \frac{1}{2} \Omega_{IJ}(\pi) \varepsilon_{ij} \partial_i \pi^I \partial_j \pi^J + \dots \right\}, \quad (2.8)$$

where Ω_{IJ} is any two-form on the vacuum manifold that respects all the symmetries.² In the interest of simplicity, we wish to forbid such terms, and will do so by imposing the \mathcal{P} invariance of the action, focusing on the symmetry breaking patterns that respect spatial parity. This condition can of course be easily relaxed, without changing our conclusions significantly.

This structure of low-energy effective theories suggests the following classification of NG modes, into two general types:

- Type A: One NG mode per broken symmetry generator (not paired by Ω_I). The low-energy dispersion relation is linear, $\omega \propto k$.
- Type B: One NG mode per each pair of broken symmetry generators (paired by Ω_I). The low-energy dispersion relation is quadratic, $\omega \propto k^2$.

In general, Type A and Type B NG modes may coexist in one system. Some examples from condensed matter theory can be found in [50].

Based on the intuition developed in the context of relativistic quantum field theory, one might be tempted to conclude that everything else would be fine tuning, as quantum corrections would be likely to generate large terms of the form (2.4) in the effective action if we attempted to tune them to zero.

We will show that in Lifshitz-type theories, h_{AB} can be small *naturally, without fine tuning*. When that happens, the low-energy behavior of the NG modes will be determined by the next term, of higher order in ∂_i . The argument can be iterated: When the terms of order ∂^4 are also small, terms with $z = 3$ will step in, etc. This results in a hierarchy of multicritical Type-A and Type-B NG modes with increasing values of z . Compared to the generic NG modes described above, these multicritical NG modes are anomalously slow at low energies.

2.2. Example of Slow Nambu-Goldstone Bosons

We will demonstrate our results by focusing on a simple but representative example of symmetry breaking, the $O(N)$ nonlinear sigma model (NLSM) with target space S^{N-1} . (For some background on Lifshitz scalar theories, see [10, 52, 53, 54, 55, 56, 57, 58].) Until stated otherwise, we will also impose time reversal invariance, to forbid Ω_A .

²For example, if $\Omega_I(\pi)$ suitable for (2.7) exist, one can take $\Omega_{IJ} = \partial_{[I} \Omega_{J]}$.

2.2.1. $z=2$ Linear and Non-linear $O(N)$ Sigma Models

Under the aforementioned assumptions, the action of the $O(N)$ -invariant $z = 2$ Lifshitz NLSM [56] is given by

$$S_{\text{NLSM}} = \frac{1}{2G^2} \int dt d^D \mathbf{x} \left\{ g_{AB} \dot{\pi}^A \dot{\pi}^B - e^2 g_{AB} \Delta \pi^A \Delta \pi^B - c^2 g_{AB} \partial_i \pi^A \partial_i \pi^B \right. \\ \left. - \lambda_1 (g_{AB} \partial_i \pi^A \partial_j \pi^B) (g_{CD} \partial_i \pi^C \partial_j \pi^D) - \lambda_2 (g_{AB} \partial_i \pi^A \partial_i \pi^B)^2 \right\}. \quad (2.9)$$

Here $\Delta \pi^A \equiv \partial_i \partial_i \pi^A + \Gamma_{BC}^A \partial_i \pi^B \partial_i \pi^C$, g_{AB} is the round metric on the unit S^{N-1} (later we will use $g_{AB} = \delta_{AB} + \pi^A \pi^B / (1 - \delta_{CD} \pi^C \pi^D)$), and Γ_{BC}^A is its connection. The Gaussian $z = 2$ RG fixed point is defined by the first two terms in (2.9) as $G \rightarrow 0$. We define scaling dimensions throughout in the units of spatial momentum, $[\partial_i] \equiv 1$. Due to its geometric origin, the NG field π^A is dimensionless, $[\pi^A] = 0$. The first four terms in S_{NLSM} are all of the same dimension, so $[e^2] = [\lambda_1] = [\lambda_2] = 0$. We can set $e = 1$ by the rescaling of space and time, and will do so henceforth. All interactions are controlled by the coupling constant G , whose dimension is $[G] = (2 - D)/2$. Thus, the critical spacetime dimension of the system, at which the first four terms in (2.9) are classically marginal, is equal to $2 + 1$. The remaining term has a coupling of dimension $[c^2] = 2$, and represents a relevant deformation away from $z = 2$, even in the non-interacting limit $G \rightarrow 0$. Since c determines the speed of the NG modes in the $\mathbf{k} \rightarrow 0$ limit, we refer to this term as the ‘‘speed term’’ for short. Given the symmetries, this relevant deformation is unique.

We are mainly interested in $3 + 1$ dimensions, so we set $D = 3$ from now on. Since this is above the critical dimension of $2 + 1$ and $[G]$ is negative, the theory described by (2.9) must be viewed as an EFT: S_{NLSM} gives the first few (most relevant) terms out of an infinite sequence of operators of growing dimension, compatible with all the symmetries. It is best to think of this EFT as descending from some UV completion. For example, we can engineer this effective NLSM by starting with the $z = 2$ linear sigma model (LSM) of the unconstrained $O(N)$ vector ϕ^I , $I = 1, \dots, N$, and action

$$S_{\text{LSM}} = \frac{1}{2} \int dt d^D \mathbf{x} \left\{ \dot{\phi}^I \dot{\phi}^I - e^2 \partial^2 \phi^I \partial^2 \phi^I - c^2 \partial_i \phi^I \partial_i \phi^I - m^4 \phi^I \phi^I - \frac{\lambda}{2} (\phi^I \phi^I)^2 \right. \\ \left. - [e_1 + e_2 \phi^I \phi^I] \phi^J \phi^J \partial_i \phi^K \partial_i \phi^K - [f_1 + f_2 \phi^I \phi^I] (\phi^J \partial_i \phi^J) (\phi^K \partial_i \phi^K) \right. \\ \left. - \sum_{s=3}^5 \frac{g_s}{s!} (\phi^I \phi^I)^s \right\}. \quad (2.10)$$

The first two terms define the Gaussian $z = 2$ fixed point. We again set $e = 1$ by rescaling space and time. At this fixed point, the field is of dimension $[\phi] = 1/2$, and the dimensions of the couplings – in the order from the marginal to the more relevant – are: $[e] = [g_5] = [e_2] = [f_2] = 0$, $[g_4] = [e_1] = [f_1] = 1$, $[g_3] = [c^2] = 2$, $[\lambda] = 3$ and $[m^4] = 4$.

This theory can be studied in the unbroken phase, the broken phase with a spatially uniform condensate (which we take to lie along the N -th component, $\langle \phi^N \rangle = v$), or in a spatially modulated phase which also breaks spontaneously some of the spacetime symmetry. We will focus on the unbroken and the uniformly broken phase. In the latter, we will write

$\phi^I = (\Pi^A, v + \sigma)$. Changing variables to $\phi^I = (r\pi^A, r\sqrt{1 - \delta_{AB}\pi^A\pi^B})$ and integrating out perturbatively the gapped radial field $r - v$ gives the NLSM (2.9) of the gapless π^A at leading order, followed by higher-derivative corrections. This is an expansion in the powers of the momenta $|\mathbf{k}|/m_{\text{gap}}$ and frequency ω/m_{gap}^2 , where m_{gap} is the gap scale of the radial mode.

2.2.2. Quantum Corrections to the Speed Term

The simplest example with a uniform broken phase is given by the special case of LSM, in which we turn off all self-interaction couplings except λ , and also set the speed term $c^2 = 0$ classically. This theory is superrenormalizable: Since $[\lambda] = 3$, the theory becomes free at asymptotically high energies, and stays weakly coupled until we reach the scale of strong coupling $m_s = \lambda^{1/3}$. Since the speed term is relevant, our intuition from the relativistic theory may suggest that once interactions are turned on, relevant terms are generated by loop corrections, with a leading power-law dependence on the UV momentum cutoff Λ . In fact, this does not happen here. To show this, consider the broken phase, with the potential minimized by

$$v = \frac{m^2}{\sqrt{\lambda}}, \quad (2.11)$$

and set $c^2 = 0$ at the classical level. The Π^A fields are gapless, and represent our NG modes. The σ has a gapped dispersion relation, $\omega^2 = |\mathbf{k}|^4 + 2m^4$. The Feynman rules in the broken phase are almost identical to those of the relativistic version of this theory [59], except for the nonrelativistic form of the propagators,

$$\begin{array}{c} A \\ \longrightarrow \\ \omega, \mathbf{k} \\ \longrightarrow \\ B \end{array} = \frac{i\delta_{AB}}{\omega^2 - |\mathbf{k}|^4 + i\epsilon}, \quad (2.12a)$$

$$\begin{array}{c} \omega, \mathbf{k} \\ \longrightarrow \end{array} = \frac{i}{\omega^2 - |\mathbf{k}|^4 - 2m^4 + i\epsilon}. \quad (2.12b)$$

Because of the $z = 2$ anisotropy, the superficial degree of divergence of a diagram with L loops, E external legs and V_3 cubic vertices is $\mathcal{D} = 8 - 2E - 3L - 2V_3$. Loop corrections to the speed term are actually finite. If we start at the classical level by setting $c^2 = 0$, this relation can be viewed as a “zeroth order natural relation” (in the sense of [59]): True classically and acquiring only finite corrections at all loops. We can even set c^2 at any order to zero by a finite local counterterm, but an infinite counterterm for c^2 is not needed for renormalizability.

How large is this finite correction to c^2 ? At one loop, five diagrams (shown in Fig. 2.1) contribute to the inverse propagator $\Gamma_{AB}(\omega, \mathbf{k}) \equiv (\omega^2 - |\mathbf{k}|^4 + \Sigma(\omega, \mathbf{k}))\delta_{AB}$. We can read off the one-loop correction to $c^2 = 0$ by expanding $\Sigma = -\delta m^4 - \delta c^2 \mathbf{k}^2 + \dots$. Four of these diagrams give a (linearly) divergent contribution to δm^4 , but both the divergent and finite contributions to δm^4 sum to zero, as Goldstone’s theorem requires (see Appendix 2.A). The next term in Σ is then proportional to \mathbf{k}^2 and finite. It gets its only one-loop contribution

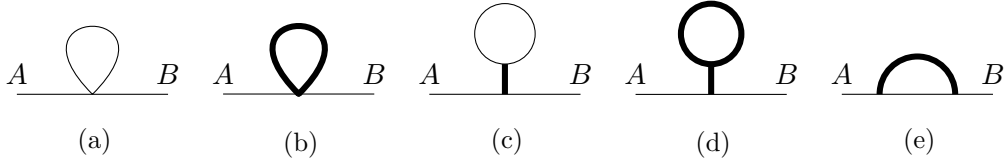


Figure 2.1: One-loop corrections to Γ_{AB} of the NG modes in the broken phase of the superrenormalizable LSM.

from diagram (e) in Fig. 2.1, whose explicit evaluation gives (see Appendix 2.A)

$$\delta c^2 = \frac{2^{\frac{7}{4}} \cdot 5}{63\pi^{\frac{5}{2}}} \left[\Gamma\left(\frac{5}{4}\right) \right]^2 \frac{\lambda}{m} \approx 0.0125 \frac{\lambda}{m}. \quad (2.13)$$

Thus, the first quantum correction to c^2 is indeed finite and nonzero. But is it small or large? There are much higher scales in the theory, such as m and Λ , yet in our weak coupling limit the correction to the speed term is found to be $\delta c^2 \propto \lambda/m$ naturally. In this sense, δc^2 is small, and so c^2 can also be small without fine tuning.

We can also calculate δc^2 at one loop in the effective NLSM. The Feynman rules derived from (2.9) for the rescaled field π^A/G involve a propagator independent of G (in which we set $c^2 = 0$), and an infinite sequence of vertices with an arbitrary even number of legs, of which we will only need the lowest one. When the radial direction of ϕ is integrated out in our superrenormalizable LSM, at the leading order we get (2.9) with $G = 1/v$, $\lambda_1 = 0$ and $\lambda_2 = 1$. In this special case, the 4-vertex is

$$\begin{array}{c} D \swarrow \quad \nearrow C \\ \omega_4, \mathbf{k}_4 \quad \omega_3, \mathbf{k}_3 \\ \omega_1, \mathbf{k}_1 \quad \omega_2, \mathbf{k}_2 \\ A \nearrow \quad \swarrow B \end{array} = -iG^2 \{ (\omega_1 + \omega_2)(\omega_3 + \omega_4) + |\mathbf{k}_1 + \mathbf{k}_2|^2 |\mathbf{k}_3 + \mathbf{k}_4|^2 \} \delta_{AB} \delta_{CD} + 2 \text{ permutations.}$$

The first quantum correction to δc^2 comes at one loop, from \bigcirc , and it is cubically divergent. With the sharp cutoff at $|\mathbf{k}| = \Lambda$, we get

$$\delta c^2 = \frac{G^2 \Lambda^3}{3\pi^2}. \quad (2.14)$$

This theory is only an EFT, and its natural cutoff scale Λ is given by m , the gap scale of the σ . With this value of the cutoff, the one-loop result (2.14) gives $\delta c^2 = \mathcal{O}(\lambda/m)$, which matches our LSM result.

If one wishes to extend the control over the LSM beyond weak coupling in λ , one can take the large- N limit, holding the 't Hooft coupling λN fixed. In this limit, the LSM and the NLSM actually become equivalent, by the same argument as in the relativistic case [5]. An explicit calculation shows that at large N , δc^2 is not just finite but actually zero, to all orders in the 't Hooft coupling (see Appendix 2.B).

2.3. Naturalness

Now, we return to the question of Naturalness of small δc^2 , in the technical context articulated in [26]. As a warm-up, consider first our superrenormalizable LSM in its unbroken phase. The leading contribution to the speed term in the inverse propagator of ϕ^I is now at two-loop order, from $\text{---}\bigcirc\text{---}$. This diagram is finite; even the leading constant, independent of ω and \mathbf{k} , only yields a finite correction to the gap m^4 . The contribution of order \mathbf{k}^2 is then also finite, and gives $\delta c^2 = \xi \lambda^2/m^4$, with ξ a pure number independent of all couplings. But is this δc^2 small?

Let us first recall a well-known fact from the relativistic $\lambda\phi^4$ theory [26]: λ and m^2 may be simultaneously small, $\sim \varepsilon$, because in the limit of $\varepsilon \rightarrow 0$, the system acquires an enhanced symmetry – in this case, the constant shift symmetry,

$$\phi^I \rightarrow \phi^I + a^I. \quad (2.15)$$

The same constant shift symmetry works also in our superrenormalizable Lifshitz LSM. Restoring dimensions, we have

$$\lambda = \mathcal{O}(\varepsilon\mu^3), \quad m^4 = \mathcal{O}(\varepsilon\mu^4). \quad (2.16)$$

Here μ is the scale at which the constant shift symmetry is broken (or other new physics steps in), and represents the *scale of naturalness*: The theory is natural until we reach the scale $\mu = \mathcal{O}(m^4/\lambda)$. This result is sensible – if we wish for the scale of naturalness to be much larger than the gap scale, $\mu \gg m$, we must keep the theory at weak coupling, $\lambda/m^3 \ll 1$. Now, how about the speed term? If we assume that c^2 is also technically small, $c^2 \sim \nu$, this assumption predicts $c^2 = \mathcal{O}(\lambda^2/m^4)$, which is exactly the result we found above in our explicit perturbative calculation. It looks like there must be a symmetry at play, protecting simultaneously the smallness of m^4 , λ as well as c^2 ! We propose that the symmetry in question is the generalized shift symmetry (2.15), with a^I now a quadratic polynomial in the spatial coordinates,

$$a^I = a_{ij}^I x^i x^j + a_i^I x^i + a_0^I. \quad (2.17)$$

The speed term $\partial_i \phi^I \partial_i \phi^I$ is forbidden by this “quadratic shift” symmetry, while $\partial^2 \phi^I \partial^2 \phi^I$ is invariant up to a total derivative. This symmetry holds in the free-field limit, and will be broken by interactions. It can be viewed as a generalization of the Galileon symmetry, much studied in cosmology [60], which acts by shifts linear in the spacetime coordinates.

As long as the coupling is weak, the unbroken phase of the LSM exhibits a natural hierarchy of scales, $c \ll m \ll \mu$, with the speed term much smaller than the gap scale. The effects of the speed term on the value of z would only become significant at low-enough energies, where the system is already gapped. Note that another interesting option is also available, since there is no obligation to keep c small at the classical level. If instead we choose c much above the gap scale m (but below the naturalness scale μ), as we go to lower energies the system will experience a crossover from $z = 2$ to $z = 1$ before reaching the gap, and the theory will flow to the relativistic $\lambda\phi^4$ in the infrared. The coupling λ can stay small throughout the RG flow from the free $z = 2$ fixed point in the UV to the $z = 1$ theory in the infrared.

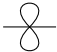
Now consider the same LSM in the broken phase. In this case, we are not trying to make m small – this is a fixed scale, setting the nonzero gap of the σ . Moreover, the π 's are gapless, by Goldstone's theorem. We claim that c^2 can be naturally small in the regime of small λ ,

$$\lambda = \mathcal{O}(\varepsilon\mu^3), \quad c^2 = \mathcal{O}(\varepsilon\mu^2), \quad (2.18)$$

as a consequence of an enhanced symmetry. The symmetry in question is again the “quadratic shift” symmetry, now acting only on the gapless NG modes in their free-field limit: $\Pi^A \rightarrow \Pi^A + a_{ij}^A x^i x^j + \dots$. It follows from (2.11) that the radius v of the vacuum manifold S^{N-1} goes to infinity with $\varepsilon \rightarrow 0$, $v = \mathcal{O}(m^2/\sqrt{\mu^3\varepsilon})$, and $v \rightarrow \infty$ corresponds to the free-field limit of the π 's. Our enhanced symmetry does not protect m from acquiring large corrections; we can view m in principle as a separate mass scale, but it is natural to take it to be of the order of the naturalness scale, $m = \mathcal{O}(\mu)$. Altogether, this predicts $\delta c^2 = \mathcal{O}(\lambda/\mu) = \mathcal{O}(\lambda/m)$, in accord with our explicit loop result (2.13).

The technically natural smallness of the speed term in our examples is not an artifact of the superrenormalizability of our LSM. To see that, consider the full renormalizable LSM (2.10), first in the unbroken phase. As we turn off all self-interactions by sending $\varepsilon \rightarrow 0$, the enhanced quadratic shift symmetry will again protect the smallness of $c^2 \sim \varepsilon$. In terms of the naturalness scale μ , this argument predicts that in the action (2.10), all the deviations from the $z = 2$ Gaussian fixed point can be naturally of order ε in the units set by μ :


$$e_2 = \mathcal{O}(\varepsilon), \quad \dots, \quad c^2 = \mathcal{O}(\varepsilon\mu^2), \quad \lambda = \mathcal{O}(\varepsilon\mu^3), \quad m^4 = \mathcal{O}(\varepsilon\mu^4).$$

If we want the naturalness scale to be much larger than the gap scale, $\mu \gg m$, all couplings must be small; for example, $e_2 = \mathcal{O}(m^4/\mu^4) \ll 1$, etc. We then get an estimate $\delta c^2 = \mathcal{O}(e_2\mu^2) = \mathcal{O}(\sqrt{e_2}m^2) \ll m^2$: As in the superrenormalizable case, the speed term can be naturally much smaller than the gap scale. This prediction can be verified by a direct loop calculation. The leading contribution to δc^2 comes from several two-loop diagrams, including  with one e_2 vertex. Each loop in this diagram is separately linearly divergent, giving $\delta c^2 \sim e_2\Lambda^2 = \mathcal{O}(\sqrt{e_2}m^2)$, in accord with our scaling argument.

The story extends naturally to the broken phase of the renormalizable LSM, although this theory is technically rather complicated: The $\langle\phi\rangle$ itself is no longer given by (2.11) but it is at the minimum of a generic fifth-order polynomial in $\phi^I\phi^I$. It is thus more practical to run our argument directly in the low-energy NLSM. The advantage is that even for the generic renormalizable LSM (2.10), the leading-order NLSM action is of the general form (2.9). The leading order of matching gives $G = 1/v$, with v the radius of the vacuum manifold S^{N-1} . The NLSM is weakly coupled when this radius is large. The enhanced “quadratic shift” symmetry of the NG modes π^A in their free-field limit implies $G^2 = \mathcal{O}(\varepsilon/\mu)$ and $c^2 = \mathcal{O}(\varepsilon\mu^2)$ with $\lambda_{1,2} = \mathcal{O}(1)$, and predicts

$$c^2 = \mathcal{O}(G^2\mu^3). \quad (2.19)$$

The naturalness scale μ is set by the gap of the σ particle, which is generally of order m . Thus, (2.19) implies that in the large- v regime of the weakly-coupled NLSM, the speed term is naturally much smaller than the naturalness scale. This can be again confirmed by

a direct loop calculation: The leading contribution to δc^2 comes from the one-loop diagram . This diagram is cubically divergent and its vertex gives a G^2 factor, leading to $\delta c^2 \sim G^2 \Lambda^3$. Setting $\Lambda \sim \mu$ confirms our scaling prediction (2.19). In the special case of our superrenormalizable LSM, we can go one step further, and use (2.11) and $G = 1/v$ to reproduce again our earlier result, $\delta c^2 = \mathcal{O}(\lambda/m)$.

2.4. Nonrelativistic Refinement of Goldstone’s Theorem

In its original form, Goldstone’s theorem guarantees the existence of a gapless mode when a global continuous internal symmetry is spontaneously broken. However, in the absence of Lorentz symmetry, it does not predict the number of such modes, or their low-energy dispersion relation.

The classification of the effective field theories which are available to describe the low-energy limit of the Nambu-Goldstone mode dynamics leads to a natural refinement of the Goldstone theorem in the nonrelativistic regime. In the specific case of spacetimes with Lifshitz symmetry, we get two hierarchies of NG modes:

- Type A: One NG mode per broken symmetry generator (not paired by Ω_I) The low-energy dispersion relation is $\omega \propto k^n$, where $n = 1, 2, 3, \dots$
- Type B: One NG mode per each pair of broken symmetry generators (paired by Ω_I). The low-energy dispersion relation is $\omega \propto k^{2n}$, where $n = 1, 2, 3, \dots$

It is natural to label the members of these two hierarchies by the value of the dynamical critical exponent of their corresponding Gaussian fixed point. We will refer to these multicritical universality classes of Nambu-Goldstone modes as “Type A_n ” and “Type B_{2n} ”, respectively.

2.5. Discussion

We have shown that Type-A NG modes can naturally have an anomalously slow speed, characterized by an effective $z = 2$ dispersion relation. Our arguments can be easily iterated, leading to Type-A NG modes with higher dispersion of $z = 3, 4, \dots$. In such higher multicritical cases, the smallness of all the relevant terms is protected by the enhanced “polynomial shift” symmetry in the free-field limit, with a^I now a polynomial in x^i of degree $2z - 2$. Our results also extend easily to Type-B NG modes. Instead of their generic $z = 2$ dispersion, they can exhibit a $z = 4$ (or higher) behavior over a large range of energy scales.

The following few comments may be useful:

- (1) The polynomial shift symmetry is easily applied to Type B NG modes as well. For example, for the quadratic shift at the Gaussian fixed point, $\Omega_I(\pi)$ of (2.7) reduces to a linear function of π , such that $\tilde{S}_{\text{eff},K}$ is invariant under the quadratic shift up to a total derivative, and the extra shift symmetry yields Type B NG modes with a quartic dispersion relation.

- (2) Type B NG modes represent a true infinite hierarchy of consistent fixed points. On the other hand, at fixed spatial dimension, the Type A pattern of multicritical symmetry breaking will eventually run into the nonrelativistic analog of the Coleman-Hohenberg-Mermin-Wagner theorem [61, 62, 63]: At the critical value of $n = D$, they develop infrared singularities and cease to exist as well-defined quantum fields. We comment on this behavior further in §4.
- (3) Type A preserve \mathcal{T} invariance, while Type B break \mathcal{T} . (This does not mean that a suitable time reversal invariance cannot be defined on Type B modes, but it would have to extend \mathcal{T} of (2.5) to act nontrivially on the fields.)
- (4) Our classification shows the existence of A_n and B_{2n} hierarchies of NG modes described by Gaussian fixed points, and therefore represents a refinement of the classifications studied in the literature so far. However, it does not pretend to completeness: We find it plausible that nontrivial fixed points (and fixed points at non-integer values of n) suitable for describing NG modes may also exist. In this sense, the full classification of all possible types of nonrelativistic NG dynamics – even under the assumption of Lifshitz symmetries – still remains a fascinating open question.
- (5) For simplicity, we worked under the assumption of spacetime Lifshitz symmetry. Obviously, this simplifying restriction can be removed, and the classification of multicritical NG modes in principle extended to cases whereby some of the the spacetime symmetries are further broken by additional features of the system – such as spatial anisotropy, layers, an underlying lattice structure, etc. We also expect that the classification can be naturally extended to Nambu-Goldstone fermions associated with spontaneous breaking of symmetries associated with supergroups. Such generalizations, however, are beyond the scope of this chapter.

The multicritical behavior of the NG modes will have consequences for their low-energy scattering, generalizing the low-energy theorems known from the relativistic case [34]. The scattering amplitudes will exhibit a higher-power effective dependence on the momenta, with the power controlled by z .

Finally, it would be very interesting to extend our analysis to the spatially modulated phases of Lifshitz theories, in which the spacetime symmetries are further broken *spontaneously*, and where one can expect spatially modulated NG modes.

The results of this work refine the classification of NG modes in non-relativistic systems, and we expect them to be useful for understanding symmetry breaking in a broad class of phenomena, including relativistic matter at nonzero density or chemical potential, and areas of condensed matter, such as superconductivity, quantum critical phenomena [64] and dynamical critical systems [1]. Since our results also shed interesting new light on the concept of Naturalness, we are hopeful that they may stimulate new insights in areas where puzzles of Naturalness have been most prominent: particle physics, quantum gravity and cosmology.

Appendix

2.A. One-loop Correction to the Mass and Speed Parameters

In this appendix, we will evaluate explicitly the five one-loop diagrams in Fig. 2.1. The three-point and four-point vertices are

$$\begin{array}{ll}
 \begin{array}{c} B \\ \diagdown \\ \text{---} \\ \diagup \\ A \end{array} = -2im^2\sqrt{\lambda}\delta_{AB}, & \begin{array}{c} \diagdown \\ \text{---} \\ \diagup \end{array} = -6im^2\sqrt{\lambda}, \\
 \begin{array}{c} B \quad C \\ \diagdown \quad \diagup \\ A \quad D \end{array} = -2i\lambda(ABCD), & \begin{array}{c} B \quad \diagup \\ \diagdown \quad \text{---} \\ A \end{array} = -2i\lambda\delta_{AB}, \\
 \begin{array}{c} \diagdown \quad \diagup \\ \text{---} \\ \diagup \quad \diagdown \end{array} = -6i\lambda, &
 \end{array}$$

where we have defined the symmetrized product of Kronecker delta symbols

$$(ABCD) \equiv \delta_{AB}\delta_{CD} + \delta_{AC}\delta_{BD} + \delta_{AD}\delta_{BC}.$$

Since there are $N - 1$ pions, one obtains

$$(ABCD)\delta_{CD} = [(N - 1) + 1 + 1]\delta_{AB} = (N + 1)\delta_{AB}.$$

Denote the Feynman integrals associated with the diagrams as follows

$$\begin{array}{ll}
 I_a = \begin{array}{c} \text{---} \\ \diagup \quad \diagdown \\ \text{---} \\ \diagdown \quad \diagup \\ \text{---} \end{array} A \quad B, & I_b = \begin{array}{c} \text{---} \\ \diagup \quad \diagdown \\ \text{---} \\ \diagdown \quad \diagup \\ \text{---} \end{array} A \quad B, \\
 I_c = \begin{array}{c} \text{---} \\ \diagup \quad \diagdown \\ \text{---} \\ \diagdown \quad \diagup \\ \text{---} \end{array} A \quad B, & I_d = \begin{array}{c} \text{---} \\ \diagup \quad \diagdown \\ \text{---} \\ \diagdown \quad \diagup \\ \text{---} \end{array} A \quad B, \\
 I_e = \begin{array}{c} \text{---} \\ \diagup \quad \diagdown \\ \text{---} \\ \diagdown \quad \diagup \\ \text{---} \end{array} A \quad B.
 \end{array}$$

Let (ω, \mathbf{k}) be the external frequency and momentum and (ν, \mathbf{p}) be the internal frequency and momentum, which are integrated over. Taking into account the symmetry factor of 2 for diagrams (a), (b), (c) and (d), one obtains

$$I = \lambda \delta_{AB} \int \frac{d\nu}{2\pi} \frac{d^3p}{(2\pi)^3} \frac{J}{(\nu^2 - p^4 + i\epsilon)(\nu^2 - p^4 - 2m^4 + i\epsilon)},$$

with $J = J_a + J_b + J_c + J_d + J_e$ and

$$\begin{aligned} J_a &= (N+1)(\nu^2 - p^4 - 2m^4 + i\epsilon), \\ J_b &= \nu^2 - p^4 + i\epsilon, \\ J_c &= -(N-1)(\nu^2 - p^4 - 2m^4 + i\epsilon), \\ J_d &= -3(\nu^2 - p^4) + i\epsilon, \\ J_e &= 4m^4 \frac{\nu^2 - p^4 - 2m^4 + i\epsilon}{(\nu + \omega)^2 - (p + k)^4 - 2m^4 + i\epsilon}. \end{aligned}$$

Therefore,

$$J = 4m^4 \left(\frac{\nu^2 - p^4 - 2m^4 + i\epsilon}{(\nu + \omega)^2 - (p + k)^4 - 2m^4 + i\epsilon} - 1 \right).$$

Expand in powers of ω and k as in

$$J = \sum_{r,n=0}^{\infty} J_{i_1 \dots i_n}^{(r,n)} \omega^r k_{i_1} \dots k_{i_n}.$$

$J^{(0,0)}$ determines the correction to the pion mass. However, this vanishes identically,

$$J^{(0,0)} = 0.$$

Therefore the pions remain exactly massless, as required by Goldstone's theorem.

It is clear that only J_e contributes $J^{(r,n)}$ when either r or n is nonzero. Therefore, let us focus on I_e :

$$I_e = 4m^4 \lambda \delta_{AB} \int \frac{d\nu}{2\pi} \frac{d^3p}{(2\pi)^3} \frac{1}{(\nu^2 - p^4 + i\epsilon)[(\nu + \omega)^2 - (p + k)^4 - 2m^4 + i\epsilon]}.$$

Introduce a Feynman parameter to write I_e as

$$I_e = 4m^4 \lambda \delta_{AB} \int_0^1 dx \int \frac{d\nu}{2\pi} \frac{d^3p}{(2\pi)^3} \frac{1}{D^2},$$

where

$$D = x[(\nu + \omega)^2 - (p + k)^4 - 2m^4 + i\epsilon] + (1-x)(\nu^2 - p^4 + i\epsilon).$$

Define

$$\xi = \nu + x\omega, \quad \ell = \mathbf{p} + x\mathbf{k}.$$

Then,

$$D = \xi^2 - \ell^4 - \alpha \ell^2 k^2 - \beta (\boldsymbol{\ell} \cdot \mathbf{k})^2 - \gamma (\boldsymbol{\ell} \cdot \mathbf{k}) k^2 - \Delta + i\epsilon,$$

where

$$\begin{aligned} \alpha &= 2x(1-x), & \gamma &= 4x(1-x)(1-2x), \\ \beta &= 4x(1-x), & \Delta &= 2xm^4 - x(1-x)[\omega^2 - (1-3x+3x^2)k^4]. \end{aligned}$$

After Wick-rotation, I_e becomes

$$I_e = 4im^4 \lambda \delta_{AB} \int_0^1 dx \int \frac{d\xi}{2\pi} \frac{d^3\ell}{(2\pi)^3} \frac{1}{D^2},$$

where

$$D = \xi^2 + \ell^4 + \alpha \ell^2 k^2 + \beta (\boldsymbol{\ell} \cdot \mathbf{k})^2 + \gamma (\boldsymbol{\ell} \cdot \mathbf{k}) k^2 + \Delta.$$

The term in I_e which contributes a correction to the speed parameter is the term which is of order $\omega^0 k^2$. We denote this term by $I_e^{(0,2)}$, given by

$$I_e^{(0,2)} = -8im^4 \lambda \delta_{AB} \int_0^1 dx \int \frac{d\xi}{2\pi} \frac{d^3\ell}{(2\pi)^3} \frac{\alpha \ell^2 k^2 + \beta (\boldsymbol{\ell} \cdot \mathbf{k})^2}{(\xi^2 + \ell^4 + 2xm^4)^3}.$$

Rotation invariance of the entire integrand except for the dot product piece allows for the substitution $(\boldsymbol{\ell} \cdot \mathbf{k})^2 \rightarrow \frac{1}{3} \ell^2 k^2$, and thus

$$I_e^{(0,2)} = -8im^4 \lambda k^2 \delta_{AB} \int_0^1 dx \left(\alpha + \frac{\beta}{3} \right) \int \frac{d\xi}{2\pi} \frac{d^3\ell}{(2\pi)^3} \frac{\ell^2}{(\xi^2 + \ell^4 + 2xm^4)^3}.$$

These are now all relatively simple integrals to evaluate. The result of the ξ integral is

$$\int \frac{d\xi}{2\pi} \frac{1}{(\xi^2 + \ell^4 + 2xm^4)^3} = \frac{3}{16(\ell^4 + 2xm^4)^{5/2}}.$$

The result of the subsequent ℓ integral is

$$\int \frac{d^3\ell}{(2\pi)^3} \frac{\ell^2}{(\ell^4 + 2xm^4)^{5/2}} = \frac{[\Gamma(\frac{5}{4})]^2}{2^{\frac{9}{4}} 3\pi^{\frac{5}{2}} m^5 x^{\frac{5}{4}}}.$$

The result of the subsequent x integral is

$$\int_0^1 dx \left(\alpha + \frac{\beta}{3} \right) x^{-\frac{5}{4}} = \frac{10}{3} \int_0^1 dx x^{-\frac{1}{4}} (1-x) = \frac{160}{63}.$$

All in all,

$$I_e^{(0,2)} = -8im^4 \lambda k^2 \delta_{AB} \frac{160}{63} \frac{[\Gamma(\frac{5}{4})]^2}{2^{\frac{9}{4}} 3\pi^{\frac{5}{2}} m^5} \frac{3}{16} = -i \left(\frac{2^{\frac{7}{4}} \cdot 5}{63\pi^{\frac{5}{2}}} [\Gamma(\frac{5}{4})]^2 \frac{\lambda}{m} \right) k^2 \delta_{AB}. \quad (2.20)$$

The term in parentheses is the one-loop correction, δc^2 . Indeed, summing over all repeated diagrams of type (e) gives the corrected propagator

$$\frac{i\delta_{AB}}{\omega^2 - k^4} \sum_{n=0}^{\infty} \left[(-i\delta c^2 k^2) \frac{i}{\omega^2 - k^4} \right]^n = \frac{i\delta_{AB}}{\omega^2 - k^4} \frac{1}{1 - \frac{\delta c^2 k^2}{\omega^2 - k^4}} = \frac{i\delta_{AB}}{\omega^2 - k^4 - \delta c^2 k^2}.$$

Therefore,

$$\delta c^2 = \frac{2^{\frac{7}{4}} \cdot 5}{63\pi^{\frac{5}{2}}} [\Gamma(\frac{5}{4})]^2 \frac{\lambda}{m} \approx 0.0125 \frac{\lambda}{m}. \quad (2.21)$$

2.B. Large- N Limit

In this appendix, we will demonstrate that the correction to the speed parameter vanishes in the large- N limit of the superrenormalizable linear sigma model, given by

$$S_{\text{LSM}} = \frac{1}{2} \int dt d^D \mathbf{x} \left\{ \dot{\phi}^I \dot{\phi}^I - \partial^2 \phi^I \partial^2 \phi^I - c^2 \partial_i \phi^I \partial_i \phi^I - m^4 \phi^I \phi^I - \frac{\lambda}{2} (\phi^I \phi^I)^2 \right\}.$$

In the broken phase, as in the relativistic case, the LSM and the NLSM become equivalent in the large- N limit [5]. To leading order, the NLSM action derived from the broken phase of the superrenormalizable LSM above is given by

$$S_{\text{NLSM}} = \frac{1}{2G^2} \int dt d^D \mathbf{x} \left\{ g_{AB} \dot{\pi}^A \dot{\pi}^B - g_{AB} \Delta \pi^A \Delta \pi^B - (g_{AB} \partial_i \pi^A \partial_i \pi^B)^2 \right\},$$

where $g_{AB} = \delta_{AB} + \pi^A \pi^B / (1 - \delta_{CD} \pi^C \pi^D)$ and $G = 1/v = \sqrt{\lambda}/m^2$ is the inverse of the vacuum expectation value of the magnitude of the vector ϕ^I . This leading order NLSM action is determined by simply setting the radial field identically equal to v , rather than expanding around v up to quadratic order and integrating out the perturbation.

The resulting 4-vertex is

$$\begin{array}{c} \begin{array}{ccc} D & & C \\ \swarrow & & \nearrow \\ \omega_4, \mathbf{k}_4 & & \omega_3, \mathbf{k}_3 \\ \nwarrow & & \nearrow \\ \omega_1, \mathbf{k}_1 & & \omega_2, \mathbf{k}_2 \\ \swarrow & & \nwarrow \\ A & & B \end{array} \\ \end{array} = -iG^2 \{ (\omega_1 + \omega_2)(\omega_3 + \omega_4) + |\mathbf{k}_1 + \mathbf{k}_2|^2 |\mathbf{k}_3 + \mathbf{k}_4|^2 \} \delta_{AB} \delta_{CD} \\ + 2 \text{ permutations.}$$

The one-loop correction to c^2 comes from $\text{---} \bigcirc \text{---}$, which can be split into two pieces, depending on the contraction of the pion indices:

$$\text{---} \bigcirc \text{---} = \text{---} \bigcirc \text{---} + \text{---} \bigcirc \text{---}$$

Due to the form of the vertex, the diagram with a self-contracted internal loop vanishes identically. On the other hand, such diagrams are the leading-order diagrams in the large- N limit since they pick up an extra factor of N from the index contraction. The large- N limit of the correction to the inverse propagator is given by so-called *cactus diagrams*, which contain only 4-point vertices and any number of self-contracted loops. However, in the present case, self-contracted loops vanish identically. Hence, the correction to c^2 vanishes identically in the large- N limit:

$$\delta c^2 \xrightarrow{N \rightarrow \infty} 0. \quad (2.22)$$

One can consider the most general situation, including all terms that can show up in the NLSM action (2.9). Surprisingly, one can derive an analytic equation for the correction to c^2 , which may be solved perturbatively in the smallness of the coupling constants. However, this result is not needed here.

Chapter 3

Scalar Field Theories with Polynomial Shift Symmetries

We continue our study of naturalness in nonrelativistic QFTs of the Lifshitz type, focusing on scalar fields that can play the role of Nambu-Goldstone (NG) modes associated with spontaneous symmetry breaking. Such systems allow for an extension of the constant shift symmetry to a shift by a polynomial of degree P in spatial coordinates. These “polynomial shift symmetries” in turn protect the technical naturalness of modes with a higher-order dispersion relation, and lead to a refinement of the proposed classification of infrared Gaussian fixed points available to describe NG modes in nonrelativistic theories. Generic interactions in such theories break the polynomial shift symmetry explicitly to the constant shift. It is thus natural to ask: Given a Gaussian fixed point with polynomial shift symmetry of degree P , what are the lowest-dimension operators that preserve this symmetry, and deform the theory into a self-interacting scalar field theory with the shift symmetry of degree P ? To answer this (essentially cohomological) question, we develop a new graph-theoretical technique, and use it to prove several classification theorems. First, in the special case of $P = 1$ (essentially equivalent to Galileons), we reproduce the known Galileon N -point invariants, and find their novel interpretation in terms of graph theory, as an equal-weight sum over all labeled trees with N vertices. Then we extend the classification to $P > 1$ and find a whole host of new invariants, including those that represent the most relevant (or least irrelevant) deformations of the corresponding Gaussian fixed points, and we study their uniqueness.

3.1. Introduction

The naturalness of the Nambu-Goldstone modes associated with the multicritical symmetry breaking described in §2 was protected by the polynomial shift symmetry. This symmetry is an approximate symmetry restored at the Gaussian infrared fixed points. In many general examples of multicritical symmetry breaking, the polynomial shift symmetry is broken by the self-interactions of the NG modes. It is then natural to ask: What if we impose the polynomial shift symmetry as an exact symmetry? What is the lowest-dimension operator that can be added to the action while preserving the symmetry? This is the task we address

in this chapter.

The classification of Lagrangians invariant under the polynomial shift of degree P up to a total derivative (which we will refer to as “ P -invariants” for short) is essentially a cohomological problem. In §3.2, we consider the polynomial-shift invariants in the simplest case of linear shifts (i.e., “1-invariants”). In order to prepare for the general case of $P > 1$, we develop a novel technique, based on graph theory. Having rephrased the defining relation for the invariants into the language of graphs, we can address the classification problem using the abstract mathematical machinery of graph theory. The basic ingredients of this technique are explained as needed in §3.2 and §3.3. However, we relegate all the technicalities of the graphical technique into a self-contained Appendix 3.B (preceded by Appendix 3.A, in which we offer a glossary of the basic terms from graph theory). Appendix 3.B is rather mathematical in nature, as it contains a systematic exposition of all our definitions, theorems and proofs that we found useful in the process of generating the invariants discussed in this chapter. Appendix 3.B is not required for the understanding of the results presented in §3.2 and §3.3: Once the invariants have been found using the techniques in Appendix 3.B, their actual invariance can be checked by explicit calculation (for example, on a computer). In this sense, the bulk of the work (§3.2 and §3.3) is also self-contained, and can be read independently of the Appendices.

The N -point 1-invariants discussed in §3.2 are known in the literature, where they have been generated in the closely related context of the relativistic Galileon theories [60]. While it is reassuring to see that our graph-theoretical technique easily reproduces these known 1-invariants, the novelty of our results presented in §3.2 lies elsewhere: We find a surprisingly simple and elegant interpretation of the known N -point 1-invariants in the language of graphs. They are simply given by the equal-weight sum over all labeled trees with N vertices!

In §3.3 we move beyond the 1-invariants, and initiate a systematic study of P -invariants with $P > 1$, organized in the order of their scaling dimension. We find several series of invariants; some of them we prove to be the unique and most relevant (or, more accurately, least irrelevant) N -point P -invariants, while others represent hierarchies of P -invariants of higher dimensions. We also show how to construct higher P -invariants from superposing several graphs that represent invariants of lower P . Appendix 3.C contains a brief discussion of the connection between our invariant Lagrangians and the Chevalley-Eilenberg Lie algebra cohomology theory. In §3.4 we present our conclusions.

For simplicity, we will focus on theories that consist of Type A_n (or Type B_{2n}) with a fixed n , and leave the generalizations to interacting systems that mix different types of NG modes for future studies.

3.1.1. Polynomial Shift Symmetries

Since the polynomial shift symmetries act on the fields $\pi^I(t, \mathbf{x})$ separately component by component, from now on we shall focus on just one field component, and rename it $\phi(t, \mathbf{x})$.

The generators of the polynomial shift symmetry of degree P act on ϕ by

$$\delta_P \phi = a_{i_1 \dots i_P} x^{i_1} \cdots x^{i_P} + \dots + a_i x^i + a. \quad (3.1)$$

The multicritical Gaussian fixed point with dynamical exponent $z = n$ is described by

$$S_n = \int dt d\mathbf{x} \left\{ \frac{1}{2} \dot{\phi}^2 - \frac{1}{2} \zeta_n^2 (\partial_{i_1} \dots \partial_{i_n} \phi) (\partial_{i_1} \dots \partial_{i_n} \phi) \right\}. \quad (3.2)$$

In fact, it is a one-parameter family of fixed points, parametrized by the real positive coupling ζ_n^2 . (Sometimes it is convenient to absorb ζ_n into the rescaling of space, and we will often do so when there is no competition between different fixed points.)

The action S_n is invariant under polynomial shift symmetries (3.1) of degree $P \leq 2n-1$: It is strictly invariant under the symmetries of degree $P < n$, and invariant up to a total derivative for degrees $n \leq P \leq 2n-1$.

Morally, this infinite hierarchy of symmetries can be viewed as a natural generalization of the Galileon symmetry, proposed in [60] and much studied since, mostly in the cosmological literature. In the case of the Galileons, the theory is relativistic, and the symmetry is linear in space-time coordinates. The requirement of relativistic invariance is presumably the main reason that has precluded the generalization of the Galileon symmetries past the linear shift: The higher polynomial shift symmetries in spacetime coordinates would lead to actions dominated by higher time derivatives, endangering perturbative unitarity.

So far, we considered shifts by generic polynomials of degree P , whose coefficients $a_{i_1 \dots i_\ell}$ are arbitrary symmetric real tensors of rank ℓ for $\ell = 0, \dots, P$. We note here in passing that for degrees $P \geq 2$, the polynomial shift symmetries allow an interesting refinement. To illustrate this feature, we use the example of the quadratic shift,

$$\delta_2 \phi = a_{ij} x^i x^j + a_i x^i + a_0. \quad (3.3)$$

The coefficient a_{ij} of the quadratic part is a general symmetric 2-tensor. It can be decomposed into its traceless part \tilde{a}_{ij} and the trace part a_{ii} ,

$$a_{ij} = \tilde{a}_{ij} + \frac{1}{D} a_{kk} \delta_{ij}. \quad (3.4)$$

Since this decomposition is compatible with the spacetime Lifshitz symmetries (2.2), one can restrict the symmetry group to be generated by a strictly smaller invariant subalgebra in the original algebra generated by a_{ij} . For example, setting the traceless part \tilde{a}_{ij} of the quadratic shift symmetry to zero reduces the number of independent generators from $(D+2)(D+1)/2$ to $D+2$, but it is still sufficient to prevent $\partial_i \phi \partial_i \phi$ from being an invariant under the smaller symmetry. This intriguing pattern extends to $P > 2$, leading to intricate hierarchies of polynomial shift symmetries whose coefficients $a_{i_1 \dots i_\ell}$ have been restricted by various invariant conditions. As another example, invariance under the traceless part has been studied in [65]. In the interest of simplicity, we concentrate in the rest of this chapter on the maximal case of polynomial shift symmetries with arbitrary unrestricted real coefficients $a_{i_1 \dots i_\ell}$.

The invariance of the action under each polynomial shift leads to a conserved Noether current. Each such current then implies a set of Ward identities on the correlation functions and the effective action. Take, for example, the case of $n = 2$ in (3.2): The currents for the infinitesimal shift by a general function $a(\mathbf{x})$ of the spatial coordinates x^i are collectively given by

$$\mathcal{J}_t = a(\mathbf{x}) \dot{\phi}, \quad \mathcal{J}_i = a(\mathbf{x}) \partial_i \partial^2 \phi - \partial_j a(\mathbf{x}) \partial_i \partial_j \phi + \partial_i \partial_j a(\mathbf{x}) \partial_j \phi - \partial_i \partial^2 a(\mathbf{x}) \phi, \quad (3.5)$$

and their conservation requires

$$\dot{\mathcal{J}}_t + \partial_i \mathcal{J}_i \equiv a(\mathbf{x}) \left\{ \ddot{\phi} + (\partial^2)^2 \phi \right\} - (\partial^2)^2 a(\mathbf{x}) \phi = 0. \quad (3.6)$$

The term in the curly brackets is zero on shell, and the current conservation thus reduces to the condition $(\partial^2)^2 a(\mathbf{x}) \phi = 0$, which is certainly satisfied by a polynomial of degree three,

$$a(\mathbf{x}) = a_{ijk} x^i x^j x^k + a_{ij} x^i x^j + a_i x^i + a. \quad (3.7)$$

Note that if we start instead with the equivalent form of the classical action

$$\tilde{S}_2 = \int dt d\mathbf{x} \left\{ \frac{1}{2} \dot{\phi}^2 - \frac{1}{2} (\partial_i \partial_i \phi)^2 \right\}, \quad (3.8)$$

the Noether currents will be related, as expected, by

$$\begin{aligned} \tilde{\mathcal{J}}_t &= \mathcal{J}_t, \\ \tilde{\mathcal{J}}_i &= a(\mathbf{x}) \partial_i \partial^2 \phi - \partial_i a(\mathbf{x}) \partial^2 \phi + \partial^2 a(\mathbf{x}) \partial_i \phi - \partial_i \partial^2 a(\mathbf{x}) \phi \\ &= \mathcal{J}_i + \partial_j [\partial_i a(\mathbf{x}) \partial_j \phi - \partial_j a(\mathbf{x}) \partial_i \phi]. \end{aligned} \quad (3.9)$$

From these conserved currents, one can formally define the charges

$$Q[a] = \int_{\Sigma} d\mathbf{x} \mathcal{J}_t. \quad (3.10)$$

However, for infinite spatial slices $\Sigma = \mathbf{R}^D$, such charges are all zero on the entire Hilbert space of states generated by the normalizable excitations of the fields ϕ . This behavior is quite analogous to the standard case of NG modes invariant under the constant shifts, and it simply indicates that the polynomial shift symmetry is being spontaneously broken by the vacuum.

3.1.2. Polynomial Shift Symmetries as Exact Symmetries

We have established a new infinite sequence of symmetries in scalar field theories, and have shown that they can protect the smallness of quantum mechanical corrections to their low-energy dispersion relations near the Gaussian fixed points. The symmetries are exact at the infrared Gaussian fixed point, and turning on interactions typically breaks them explicitly – as we have seen in the series of examples in §2. Yet, the polynomial shift symmetry at the Gaussian fixed point is useful for the interacting theory as well: It controls the interaction terms, allowing them to be naturally small, parametrized by the amount ε of the explicit polynomial symmetry breaking near the fixed point.

Generally, this explicit breaking by interactions breaks the polynomial shift symmetries of NG modes all the way to the constant shift, which remains mandated by the original form of the Goldstone theorem (guaranteeing the existence of gapless modes).¹ However,

¹Strictly speaking, moving away from the Gaussian fixed point by turning on self-interactions generally yields additional corrections to the constant shift symmetry, if the underlying symmetry group of the interacting theory is non-Abelian. Such non-Abelian corrections vanish at the Gaussian fixed point, and each NG component effectively becomes an Abelian field with its own constant shift symmetry. We will concentrate solely on the simplest Abelian case, with one Type A NG field ϕ and the symmetry group $U(1)$.

one can now turn the argument around, and ask the following question: Starting at a given Type A_n or B_{2n} fixed point, what are the lowest-dimension scalar composite operators that involve N fields ϕ and respect the polynomial shift symmetry of degree P exactly, up to a total derivative? Such operators can be added to the action, and for $N = 3, 4, \dots$ they represent self-interactions of the system, invariant under the polynomial shift of degree P . More generally, one can attempt to classify all independent composite operators invariant under the polynomial shift symmetry of degree P , organized in the order of their increasing dimensions.

These are the questions on which we focus in the rest of this chapter. In order to provide some answers, we will first translate this classification problem into a more precise mathematical language, and then we will develop techniques – largely based on abstract graph theory – that lead us to systematic answers. For some low values of the degree P of the polynomial symmetry and of the number N of fields involved, we can even find the most relevant invariants and prove their uniqueness.

3.2. Galileon Invariants

Consider a quantum field theory of a single scalar field $\phi(t, \mathbf{x})$ in D spatial dimensions and one time dimension. Consider the transformation of the field which is linear in spatial coordinates: $\delta\phi = a_i x^i + a_0$, where a_i and a_0 are arbitrary real coefficients. Other than the split between time and space and the exclusion of the time coordinate from the linear shift transformation, this is the same as the theory of the Galileon [60].

The goal is to find Lagrangian terms which are invariant (up to a total derivative) under this linear shift transformation. We will classify the Lagrangian terms by their numbers of fields N and derivatives 2Δ . Imposing spatial rotation invariance requires that spatial derivatives be contracted in pairs by the flat metric δ_{ij} . Thus Δ counts the number of contracted pairs of derivatives. It is easy to find Lagrangian terms which are exactly invariant (i.e., not just up to a total derivative): Let $\Delta \geq N$ and let at least two spatial derivatives act on every ϕ . For the linear shift case, all terms with at least twice as many derivatives as there are fields are equal to exact invariants, up to total derivatives (Theorem 4). However, it is possible for a term to have fewer derivatives than this and still be invariant up to a non-vanishing total derivative. For fixed N , the terms with the lowest Δ are more relevant in the sense of the renormalization group. Therefore, we will focus on invariant terms with the lowest number of derivatives, which we refer to as *minimal invariants*.

These minimal invariants have already been classified for the case of the linear shift. There is a unique (up to total derivatives and an overall constant prefactor) N -point minimal invariant, which contains $2(N - 1)$ derivatives (i.e., $\Delta = N - 1$). These are listed below up

to $N = 5$.

$$L_{1\text{-pt}} = \phi, \quad (3.11a)$$

$$L_{2\text{-pt}} = \partial_i \phi \partial_i \phi, \quad (3.11b)$$

$$L_{3\text{-pt}} = 3 \partial_i \phi \partial_j \phi \partial_i \partial_j \phi, \quad (3.11c)$$

$$L_{4\text{-pt}} = 12 \partial_i \phi \partial_i \partial_j \phi \partial_j \partial_k \phi \partial_k \phi + 4 \partial_i \phi \partial_j \phi \partial_k \phi \partial_i \partial_j \partial_k \phi, \quad (3.11d)$$

$$L_{5\text{-pt}} = 60 \partial_i \phi \partial_i \partial_j \phi \partial_j \partial_k \phi \partial_k \partial_\ell \phi \partial_\ell \phi + 60 \partial_i \phi \partial_i \partial_j \phi \partial_j \partial_k \phi \partial_\ell \phi \partial_k \phi \partial_\ell \phi + 5 \partial_i \phi \partial_j \phi \partial_k \phi \partial_\ell \phi \partial_i \partial_j \partial_k \partial_\ell \phi. \quad (3.11e)$$

These are not identical to the usual expressions (e.g., in [60]), but one can easily check that they are equivalent.

3.2.1. The Graphical Representation

We can represent the terms in (3.11) as formal linear combinations of graphs. In these graphs, ϕ is represented by a \bullet -vertex. An edge joining two vertices represents a pair of contracted derivatives, one derivative acting on each of the ϕ 's representing the endpoints of the edge. The graphical representations of the above terms are given below:

$$L_{1\text{-pt}} = \bullet, \quad (3.12a)$$

$$L_{2\text{-pt}} = \bullet \text{---} \bullet, \quad (3.12b)$$

$$L_{3\text{-pt}} = 3 \begin{array}{c} \bullet \\ / \\ \bullet \text{---} \bullet \end{array}, \quad (3.12c)$$

$$L_{4\text{-pt}} = 12 \begin{array}{c} \bullet \quad \bullet \\ | \quad | \\ \bullet \text{---} \bullet \end{array} + 4 \begin{array}{c} \bullet \quad \bullet \\ / \quad | \\ \bullet \text{---} \bullet \end{array}, \quad (3.12d)$$

$$L_{5\text{-pt}} = 60 \begin{array}{c} \bullet \quad \bullet \\ / \quad \backslash \\ \bullet \quad \bullet \end{array} + 60 \begin{array}{c} \bullet \quad \bullet \\ / \quad / \\ \bullet \text{---} \bullet \end{array} + 5 \begin{array}{c} \bullet \\ / \quad \backslash \\ \bullet \quad \bullet \end{array}. \quad (3.12e)$$

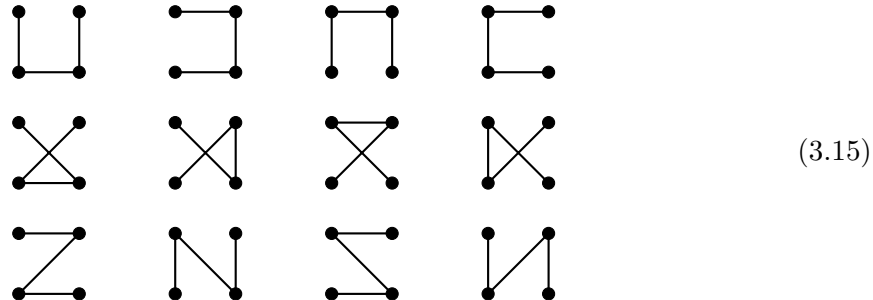
The structure of the graph (i.e., the connectivity of the vertices) is what distinguishes graphs; the placement of the vertices is immaterial. This reflects the fact that the order of the ϕ 's in the algebraic expressions is immaterial and the only thing that matters is which contracted pairs of derivatives act on which pairs of ϕ 's. Therefore, for example, the graphs below all represent the same algebraic expression.

$$\begin{array}{ccc} \begin{array}{c} \bullet \\ / \\ \bullet \text{---} \bullet \end{array} & \begin{array}{c} \bullet \\ \backslash \quad / \\ \bullet \quad \bullet \end{array} & \begin{array}{c} \bullet \\ \backslash \\ \bullet \text{---} \bullet \end{array} \end{array} \quad (3.13)$$

Similarly, the four graphs below represent the same algebraic expression.

$$\begin{array}{cccc} \begin{array}{c} \bullet \quad \bullet \\ / \quad | \\ \bullet \text{---} \bullet \end{array} & \begin{array}{c} \bullet \quad \bullet \\ \backslash \quad | \\ \bullet \text{---} \bullet \end{array} & \begin{array}{c} \bullet \quad \bullet \\ / \quad / \\ \bullet \text{---} \bullet \end{array} & \begin{array}{c} \bullet \quad \bullet \\ / \quad \backslash \\ \bullet \quad \bullet \end{array} \end{array} \quad (3.14)$$

A more nontrivial example is given by the following twelve graphs, which all represent the same algebraic expression.



The graphs in the second line above appear to have intersecting edges. However, since there is no \bullet -vertex at the would-be intersection, these edges do not actually intersect.

3.2.2. Galileon Invariants as Equal-Weight Sums of Trees

There are three times as many graphs in (3.15) as there are in (3.14). It so happens that the coefficient with which the first graph in (3.15) appears in $L_{4\text{-pt}}$ (3.12d) is also three times the coefficient with which the first graph in (3.14) appears in $L_{4\text{-pt}}$. This suggests that the coefficient with which a graph appears in a minimal term is precisely the number of graphs with the exact same structure (i.e., isomorphic), just with various vertices and edges permuted.

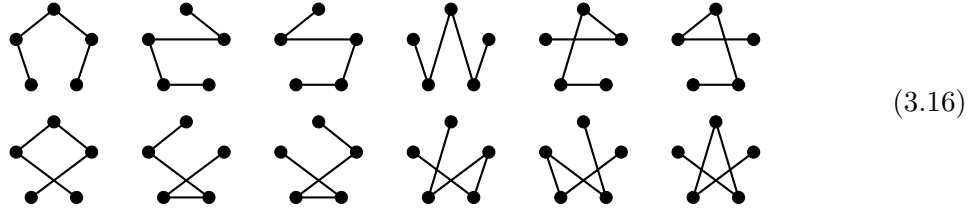
One simple way to state this is to actually label the vertices in the graphs. If the vertices were labeled, and thus distinguished from each other, then all of the graphs in each one of (3.13), (3.14) and (3.15) would actually be distinct graphs. Of course, this means that the corresponding algebraic expressions have ϕ 's similarly labeled, but this labeling is fiducial and may be removed afterwards. Note the simplicity that this labeled convention introduces: $L_{4\text{-pt}}$ is the sum of all of the graphs in (3.14) and (3.15) with unit coefficients.

The graphs in (3.14) and (3.15) have an elegant and unified interpretation in graph theory. These graphs are called *trees*. A tree is a graph which is connected (i.e., cannot be split into two or more separate graphs without cutting an edge), and contains no loops (edges joining a vertex to itself) or cycles (edges joining vertices in a closed cyclic manner). One can check that there are exactly 16 trees with four vertices and they are given by (3.14) and (3.15). Cayley's formula, a well-known result in graph theory, says that the number of trees with N vertices is N^{N-2} .

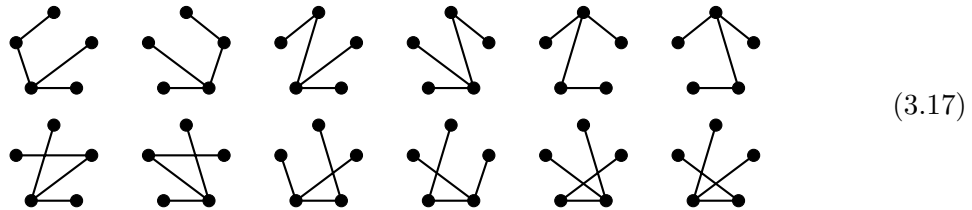
For $N = 3$, the $3^{3-2} = 3$ trees are in (3.13), and we indeed find that $L_{3\text{-pt}}$ is the sum of all three graphs with unit coefficients. The same can be said for $L_{2\text{-pt}}$ and $L_{1\text{-pt}}$. Therefore, the minimal terms for $N = 1, 2, 3$ and 4 are represented graphically as a sum of trees with unit coefficients (an equal-weight sum of trees). If this were to hold for the $N = 5$ case, it would strongly suggest that this may hold for all N .

There are $5^3 = 125$ trees for $N = 5$. They can be divided into three sets such that the trees in each set are isomorphic to one of the three graphs appearing in $L_{5\text{-pt}}$ (3.12e). There are 60 graphs which are isomorphic to the first graph appearing in $L_{5\text{-pt}}$; 12 of these are

listed below and the rest are given by the five rotations acting on each of these 12 graphs:



There are 60 graphs which are isomorphic to the second graph appearing in $L_{5\text{-pt}}$; 12 of these are listed below and the rest are given by their rotations:



Finally, there are five graphs which are isomorphic to the third graph appearing in $L_{5\text{-pt}}$, which are simply the five rotations acting on that graph. Therefore, $L_{5\text{-pt}}$ is indeed the sum with unit coefficients of all trees with five vertices!

Thus, we arrive at the main result of this section (proven in Appendix 3.B.3):

The unique minimal N -point linear shift-invariant Lagrangian term is represented graphically as a sum with unit coefficients of all labeled trees with N vertices.

3.3. Beyond the Galileons

Now, we extend the linear shift transformation to polynomials of higher degree. We will need to develop the graphical approach further in order to tackle this problem and numerous technicalities will arise. However, a rather elegant and beautiful description of these polynomial shift invariants will emerge.

Consider the problem of determining all possible terms in a Lagrangian that are invariant under the polynomial shift symmetry:

$$\phi(t, x^i) \rightarrow \phi(t, x^i) + \delta_P \phi, \quad \delta_P \phi = a_{i_1 \dots i_P} x^{i_1} \dots x^{i_P} + \dots + a_i x^i + a. \quad (3.18)$$

The a 's are arbitrary real coefficients that parametrize the symmetry transformation, and are symmetric in any pair of indices. $P = 0, 1, 2, \dots$ corresponds to constant shift, linear shift, quadratic shift, and so on. Obviously, if a term is invariant under a polynomial shift of order P , then it is also invariant under a polynomial shift of order P' with $0 \leq P' \leq P$.

We will call a term with N fields and 2Δ derivatives an (N, Δ) term. We are interested in interaction terms, for which $N \geq 3$. As previously mentioned, terms with the lowest possible value of Δ are of greatest interest. It is straightforward to write down invariant terms with $\Delta \geq \frac{1}{2}N(P+1)$ since, if each ϕ has more than P derivatives acting on it, then the term is exactly invariant. Are there any invariant terms with lower values of Δ ? If so, then these invariant terms will be more relevant than the exact invariants.

To be invariant, a term must transform into a total derivative under the polynomial shift symmetry. In other words, for a specific P and given (N, Δ) , we are searching for terms L such that

$$\delta_P L = \partial_i(L_i). \quad (3.19)$$

Here L is a linear combination of terms with N ϕ 's and 2Δ ∂ 's, and L_i is a linear combination of terms with $N - 1$ ϕ 's. Such L 's are called *P-invariants*.

How might we determine such invariant terms in general? For a given (N, Δ) , the most brute-force method for determining invariant terms can be described as follows. First, write down all possible terms in the Lagrangian with a given (N, Δ) and ensure that they are independent up to integration by parts. Next, take the variation of all these terms under the polynomial shift. There may exist linear combinations of these variations which are equal to a total derivative, which we call *total derivative relations*. If we use these total derivative relations to maximally reduce the number of variation terms, then the required P -invariants form the kernel of the map from the independent Lagrangian terms to the independent variation terms (Corollary 6). Let us consider some examples of this brute-force procedure in action.

3.3.1. Brute-force Examples

$$(P, N, \Delta) = (1, 3, 2)$$

In this case, a general Lagrangian is made up of two independent terms, after integrating by parts, given by

$$L_1 = \partial_i \phi \partial_j \phi \partial_i \partial_j \phi, \quad L_2 = \phi \partial_i \partial_j \phi \partial_i \partial_j \phi.$$

The variation under the linear shift symmetry (for $P = 1$) of these terms is given by

$$\delta_1(L_1) = 2L_a^\times, \quad \delta_1(L_2) = L_b^\times,$$

where $L_a^\times = a_i \partial_j \phi \partial_i \partial_j \phi$ and $L_b^\times = (a_k x^k + a) \partial_i \partial_j \phi \partial_i \partial_j \phi$. There is only one total derivative that can be formed from these terms, namely

$$\partial_i(a_i \partial_j \phi \partial_j \phi) = 2L_a^\times.$$

Therefore, there is a single invariant term for $(P, N, \Delta) = (1, 3, 2)$, given by

$$L_1 = \partial_i \phi \partial_j \phi \partial_i \partial_j \phi.$$

$$(P, N, \Delta) = (3, 3, 4)$$

In this case, a general Lagrangian is made up of four independent terms, after integrating by parts, given by

$$\begin{aligned} L_1 &= \partial_i \partial_j \phi \partial_k \partial_l \phi \partial_i \partial_j \partial_k \partial_l \phi, & L_2 &= \partial_i \partial_j \phi \partial_i \partial_k \partial_l \phi \partial_j \partial_k \partial_l \phi, \\ L_3 &= \partial_i \phi \partial_j \partial_k \partial_l \phi \partial_i \partial_j \partial_k \partial_l \phi, & L_4 &= \phi \partial_i \partial_j \partial_k \partial_l \phi \partial_i \partial_j \partial_k \partial_l \phi. \end{aligned}$$

The variation under the cubic shift symmetry (for $P = 3$) of these terms is given by

$$\begin{aligned}\delta_3(L_1) &= 2L_a^\times, & \delta_3(L_2) &= L_b^\times + 2L_c^\times, \\ \delta_3(L_3) &= L_d^\times + L_e^\times, & \delta_3(L_4) &= L_f^\times.\end{aligned}$$

where

$$\begin{aligned}L_a^\times &= (6a_{ijm}x^m + 2a_{ij})\partial_k\partial_l\phi\partial_i\partial_j\partial_k\partial_l\phi \\ L_b^\times &= (6a_{ijm}x^m + 2a_{ij})\partial_i\partial_k\partial_l\phi\partial_j\partial_k\partial_l\phi \\ L_c^\times &= 6a_{ikl}\partial_i\partial_j\phi\partial_j\partial_k\partial_l\phi \\ L_d^\times &= (3a_{imn}x^m x^n + 2a_{im}x^m + a_i)\partial_i\phi\partial_j\partial_k\partial_l\phi\partial_i\partial_j\partial_k\partial_l\phi \\ L_e^\times &= 6a_{jkl}\partial_i\phi\partial_i\partial_j\partial_k\partial_l\phi \\ L_f^\times &= (a_{mnp}x^m x^n x^p + a_{mn}x^m x^n + a_m x^m + a)\partial_i\partial_j\partial_k\partial_l\phi\partial_i\partial_j\partial_k\partial_l\phi.\end{aligned}$$

There are three independent total derivatives that can be formed out of these:

$$\begin{aligned}\partial_i[2(6a_{ijm}x^m + 2a_{ij})\partial_k\partial_l\phi\partial_j\partial_k\partial_l\phi - 6a_{ijj}\partial_k\partial_l\phi\partial_k\partial_l\phi] &= 2(L_a^\times + L_b^\times), \\ \partial_i[6a_{ijk}\partial_j\partial_l\phi\partial_k\partial_l\phi] &= 2L_c^\times, \\ \partial_i[6a_{ijk}\partial_j\partial_k\partial_l\phi\partial_l\phi] &= L_c^\times + L_e^\times.\end{aligned}$$

It is a non-trivial exercise to find and verify this, and a more systematic way of finding the total derivative relations will be introduced later.

Applying these relations, one finds a single invariant for $(P, N, \Delta) = (3, 3, 4)$:

$$L_1 + 2L_2 = \partial_i\partial_j\phi\partial_k\partial_l\phi\partial_i\partial_j\partial_k\partial_l\phi + 2\partial_i\partial_j\phi\partial_i\partial_k\partial_l\phi\partial_j\partial_k\partial_l\phi.$$

Note that $\delta_3(L_1 + 2L_2) = 2(L_a^\times + L_b^\times) + 2(2L_c^\times)$, which is a total derivative.

3.3.2. Introduction to the Graphical Representation

It is clear that even for these simple examples, the calculations quickly become unwieldy, and it becomes increasingly difficult to classify all of the total derivative relations. At this point we will rewrite these results in a graphical notation which will make it easier to keep track of the contractions of indices in the partial derivatives. Full details about this graphical approach can be found in Appendix 3.B, but we will summarize them here. In addition to the \bullet -vertex and edges we introduced in §3.2, we represent $\delta_P\phi$ by a \otimes (a \times -vertex). Note that there are at most P edges incident to a \times -vertex since $P+1$ derivatives acting on $\delta_P\phi$ yields zero, whereas an arbitrary number of edges can be incident to a \bullet -vertex. Moreover, we introduce another vertex, called a \star -vertex, which will be used to represent terms that are total derivatives. We require that a \star -vertex always be incident to exactly one edge, and that this edge be incident to a \bullet -vertex or \times -vertex. This edge represents a derivative acting on the entire term as a whole, and the index of that derivative is contracted with the index of another derivative acting on the ϕ or $\delta_P\phi$ of the \bullet - or \times -vertex, respectively, to which the \star -vertex is adjacent. Therefore, directly from the definition, any graph with a \star -vertex represents a total derivative term. The expansion of this derivative using the Leibniz rule is graphically represented by the summation of the graphs formed by removing

the \star -vertex and attaching the edge that was incident to the \star -vertex to each remaining vertex. This operation is denoted by the *derivative map* ρ . The symbols $N(\bullet)$, $N(\times)$ and $N(\star)$ represent the numbers of each type of vertex. Note that $N = N(\bullet) + N(\times)$ does not include $N(\star)$ since \star -vertices represent neither ϕ nor $\delta_P\phi$.

We define three special types of graphs: A *plain-graph* is a graph in which all vertices are \bullet -vertices. A \times -*graph* is a plain-graph with one \bullet -vertex replaced with a \times -vertex. A \star -*graph* is a graph with one \times -vertex and at least one \star -vertex.

Note that the variation δ_P of a plain-graph under the polynomial shift symmetry is given by summing over all graphs that have exactly one \bullet -vertex in the original graph replaced with a \times -vertex. To illustrate the graphical approach, we rewrite the examples from sections 3.3.1 and 3.3.1 using this new graphical notation. Since the algebraic expressions have unlabeled ϕ 's, the graphs in this section will be unlabeled.

$$(P, N, \Delta) = (1, 3, 2)$$

The two independent terms are written in the graphical notation as

$$L_1 = \begin{array}{c} \bullet \\ | \\ \bullet \text{---} \bullet \end{array} \qquad L_2 = \begin{array}{c} \bullet \\ \text{---} \bullet \\ \text{---} \bullet \end{array}$$

The variation under the linear shift symmetry (for $P = 1$) is given by

$$\delta_1 \left(\begin{array}{c} \bullet \\ | \\ \bullet \text{---} \bullet \end{array} \right) = 2 \begin{array}{c} \otimes \\ | \\ \bullet \text{---} \bullet \end{array} \qquad \delta_1 \left(\begin{array}{c} \bullet \\ \text{---} \bullet \\ \text{---} \bullet \end{array} \right) = \begin{array}{c} \otimes \\ \text{---} \bullet \\ \text{---} \bullet \end{array}$$

The only independent total derivative that can be formed out of these terms is

$$\rho \left(\begin{array}{c} \otimes \text{---} \star \\ \text{---} \bullet \end{array} \right) = 2 \begin{array}{c} \otimes \\ | \\ \bullet \text{---} \bullet \end{array}$$

As before, there is a single invariant for $(P, N, \Delta) = (1, 3, 2)$ given by L_1 . In this case, the graphical version of (3.19) is given by

$$\delta_1 \left(\begin{array}{c} \bullet \\ | \\ \bullet \text{---} \bullet \end{array} \right) = 2 \begin{array}{c} \otimes \\ | \\ \bullet \text{---} \bullet \end{array} = \rho \left(\begin{array}{c} \otimes \text{---} \star \\ \text{---} \bullet \end{array} \right)$$

$$(P, N, \Delta) = (3, 3, 4)$$

The four independent terms are written in the graphical notation as

$$L_1 = \begin{array}{c} \bullet \\ \text{---} \bullet \\ \text{---} \bullet \end{array} \qquad L_2 = \begin{array}{c} \bullet \\ \text{---} \bullet \\ \text{---} \bullet \end{array} \qquad L_3 = \begin{array}{c} \bullet \\ | \\ \bullet \text{---} \bullet \end{array} \qquad L_4 = \begin{array}{c} \bullet \\ \text{---} \bullet \\ \text{---} \bullet \end{array}$$

The variation under the cubic shift symmetry (for $P = 3$) is given by

$$\begin{aligned} \delta_3 \left(\begin{array}{c} \bullet \\ | \\ \bullet \\ \text{---} \\ \bullet \end{array} \right) &= 2 \begin{array}{c} \otimes \\ | \\ \bullet \\ \text{---} \\ \bullet \end{array} \\ \delta_3 \left(\begin{array}{c} \bullet \\ / \backslash \\ \bullet \text{---} \bullet \\ \text{---} \\ \bullet \end{array} \right) &= \begin{array}{c} \otimes \\ / \backslash \\ \bullet \text{---} \bullet \\ \text{---} \\ \bullet \end{array} + 2 \begin{array}{c} \otimes \\ / \backslash \\ \bullet \text{---} \bullet \\ \text{---} \\ \bullet \end{array} \\ \delta_3 \left(\begin{array}{c} \bullet \\ | \\ \bullet \\ \text{---} \\ \bullet \end{array} \right) &= \begin{array}{c} \otimes \\ | \\ \bullet \\ \text{---} \\ \bullet \end{array} + \begin{array}{c} \otimes \\ | \\ \bullet \\ \text{---} \\ \bullet \end{array} \\ \delta_3 \left(\begin{array}{c} \bullet \\ \text{---} \\ \bullet \end{array} \right) &= \begin{array}{c} \otimes \\ \text{---} \\ \bullet \end{array} \end{aligned}$$

The independent total derivatives that can be formed out of these terms are

$$\begin{aligned} \rho \left(2 \begin{array}{c} \otimes \star \\ | \\ \bullet \text{---} \bullet \end{array} - \begin{array}{c} \otimes \star \\ \curvearrowright \\ \bullet \text{---} \bullet \end{array} \right) &= 2 \begin{array}{c} \otimes \\ | \\ \bullet \\ \text{---} \\ \bullet \end{array} + 2 \begin{array}{c} \otimes \\ / \backslash \\ \bullet \text{---} \bullet \\ \text{---} \\ \bullet \end{array} \\ \rho \left(\begin{array}{c} \otimes \star \\ / \backslash \\ \bullet \text{---} \bullet \end{array} \right) &= 2 \begin{array}{c} \otimes \\ / \backslash \\ \bullet \text{---} \bullet \\ \text{---} \\ \bullet \end{array} \\ \rho \left(\begin{array}{c} \otimes \star \\ | \\ \bullet \text{---} \bullet \end{array} \right) &= \begin{array}{c} \otimes \\ / \backslash \\ \bullet \text{---} \bullet \\ \text{---} \\ \bullet \end{array} + \begin{array}{c} \otimes \\ | \\ \bullet \\ \text{---} \\ \bullet \end{array} \end{aligned}$$

Once again, there is a single invariant for $(P, N, \Delta) = (3, 4)$ given by $L_1 + 2L_2$. The graphical version of (3.19) is given by

$$\begin{aligned} \delta_3 \left(\begin{array}{c} \bullet \\ | \\ \bullet \\ \text{---} \\ \bullet \end{array} + 2 \begin{array}{c} \bullet \\ / \backslash \\ \bullet \text{---} \bullet \\ \text{---} \\ \bullet \end{array} \right) &= 2 \begin{array}{c} \otimes \\ | \\ \bullet \\ \text{---} \\ \bullet \end{array} + 2 \begin{array}{c} \otimes \\ / \backslash \\ \bullet \text{---} \bullet \\ \text{---} \\ \bullet \end{array} + 4 \begin{array}{c} \otimes \\ / \backslash \\ \bullet \text{---} \bullet \\ \text{---} \\ \bullet \end{array} \\ &= \rho \left(2 \begin{array}{c} \otimes \star \\ | \\ \bullet \text{---} \bullet \end{array} - \begin{array}{c} \otimes \star \\ \curvearrowright \\ \bullet \text{---} \bullet \end{array} + 2 \begin{array}{c} \otimes \star \\ / \backslash \\ \bullet \text{---} \bullet \end{array} \right) \end{aligned} \quad (3.20)$$

So far all we have done is rewrite our results in a new notation. But the graphical notation is more than just a succinct visual way of expressing the invariant terms. The following section illustrates the virtue of this approach.

3.3.3. New Invariants via the Graphical Approach

As shown in Appendix 3.B, the graphical approach allows us to prove many general theorems. In particular, we have the following useful outcomes:

1. Without loss of generality, we can limit our search for invariants to graphs with very specific properties (Appendix 3.B.2).
2. There is a simple procedure for obtaining all the independent total derivative relations between the variation terms for each P , N and Δ (Theorem 1).
3. The graphical method allows a complete classification of 1-invariants (Theorem 4).
4. The graphical method allows many higher P -invariant terms to be constructed from lower P invariants (Appendix 3.B.4).

We will expound upon the above points by presenting explicit examples. These examples are generalizable and their invariance is proven in Appendix 3.B. However, the reader can also check by brute force that the terms we present are indeed invariant. We will now summarize points 1 and 2 and will return to point 4 in §3.3.4. Point 3 was discussed in §3.2 with technical details in Appendix 3.B.3.

When building invariants, we need only consider loopless plain-graphs (Proposition 2), since a loop represents $\partial_i \partial_i$ acting on a single ϕ and one can always integrate by parts to move one of the ∂_i 's to act on the remaining ϕ 's. We can also restrict to plain-graphs with vertices of degree no less than $\frac{1}{2}(P+1)$ (Proposition 7). This represents a significant simplification from the previous procedure (§3.3.2). For instance, in §3.3.2, the graphs L_3 and L_4 are immediately discarded.

Taking the variation of these terms yields \times -graphs and we need to determine the total derivative relations between them. Since all plain-graphs we are considering are loopless, any \times -graphs involved in these total derivative relations are also loopless. The total derivative relations that we need to consider can be obtained with the use of graphs called *Medusas* (Definition 10). A Medusa is a loopless \star -graph with all of its \star -vertices adjacent to the \times -vertex and such that the degree of the \times -vertex is given by:

$$\text{deg}(\times) = P + 1 - N(\star), \quad (3.21)$$

where, again, $N(\star)$ is the number of \star -vertices. Note that because $\text{deg}(\times) \geq N(\star)$ for a Medusa, (3.21) implies that $N(\star) \leq \frac{1}{2}(P+1) \leq \text{deg}(\times)$ for any Medusa. Furthermore, we need only consider Medusas with \times -vertex and \bullet -vertices of degree no less than $\frac{1}{2}(P+1)$ (Proposition 8). From each of these Medusas, we obtain a total derivative relation, containing only loopless \times -graphs, by applying the map ρ and then omitting all looped graphs (Proposition 4). This map is denoted as $\rho^{(0)}$ in Definition 13. In §3.3.3, we will give an introduction to the construction of such total derivative relations from Medusas. Moreover, this procedure captures all relevant total derivative relations (Theorem 1). Appendix 3.B.2 provides a systematic treatment of Medusas.

In general, for given N and P , we call an invariant consisting of graphs containing the lowest possible value of Δ a *minimal* invariant (Definition 16). Minimal invariants are of particular interest in a QFT, since they are the most relevant N -point interactions. In §3.3.3 and §3.3.3 we apply the graphical approach to classify all minimal invariants for $N = 4$ and $P = 2, 3$.

The Minimal Invariant: $(P, N, \Delta) = (2, 4, 5)$

As our first example, let us find the minimal 2-invariant for $N = 4$. For $P = 2$, any Medusa must have $N(\star) \leq \frac{1}{2}(P+1) = \frac{3}{2}$, and thus there is exactly one \star -vertex in a $P = 2$ Medusa. Furthermore, we need only consider Medusas in which each vertex has degree at least 2, since $\frac{1}{2}(P+1) = \frac{3}{2}$. Therefore, the counting implies that we need only consider $P = 2$ Medusas with $\Delta \geq N + 1$. In particular, when $N = 4$, the minimal Δ is 5 (representing terms with 10 derivatives). In the following we show that there is exactly one 2-invariant

with $\Delta = 5$. The relevant Medusas are:

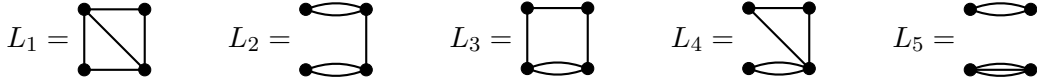


The resulting loopless total derivative relations are:

$$\begin{aligned} \rho^{(0)}(M_1) &= 2 \begin{array}{c} \text{circle with } x \\ \diagup \\ \text{square} \end{array} + \begin{array}{c} \text{circle with } x \\ \text{square} \end{array} \equiv 2L_a^\times + L_e^\times \\ \rho^{(0)}(M_2) &= \begin{array}{c} \text{circle with } x \\ \text{square} \end{array} + \begin{array}{c} \text{circle with } x \\ \text{square} \end{array} + \begin{array}{c} \text{circle with } x \\ \text{square} \end{array} \equiv L_b^\times + L_c^\times + L_d^\times \end{aligned} \quad (3.22)$$

Note that, when acting on these $P = 2$ Medusas, ρ and $\rho^{(0)}$ are in fact the same.

On the other hand, the invariants must be constructed out of plain-graphs containing vertices of degree no less than $\frac{1}{2}(P+1) = \frac{3}{2}$. The only possibilities are:



The invariant cannot be constructed out of L_5 since $\delta_2(L_5)$ is absent from the total derivative relations (3.22). Hence, we need only consider the variations of L_1, L_2, L_3 and L_4 .

We can now determine the 2-invariants. The total derivative relations allow us to identify $L_d^\times \sim -L_b^\times - L_c^\times$ and $L_e^\times \sim -2L_a^\times$. Up to total derivatives,

$$\delta_2 \begin{pmatrix} L_1 \\ L_2 \\ L_3 \\ L_4 \end{pmatrix} = \begin{pmatrix} 2 & 0 & 0 & 0 & 0 \\ 0 & 2 & 0 & 0 & 0 \\ 0 & 0 & 2 & 0 & 0 \\ 0 & 0 & 0 & 2 & 1 \end{pmatrix} \begin{pmatrix} L_a^\times \\ L_b^\times \\ L_c^\times \\ L_d^\times \\ L_e^\times \end{pmatrix} \sim \begin{pmatrix} 2 & 0 & 0 \\ 0 & 2 & 0 \\ 0 & 0 & 2 \\ -2 & -1 & -1 \end{pmatrix} \begin{pmatrix} L_a^\times \\ L_b^\times \\ L_c^\times \end{pmatrix} \quad (3.23)$$

The invariants form the nullspace of the transpose of the final 4×3 matrix in (3.23). The nullspace is spanned by $(1, 1, 1, 1)$. Therefore, there is one 2-invariant given by the linear combination $L_1 + L_2 + L_3 + L_4$, i.e.,

$$\begin{array}{c} \text{square with diagonal} \\ + \\ \text{square with top/bottom edges} \\ + \\ \text{square with left/right edges} \\ + \\ \text{square with diagonal and top/bottom edges} \end{array} \quad (3.24)$$

Therefore, (3.24) gives the only independent minimal 2-invariant for $N = 4$.

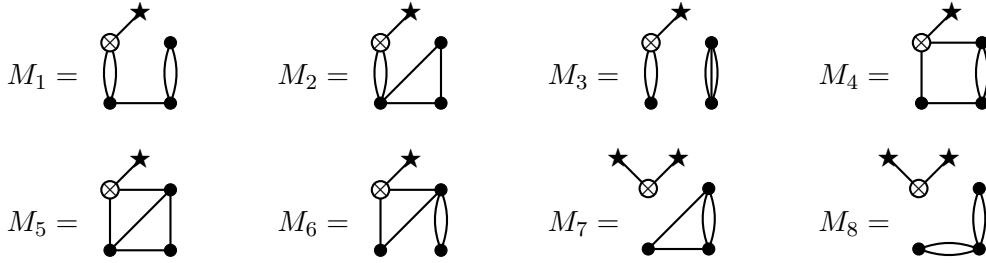
The Minimal Invariant: $(P, N, \Delta) = (3, 4, 6)$

Next, let us consider $P = 3, N = 4$, for which each vertex degree must be at least $\frac{1}{2}(P+1) = 2$. Again we would like to find the minimal invariant in this case. By counting alone, it is possible to write down Medusas with $\Delta = 5$. In fact, a 3-invariant with $N = 4$ and $\Delta = 5$ would also be 2-invariant. The only possible 2-invariant with $(N, \Delta) = (4, 5)$ is (3.24).

However, this is not a 3-invariant because it is impossible for some graphs contained in it to appear in a 3-invariant. For example, by replacing a degree-2 vertex in L_2 in (3.24) with a \times -vertex, a \times -graph Γ^\times is produced; Γ^\times and the only $P = 3$ Medusa M that generates Γ^\times are given below:



But M contains a \bullet -vertex of degree lower than 2, and therefore (3.24) cannot be 3-invariant. This sets a lower bound for Δ : $\Delta \geq 6$. For $\Delta = 6$, the Medusas are:

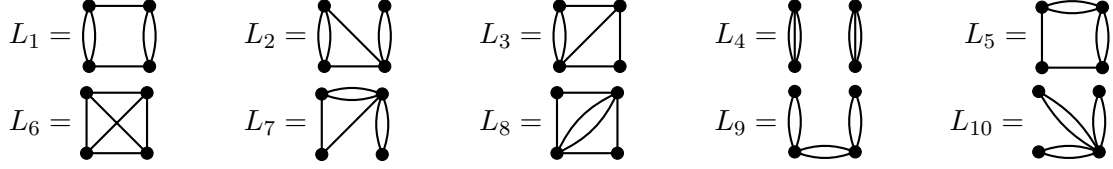


These give the following total derivative relations:

$$\begin{aligned}
 \rho^{(0)}(M_1) &= \text{[Diagram 1]} + \text{[Diagram 2]} + \text{[Diagram 3]} \equiv L_a^\times + L_b^\times + L_c^\times \\
 \rho^{(0)}(M_2) &= \text{[Diagram 4]} + 2 \text{[Diagram 5]} \equiv L_d^\times + 2L_e^\times \\
 \rho^{(0)}(M_3) &= \text{[Diagram 6]} + 2 \text{[Diagram 7]} \equiv L_f^\times + 2L_g^\times \\
 \rho^{(0)}(M_4) &= \text{[Diagram 8]} + \text{[Diagram 9]} + \text{[Diagram 10]} \equiv L_a^\times + L_h^\times + L_i^\times \\
 \rho^{(0)}(M_5) &= 2 \text{[Diagram 11]} + \text{[Diagram 12]} \equiv 2L_e^\times + L_j^\times \\
 \rho^{(0)}(M_6) &= \text{[Diagram 13]} + \text{[Diagram 14]} + \text{[Diagram 15]} \equiv L_b^\times + L_k^\times + L_h^\times \\
 \rho^{(0)}(M_7) &= 2 \text{[Diagram 16]} + \text{[Diagram 17]} + 4 \text{[Diagram 18]} + 2 \text{[Diagram 19]} \equiv 2L_\ell^\times + L_m^\times + 4L_n^\times + 2L_o^\times \\
 \rho^{(0)}(M_8) &= 2 \text{[Diagram 20]} + \text{[Diagram 21]} + 2 \text{[Diagram 22]} + 4 \text{[Diagram 23]} \equiv 2L_p^\times + L_q^\times + 2L_r^\times + 4L_s^\times
 \end{aligned}$$

Then the invariants must be made up of plain-graphs whose variations are contained in the

total derivative relations above. In other words, the invariants are made from:



We can now determine the 3-invariants. After imposing the total derivative relations,

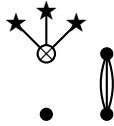
$$\delta_3 \begin{pmatrix} L_1 \\ L_2 \\ L_3 \\ L_4 \\ L_5 \\ L_6 \\ L_7 \\ L_8 \\ L_9 \\ L_{10} \end{pmatrix} \sim \begin{pmatrix} 4 & 0 & 0 & 0 & 0 & 0 & 0 & 0 & 0 & 0 & 0 \\ 0 & 2 & 0 & 0 & 0 & -2 & -4 & -2 & 0 & 0 & 0 \\ 0 & 0 & 1 & 0 & 1 & 0 & 1 & 0 & 0 & 0 & 0 \\ 0 & 0 & 0 & 4 & 0 & 0 & 0 & 0 & 0 & 0 & 0 \\ -2 & 0 & 0 & 0 & -2 & 0 & 0 & 0 & 0 & 1 & 0 \\ 0 & 0 & -8 & 0 & 0 & 0 & 0 & 0 & 0 & 0 & 0 \\ 0 & -1 & 0 & 0 & -1 & 1 & 0 & 0 & 0 & 0 & 1 \\ 0 & 0 & 0 & 0 & 0 & 0 & 0 & 2 & 0 & 0 & 0 \\ 0 & 0 & 0 & 0 & 0 & 0 & 0 & 0 & 2 & 0 & 0 \\ 0 & 0 & 0 & 0 & 0 & 0 & 0 & 0 & -6 & -6 & -12 \end{pmatrix} \begin{pmatrix} L_a^\times \\ L_b^\times \\ L_e^\times \\ L_f^\times \\ L_h^\times \\ L_l^\times \\ L_n^\times \\ L_o^\times \\ L_p^\times \\ L_r^\times \\ L_s^\times \end{pmatrix}$$

The nullspace of the transpose of this matrix is spanned by $(3, 6, 24, 0, 6, 3, 12, 6, 3, 1)$, giving the only invariant linear combination,

$$\begin{aligned} & 3 \begin{matrix} \bullet & \bullet \\ | & | \\ \bullet & \bullet \end{matrix} + 6 \begin{matrix} \bullet & \bullet \\ | & | \\ \bullet & \bullet \\ \diagdown & / \end{matrix} + 24 \begin{matrix} \bullet & \bullet \\ | & | \\ \bullet & \bullet \\ \diagup & \diagdown \end{matrix} \\ & + 6 \begin{matrix} \bullet & \bullet \\ | & | \\ \bullet & \bullet \\ \diagup & \diagdown \end{matrix} + 3 \begin{matrix} \bullet & \bullet \\ | & | \\ \bullet & \bullet \\ \diagdown & / \end{matrix} + 12 \begin{matrix} \bullet & \bullet \\ | & | \\ \bullet & \bullet \\ \diagup & \diagdown \end{matrix} \\ & + 6 \begin{matrix} \bullet & \bullet \\ | & | \\ \bullet & \bullet \\ \diagdown & / \end{matrix} + 3 \begin{matrix} \bullet & \bullet \\ | & | \\ \bullet & \bullet \\ \diagup & \diagdown \end{matrix} + \begin{matrix} \bullet & \bullet \\ | & | \\ \bullet & \bullet \\ \diagup & \diagdown \end{matrix} \end{aligned} \tag{3.25}$$

This gives the only independent minimal 3-invariant for $N = 4$.

Note that L_4 does not appear in the invariant. Indeed, it can be discarded immediately, since the unique Medusa associated with L_4 is



This Medusa has an empty vertex, which violates the lower bound on vertex degree.

Medusas and Total Derivative Relations

We have seen that Medusas play a central role in the search for P -invariants. It is thus worthwhile to discuss the key features of Medusas and to demonstrate how a total derivative relation consisting of loopless \times -graphs is constructed from a Medusa. Given any Medusa, $\rho^{(0)}(M)$ is in fact a total derivative relation, as can be seen from the following construction.

For fixed P and N , consider a Medusa M that contains $N(\star)$ \star -vertices. Then, by definition, it has a \times -vertex of degree $\deg(\times) = P + 1 - N(\star)$. Since the maximal degree of a \times -vertex is P , graphs in $\rho(M)$ contain at most $N(\star) - 1$ loops. Form a \star -graph $\Gamma^{(\ell)}$ from M by deleting $\ell \leq N(\star) - 1$ \star -vertices in M and then adding ℓ loops to the \times -vertex. By this definition, $M = \Gamma^{(0)}$. In the algebraic expression represented by $\Gamma^{(\ell)}$, the $N(\star) - \ell$ \star -vertices stand for $N(\star) - \ell$ partial derivatives acting on the whole term. Distributing $N(\star) - \ell - 1$ ∂ 's over all ϕ 's in this algebraic expression will result in a linear combination of total derivative terms. In the graphical representation, this is equivalent to acting ρ on $\Gamma^{(\ell)}$ but keeping fixed exactly one \star -vertex and its incident edge. Setting to zero all coefficients of graphs in the resulting linear combination, except for the ones containing exactly ℓ loops, generates a linear combination $L^{(\ell)}$ of \star -graphs, each containing exactly one \star -vertex. By construction,

$$\rho^{(0)}(M) = \rho \left(\sum_{\alpha=0}^{N(\star)-1} (-1)^\alpha L^{(\alpha)} \right). \tag{3.26}$$

The algebraic form of the RHS of (3.26) is explicitly a total derivative relation. For a rigorous treatment of the above discussion, refer to Proposition 4 in Appendix 3.B.2.

As a simple example, we consider the Medusa M_7 referred to in §3.3.3. We have

$$M_7 = \begin{array}{c} \star \\ \diagup \quad \diagdown \\ \times \\ \diagdown \quad \diagup \\ \bullet \quad \bullet \\ \diagup \quad \diagdown \\ \bullet \quad \bullet \end{array} \Rightarrow \rho^{(0)}(M_7) = \rho \left(\begin{array}{c} \star \\ \diagup \quad \diagdown \\ \times \\ \diagdown \quad \diagup \\ \bullet \quad \bullet \\ \diagup \quad \diagdown \\ \bullet \quad \bullet \end{array} + 2 \begin{array}{c} \star \\ \diagup \quad \diagdown \\ \times \\ \diagdown \quad \diagup \\ \bullet \quad \bullet \\ \diagup \quad \diagdown \\ \bullet \quad \bullet \end{array} - \begin{array}{c} \star \\ \diagup \quad \diagdown \\ \times \\ \diagdown \quad \diagup \\ \bullet \quad \bullet \\ \diagup \quad \diagdown \\ \bullet \quad \bullet \end{array} \right)$$

For a second example, we consider $(P, N, \Delta) = (5, 3, 6)$ and the Medusa

$$M = \begin{array}{c} \star \\ \diagup \quad \diagdown \\ \times \\ \diagdown \quad \diagup \\ \star \\ \diagup \quad \diagdown \\ \bullet \quad \bullet \\ \diagup \quad \diagdown \\ \bullet \quad \bullet \end{array}$$

By (3.26), we obtain

$$\rho^{(0)}(M) = \rho \left(2 \begin{array}{c} \star \\ \diagup \quad \diagdown \\ \times \\ \diagdown \quad \diagup \\ \bullet \quad \bullet \\ \diagup \quad \diagdown \\ \bullet \quad \bullet \end{array} + 2 \begin{array}{c} \star \\ \diagup \quad \diagdown \\ \times \\ \diagdown \quad \diagup \\ \bullet \quad \bullet \\ \diagup \quad \diagdown \\ \bullet \quad \bullet \end{array} - 2 \begin{array}{c} \star \\ \diagup \quad \diagdown \\ \times \\ \diagdown \quad \diagup \\ \bullet \quad \bullet \\ \diagup \quad \diagdown \\ \bullet \quad \bullet \end{array} + \begin{array}{c} \star \\ \diagup \quad \diagdown \\ \times \\ \diagdown \quad \diagup \\ \bullet \quad \bullet \\ \diagup \quad \diagdown \\ \bullet \quad \bullet \end{array} \right).$$

This Medusa is involved in a 5-invariant that we will construct in §3.3.4.

3.3.4. Superposition of Graphs

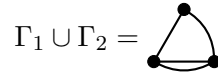
In §3.2, we discovered an intriguing construction of the minimal 1-invariant for given N , which is a sum with equal coefficients of all possible trees with N vertices. A close study

of the P -invariants with $P > 1$ in §3.3 also reveals an elegant structure in these invariants: They can all be decomposed as a *superposition* of equal-weight tree summations and *exact* invariants. Recall that an exact invariant is a linear combination that is invariant exactly, instead of up to a total derivative. In the graphical representation, a linear combination of graphs is an exact P_E -invariant if and only if all vertices are of degree larger than P_E (Corollary 4). Each graph in an exact invariant is itself exactly invariant.

Next we illustrate “the superposition of linear combinations” by explicit examples. When appropriate, we will consider labeled graphs and only remove the labels at the end. Consider two labeled graphs,



The superposition of Γ_1 and Γ_2 is defined to be the graph formed by taking all edges in Γ_2 and adding them to Γ_1 , i.e.,



The superposition of two linear combinations, $L_A = \sum_{i=1}^{k_A} a_i \Gamma_i^A$ and $L_B = \sum_{i=1}^{k_B} b_i \Gamma_i^B$, of plain graphs Γ_i^A, Γ_j^B with the same N , is defined as

$$L_A \cup L_B \equiv \sum_{i=1}^{k_A} \sum_{j=1}^{k_B} a_i b_j \Gamma_i^A \cup \Gamma_j^B.$$

In the following we present numerous examples of invariants constructed by superposing equal-weight tree summations and exact invariants for various P 's. In fact, Theorem 7 of Appendix 3.B.4 states:

For fixed N , the superposition of an exact P_E -invariant with the superposition of Q minimal loopless 1-invariants results in a P -invariant, provided $P_E + 2Q \geq P$.²

We conjecture that the above result captures all P -invariants, up to total derivatives. Since we have classified all exact invariants and all 1-invariants (Theorem 4), it is straightforward to construct the P -invariants in the above statement for any specific case. We now proceed to construct the minimal P -invariants for some important cases.

Quadratic Shift ($P=2$)

$N = 3$ Case: A 2-invariant can be constructed by superposing an equal-weight tree summation with an exact 0-invariant. In the labeled representation, all possible trees for $N = 3$ are given by (3.13),

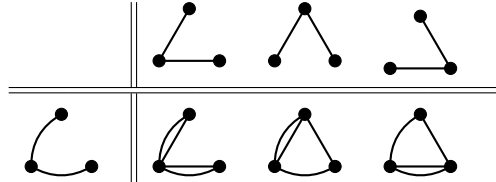


²Note that this theorem also applies when $P_E < 0$, where we take an exact P_E -invariant for $P_E < 0$ to mean any linear combination of plain-graphs. In particular, the plain-graph consisting only of empty vertices is a P_E -invariant for any $P_E < 0$, and superposing this graph on any other is equivalent to not superposing anything at all.

The sum of all three $N = 3$ trees with unit coefficients gives a 1-invariant, $L_{3\text{-pt}}$. On the other hand, up to total derivatives, an exact 0-invariant with $\Delta = 2$ is isomorphic to

$$\Gamma_0 = \begin{array}{c} \bullet \\ \diagdown \\ \bullet \text{---} \bullet \end{array}$$

Then $\Gamma_0 \cup L_{3\text{-pt}}$ contains the three superposed graphs as follows:



Summing over all superposed graphs with unit coefficients gives a 2-invariant for $N = 3$ (after identifying isomorphic graphs),

$$\delta_2 \left(\begin{array}{c} \bullet \\ \diagdown \\ \bullet \text{---} \bullet \\ \text{---} \bullet \end{array} + 2 \begin{array}{c} \bullet \\ \diagdown \\ \bullet \text{---} \bullet \\ \diagup \\ \bullet \end{array} \right) = \rho^{(0)} \left(2 \begin{array}{c} \otimes \text{---} \star \\ \diagdown \\ \bullet \text{---} \bullet \\ \diagup \\ \bullet \end{array} \right). \tag{3.27}$$

Note that for $P = 2$ and $N = 3$, we need only consider Medusas with at least four edges, since the \times -vertex and \bullet -vertices have degree no less than 2. The Medusa in (3.27) is the only such Medusa with $\Delta = 4$. Therefore, this is the only independent minimal 2-invariant. Note that the 2-invariant given in (3.27) and the 3-invariant in (3.20) happen to be the same.

In fact, we can prove a general minimality statement for $N = 3$. Consider a Medusa with $\Delta = P + 1$ for odd P , and $\Delta = P + 2$ for even P . The \bullet -vertices of this Medusa have degree at least $\frac{1}{2}\Delta$. For odd P this already saturates the lower bound for the degree of a \bullet -vertex; no edge joining the two \bullet -vertices can be removed and thus Δ cannot be lowered further. For even P , one \bullet -vertex saturates the lower bound on vertex degree and the other \bullet -vertex has an excess of exactly one edge. Nevertheless, the same conclusion holds.

$N = 4$ Case: In §3.3.3 we found that (3.24) gives the only independent minimal 2-invariant for $N = 4$. It has the structure of a superposition of the sum with unit coefficients of all $N = 4$ trees (Figure 3.1a) and an exact 0-invariant:

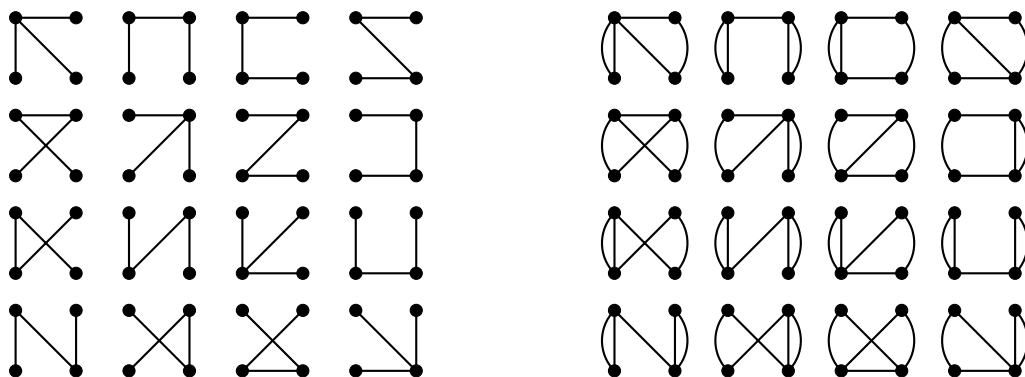
$$\begin{array}{c} \bullet \quad \bullet \\ \diagdown \quad \diagup \\ \bullet \quad \bullet \end{array} \tag{3.28}$$

The superposition of this 0-invariant with the trees in Figure 3.1a is given in Figure 3.1b. The sum of all graphs in Figure 3.1b with unit coefficients gives the 2-invariant in (3.24) (with an overall prefactor of 4).

Cubic Shift ($P=3$)

$N = 3$ Case: For $P = 3$, the only independent minimal invariant for $N = 3$ is given in (3.20), which can be written as a superposition of two equal-weight tree summations, as shown in Figure 3.2.

³The trees are arranged in order of their Prüfer sequences [66].



(a) All 16 trees for $N = 4$.³

(b) Superposition of (3.28) and the 16 trees.

Figure 3.1: The most relevant 2-invariant for $N = 4$ from superposition of graphs.

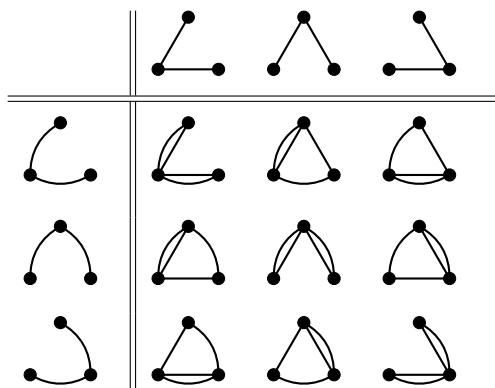


Figure 3.2: The superposition of two $n = 3$ tree summations.

As we already pointed out, this 3-invariant happens to be the minimal 2-invariant as well.

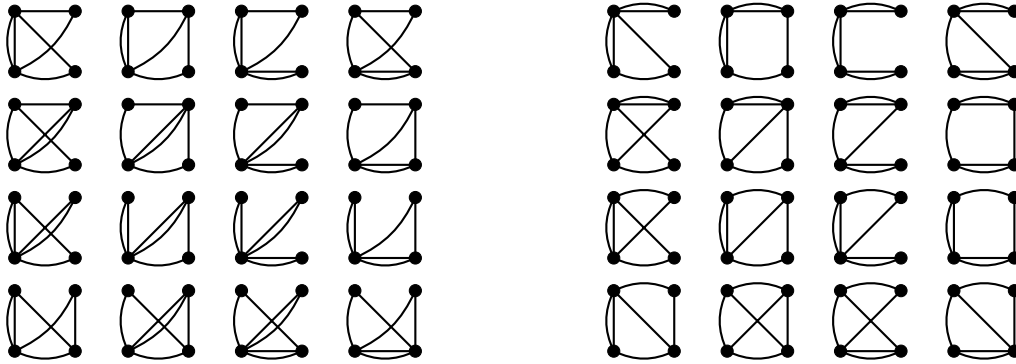
We can produce more 3-invariants by superposing an exact 1-invariant on the equal-weight sum of $N = 3$ trees. This would have two more derivatives compared to the minimal term above. For example, there are two independent exact 1-invariants for $N = 3$ with 3 edges:



which yield the following two 3-invariants:



$N = 4$ Case: In §3.3.3 we found that (3.25) gives the only independent minimal 3-invariant



(a) Superposition of T_A and Figure 3.1a.

(b) Superposition of T_B and Figure 3.1a.

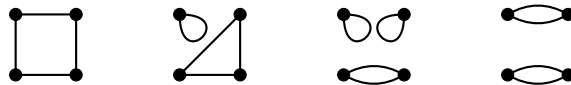
Figure 3.3: Superposition of graphs in (3.29) on trees in Figure 3.1a.

for $N = 4$. It has the structure of a superposition of two sums with unit coefficients of all trees in Figure 3.1a. As mentioned in §3.2, there are two isomorphism classes of $N = 4$ trees:

$$T_A = \begin{array}{c} \bullet \\ \diagup \quad \diagdown \\ \bullet \quad \bullet \\ \diagdown \quad \diagup \\ \bullet \end{array} \quad T_B = \begin{array}{c} \bullet \\ \diagup \quad \diagdown \\ \bullet \quad \bullet \\ \diagdown \quad \diagup \\ \bullet \end{array} \quad (3.29)$$

Superposing these graphs on the $N = 4$ trees produces the graphs in Figure 3.3. If T and T' are isomorphic trees, then superposing T on the trees in Figure 3.1a produces 16 graphs which are isomorphic to the 16 graphs formed by superposing T' on the same trees. There are four trees in the isomorphism class of T_A and twelve for T_B . Therefore, we just have to give the 16 graphs in Figure 3.3a weight 4 and the 16 graphs in Figure 3.3b weight 12 and then add them all up. The result is (3.25) with an overall prefactor of 4. Again, we have already shown that this is the unique minimal 3-invariant for $N = 4$.

As in the $N = 3$ case, we can produce non-minimal 3-invariants by superposing an exact 1-invariant on the equal-weight sum of $N = 4$ trees. For example, there are four independent exact 1-invariants for $N = 4$ with the lowest number of edges:



Quartic Shift ($P=4$)

$N = 3$ Case: As argued earlier, $\Delta_{\min} = 6$ in this case. There are two Medusas with the fewest edges such that the \times -vertex and the \bullet -vertices have degree no less than 3 (note that $\frac{1}{2}(P + 1) = \frac{5}{2}$ in this case):



There is exactly one minimal 4-invariant in this case, which is constructed by superposing two equal-weight sums of trees with an exact 0-invariant:



Note that the sum of the coefficients is 9, as it should be, since there are three $N = 3$ trees, and thus there are nine superpositions of two $N = 3$ trees.

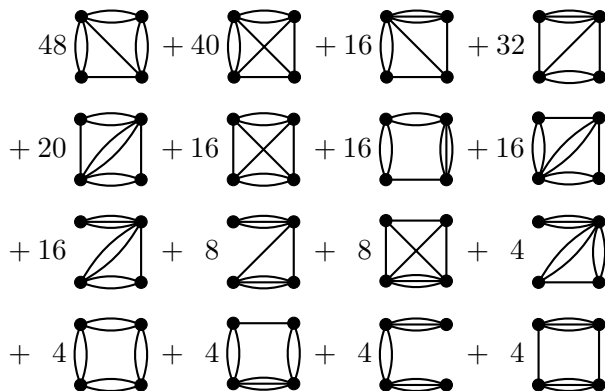
Examples of non-minimal invariants can be constructed by superposing an equal-weight sum of trees with an exact 2-invariant, or two equal-weight sums of trees with an exact 1-invariant.

The proofs of uniqueness and minimality for the remaining $N = 4$ examples are lengthy and involve many more Medusas than the previous examples, but the process is the same. Therefore, we will simply write the invariants and state that they are unique and minimal.

$N=4$ Case: We construct the minimal 4-invariant by superposing two copies of equal-weight sums of trees with an exact 0-invariant. There is one independent exact 0-invariant:



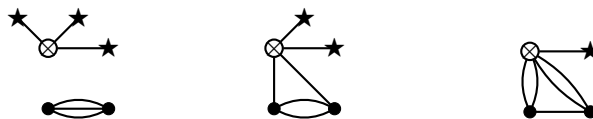
Superposing this on the superposition of two copies of equal-weight sums of trees yields



Note that the sum of the coefficients is $256 = 16^2$.

Quintic Shift ($P=5$)

$N = 3$ Case: In this case, $\Delta_{\min} = 6$. There are three Medusas with the fewest edges such that the \times -vertex and the \bullet -vertices have degree no less than 3 (note that $\frac{1}{2}(P + 1) = 3$):



There is exactly one minimal 5-invariant in this case, which is constructed by superposing three equal-weight sums of trees:

$$3 \begin{array}{c} \bullet \\ \diagup \quad \diagdown \\ \bullet \quad \bullet \\ \diagdown \quad \diagup \\ \bullet \quad \bullet \end{array} + 18 \begin{array}{c} \bullet \\ \diagup \quad \diagdown \\ \bullet \quad \bullet \\ \diagdown \quad \diagup \\ \bullet \quad \bullet \end{array} + 6 \begin{array}{c} \bullet \\ \diagup \quad \diagdown \\ \bullet \quad \bullet \\ \diagdown \quad \diagup \\ \bullet \quad \bullet \end{array}$$

Note that the sum of the coefficients is $27 = 3^3$. Also, note that this is proportional to the unique independent minimal 4-invariant found in the previous section, which was the superposition of two equal-weight sums of trees and an exact 0-invariant.

$N = 4$ Case: The superposition of three equal-weight sums of $N = 4$ trees yields

$$\begin{array}{cccccc} 4 & + & 12 & + & 108 & + & 432 & + & 288 \\ \begin{array}{c} \bullet \\ \diagup \quad \diagdown \\ \bullet \quad \bullet \\ \diagdown \quad \diagup \\ \bullet \quad \bullet \end{array} & & \begin{array}{c} \bullet \quad \bullet \\ \diagdown \quad \diagup \\ \bullet \quad \bullet \end{array} & & \begin{array}{c} \bullet \quad \bullet \\ \diagdown \quad \diagup \\ \bullet \quad \bullet \end{array} & & \begin{array}{c} \bullet \quad \bullet \\ \diagdown \quad \diagup \\ \bullet \quad \bullet \end{array} & & \begin{array}{c} \bullet \quad \bullet \\ \diagdown \quad \diagup \\ \bullet \quad \bullet \end{array} \\ + & 72 & + & 216 & + & 216 & + & 36 & + & 72 \\ \begin{array}{c} \bullet \quad \bullet \\ \diagdown \quad \diagup \\ \bullet \quad \bullet \end{array} & & \begin{array}{c} \bullet \quad \bullet \\ \diagdown \quad \diagup \\ \bullet \quad \bullet \end{array} & & \begin{array}{c} \bullet \quad \bullet \\ \diagdown \quad \diagup \\ \bullet \quad \bullet \end{array} & & \begin{array}{c} \bullet \quad \bullet \\ \diagdown \quad \diagup \\ \bullet \quad \bullet \end{array} & & \begin{array}{c} \bullet \quad \bullet \\ \diagdown \quad \diagup \\ \bullet \quad \bullet \end{array} \\ + & 72 & + & 144 & + & 144 & + & 612 & + & 144 \\ \begin{array}{c} \bullet \quad \bullet \\ \diagdown \quad \diagup \\ \bullet \quad \bullet \end{array} & & \begin{array}{c} \bullet \quad \bullet \\ \diagdown \quad \diagup \\ \bullet \quad \bullet \end{array} & & \begin{array}{c} \bullet \quad \bullet \\ \diagdown \quad \diagup \\ \bullet \quad \bullet \end{array} & & \begin{array}{c} \bullet \quad \bullet \\ \diagdown \quad \diagup \\ \bullet \quad \bullet \end{array} & & \begin{array}{c} \bullet \quad \bullet \\ \diagdown \quad \diagup \\ \bullet \quad \bullet \end{array} \\ + & 216 & + & 72 & + & 72 & + & 432 & + & 72 \\ \begin{array}{c} \bullet \quad \bullet \\ \diagdown \quad \diagup \\ \bullet \quad \bullet \end{array} & & \begin{array}{c} \bullet \quad \bullet \\ \diagdown \quad \diagup \\ \bullet \quad \bullet \end{array} & & \begin{array}{c} \bullet \quad \bullet \\ \diagdown \quad \diagup \\ \bullet \quad \bullet \end{array} & & \begin{array}{c} \bullet \quad \bullet \\ \diagdown \quad \diagup \\ \bullet \quad \bullet \end{array} & & \begin{array}{c} \bullet \quad \bullet \\ \diagdown \quad \diagup \\ \bullet \quad \bullet \end{array} \\ + & 72 & + & 72 & + & 216 & + & 192 & + & 108 \\ \begin{array}{c} \bullet \quad \bullet \\ \diagdown \quad \diagup \\ \bullet \quad \bullet \end{array} & & \begin{array}{c} \bullet \quad \bullet \\ \diagdown \quad \diagup \\ \bullet \quad \bullet \end{array} & & \begin{array}{c} \bullet \quad \bullet \\ \diagdown \quad \diagup \\ \bullet \quad \bullet \end{array} & & \begin{array}{c} \bullet \quad \bullet \\ \diagdown \quad \diagup \\ \bullet \quad \bullet \end{array} & & \begin{array}{c} \bullet \quad \bullet \\ \diagdown \quad \diagup \\ \bullet \quad \bullet \end{array} \end{array}$$

Note that the sum of the coefficients is $4096 = 16^3$.

To facilitate the check of the invariance of the above linear combination, denoted as L , we provide the linear combination of Medusas L_M such that $\delta_5(L) = \rho^{(0)}(L_M)$:

$$\begin{array}{cccccc} 12 & + & 72 & + & 24 & + & 72 & + & 72 & + & 144 \\ \begin{array}{c} \star \\ \diagup \quad \diagdown \\ \circ \quad \circ \\ \diagdown \quad \diagup \\ \bullet \quad \bullet \end{array} & & \begin{array}{c} \star \\ \diagup \quad \diagdown \\ \circ \quad \circ \\ \diagdown \quad \diagup \\ \bullet \quad \bullet \end{array} & & \begin{array}{c} \star \\ \diagup \quad \diagdown \\ \circ \quad \circ \\ \diagdown \quad \diagup \\ \bullet \quad \bullet \end{array} & & \begin{array}{c} \star \\ \diagup \quad \diagdown \\ \circ \quad \circ \\ \diagdown \quad \diagup \\ \bullet \quad \bullet \end{array} & & \begin{array}{c} \star \\ \diagup \quad \diagdown \\ \circ \quad \circ \\ \diagdown \quad \diagup \\ \bullet \quad \bullet \end{array} & & \begin{array}{c} \star \\ \diagup \quad \diagdown \\ \circ \quad \circ \\ \diagdown \quad \diagup \\ \bullet \quad \bullet \end{array} \\ + & 144 & + & 216 & + & 72 & + & 72 & + & 72 & + & 288 \\ \begin{array}{c} \star \\ \diagup \quad \diagdown \\ \circ \quad \circ \\ \diagdown \quad \diagup \\ \bullet \quad \bullet \end{array} & & \begin{array}{c} \star \\ \diagup \quad \diagdown \\ \circ \quad \circ \\ \diagdown \quad \diagup \\ \bullet \quad \bullet \end{array} & & \begin{array}{c} \star \\ \diagup \quad \diagdown \\ \circ \quad \circ \\ \diagdown \quad \diagup \\ \bullet \quad \bullet \end{array} & & \begin{array}{c} \star \\ \diagup \quad \diagdown \\ \circ \quad \circ \\ \diagdown \quad \diagup \\ \bullet \quad \bullet \end{array} & & \begin{array}{c} \star \\ \diagup \quad \diagdown \\ \circ \quad \circ \\ \diagdown \quad \diagup \\ \bullet \quad \bullet \end{array} & & \begin{array}{c} \star \\ \diagup \quad \diagdown \\ \circ \quad \circ \\ \diagdown \quad \diagup \\ \bullet \quad \bullet \end{array} \\ + & 432 & + & 108 & + & 216 & + & 144 & + & 216 \\ \begin{array}{c} \star \\ \diagup \quad \diagdown \\ \circ \quad \circ \\ \diagdown \quad \diagup \\ \bullet \quad \bullet \end{array} & & \begin{array}{c} \star \\ \diagup \quad \diagdown \\ \circ \quad \circ \\ \diagdown \quad \diagup \\ \bullet \quad \bullet \end{array} & & \begin{array}{c} \star \\ \diagup \quad \diagdown \\ \circ \quad \circ \\ \diagdown \quad \diagup \\ \bullet \quad \bullet \end{array} & & \begin{array}{c} \star \\ \diagup \quad \diagdown \\ \circ \quad \circ \\ \diagdown \quad \diagup \\ \bullet \quad \bullet \end{array} & & \begin{array}{c} \star \\ \diagup \quad \diagdown \\ \circ \quad \circ \\ \diagdown \quad \diagup \\ \bullet \quad \bullet \end{array} \end{array}$$

3.4. Outlook

We studied nonrelativistic scalar field theories with polynomial shift symmetries. In the free-field limit, such field theories arise in the context of Goldstone's theorem, where they

lead to the hierarchies of possible universality classes of Nambu-Goldstone modes, as shown in §2. Our main focus in §3.2 and §3.3 has been on *interacting* effective field theories which respect the polynomial shift symmetries of degree $P = 1, 2, \dots$. In order to find such theories, one needs to identify possible Lagrangian terms invariant under the polynomial shift up to total derivatives, and organize them by their scaling dimension, starting from the most relevant. As we showed in §3.2, §3.3 and Appendix 3.B, this essentially cohomological classification problem can be usefully translated into the language of graph theory. This graphical technique is important for two reasons. First, it is quite powerful: The translation of the classification problem into a graph-theory problem allows us to generate sequences of invariants for various values of P , number N of fields, the number 2Δ of spatial derivatives, and as a function of the spatial dimension D , in a way that is much more efficient than any “brute force” technique. Secondly, and perhaps more importantly, the graphical technique reveals some previously hidden structure even in those invariants already known in the literature. For example, the known Galileon N -point invariants are given by the equal-weight sums of all labeled trees with N vertices! This hidden simplicity of the Galileon invariants is a feature previously unsuspected in the literature, and its mathematical explanation deserves further study. In addition, we also discovered patterns that allow the construction of higher polynomials from the superposition of graphs representing a collection of invariants of a lower degree – again a surprising result, revealing glimpses of intriguing connections among the *a priori* unrelated spaces of invariants across the various values of P , N and Δ .

We focused for simplicity on the unrestricted polynomial shift symmetries of degree P , whose coefficients $a_{i_1 \dots i_\ell}$ are general real symmetric tensors of rank $\ell = 0, \dots, P$. As we pointed out in §3.1.1, at $P \geq 2$, this maximal polynomial shift symmetry algebra allows various subalgebras, obtained by imposing additional conditions on the structure of $a_{i_1 \dots i_\ell}$'s. While this refinement does not significantly impact the classification of Gaussian fixed points, reducing the symmetry to one of the subalgebras inside the maximal polynomial shift symmetry can lead to new N -point invariants, beyond the ones presented in this chapter. It is possible to extend our graphical technique to the various reduced polynomial shift symmetries, and to study the refinement of the structure of polynomial shift invariants associated with the reduced symmetries.

Our main motivation for the study of scalar field theories with polynomial shift symmetries has originated from our desire to map out phenomena in which technical naturalness plays a crucial role, in general classes of field theories with or without relativistic symmetries. The refined classification of the universality classes of NG modes and the non-relativistic refinement of Goldstone's theorem have provided an example of scenarios where our naive relativistic intuition about technical naturalness may be misleading, and new interesting phenomena can emerge. We anticipate that other surprises of naturalness are still hidden not only in the landscape of quantum field theories, but also in the landscape of nonrelativistic theories of quantum gravity.

Appendix

3.A. Glossary of Graph Theory

In this section, we list the standard terminologies in graph theory to which we will refer. (These essentially coincide with the ones in [66].)

Graph A *graph* Γ is an ordered pair $(V(\Gamma), E(\Gamma))$ consisting of a set $V(\Gamma)$ of *vertices* and a set $E(\Gamma)$, disjoint from $V(\Gamma)$, of *edges*, together with an *incident function* Ψ_Γ that associates with each edge of Γ an ordered pair of (not necessarily distinct) vertices of Γ . If e is an edge and u and v are vertices such that $\Psi_\Gamma(e) = \{u, v\}$, then e is said to *join* u and v .

Isomorphism Two graphs Γ_A and Γ_B are *isomorphic* if there exist a pair of bijections $f : V(\Gamma_A) \rightarrow V(\Gamma_B)$ and $\phi : E(\Gamma_A) \rightarrow E(\Gamma_B)$ such that $\Psi_{\Gamma_A}(e) = \{u, v\}$ if and only if $\Psi_{\Gamma_B}(\phi(e)) = \{f(u), f(v)\}$.

Identical Graphs Two graphs are *identical*, written $\Gamma_A = \Gamma_B$, if $V(G) = V(H)$, $E(G) = E(H)$ and $\Psi_G = \Psi_H$.

Labeled Graph A graph in which the vertices are labeled but the edges are not, is called a *labeled graph*. This will be the notion of graphs that we will refer to most frequently.

Unlabeled Graph An *unlabeled graph* is a representative of an equivalence class of isomorphic graphs.

Finite Graph A graph is *finite* if both of its vertex set and edge set are finite.

Null Graph The graph with no vertices (and hence no edges) is the *null graph*.

Incident The ends of an edge are said to be *incident* to the edge, and *vice versa*.

Adjacent Two vertices which are incident to a common edge are *adjacent*.

Loop A *loop* is an edge that joins a vertex to itself.

Cycle A *cycle* on two or more vertices is a graph in which the vertices can be arranged in a cyclic sequence such that two vertices are joined by exactly one edge if they are consecutive in the sequence, and are nonadjacent otherwise. A *cycle* on one vertex is a graph consisting of a single vertex with a loop.

Loopless Graph A *loopless* graph contains no loops. Note that a loopless graph may still contain cycles on two or more vertices.

Vertex Degree The *degree* of a vertex v , denoted by $\deg(v)$, in a graph Γ is the number of edges of Γ incident to v , with each loop counting as two edges.

Empty Vertex A vertex of degree 0 is called an *empty vertex*.

Leaf A vertex of degree 1 is called a *leaf*.

Edge Deletion The *edge deletion* of an edge e in a graph Γ is defined by deleting from Γ the edge e but leaving the vertices and the remaining edges intact.

Vertex Deletion The *vertex deletion* of a vertex v in a graph Γ is defined by deleting from Γ the vertex v together with all the edges incident to v . The resulting graph is denoted by $\Gamma - v$.

Connected Graph A graph is *connected* if, for every partition of its vertex set into two nonempty sets X and Y , there is an edge with one end in X and one end in Y .

Connected Component A *connected component* of a graph Γ is a connected subgraph Γ' of Γ such that any vertex v in Γ' satisfies the following condition: all edges incident to v in Γ are also contained in Γ' .

Tree A *tree* is a connected graph that contains no cycles. In particular, note that a tree has no empty vertices if it contains more than one vertex.

Cayley's Formula The number of labeled trees on N vertices is N^{N-2} .

3.B. Theorems and Proofs

3.B.1. The Graphical Representation

Consider the polynomial shift symmetry applied to a real scalar field ϕ ,

$$\phi(t, x^i) \rightarrow \phi(t, x^i) + \delta_P \phi, \quad \delta_P \phi = a_{i_1 \dots i_P} x^{i_1} \dots x^{i_P} + \dots + a_i x^i + a. \quad (3.30)$$

The polynomial ends at P^{th} order in the spatial coordinate x^i with $P = 0, 1, 2, \dots$, respectively corresponding to constant shift, linear shift, quadratic shift, and so on. The a 's are arbitrary real coefficients that parametrize the symmetry transformation, and are symmetric in any pair of indices. In the algebraic language, for a specific P , we are searching for a Lagrangian that is invariant under the polynomial shift up to a total derivative. Let L be a term in the Lagrangian with N ϕ 's and 2Δ spatial derivatives. Then,

$$\delta_P(L) = \partial_i(L_i), \quad (3.31)$$

where L_i is an expression containing $N - 1$ ϕ 's and an index i , which is not contracted. Such L 's are called *P-invariants*. We will mainly focus on interaction terms, i.e., $N \geq 3$.

We want to express these *P-invariants* using a graphical representation. The ingredients of the graphical representation are:

1. \bullet -vertices, denoted in a graph by \bullet .
2. \times -vertices, denoted in a graph by \otimes .
3. \star -vertices, denoted in a graph by \star .
4. Edges, denoted in a graph by a line, that join the above vertices.

In this context, a graph contains up to three types of vertices. This means that these graphs carry an additional structure regarding vertex type, compared to the conventional definition of a graph in Appendix 3.A.

We construct graphs using the following rules:

1. The maximal degree of a \times -vertex is P . Any graph containing a \times -vertex of degree greater than P is identified with the null graph.
2. There is at most one \times -vertex in a graph.
3. A \star -vertex is always a leaf (i.e., it has degree one).
4. Two \star -vertices are not allowed to be adjacent to each other.

We now describe what these graph ingredients represent. A \bullet -vertex represents a ϕ and a \times -vertex represents $\delta_P\phi$. A pair of derivatives with contracted indices, each one acting on a certain ϕ or $\delta_P\phi$, is represented by an edge joining the relevant \bullet - and \times -vertices. Note that Rule 1, which requires that there be at most P edges incident to the \times -vertex, is justified since $P + 1$ derivatives acting on $\delta_P\phi$ gives zero.

A graph with \star -vertices will represent terms which are total derivatives. By Rules 3 and 4, a \star -vertex must always have exactly one edge incident to it, and this edge is incident to a \bullet -vertex or \times -vertex. This edge represents a derivative acting on the entire term as a whole, and the index of that derivative is contracted with the index of another derivative acting on the ϕ or $\delta_P\phi$ of the \bullet - or \times -vertex, respectively, to which the \star -vertex is adjacent. Therefore, any graph with a \star -vertex represents a total derivative term.

Since the Lagrangian terms that these graphs represent have a finite number of ϕ 's and ∂ 's, we will consider only finite graphs. In addition, by the definition of graphs, all vertices and edges are automatically labeled, due to the fact that all elements in a set are distinct from each other. Therefore, a graph represents an algebraic expression in which each ϕ and ∂ carries a label. It will be convenient to keep the labels on ϕ , but it is unnecessary to label the derivatives. This motivates the definition given in Appendix 3.A for "labeled" graphs. In the rest of Appendix 3.B, unless otherwise stated, a graph is understood to be a labeled graph.

The desired algebraic expressions in which all ϕ 's are identical can be recovered by identifying all isomorphic graphs (for examples, refer to §3.2). In fact, the labeled P -invariants already capture all of the unlabeled ones (Appendix 3.B.5).

Note that not all algebraic expressions are captured in the graphical representation described above. For example, $\partial^2(\partial_j\phi\partial_j\phi)$ cannot be represented by a graph, since two \star -vertices are forbidden to be adjacent to each other by Rule 4. However, this algebraic expression can be written as $2\partial_i(\partial_i\partial_j\phi\partial_j\phi)$, which is graphically represented in Figure



Figure 3.B.1: Examples for the graphical representation of algebraic expressions.

3.B.1a, disregarding the coefficient 2. Another peculiar example is $\partial_i(\partial_j\phi\partial_j\phi)\partial_i\partial^2\phi$, which is equal to $4(\partial_i\partial_j\phi)(\partial_j\phi)(\partial_i\partial^2\phi)$. Although the graphical representation for the former expression is beyond the current framework, the graphical representation for the latter one is given in Figure 3.B.1b. One could generalize the graphical representation to include all possible algebraic expressions. However, for our purposes, the present framework will suffice.

Types of Graphs and Vector Spaces

We classify graphs by different combinations of vertices:

Definition 1.

1. A plain-graph is a graph in which all vertices are \bullet 's.
2. A \star -ed plain-graph is a graph with vertex set consisting of only \bullet -vertices and at least one \star -vertex.
3. A \times -graph is a plain-graph with one \bullet -vertex replaced with a \times -vertex.
4. A \star -graph is a graph with one \times -vertex and at least one \star -vertex.

We define sets of graphs and the real vector spaces that they generate:

Definition 2.

1. $\mathcal{G}_{N,\Delta}$ is the set of plain-graphs with N \bullet -vertices and Δ edges.
2. $\mathcal{G}_{N,\Delta}^\times$ is the set of \times -graphs with $N - 1$ \bullet -vertices, one \times -vertex and Δ edges.
3. $\mathcal{G}_{N,\Delta}^\star$ is the set of \star -graphs with $N - 1$ \bullet -vertices, one \times -vertex, at least one \star -vertex and Δ edges.

In the above graphs, we choose the labels of the \bullet - and \times -vertices to go from v_1 to v_N and the labels of the \star -vertices to go from v_1^\star to $v_{N(\star)}^\star$, where $N(\star)$ is the number of \star -vertices. Let $\mathcal{L}_{N,\Delta}$, $\mathcal{L}_{N,\Delta}^\times$ and $\mathcal{L}_{N,\Delta}^\star$ be the real vector spaces of formal linear combinations generated by $\mathcal{G}_{N,\Delta}$, $\mathcal{G}_{N,\Delta}^\times$ and $\mathcal{G}_{N,\Delta}^\star$, respectively. The zero vector in any of these vector spaces is the null graph.

Note that $N = N(\bullet) + N(\times)$, where $N(\bullet)$ is the number of \bullet -vertices and $N(\times)$ is the number of \times -vertices. N does not include $N(\star)$ since \star -vertices represent neither ϕ nor $\delta_P\phi$. These sets of graphs are finite and therefore the vector spaces of formal linear combinations are finite-dimensional.

By Definition 2, graphs in a linear combination $L \in \mathcal{L}_{N,\Delta}$ ($\mathcal{L}_{N,\Delta}^\times$ or $\mathcal{L}_{N,\Delta}^\star$) share the same number of N and Δ . In most of the following discussion, N and Δ are fixed. We will therefore omit these subscripts as long as no confusion arises. However, the number of \star -vertices $N(\star)$ is not fixed in a generic linear combination of \star -graphs.

Maps

We now define some maps between the sets and vector spaces in Definition 2. This will model the operations that act on the algebraic expressions represented by the graphs.

Firstly, the variation under the polynomial shift δ_P of an algebraic term, expressed by a graph Γ , is represented graphically by summing over all graphs that have one \bullet -vertex in Γ replaced with a \times -vertex.

Definition 3 (Variation Map). *Given a plain-graph $\Gamma \in \mathcal{G}$, with $V(\Gamma) = (v_1, \dots, v_N)$, the map $\delta_P : \mathcal{G} \rightarrow \mathcal{L}^\times$ is defined by $\delta_P(\Gamma) = \sum_{i=1}^N \Gamma_i^\times$, where Γ_i^\times is a graph given by replacing v_i with a \times -vertex. This map extends to $\mathcal{L} \rightarrow \mathcal{L}^\times$ by distributing δ_P over the formal sum.*

Note that Γ_i^\times is the null graph if v_i has degree greater than P . We will omit the subscript P in δ_P as long as no confusion arises. It is also necessary to define a map that operates in the reverse direction:

Definition 4. *The map $v : \mathcal{G}^\times \rightarrow \mathcal{G}$ is defined by replacing the \times -vertex with a \bullet -vertex.*

In the algebraic expressions, a total derivative term looks like $\partial_i L_i$, and the ∂_i can be distributed over L_i as usual, by applying the Leibniz rule. This feature will be captured by the graphical representation in the following definition.

Definition 5 (Derivative Map). *For a given \star -graph $\Gamma^\star \in \mathcal{G}^\star$, the derivative map $\rho : \mathcal{G}^\star \rightarrow \mathcal{L}^\times$ is defined using the following construction:*

1. *For the \star -graph Γ^\star , denote the \bullet -vertices by v_1, \dots, v_{N-1} , the \times -vertex by v_N and the \star -vertices by $v_1^\star, \dots, v_k^\star$, $k = N(\star)$. Take any \star -vertex v_i^\star in Γ^\star . For each $j_1 \in \{1, \dots, N\}$, form a graph Γ_{j_1} by deleting v_1^\star in Γ^\star and then adding an edge joining v_{j_1} and the vertex that was adjacent to v_1^\star in Γ^\star .*
2. *Apply the above procedure to each of the Γ_{j_1} to form $\Gamma_{j_1 j_2}$ by removing the next v_2^\star . Iterate this procedure until all \star -vertices have been removed, forming the \times -graph $\Gamma_{j_1 \dots j_k}$.*
3. *Define $\rho(\Gamma^\star) \equiv \sum_{j_1, \dots, j_k=1}^N \Gamma_{j_1 \dots j_k}^\times$.*

The domain of this map can be extended to \mathcal{L}^\star by distributing ρ over the formal sum. The derivative map ρ can be similarly defined on \star -ed plain-graphs. Furthermore, we take ρ to be the identity map when it acts on \times -graphs.

Note that the above definition is well-defined since ρ is independent of the order in which the \star -vertices are deleted.

Relations

There are many linear combinations of plain- and \times -graphs representing terms that can be written as a total derivative. To take this feature into account, we define two notions of relations for plain- and \times -graphs, respectively.

Definition 6 (Relations). *If a linear combination of plain-graphs $L \in \mathcal{L}$ can be written as $\rho(L')$, where L' is a sum of \star -ed plain-graphs, then L is called a plain-relation. If a linear combination of \times -graphs $L^\times \in \mathcal{L}^\times$ can be written as $\rho(L^\star)$, with L^\star a sum of \star -graphs, then L^\times is called a \times -relation.*

We shall denote the set of all plain-relations by \mathcal{R} and the set of all \times -relations by \mathcal{R}^\times . \mathcal{R} and \mathcal{R}^\times have a natural vector space structure and are subspaces of \mathcal{L} and \mathcal{L}^\times , respectively.

The Consistency Equation and Associations

Recall that P -invariants are defined algebraically by equation (3.31), $\delta_P(L) = \partial_i(L_i)$. This equation is written in the graphical representation as

$$\delta_P(L) = \rho(L^\star), \quad (3.32)$$

for $L \in \mathcal{L}$ and $L^\star \in \mathcal{L}^\star$. We call (3.32) the *consistency equation*. Searching for P -invariants is equivalent to constructing all consistency equations. Note that, by Definition 6, the consistency equation implies that $\delta_P(L)$ is a \times -relation and so we make the following definition:

Definition 7 (P -Invariant). *$L \in \mathcal{L}$ is a P -invariant if $\delta_P(L) \in \mathcal{R}^\times$.*

Furthermore, there is a simple class of P -invariants, which we call *exact P -invariants*. These represent terms which are *exactly* invariant under the polynomial shift symmetry (3.30), not just up to a total derivative.

Definition 8 (Exact P -Invariant). *$L \in \mathcal{L}$ is an exact P -invariant if $\delta_P(L) = 0$.*

The following notion, called “association between graphs”, will turn out to be indispensable in constructing consistency equations.

Definition 9 (Associations). *The associations between pairs of plain- and \times -graphs, plain- and plain-graphs, \star - and \times -graphs, \star - and \star -graphs and plain- and \star -graphs are defined as follows:*

1. $\Gamma \in \mathcal{G}$ and $\Gamma^\times \in \mathcal{G}^\times$ are associated with each other if Γ^\times is contained in $\delta_P(\Gamma)$, or, equivalently, $v(\Gamma^\times) = \Gamma$.
2. Any two graphs $\Gamma_1, \Gamma_2 \in \mathcal{G}$ are associated with each other if either they are associated with the same $\Gamma^\times \in \mathcal{G}^\times$, or Γ_1 is identical to Γ_2 .
3. $\Gamma^\star \in \mathcal{G}^\star$ and $\Gamma^\times \in \mathcal{G}^\times$ are associated with each other if Γ^\times is contained in $\rho(\Gamma^\star)$.
4. Any two graphs $\Gamma_1^\star, \Gamma_2^\star \in \mathcal{G}^\star$ are associated with each other if either they are associated with the same $\Gamma^\times \in \mathcal{G}^\times$, or Γ_1^\star and Γ_2^\star are identical to each other.

5. Any two graphs $\Gamma \in \mathcal{G}$ and $\Gamma^* \in \mathcal{G}^*$ are associated with each other if they are associated with the same $\Gamma^\times \in \mathcal{G}^\times$.

It turns out that the associations between only plain-graphs and \times -graphs have a simple structure. Note that for any \times -graph $\Gamma^\times \in \mathcal{G}^\times$, $v(\Gamma^\times)$ uniquely defines the associated plain-graph. Hence,

Proposition 1. *A \times -graph is associated with exactly one plain-graph.*

The corollaries below directly follow:

Corollary 1. *For $L \in \mathcal{L}$ and Γ^\times a \times -graph in $\delta(L)$, L contains the plain-graph $v(\Gamma^\times)$.*

Corollary 2. *Any two associated plain-graphs are identical to each other.*

Proof. If two distinct plain-graphs are associated with each other, then they are associated with a common \times -graph, which violates Proposition 1. Therefore, only identical plain-graphs are associated with each other. \square

Corollary 3. *For $L \in \mathcal{L}$ and a plain-graph Γ in L , $\delta(L)$ contains all \times -graphs in $\delta(\Gamma)$.*

Proof. Without loss of generality, suppose Γ appears in L with unit coefficient (otherwise, simply divide L by the coefficient of Γ). Let Γ^\times be a \times -graph in $\delta(\Gamma)$. By Proposition 1, Γ is the only plain-graph associated with Γ^\times . Therefore, Γ^\times cannot drop out of $\delta(\Gamma + L')$ for any $L' \in \mathcal{L}$ that does not contain Γ . Applying this statement to $L' = L - \Gamma$ proves that Γ^\times must appear in $\delta(L)$. \square

This now allows us to find all *exact* P -invariants in a simple manner:

Corollary 4. *$L \in \mathcal{L}$ is an exact P -invariant if and only if all vertices in all graphs contained in L have degree at least $P + 1$.*

Proof. If there is a vertex v in some plain-graph Γ in L of degree lower than $P + 1$, then $\delta_P(\Gamma)$ contains the \times -graph where v is replaced with a \times -vertex. But by Corollary 3, this means that $\delta_P(L)$ also contains this \times -graph, which contradicts $\delta_P(L) = 0$. \square

All of the above definitions and conclusions make sense when extended to $P < 0$. Even though $P < 0$ no longer corresponds to any polynomial shift symmetry, it will occasionally be useful to consider graphs with $P < 0$. Since any vertex has a non-negative degree, Corollary 4 implies:

Corollary 5. *If $P < 0$, any $L \in \mathcal{L}$ is an exact P -invariant.*

Associations between \star -graphs and \times -graphs also have a simple and useful property:

Lemma 1. *Suppose that a \times -graph $\Gamma^\times \in \mathcal{G}^\times$ is associated with a \star -graph $\Gamma^* \in \mathcal{G}^*$ that contains a single \star -vertex. Then Γ^\times appears in $\rho(\Gamma^*)$ with coefficient 1.*

In general, a \times -graph can be associated with more than one \star -graph. Figure 3.B.2 presents a simple example with $(P, N, \Delta) = (2, 3, 2)$. Consequently, there can exist multiple consistency equations for the same P -invariant. In the next section we will develop techniques to deal with this difficulty.

$$\rho \left(\begin{array}{c} \otimes \text{---} \star \\ \diagdown \star \\ \bullet \quad \bullet \end{array} \right) = 2 \begin{array}{c} \otimes \\ | \\ \bullet \end{array} \text{---} \bullet + \begin{array}{c} \otimes \\ | \\ \bullet \end{array} \text{---} \bullet + \begin{array}{c} \otimes \\ \diagup \diagdown \\ \bullet \quad \bullet \end{array} = \rho \left(\begin{array}{c} \otimes \text{---} \star \\ | \\ \bullet \quad \bullet \end{array} + \begin{array}{c} \otimes \text{---} \star \\ \diagdown \\ \bullet \quad \bullet \end{array} \right)$$

Figure 3.B.2: Two different linear combinations of \star -graphs result in an identical \times -relation for $P = 2$. In particular, the \times -graph with a coefficient 2 is associated with all three \star -graphs in the figure.

3.B.2. Building Blocks for Consistency Equations

In this section, we introduce the building blocks with which we will construct the consistency equation (3.32), $\delta_P(L) = \rho(L^*)$. Any polynomial shift-invariant can be generated using these building blocks. We show that we can constrain L to contain only loopless plain-graphs, and all other invariants are equal to these ones up to total derivatives. Consequently, $\delta_P(L)$, and thus $\rho(L^*)$, contains only loopless \times -graphs. Therefore, $\rho(L^*) = \rho^{(0)}(L^*)$, where $\rho^{(0)}$ acts in the same way as ρ but omits any looped graphs (Definition 13). In fact, we can restrict L^* to be a linear combination L_M of a particular type of \star -graph, such that $\rho^{(0)}(L^*) = \rho^{(0)}(L_M)$. These \star -graphs will be called Medusas (Definition 10). In Appendix 3.B.2 we determine a lower bound on the degree of a vertex in any graph that appears in the consistency equation.

The Loopless Realization of \mathcal{L}/\mathcal{R}

There are usually many alternative expressions for a single P -invariant algebraic term, which are equal to each other up to total derivatives. In the graphical language, the graphs representing these equivalent expressions are related by plain-relations. Therefore, we are interested in the space of linear combinations of plain-graphs modding out plain-relations, i.e., the quotient space \mathcal{L}/\mathcal{R} . We need to find subset of graphs, $\mathcal{B} \subset \mathcal{G}$, whose span is isomorphic to \mathcal{L}/\mathcal{R} . In other words, every element of \mathcal{L} can be written as a linear combination of graphs in \mathcal{B} and plain-relations. Furthermore, this means that there are no plain-relations between elements in the set \mathcal{B} . The following proposition shows that the set of loopless plain-graphs realizes the set \mathcal{B} .

Proposition 2 (Loopless Basis). *The span of loopless plain-graphs is isomorphic to \mathcal{L}/\mathcal{R} .*

Proof. Denote the span of all loopless plain-graphs by $\mathcal{L}_{\text{loopless}}$. If $\partial_i \partial_i$ acts on a single ϕ , then one can always integrate by parts to move one of the ∂_i 's to act on the remaining ϕ 's. In the graphical language, this means that any graph with loops can always be written as a linear combination of loopless graphs up to a plain-relation. This proves $\mathcal{L}/\mathcal{R} \subset \mathcal{L}_{\text{loopless}}$.

Now, we show that there are no plain-relations between the loopless plain-graphs. Suppose there exists a linear combination of loopless plain-graphs L that is a plain-relation. That is, there exists a linear combination L' of \star -ed plain-graphs such that $L = \rho(L')$. Let Γ' be a \star -ed plain-graph in L' . Then, $\rho(\Gamma')$ is a linear combination of plain-graphs each of which has a number of loops no greater than the number of \star -vertices in Γ' . There

will be exactly one graph, $\Gamma_{\text{f.l.}}$, which is fully-looped (with the number of loops equal to the number of \star -vertices in Γ'), produced when all the original \star -vertices (and the edges incident to them) are replaced with loops. Furthermore, $\Gamma_{\text{f.l.}}$ uniquely determines Γ' by replacing each loop in $\Gamma_{\text{f.l.}}$ with an edge incident to an extra \star -vertex. Choose the \star -ed plain-graph appearing in L' with the largest number of \star -vertices (the maximally \star -ed plain-graphs). This maximum exists since the number of the edges incident to the \star -vertices is bounded above by the number of edges Δ . The fully-looped graphs formed from these maximally \star -ed plain-graphs cannot cancel each other (by uniqueness) and cannot be canceled by any other graphs that are not fully-looped (by maximality). Therefore $\rho(L')$ is a linear combination containing looped graphs, which contradicts the initial assumption that L only consists of loopless graphs. This proves $\mathcal{L}_{\text{loopless}} \subset \mathcal{L}/\mathcal{R}$.

Therefore, $\mathcal{L}_{\text{loopless}} \cong \mathcal{L}/\mathcal{R}$. \square

Henceforth, we can restrict our search for P -invariants to $\mathcal{L}_{\text{loopless}}$. Note that if $L \in \mathcal{L}_{\text{loopless}}$, then all the graphs in $\delta(L)$ are also loopless, so it is sufficient to consider only loopless \times -graphs. We can also restrict to loopless \times -relations, $\mathcal{R}_{\text{loopless}}^\times \subset \mathcal{R}^\times$, which is the vector space consisting of \times -relations that are linear combinations of loopless graphs. We summarize this discussion in the following corollary:

Corollary 6. *The P -invariants that are independent up to total derivatives are represented by $L \in \mathcal{L}_{\text{loopless}}$ with $\delta(L) \in \mathcal{R}_{\text{loopless}}^\times$. Equivalently, they span the kernel of the map:*

$$q \circ \delta : \mathcal{L}_{\text{loopless}} \rightarrow \mathcal{L}_{\text{loopless}}^\times / \mathcal{R}_{\text{loopless}}^\times,$$

where q is the quotient map $q : \mathcal{L}_{\text{loopless}}^\times \rightarrow \mathcal{L}_{\text{loopless}}^\times / \mathcal{R}_{\text{loopless}}^\times$.

Medusas and Spiders

Corollary 6 motivates us to look for a basis of $\mathcal{R}_{\text{loopless}}^\times$, the \times -relations that are linear combinations of loopless graphs. To classify all such loopless \times -relations, we are led to study the linear combinations of \star -graphs that give rise to these relations under the derivative map ρ . We will realize a convenient choice for the basis of $\mathcal{R}_{\text{loopless}}^\times$, which will tremendously simplify our calculations: It turns out that the basis of $\mathcal{R}_{\text{loopless}}^\times$ is in one-to-one correspondence with a particular subset of loopless \star -graphs, which we now define.

Definition 10 (Medusa). *A Medusa is a loopless \star -graph with all \star -vertices adjacent to the \times -vertex, such that the degree of the \times -vertex $\deg(\times)$ and the number of \star -vertices $N(\star)$ satisfy $\deg(\times) = P + 1 - N(\star)$. We denote the set of Medusas by $\mathcal{M}_{N,\Delta}$.*

We should point out that applying ρ to a Medusa does not necessarily generate a \times -relation in $\mathcal{R}_{\text{loopless}}^\times$; it will sometimes produce \times -graphs with loops. In order to form a loopless \times -relation, these looped \times -graphs must be canceled by contributions from other \star -graphs.

In the proof of the one-to-one correspondence between the basis of $\mathcal{R}_{\text{loopless}}^\times$ and the subset of Medusas, we will frequently refer to the following definitions.

Definition 11 (Primary \star -Graphs). *A primary \star -graph is a \star -graph that contains exactly one \star -vertex.*

Definition 12 (Spider). *A spider is a primary \star -graph with the \star -vertex adjacent to the \times -vertex and $\deg(\times) = P$.*

Since $\deg(\times) \geq N(\star)$ for a Medusa, we have $\frac{1}{2}(P+1) \leq \deg(\times) \leq P$. In particular, if $P = 1$ or 2 , then $\deg(\times) = P$ and $N(\star) = 1$ (i.e., a Medusa is a loopless spider for $P = 1$ or 2). Spiders will play an important role in sorting out all independent loopless \times -relations in Appendix 3.B.2, and loopless spiders will lead us to the classification of 1-invariants in Appendix 3.B.3.

In 3.B.2 and 3.B.2 we will construct $\mathcal{R}_{\text{loopless}}^\times$ by spiders and Medusas. We will need to keep track of graphs containing specific numbers of loops, and the following refinement of the derivative map ρ (Definition 5) will allow us to formulate the graphical operations algebraically.

Definition 13. *The map $\rho^{(\ell)} : \mathcal{L}^\star \rightarrow \mathcal{L}^\times$ is defined such that, for $L^\star \in \mathcal{L}^\star$, $\rho^{(\ell)}(L^\star)$ is equal to $\rho(L^\star)$, with the coefficient of any graph that does not contain ℓ loops set to zero.*

Note that $\rho = \sum_{i=0}^{\infty} \rho^{(i)}$. If $\Gamma^\star \in \mathcal{G}^\star$ contains a loop, then $\rho^{(0)}(\Gamma^\star)$ is identically zero. In Theorem 1 we will show that the map $\rho^{(0)}$ defines the one-to-one correspondence between \mathcal{M} and the preferred basis of $\mathcal{R}_{\text{loopless}}^\times$.

It is also useful to introduce the operation of “undoing” loops.

Definition 14. *Given a $\Gamma \in \mathcal{G}^\times \cup \mathcal{G}^\star$ which contains ℓ loops, labeled from 1 to ℓ , the map $\theta_i : \mathcal{G}^\times \cup \mathcal{G}^\star \rightarrow \mathcal{G}^\star$ is defined such that $\theta_i(\Gamma)$ is a \star -graph constructed by deleting the i^{th} loop from Γ , adding an extra \star -vertex v^\star and adding an edge joining v^\star to the vertex at which the i^{th} deleted loop ended. Define $\theta : \mathcal{G}^\times \cup \mathcal{G}^\star \rightarrow \mathcal{G}^\star$ by $\theta(\Gamma) \equiv \theta_1 \circ \dots \circ \theta_\ell(\Gamma)$. This map extends to $\mathcal{L}^\times \cup \mathcal{L}^\star \rightarrow \mathcal{L}^\star$ by distributing θ over the formal sum. The map θ can be similarly defined on \star -ed plain-graphs.*

We will need to distinguish different types of loops:

Definition 15. *A loop at the \times -vertex is called a \times -loop, and a loop at a \bullet -vertex is a \bullet -loop. A graph that contains ℓ loops is called ℓ -looped.*

We can now prove a key formula:

Proposition 3. *If an ℓ -looped \star -graph Γ^\star contains a loop at vertex v_A , then*

$$\rho^{(\ell-1)} \circ \theta_A(\Gamma^\star) = \rho^{(\ell-1)} \circ \theta_A \circ \rho^{(\ell)}(\Gamma^\star) + \rho^{(\ell-1)} \left(\mathbf{L}_{\text{spider}}^{(\ell-1)} \right), \quad (3.33)$$

where θ_A undoes a loop at v_A , and $\mathbf{L}_{\text{Spider}}^{(\ell-1)}$ is a linear combination of $(\ell-1)$ -looped spiders. Every graph in a nonzero $\mathbf{L}_{\text{Spider}}^{(\ell-1)}$ has one fewer \times -loop than Γ^\star . $\mathbf{L}_{\text{Spider}}^{(\ell-1)}$ is nonzero if and only if the following three conditions are satisfied:

- (a) v_A is the \times -vertex;
- (b) There is a \star -vertex that is not adjacent to the \times -vertex;
- (c) $\deg(\times) \geq P+1 - N^\bullet(\star)$, where $N^\bullet(\star)$ is the number of \star -vertices in Γ^\star that are adjacent to \bullet -vertices.

Proof. Denote the vertices in Γ^\star adjacent to \star -vertices by v_i , $i = 1, \dots, k$, and the \times -vertex by v^\times . Note that v^\times and v_A may coincide with each other and with some of the v_i 's. Form an $(\ell - 1)$ -looped graph Γ from Γ^\star by deleting all \star -vertices and deleting a loop at v_A . We now show that all graphs in $\rho^{(\ell-1)} \circ \theta_A(\Gamma^\star)$ and $\rho^{(\ell-1)} \circ \theta_A \circ \rho^{(\ell)}(\Gamma^\star)$ in (3.33) contain Γ as a subgraph:

- $\rho^{(\ell-1)} \circ \theta_A(\Gamma^\star)$: Define $\Gamma_{v_{\beta_1} \dots v_{\beta_k}}$ to be a graph formed from Γ by adding k edges joining v_i and v_{β_i} , respectively. Then

$$\rho^{(\ell-1)} \circ \theta_A(\Gamma^\star) = \sum_{v_\alpha \neq v_A} \sum_{v_{\beta_1} \neq v_1} \dots \sum_{v_{\beta_k} \neq v_k} \Gamma_{v_{\beta_1} \dots v_{\beta_k}}^{v_\alpha}, \quad (3.34)$$

where $\Gamma_{v_{\beta_1} \dots v_{\beta_k}}^{v_\alpha}$ is the graph $\Gamma_{v_{\beta_1} \dots v_{\beta_k}}$ with an extra edge joining v_A and v_α . Note that the graphs formed from Γ by adding edges joining v_A (or v_i) to itself are not included in this sum, because these graphs are not $(\ell - 1)$ -looped.

- $\rho^{(\ell-1)} \circ \theta_A \circ \rho^{(\ell)}(\Gamma^\star)$: Define Γ_A to be the graph Γ with a loop added at v_A . Then $\rho^{(\ell)}(\Gamma^\star) = \sum_{v_{\beta_i} \neq v_i} \tilde{\Gamma}_{v_{\beta_1} \dots v_{\beta_k}}$, where $\tilde{\Gamma}_{v_{\beta_1} \dots v_{\beta_k}}$ is the graph formed from Γ_A by adding k edges joining v_i and v_{β_i} , respectively. $v_{\beta_i} \neq v_i$ in the sum because only ℓ -looped graphs are included. Applying $\rho^{(\ell-1)} \circ \theta_A$ gives:

$$\rho^{(\ell-1)} \circ \theta_A \circ \rho^{(\ell)}(\Gamma^\star) = \sum_{v_\alpha \neq v_A} \sum_{v_{\beta_1} \neq v_1} \dots \sum_{v_{\beta_k} \neq v_k} \tilde{\Gamma}_{v_{\beta_1} \dots v_{\beta_k}}^{v_\alpha}, \quad (3.35)$$

where $\tilde{\Gamma}_{v_{\beta_1} \dots v_{\beta_k}}^{v_\alpha}$ is formed from $\tilde{\Gamma}_{v_{\beta_1} \dots v_{\beta_k}}$ by deleting a loop at v_A and adding an edge joining v_A and v_α . $v_\alpha \neq v_A$ in the sum because only $(\ell - 1)$ -looped graphs are included.

We now want to compare $\Gamma_{v_{\beta_1} \dots v_{\beta_k}}^{v_\alpha}$ and $\tilde{\Gamma}_{v_{\beta_1} \dots v_{\beta_k}}^{v_\alpha}$ for $v_\alpha \neq v_A$ and $v_{\beta_i} \neq v_i$. At first it might seem that $\Gamma_{v_{\beta_1} \dots v_{\beta_k}}^{v_\alpha} = \tilde{\Gamma}_{v_{\beta_1} \dots v_{\beta_k}}^{v_\alpha}$, since both ultimately involve taking Γ and adding an edge joining v_A and v_α , and edges joining v_i and v_{β_i} . However, there is a subtlety involved: Recall that graphs containing a \times -vertex of degree larger than P are identified with the null graph. Therefore, $\Gamma_{v_{\beta_1} \dots v_{\beta_k}}^{v_\alpha} = \tilde{\Gamma}_{v_{\beta_1} \dots v_{\beta_k}}^{v_\alpha}$, provided neither side is null or both sides are null; when one side of this equation represents the null graph and the other does not, then this equation will not hold. This violation happens only if there is a difference in $\deg(\times)$ of the graphs formed during the construction of $\Gamma_{v_{\beta_1} \dots v_{\beta_k}}^{v_\alpha}$ and $\tilde{\Gamma}_{v_{\beta_1} \dots v_{\beta_k}}^{v_\alpha}$. Note that we add the same k edges (joining v_i and v_{β_i}) to both Γ and Γ_A to form the intermediate graphs, $\Gamma_{v_{\beta_1} \dots v_{\beta_k}}$ and $\tilde{\Gamma}_{v_{\beta_1} \dots v_{\beta_k}}$, respectively. Thus the difference between the latter two graphs is the same as the difference between Γ and Γ_A : There is an extra loop at v_A in Γ_A compared to Γ , which will only be deleted after the edges have been added. Hence, the violation of the equality, $\Gamma_{v_{\beta_1} \dots v_{\beta_k}}^{v_\alpha} = \tilde{\Gamma}_{v_{\beta_1} \dots v_{\beta_k}}^{v_\alpha}$, happens only if $v_A = v^\times$. This is condition (a).

From now on, we assume $v_A = v^\times$. In addition, there must exist at least one $v_{\beta_i} = v^\times$ in order for the violation to occur, since otherwise $\deg(\times)$ in any graph we are considering never exceeds the one in Γ^\star , and thus no graph in (3.34) and (3.35) is null. Hence for at least one v_{β_i} , $v^\times = v_{\beta_i} \neq v_i$, which implies condition (b). From now on we assume $v^\times = v_{\beta_i} \neq v_i$, for at least one v_{β_i} , and denote the number of v_{β_i} equal to v^\times by b , where $1 \leq b \leq N^\bullet(\star)$.

We know that $\deg(\times)$ in $\tilde{\Gamma}_{v_{\beta_1} \dots v_{\beta_k}}$ is 2 higher than $\deg(\times)$ in $\Gamma_{v_{\beta_1} \dots v_{\beta_k}}$, due to the one extra loop at v_A in Γ_A .

Therefore, if $\Gamma_{v_{\beta_1} \dots v_{\beta_k}}^{v_\alpha}$ vanishes, then $\tilde{\Gamma}_{v_{\beta_1} \dots v_{\beta_k}}^{v_\alpha}$ should also vanish, since $\tilde{\Gamma}_{v_{\beta_1} \dots v_{\beta_k}}$ already has a higher $\deg(\times)$. Furthermore, $\deg(\times)$ in $\tilde{\Gamma}_{v_{\beta_1} \dots v_{\beta_k}}$ is 1 higher than $\deg(\times)$ in $\Gamma_{v_{\beta_1} \dots v_{\beta_k}}^{v_\alpha}$, and thus $\Gamma_{v_{\beta_1} \dots v_{\beta_k}}^{v_\alpha} \neq \tilde{\Gamma}_{v_{\beta_1} \dots v_{\beta_k}}^{v_\alpha}$ if and only if $\deg(\times) = P$ in $\Gamma_{v_{\beta_1} \dots v_{\beta_k}}^{v_\alpha}$. In this case, $\Gamma_{v_{\beta_1} \dots v_{\beta_k}}^{v_\alpha}$ does not vanish, but $\tilde{\Gamma}_{v_{\beta_1} \dots v_{\beta_k}}^{v_\alpha}$ contains a \times -vertex of degree $P + 1$ and is identified with the null graph, which means $\tilde{\Gamma}_{v_{\beta_1} \dots v_{\beta_k}}^{v_\alpha}$ is also null. So the equality is violated if and only if $\deg(\times) = P + 1$ in $\tilde{\Gamma}_{v_{\beta_1} \dots v_{\beta_k}}$. We want to write this condition in terms of $\deg(\times)$ in Γ^* . Note that $\deg(\times) = P + 1$ in $\tilde{\Gamma}_{v_{\beta_1} \dots v_{\beta_k}}$ if and only if $\deg(\times) = P + 1 - b - (k - N^\bullet(\star))$ in Γ_A , and $\deg(\times) = P - 1 - b - (k - N^\bullet(\star))$ in Γ . Finally this implies $\deg(\times) = P + 1 - b$ in Γ^* . Since $1 \leq b \leq N^\bullet(\star)$, we have that $P \geq \deg(\times) \geq P + 1 - N^\bullet(\star)$, which is condition (c). Moreover,

$$\sum_{v_\alpha \neq v_A} \Gamma_{v_{\beta_1} \dots v_{\beta_k}}^{v_\alpha} = \rho(\Gamma_{\text{spider}}),$$

where Γ_{spider} is an $(\ell - 1)$ -looped spider formed from $\Gamma_{v_{\beta_1} \dots v_{\beta_k}}$ by adding a \star -vertex and then adding an edge that joins this \star -vertex and the \times -vertex. By construction, Γ_{spider} has one fewer \times -loop than Γ^* . Such spiders form the desired $L_{\text{spider}}^{(\ell-1)}$ in (3.33). \square

Constructing Loopless \times -Relations

Constructing a basis for $\mathcal{R}_{\text{loopless}}^\times$ requires a thorough examination of \star -graphs. The next lemma shows that any \times -relation can be written as a derivative map acting on a linear combination of primary \star -graphs, which allows us to restrict to primary \star -graphs in classifying all loopless \times -relations.

Lemma 2. *For any $L^\times \in \mathcal{R}^\times$, there exists $L^\star \in \mathcal{L}^\star$ that contains only primary \star -graphs, satisfying $L^\times = \rho(L^\star)$.*

Proof. Since L^\times is a \times -relation, there exists $\tilde{L}^\star = \sum_i b_i \Gamma_i^\star \in \mathcal{L}^\star$ such that $\rho(\tilde{L}^\star) = L^\times$. Starting with Γ_i^\star , one can follow steps 1 and 2 in Definition 5 to construct a series of \star -graphs, $(\Gamma_i^\star)_{j_1}, (\Gamma_i^\star)_{j_1 j_2}, \dots, (\Gamma_i^\star)_{j_1 \dots j_{k-1}}$, with $j_\alpha = 0, \dots, n - 1$ and $\alpha = 1, \dots, k$. By construction, $(\Gamma_i^\star)_{j_1 \dots j_{k-1}}$ contains exactly one \star -vertex (which makes it a primary \star -graph), and $\rho(\Gamma_i^\star) = \rho\left(\sum_{j_1, \dots, j_{k-1}=0}^{n-1} (\Gamma_i^\star)_{j_1 \dots j_{k-1}}\right)$. Therefore,

$$L^\times = \sum_i b_i \cdot \rho(\Gamma_i^\star) = \rho\left(\sum_i \sum_{j_1, \dots, j_{k-1}=0}^{N-1} b_i (\Gamma_i^\star)_{j_1 \dots j_{k-1}}\right).$$

This linear combination of primary \star -graphs $(\Gamma_i^\star)_{j_1 \dots j_{k-1}}$ defines the desired L^\star . Operationally, such L^\star is constructed from \tilde{L}^\star by removing the \star -vertices one by one, as per the steps in the definition of ρ , until only one \star -vertex remains. \square

The following proposition presents a general construction for loopless \times -relations. In the next section we will prove that this procedure generates all elements in $\mathcal{R}_{\text{loopless}}^\times$.

Proposition 4. *Let $L^\star \in \mathcal{L}^\star$ be a linear combination of ℓ -looped primary \star -graphs such that all \times -graphs in $\rho(L^\star)$ are ℓ -looped. There exists an $L_\ell^\star \in \mathcal{L}^\star$, such that*

- (a) $L_\ell^\star - L^\star$ contains no graph with more than $\ell - 1$ loops;
- (b) $\rho(L_\ell^\star) = (-1)^\ell \rho^{(0)} \circ \theta(L^\star + \mathsf{L}_{\text{spider}}) \in \mathcal{R}_{\text{loopless}}^\times$. $\mathsf{L}_{\text{spider}}$ is a linear combination of spiders.

Proof. Since each graph in $\rho(L^\star)$ is ℓ -looped, $\rho(L^\star) = \rho^{(\ell)}(L^\star)$. Let $\rho^{(\ell)}(L^\star) \equiv \sum_{i=1}^k b_i \Gamma_i^\times$, where each Γ_i^\times contains ℓ loops. For each Γ_i^\times , label the loops from 1 to ℓ . By Definition 14, θ_1 undoes the 1st loop, and $\theta_1(\Gamma_i^\times)$ defines a primary \star -graph with $\ell - 1$ loops that is associated with Γ_i^\times . By Lemma 1, Γ_i^\times drops out of $\rho(L^\star - b_i \cdot \theta_1(\Gamma_i^\times))$. Moreover, all \times -graphs in $\rho \circ \theta_1(\Gamma_i^\times)$, except for Γ_i^\times , are $(\ell - 1)$ -looped. Then

$$L_1^\star \equiv L^\star - \sum_{i=1}^k b_i \cdot \theta_1(\Gamma_i^\times) = L^\star - \theta_1 \circ \rho^{(\ell)}(L^\star)$$

defines an L_1^\star that satisfies $\rho(L_1^\star) = \rho^{(\ell-1)}(L_1^\star)$. Repeat this procedure for L_1^\star and the 2nd loop, in place of L^\star and the 1st loop, obtaining

$$L_2^\star \equiv L_1^\star - \theta_2 \circ \rho^{(\ell-1)}(L_1^\star) = L^\star - \theta_1 \circ \rho^{(\ell)}(L^\star) + \theta_2 \circ \rho^{(\ell-1)} \circ \theta_1 \circ \rho^{(\ell)}(L^\star).$$

The second equality holds because $\rho^{(\ell-1)}(L^\star) = 0$. Furthermore, $\rho(L_2^\star) = \rho^{(\ell-2)}(L_2^\star)$. Iterating this ℓ times, we will reach a linear combination of primary \star -graphs

$$L_\ell^\star \equiv L^\star + \sum_{i=1}^{\ell} (-1)^i X_i^\star, \quad X_i^\star \equiv \theta_i \circ \rho^{(\ell-i+1)} \circ \dots \circ \theta_2 \circ \rho^{(\ell-1)} \circ \theta_1 \circ \rho^{(\ell)}(L^\star). \quad (3.36)$$

Here $\rho(L_\ell^\star) = \rho^{(0)}(L_\ell^\star) \in \mathcal{R}_{\text{loopless}}^\times$. Moreover, X_i^\star only contains $(\ell - i)$ -looped graphs. This means that graphs in $L_\ell^\star - L^\star = \sum_{i=1}^{\ell} (-1)^i X_i^\star$ contain at most $\ell - 1$ loops. Therefore, L_ℓ^\star satisfies condition (a) of the proposition.

To prove that L_ℓ^\star also satisfies condition (b), take $\mathsf{L}_{\text{spider}}^{(i)}$ to stand for ‘‘any linear combination of i -looped spiders’’ and, for $0 < k \leq \ell$, define

$$Z_{\ell-k}^\star \equiv \theta_k \circ \dots \circ \theta_1(L^\star) - \sum_{\alpha=2}^k \theta_k \circ \dots \circ \theta_\alpha \left(\mathsf{L}_{\text{spider}}^{(\ell-\alpha+1)} \right) - \mathsf{L}_{\text{spider}}^{(\ell-k)}$$

which contains only $(\ell - k)$ -looped graphs. Define $Z_\ell^\star \equiv L^\star$. Therefore, for $0 \leq k \leq \ell$, applying Proposition 3,

$$\begin{aligned} & \rho^{(\ell-k-1)} \circ \theta_{k+1} \circ \rho^{(\ell-k)}(Z_{\ell-k}^\star) = \rho^{(\ell-k-1)} \left[\theta_{k+1} \left(\mathsf{L}_{\text{spider}}^{(\ell-k-1)} \right) \right] \\ & = \rho^{(\ell-k-1)} \left[\theta_{k+1} \circ \dots \circ \theta_1(L^\star) - \sum_{\alpha=2}^{k+1} \theta_{k+1} \circ \dots \circ \theta_\alpha \left(\mathsf{L}_{\text{spider}}^{(\ell-\alpha+1)} \right) - \mathsf{L}_{\text{spider}}^{(\ell-k-1)} \right], \end{aligned}$$

i.e.,

$$\rho^{(\ell-k-1)} \circ \theta_{k+1} \circ \rho^{(\ell-k)}(Z_{\ell-k}^\star) = \rho^{(\ell-k-1)}(Z_{\ell-k-1}^\star). \quad (3.37)$$

Note that $\rho^{(0)}(L^\star) = 0$ and $\rho^{(0)}(X_i^\star) = 0$ for $i = 1, \dots, \ell - 1$. Then, by (3.36) and (3.37),

$$\begin{aligned}
\rho^{(0)}(L_\ell^\star) &= (-1)^\ell \rho^{(0)}(X_\ell^\star) \\
&= (-1)^\ell \rho^{(0)} \circ \theta_\ell \circ \rho^{(1)} \circ \dots \circ \theta_2 \circ \rho^{(\ell-1)} \circ \theta_1 \circ \rho^{(\ell)}(Z_\ell^\star) \\
&= (-1)^\ell \rho^{(0)} \circ \theta_\ell \circ \rho^{(1)} \circ \dots \circ \theta_2 \circ \rho^{(\ell-1)}(Z_{\ell-1}^\star) = \dots = (-1)^\ell \rho^{(0)}(Z_0^\star) \\
&= (-1)^\ell \rho^{(0)} \left(\theta_\ell \circ \dots \circ \theta_1(L^\star) - \sum_{\alpha=2}^{\ell} \theta_\ell \circ \dots \circ \theta_\alpha \left(L_{\text{spider}}^{(\ell-\alpha+1)} \right) - L_{\text{spider}}^{(0)} \right) \\
&= (-1)^\ell \rho^{(0)} \circ \theta \left(L^\star - \sum_{\alpha=2}^{\ell+1} L_{\text{spider}}^{(\ell-\alpha+1)} \right).
\end{aligned}$$

Hence,

$$\rho(L_\ell^\star) = \rho^{(0)}(L_\ell^\star) = (-1)^\ell \rho^{(0)} \circ \theta(L^\star + L_{\text{spider}}) \in \mathcal{R}_{\text{loopless}}^\times.$$

This gives condition (b), with $L_{\text{spider}} = -\sum_{\alpha=2}^{\ell+1} L_{\text{spider}}^{(\ell-\alpha+1)}$. \square

Corollary 7. *Given L_s , a linear combination of spiders, $\rho^{(0)} \circ \theta(L_s) \in \mathcal{R}_{\text{loopless}}^\times$.*

Proof. It is enough to show that this corollary is true for one spider S . We claim that Proposition 4 holds for $L^\star = S$ and where L_{spider} is null if we order the loops such that loops 1 to ℓ^\times are \times -loops and $\ell^\times + 1$ to ℓ are \bullet -loops and the loops are removed in this order. Define $Z_{\ell-k}^\star \equiv \theta_k \circ \dots \circ \theta_1(S)$ and $Z_\ell^\star \equiv S$. As in the proof of Proposition 4, we are done if we can prove (3.37), but with this new definition of $Z_{\ell-k}^\star$ (i.e., when L_{spider} is always taken to be zero).

For $k = 0$, $Z_\ell^\star = S$, a spider, which has no \star -vertex adjacent to a \bullet -vertex in violation of Proposition 3(b). Thus, $\rho^{(\ell-1)} \circ \theta_1 \circ \rho^{(\ell)}(Z_\ell^\star) = \rho^{(\ell-1)} \circ \theta_1(Z_\ell^\star) = \rho^{(\ell-1)}(Z_{\ell-1}^\star)$. This holds regardless of which loop is chosen to be undone first. However, if the first loop is a \times -loop, then $Z_{\ell-1}^\star = \theta_1(S)$ will continue to violate Proposition 3(b). Therefore, if all of the \times -loops are undone first, then $\rho^{(\ell-k-1)} \circ \theta_{k+1} \circ \rho^{\ell-k}(Z_{\ell-k}^\star) = \rho^{(\ell-k-1)}(Z_{\ell-k-1}^\star)$ holds for $0 \leq k \leq \ell^\times$.

Now, there are no longer any \times -loops. Whenever there are \bullet -loops, $Z_{\ell-k}^\star$ will violate Proposition 3(a). Thus, $\rho^{(\ell-k-1)} \circ \theta_{k+1} \circ \rho^{\ell-k}(Z_{\ell-k}^\star) = \rho^{(\ell-k-1)}(Z_{\ell-k-1}^\star)$ continues to hold all the way until $k = \ell$. \square

A Basis for $\mathcal{R}_{\text{loopless}}^\times$

To find a basis for $\mathcal{R}_{\text{loopless}}^\times$, we first show that any loopless \times -relation can be written as $\rho^{(0)} \circ \theta$ acting on a linear combination of spiders. We start with the following lemmas:

Lemma 3. *Let $L^\times \in \mathcal{R}_{\text{loopless}}^\times$ satisfy $L^\times = \rho(L^\star)$, with L^\star a linear combination of primary \star -graphs. For any Γ_A^\star in L^\star that is associated with a looped \times -graph Γ^\times , there exists another \star -graph $\Gamma_B^\star \neq \Gamma_A^\star$ in L^\star , such that Γ^\times is not contained in $\rho(\Gamma_A^\star - \Gamma_B^\star)$.*

Proof. Suppose Γ_A^\star is the only \star -graph in L^\star that is associated with Γ_A^\star . Assume that the coefficient of Γ_A^\star in L^\star is $b_A \neq 0$. Therefore, none of the \star -graphs in $L^\star - b_A \Gamma_A^\star$ is associated with Γ^\times , and thus Γ^\times is not contained in $\rho(L^\star - b_A \Gamma_A^\star)$. Hence, the looped \times -graph Γ^\times

appears in $\rho(L^*) = \rho(L^* - b_A \Gamma_A^*) + b_A \cdot \rho(\Gamma_A^*)$ with coefficient $b_A \neq 0$, which contradicts the fact that $\rho(L^*) \in \mathcal{R}_{\text{loopless}}^\times$.

The above argument shows that there exists a $\Gamma_B^* \neq \Gamma_A^*$ in L^* that is associated with Γ^\times . By Lemma 1, Γ^\times appears in both $\rho(\Gamma_A^*)$ and $\rho(\Gamma_B^*)$ with coefficient 1. Then, $\rho(\Gamma_A^* - \Gamma_B^*)$ does not contain Γ^\times . \square

Specifically, if Γ_A^* is ℓ -looped and Γ^\times is $(\ell + 1)$ -looped, then Γ_B^* is also ℓ -looped.

Lemma 4. *If $\Gamma_A^*, \Gamma_B^* \in \mathcal{G}^*$ are ℓ -looped primary \star -graphs that are associated with the same $(\ell + 1)$ -looped \times -graph, then $\theta(\Gamma_A^* - \Gamma_B^*) = 0$.*

Proof. Since Γ_A^* and Γ_B^* are both associated with the same $(\ell + 1)$ -looped \times -graph, Γ^\times , $\theta(\Gamma_A^*) = \theta(\Gamma_B^*) = \theta(\Gamma^\times)$. Therefore, $\theta(\Gamma_A^* - \Gamma_B^*) = 0$. \square

Proposition 5. *For any loopless \times -relation $L^\times \in \mathcal{R}_{\text{loopless}}^\times$, there exists a linear combination of spiders L_s , such that $L^\times = \rho^{(0)} \circ \theta(L_s)$.*

Proof. In the following, we take L_{spider} to stand for ‘‘any linear combination of spiders’’. Since L^\times is a \times -relation, there exists $L^* \in \mathcal{L}^*$, consisting of primary \star -graphs, such that $L^\times = \rho(L^*)$. Take the set, $\mathcal{H}_\ell = \{\Gamma_1^*, \dots, \Gamma_{H_\ell}^*\}$, of \star -graphs in L^* that contain the highest number, ℓ , of loops. Let b_ℓ^i be the coefficient of Γ_i^* in L^* . Therefore, $L^* - \sum_{i=1}^{H_\ell} b_\ell^i \Gamma_i^*$ contains no graphs with more than $\ell - 1$ loops. We implement the following procedure for all graphs in \mathcal{H}_ℓ in order from Γ_1^* to $\Gamma_{H_\ell}^*$:

1. Define $\beta_\ell^{(1)} \equiv b_\ell^{(1)}$. Apply to Γ_1^* the construction outlined in Proposition 4:
 - (a) If Γ_1^* is a spider: By Corollary 7, Proposition 4(b) becomes that there exists a linear combination of primary \star -graphs $L_\ell^{(1)}$, such that

$$\rho(L_\ell^{(1)}) = \rho^{(0)} \circ \theta(\Gamma_1^*) = \rho^{(0)} \circ \theta(L_{\text{spider}}) \in \mathcal{R}_{\text{loopless}}^\times.$$

By Proposition 4(a), graphs in $L_\ell^{(1)} - \Gamma_1^*$ contain at most $\ell - 1$ loops.

- (b) If Γ_1^* is not a spider: $\rho(\Gamma_1^*)$ contains an $(\ell + 1)$ -looped \times -graph Γ^\times . By Lemma 3, there exists an ℓ -looped \star -graph $\Gamma_j^* \in \mathcal{H}$, $\Gamma_j^* \neq \Gamma_1^*$, that is associated with Γ^\times and Γ^\times is not in $\rho(\Gamma_1^* - \Gamma_j^*)$. By Lemma 4, $\theta(\Gamma_1^* - \Gamma_j^*) = 0$. By Proposition 4,

$$\rho(L_\ell^{(1)}) = \rho^{(0)} \circ \theta(L_{\text{spider}}) \in \mathcal{R}_{\text{loopless}}^\times,$$

where graphs in $L_\ell^{(1)} - (\Gamma_1^* - \Gamma_j^*)$ contain at most $\ell - 1$ loops.

2. Define $\beta_\ell^{(i)}$, for $i > 1$, as the coefficient (which may be zero) of Γ_i^* in $L^* - \beta_\ell^{(1)} L_\ell^{(1)}$.
3. If $\beta_\ell^{(2)} = 0$, skip this step; if not, repeat step 1 for Γ_2^* , resulting in an $L_\ell^{(2)}$ with

$$\rho(L_\ell^{(2)}) = \rho^{(0)} \circ \theta(L_{\text{spider}}) \in \mathcal{R}_{\text{loopless}}^\times.$$

Redefine $\beta_\ell^{(i)}$, for $i > 2$, to be the coefficient of Γ_i^* in $(L^* - \beta_\ell^{(1)} L_\ell^{(1)}) - \beta_\ell^{(2)} L_\ell^{(2)}$.

4. Repeat step 3 for $\Gamma_\ell^{(3)}, \dots, \Gamma_\ell^{(H_\ell)}$ in sequence. This will eventually generate a linear combination of \star -graphs, $L^\star - \sum_{i=1}^{H_\ell} \beta_\ell^{(i)} L_\ell^{(i)}$, where

$$\rho \left(\sum_{i=1}^{H_\ell} \beta_\ell^{(i)} L_\ell^{(i)} \right) = \rho^{(0)} \circ \theta(L_{\text{spider}}) \in \mathcal{R}_{\text{loopless}}^\times,$$

and all graphs in $L^\star - \sum_{i=1}^{H_\ell} \beta_\ell^{(i)} L_\ell^{(i)}$ contain at most $\ell - 1$ loops.

We can now repeat this procedure for $L^\star - \sum_{i=1}^{H_\ell} \beta_\ell^{(i)} L_\ell^{(i)}$. We will obtain

$$L^\star - \sum_{i=1}^{H_\ell} \beta_\ell^{(i)} L_\ell^{(i)} - \sum_{i=1}^{H_{\ell-1}} \beta_{\ell-1}^{(i)} L_{\ell-1}^{(i)}, \quad \rho \left(\sum_{i=1}^{H_{\ell-1}} \beta_{\ell-1}^{(i)} L_{\ell-1}^{(i)} \right) = \rho^{(0)} \circ \theta(L_{\text{spider}}) \in \mathcal{R}_{\text{loopless}}^\times.$$

In the first expression graphs contain at most $\ell - 2$ loops. Iterate ℓ times to get

$$\tilde{L}^\star \equiv L^\star - \sum_{\alpha=1}^{\ell} \sum_{i=1}^{H_\alpha} \beta_\alpha^i L_\alpha^{(i)},$$

which contains only loopless primary \star -graphs. In addition,

$$\rho \left(\sum_{\alpha=1}^{\ell} \sum_{i=1}^{H_\alpha} \beta_\alpha^i L_\alpha^{(i)} \right) = \rho^{(0)} \circ \theta(L_{\text{spider}}) \in \mathcal{R}_{\text{loopless}}^\times.$$

Therefore,

$$\rho(\tilde{L}^\star) = L^\times - \rho \left(\sum_{\alpha=1}^{\ell} \sum_{i=1}^{H_\alpha} \beta_\alpha^i L_\alpha^{(i)} \right) \in \mathcal{R}_{\text{loopless}}^\times.$$

Next we show that \tilde{L}^\star is a linear combination of spiders. Suppose there exists a \star -graph Γ_A^\star in \tilde{L}^\star that is not a spider. Then, by Lemma 3, there should exist another \star -graph $\Gamma_B^\star \neq \Gamma_A^\star$ in \tilde{L}^\star that is associated with the 1-looped \times -graph Γ^\times in $\rho(\Gamma_A^\star)$. But since Γ^\times is associated with a unique loopless \star -graph (resulting from undoing the loop), this is impossible. Therefore, graphs in \tilde{L}^\star are loopless spiders, and thus $\rho(\tilde{L}^\star) = \rho^{(0)} \circ \theta(\tilde{L}^\star)$. Hence,

$$L^\times = \rho \left(\tilde{L}^\star + \sum_{\alpha=1}^{\ell} \sum_{i=1}^{H_\alpha} \beta_\alpha^i L_\alpha^{(i)} \right) = \rho^{(0)} \circ \theta(L_{\text{spider}}).$$

The L_{spider} within the last pair of parentheses is the desired L_s . \square

Thus we have shown that any loopless \times -relation can be written as $\rho^{(0)} \circ \theta(L_s)$. In fact, we can go further and show that it is equal to $\rho^{(0)}(L_M)$, where L_M is a linear combination of Medusas. We start with the following Lemma:

Lemma 5. *Given a spider S that contains ℓ^\times \times -loops, there exist two linear combinations of spiders Y^\star , with graphs containing ℓ^\times \times -loops but no \bullet -loop, and W^\star , with graphs containing fewer than ℓ^\times \times -loops, such that $\rho^{(0)} \circ \theta(Y^\star) = \rho^{(0)} \circ \theta(S + W^\star)$.*

Proof. Suppose S contains ℓ^\bullet \bullet -loops, labeled from 1 to ℓ^\bullet . Denote the total number of loops in S to be $\ell = \ell^\times + \ell^\bullet$. Label the \times -loops in S from $\ell^\bullet + 1$ to ℓ . We will follow the proof of Proposition 4 to undo these \bullet -loops. However, we want to keep the \star -vertex in S untouched. Therefore, define ρ_s to be the usual derivative map except that it keeps the original \star -vertex in S untouched; we can grade ρ_s by number of loops in analogy with ρ .

Apply θ_1 to S to undo the 1st \bullet -loop. Define $Y_1^\star \equiv S - \rho_s \circ \theta_1(S)$ and note that S drops out of Y_1^\star . Furthermore, since S is the only ℓ -looped graph in $\rho_s \circ \theta(S)$,

$$Y_1^\star = S - \rho_s \circ \theta_1(S) = -\rho_s^{(\ell-1)} \circ \theta_1(S).$$

Repeat this procedure for all graphs in Y_1^\star and the 2nd \bullet -loop, in place of S and the 1st \bullet -loop, obtaining $Y_2^\star \equiv Y_1^\star - \rho_s \circ \theta_2(Y_1^\star)$, which is a linear combination of $(\ell - 2)$ -looped graphs. However, since all graphs in Y_1^\star are $(\ell - 1)$ -looped, we have

$$Y_2^\star = (-1)^2 \rho_s^{(\ell-2)} \circ \theta_2 \circ \rho_s^{(\ell-1)} \circ \theta_1(S).$$

Iterate this ℓ^\bullet times, resulting in

$$Y_{\ell^\bullet}^\star = (-1)^{\ell^\bullet} \rho_s^{(\ell-\ell^\bullet)} \circ \theta_{\ell^\bullet} \circ \dots \circ \rho_s^{(\ell-2)} \circ \theta_2 \circ \rho_s^{(\ell-1)} \circ \theta_1(S).$$

Graphs in $Y_{\ell^\bullet}^\star$ contain no \bullet -loops. As in the derivation of (6.98) in Proposition 4,

$$Y_{\ell^\bullet}^\star = (-1)^{\ell^\bullet} \rho_s^{(\ell-\ell^\bullet)} \left(\theta_{\ell^\bullet} \circ \dots \circ \theta_1(S) - \sum_{\alpha=2}^{\ell^\bullet} \theta_{\ell^\bullet} \circ \dots \circ \theta_\alpha \left(L_{\text{spider}}^{(\ell-\alpha+1)} \right) - L_{\text{spider}}^{(\ell-\ell^\bullet)} \right) \quad (3.38)$$

By Proposition 3, each graph in $L_{\text{spider}}^{(\ell-\alpha+1)}$ and $L_{\text{spider}}^{(\ell-\ell^\bullet)}$ contains fewer than ℓ^\times \times -loops.

Take $Y^\star = (-1)^{\ell^\bullet} Y_{\ell^\bullet}^\star$. Then, by Proposition 3,

$$\rho^{(0)} \circ \theta(Y^\star) = \rho^{(0)} \circ \theta_{\ell^\bullet} \circ \dots \circ \theta_{\ell^\bullet+1}(Y^\star) = \rho^{(0)} \circ \theta(S + W^\star),$$

where W^\star is a linear combination of spiders containing fewer than ℓ^\times \times -loops. \square

The next proposition finally allows us to relate spiders and Medusas.

Proposition 6. *For any linear combination of spiders $L_s \in \mathcal{L}^\star$, there exists a linear combination of Medusas L_M , such that $\rho^{(0)} \circ \theta(L_s) = \rho^{(0)}(L_M)$.*

Proof. Take the set,

$$\mathcal{H}_{\ell^\times} = \left\{ S_1^{(\ell^\times)}, \dots, S_{H_{\ell^\times}}^{(\ell^\times)} \right\},$$

of spiders in L_s that contain the highest number, ℓ^\times , of \times -loops. Denote the coefficient of $S_i^{(\ell^\times)}$ in L_s as $b_i^{(\ell^\times)}$. Therefore, graphs in $L_s - \sum_{i=1}^{H_{\ell^\times}} b_i^{(\ell^\times)} S_i^{(\ell^\times)}$ contain at most $\ell^\times - 1$ \times -loops. Applying Lemma 5 to each $S_i^{(\ell^\times)}$ yields two linear combinations of spiders $Y^{(\ell^\times)}$, comprised of graphs containing ℓ^\times \times -loops but no \bullet -loop, and $W^{(\ell^\times)}$, comprised of graphs containing fewer than ℓ^\times \times -loops, such that

$$\sum_{i=1}^{H_{\ell^\times}} \rho^{(0)} \circ \theta \left(b_i^{(\ell^\times)} S_i^{(\ell^\times)} \right) = \rho^{(0)} \circ \theta \left(Y^{(\ell^\times)} - W^{(\ell^\times)} \right). \quad (3.39)$$

Furthermore,

$$L_s - \left(\sum_{i=1}^{H_{\ell^\times}} b_i^{(\ell^\times)} S_i^{(\ell^\times)} + W^{(\ell^\times)} \right) \quad (3.40)$$

is a linear combination of spiders that contain at most $\ell^\times - 1$ \times -loops. Replace L_s with (3.40), and the above procedure applies, resulting in a linear combination of spiders that contain at most $\ell^\times - 2$ \times -loops. Iterating ℓ^\times times, we will obtain

$$L_s^{(0)} \equiv L_s - \sum_{\alpha=1}^{\ell^\times} \left(\sum_{i=1}^{H_\alpha} b_i^{(\alpha)} S_i^{(\alpha)} + W^{(\alpha)} \right), \quad (3.41)$$

By construction, $L_s^{(0)}$ is a linear combination of spiders containing no \times -loop. Moreover,

$$\rho^{(0)} \circ \theta \left(Y^{(\alpha)} \right) = \rho^{(0)} \circ \theta \left(\sum_{i=1}^{H_\alpha} b_i^{(\alpha)} S_i^{(\alpha)} + W^{(\alpha)} \right), \quad (3.42)$$

in analogy with (3.39). Finally, repeat the same procedure one last time with $L_s^{(0)}$ in (3.41) in place of L_s . Since there are no longer any \times -loops in $L_s^{(0)}$, no $W^{(\alpha)}$'s will arise. We obtain

$$L_s^{(0)} = \sum_{i=1}^{H_0} b_i^{(0)} S_i^{(0)}, \quad \rho^{(0)} \circ \theta \left(Y^{(0)} \right) = \rho^{(0)} \circ \theta \left(\sum_{i=1}^{H_0} b_i^{(0)} S_i^{(0)} \right). \quad (3.43)$$

Combining (3.41), (3.42) and (3.43), we obtain

$$\rho^{(0)} \circ \theta (L_s) = \rho^{(0)} \circ \theta \left(\sum_{\alpha=0}^{\ell^\times} Y^{(\alpha)} \right).$$

Since the $Y^{(\alpha)}$'s are linear combinations of spiders with no \bullet -loops and α \times -loops, $\theta(Y^{(\alpha)})$, is a linear combination of loopless \star -graphs with $\deg(\times) = P - \alpha$ and $N(\star) = \alpha + 1$. This means $\deg(\times) + N(\star) = P + 1$ in these loopless \star -graphs. By Definition 10, such graphs are Medusas. Therefore,

$$L_M = \theta \left(\sum_{\alpha=0}^{\ell^\times} Y^{(\alpha)} \right)$$

gives the desired linear combination of Medusas in $\rho^{(0)} \circ \theta (L_s) = \rho^{(0)} (L_M)$. \square

Theorem 1. $\rho^{(0)}(\mathcal{M})$ forms a basis of $\mathcal{R}_{\text{loopless}}^\times$.

Proof. Proposition 5 states that any $L^\times \in \mathcal{R}_{\text{loopless}}^\times$ can be written as $\rho^{(0)} \circ \theta(L_s)$, with L_s a linear combination of spiders. Proposition 6 states that there exists a linear combination of Medusas L_M , such that $\rho^{(0)} \circ \theta(L_s) = \rho^{(0)}(L_M)$. Therefore, $L^\times = \rho^{(0)}(L_M)$. This proves the completeness.

Suppose that there exists a linear combination of Medusas $L_M = \sum_{i=1}^k \alpha_i M_i \neq 0$, such that $\rho^{(0)}(L_M) = 0$. Note that if two Medusas M_A and M_B have \times -vertices of different degrees, then $\rho^{(0)}(M_A)$ and $\rho^{(0)}(M_B)$ do not have \times -graphs in common. Therefore, without loss of generality, we can assume that the \times -vertices in all M_i have the same degree. By the definition of Medusas, $P = \deg(\times) + N(\star) - 1$, and this implies that they also have the same number of \star -vertices. Furthermore, we can assume that, after deleting the \times -vertex, all M_i 's are identical since this must be the case in order for the $\rho^{(0)}(M_i)$ to cancel each other. Therefore, the only differences between the M_i are in the edges incident to the \times -vertex.

For any \bullet -vertex, v , take the set $\mathcal{H} = \{\tilde{M}_1, \dots, \tilde{M}_H\}$ of distinct Medusas in L_M , such that each \tilde{M}_i contains the highest number, E , of edges that join v and the \times -vertex among all Medusas in L_M . For each \tilde{M}_i , form a specific graph, Γ_i^\times , in $\rho^{(0)}(\tilde{M}_i)$ by deleting all $N(\star)$ \star -vertices and adding $N(\star)$ edges joining the \times -vertex and v . Now, Γ_i^\times contains $E + N(\star)$ edges joining v and the \times -vertex. By construction, the Γ_i^\times contain the highest number of edges joining v and the \times -vertex, among all \times -graphs in $\rho^{(0)}(L_M)$. Therefore, the Γ_i^\times can only be canceled among $\rho^{(0)}(\tilde{M}_i)$'s. Thus in order for Γ_i^\times to be canceled, we need $\Gamma_i^\times = \Gamma_j^\times$ for some $i \neq j$ (note that this Γ_i^\times appears in $\rho^{(0)}(\tilde{M}_i)$ with unit coefficient). But this means $\tilde{M}_i = \tilde{M}_j$ which is a contradiction since the \tilde{M}_i are distinct. This proves independence. \square

We can use this result to systematically find any P -invariant. When $P = 0$ or $P = 1$, a simple classification is possible for any N . The case $P = 1$ is studied in detail in Appendix 3.B.3 and $P = 0$ is dealt with in the following corollary.

Corollary 8. *Any loopless 0-invariant is an exact 0-invariant.*

Proof. There are no Medusas in $P = 0$ (since Medusas require $N(\star) \geq 1$ and $N(\star) \leq \deg(\times) = P + 1 - N(\star) \leq P$). Therefore $\mathcal{R}_{\text{loopless}}^\times = \{0\}$. \square

Since we have already identified all exact invariants in Corollary 4, this classifies all loopless 0-invariants.

Lower Bound on Vertex Degree

Within the loopless basis, we will set a lower bound on the degree of any \bullet - or \times -vertex in any graph appearing in a consistency equation for a P -invariant.

Proposition 7. *The vertices of a plain-graph Γ in a P -invariant $L \in \mathcal{L}_{\text{loopless}}$ are of degree no less than $\frac{1}{2}(P + 1)$.*

Proof. Let v be a vertex in Γ of degree less than $\frac{1}{2}(P + 1)$. Let Γ^\times in $\delta(\Gamma)$ be the term given by replacing v with a \times -vertex. By Corollary 3, Γ^\times is in $\delta(L)$. Since L is P -invariant, by Theorem 1, $\delta(L) = \rho^{(0)}(\sum_i \alpha_i M_i)$ for $M_i \in \mathcal{M}$ and thus, Γ^\times is in $\rho^{(0)}(M_j)$ for some j . Since M_j is a Medusa, the \times -vertex in M_j is of degree no less than $\frac{1}{2}(P + 1)$. This contradicts the fact that the \times -vertex in Γ^\times is of degree less than $\frac{1}{2}(P + 1)$. \square

Proposition 8. *If $L \in \mathcal{L}_{\text{loopless}}$ is a P -invariant and L_M is a linear combination of Medusas, such that $\delta L = \rho^{(0)}(L_M)$, then the vertices of any Medusa in L_M are of degree no less than $\frac{1}{2}(P + 1)$.*

Proof. Suppose that a Medusa M_0 in L_M has a vertex, v , of degree lower than $\frac{1}{2}(P+1)$. For an interaction term, there exists at least one other vertex v_0 in M_0 to which the \star -vertices can be joined such that v_0 is neither v nor the \times -vertex. The resulting graph in $\rho^{(0)}(M_0)$ is a \times -graph Γ_0^\times with vertex v of degree lower than $\frac{1}{2}(P+1)$, and thus, by Proposition 7, does not appear in $\delta(L)$. Therefore, there must exist another Medusa M_1 in L_M such that $M_0 \neq M_1$ and Γ_0^\times is absent from $\rho^{(0)}(M_0 - M_1)$. Therefore, M_1 must produce Γ_0^\times after deleting the \star -vertices and adding the same number, $N(\star)$, of edges joining the \times -vertex and the other vertices. Since $M_0 \neq M_1$ at least one of these other vertices is not v_0 , so the degree of v_0 is larger in M_1 than in M_0 . Now, form another \times -graph, Γ_1^\times , in $\rho^{(0)}(M_1)$ by deleting the \star -vertices in M_1 and adding the same number of edges joining the \times -vertex and v_0 . Γ_1^\times again contains v with degree lower than $\frac{1}{2}(P+1)$. This \times -graph must be canceled by introducing a third Medusa M_2 . This procedure can be iterated to obtain an infinite sequence of Medusas M_0, M_1, M_2, \dots in L_M , with the number of edges incident to v_0 in M_i monotonically increasing with i . But this is impossible since the Medusas have a fixed finite number of edges and thus we have a contradiction. \square

3.B.3. Linear Shift Symmetry, Trees and Galileons

For $P = 1$, Medusas have a very limited configuration: A Medusa M has two subgraphs, which are disconnected from each other, one of which is $\star \text{---} \otimes$, and the other of which is a loopless plain-graph. This strongly restricts the possible associations between graphs. In addition, for $P = 1$, $\rho(M) = \rho^{(0)}(M)$ for any Medusa M .

Proposition 9. *For $P = 1$, a loopless \times -graph is associated with at most one Medusa.*

Proof. If the \times -vertex in the loopless \times -graph has degree zero, then it cannot be associated with a Medusa. If the \times -vertex in the loopless \times -graph has degree one, then the loopless \times -graph takes the form of a \times -vertex and an edge joining this \times -vertex to a vertex in a loopless plain-graph, Γ . The unique Medusa associated with this \times -graph is given by deleting the edge incident to the \times -vertex and adding a \star -vertex together with an edge joining the \star -vertex and the \times -vertex. \square

Following the same logic as in the proofs of Corollary 2 and 3, we obtain:

Corollary 9. *For $P = 1$, any two associated Medusas are identical to each other.*

Corollary 10. *For $P = 1$, if M is a Medusa in a sum of Medusas L_M , then $\rho(L_M)$ contains all graphs in $\rho(M)$.*

Corollary 11. *For $P = 1$, if a Medusa M is associated with a plain-graph in a 1-invariant, $L \in \mathcal{L}_{loopless}$, then $\delta(L)$ contains all graphs in $\rho(M)$.*

Proof. If M is associated with Γ in the 1-invariant L , then there exists Γ^\times shared by $\delta(\Gamma)$ and $\rho(M)$. Corollary 3 implies Γ^\times is in $\delta(L)$. Theorem 1 implies $\delta(L) = \rho(L_M)$ where L_M is a sum of Medusas. Therefore, Γ^\times is in $\rho(L_M)$. Proposition 9 implies M is in L_M . Corollary 10 implies $\rho(L_M)$ contains $\rho(M)$ and thus $\delta(L)$ contains $\rho(M)$. \square

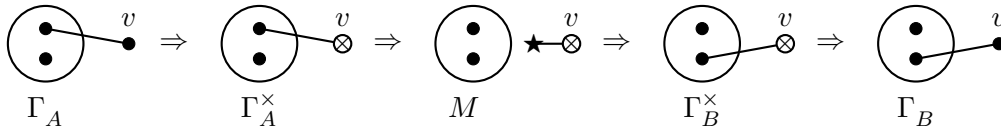
Minimal Invariants

Definition 16. A nonzero P -invariant $L_{N,\Delta}$ is minimal if there is no nonzero P -invariant $L'_{N,\Delta'}$ for any $\Delta' < \Delta$. For a given P and N , let Δ_{min} denote the minimum Δ for which a P -invariant exists.

Now, we prove that a minimal 1-invariant is a sum of trees. We start with the following lemma.

Lemma 6 (Leaf Shuffling). *If a graph Γ_A that contains a leaf v appears in a 1-invariant L , then any graph Γ_B that contains v as a leaf and satisfies $\Gamma_B - v = \Gamma_A - v$ is also contained in L .*

Proof. Depicted below is a series of graphs, which are all associated with each other:



where the circles denote subgraphs. In particular, both Γ_A and Γ_B are associated with the Medusa M . By Corollary 11, δL contains all graphs in $\rho(M)$. Furthermore, by Corollary 1, L contains both Γ_A and Γ_B . \square

We call the procedure that relates Γ_B to Γ_A described in the above lemma *leaf shuffling*. The corollaries below follow immediately.

Corollary 12. *If a plain-graph Γ_A is contained in a 1-invariant L , and Γ_B is formed from Γ_A by shuffling leaves, then Γ_B is also contained in L .*

Corollary 13. *If a plain-graph Γ in a loopless 1-invariant L contains more than one connected component, then none of these connected components is a tree.*

Proof. Note that there are at least two leaves in a tree, if the tree is not an empty vertex. If in Γ there is a connected component T that is a tree, then we can shuffle all leaves in T to be joined to other connected components, while turning T into another tree with at least one fewer vertex. This procedure can be iterated until all but one vertex in T are shuffled to be joined to other connected components, which turns Γ into a graph $\tilde{\Gamma}$ containing an empty vertex. By Corollary 12, since L contains Γ , it also contains $\tilde{\Gamma}$, which violates the lower bound on vertex degree. Therefore, such Γ cannot appear in loopless 1-invariants. \square

Proposition 10. *If L is a nonzero minimal N -point loopless 1-invariant, then it contains all trees with N vertices.*

Proof. If L contains no plain-graphs with leaves, then the vertices in L have degree at least 2 (note that an empty vertex is disallowed by Proposition 7). Then the number of edges Δ satisfies

$$\Delta \geq N. \quad (3.44)$$

Otherwise, consider a plain-graph Γ contains a leaf v and appears in L . If there exist any other leaves in Γ , shuffle them to be adjacent to v . Iterate for the resulting graphs

until reaching a plain-graph Γ_0 in which all leaves are adjacent to v . By Corollary 12, Γ_0 is also contained in L . Denote the subgraph of Γ_0 consisting of all leaves in Γ_0 and v by T , which is a particular type of tree usually called a *star*. Define Γ' as a subgraph of Γ_0 that is formed by deleting from Γ_0 all vertices in T .

If Γ' is not null, by Corollary 13, T cannot be disconnected from Γ' , since otherwise T would be a tree disconnected from at least one other connected component in Γ_0 . Moreover, since v is a leaf in Γ , Γ' is joined to T by exactly one edge incident to v . Define N_T as the number of vertices in T and N' as the number of vertices in Γ' , then $N = N_T + N'$. Note that there is no leaf in Γ' , and thus the vertices in Γ' have degree at least 2. Therefore,

$$\Delta \geq (N_T - 1) + N' + 1 = N. \quad (3.45)$$

If Γ' is null, then $\Gamma_0 = T$ and the original graph Γ is a tree. In this case, $\Delta = N - 1$, which is lower than the bounds ((3.44) and (3.45)) for the other cases. By Corollary 12, L contains T . The Galileon invariants presented in §3.2 realize this bound $\Delta_{\min} = N - 1$. In fact, any tree with N vertices can be turned into a star by shuffling leaves. Since L contains the star with N vertices, it contains all trees with N vertices. \square

Next, we prove the uniqueness of the minimal term.

Proposition 11. *The minimal N -point loopless 1-invariant with $\Delta = N - 1$ is unique up to proportionality.*

Proof. Let L_1 and L_2 be minimal N -point loopless 1-invariants with $\Delta = N - 1$. Let T be a tree in L_1 and L_2 , which exists by Proposition 10. Rescale L_1 and L_2 so that T appears in each with unit coefficient. Then, T is not in $L_1 - L_2$. However, $L_1 - L_2$ is a minimal N -point loopless 1-invariant. Therefore, Proposition 10 implies that $L_1 - L_2$ vanishes. \square

Finally, we prove the existence of the minimal N -point loopless 1-invariant with $\Delta = N - 1$:

Theorem 2. *Any minimal N -point loopless 1-invariant is proportional to the sum with unit coefficients of all trees with N vertices.*

Proof. Let T_N be a general tree with N \bullet -vertices. Let T_N^\times be a general tree with $(N - 1)$ \bullet -vertices and one \times vertex. Let T_N^\star have two connected components, one of which is $\star \text{---} \otimes$ and the other is a tree T_{N-1} . Let L , L^\times and L^\star be the sum with unit coefficients of all T_N , T_N^\times and T_N^\star , respectively. Replacing a \bullet -vertex in T_N with a \times produces a unique T_N^\times , since vertices are labeled. Therefore, $\delta(L)$ is simply L^\times . Similarly, $\rho(L^\star) = L^\times$. Therefore, $\delta(L) = \rho(L^\star)$ and L is 1-invariant, which is unique by virtue of Proposition 11. \square

It is shown in [60] that the Galileon-like term in spacetime dimension $d = D + 1 \geq N$:

$$\epsilon^{i_1 \dots i_{N-1} k_N \dots k_D} \epsilon^{j_1 \dots j_{N-1}}{}_{k_N \dots k_D} \partial_{i_1} \phi \partial_{j_1} \phi \partial_{i_2} \partial_{j_2} \phi \dots \partial_{i_{N-1}} \partial_{j_{N-1}} \phi, \quad (3.46)$$

is invariant up to a total derivative. By Theorem 2, the sum with unit coefficients of all trees with N vertices is proportional to (3.46), up to a total derivative. In fact, the constant of proportionality is 1.

Non-minimal Invariants

So far we have found the unique minimal 1-invariant for each N , that is with $\Delta = N - 1$. In what follows we argue that any non-minimal 1-invariant ($\Delta > N - 1$) is equal to an exact 1-invariant up to a plain-relation (a total derivative). We begin with the following definition:

Definition 17 (Frame). *For $\Gamma \in \mathcal{G}_{N,\Delta}$, delete all edges incident to leaves; iterate this procedure until reaching a graph Γ_f that contains no leaves. We call Γ_f the frame of Γ .*

Note that, by definition, after deleting from Γ all edges that appear in Γ_f , each of the connected components in the resulting graph is a tree. We also define:

Definition 18 (Frame Invariant). *A loopless 1-invariant $L = \sum_{i=1}^k \alpha_i \Gamma_i$ is a frame invariant if the frames of Γ_i for all $i = 1, \dots, k$ are identical.*

For convenience, we define a map f on frame invariants, such that $f(L)$ is the frame which is common to all of the graphs contained in L .

By definition, the nonempty vertices in any frame have degree greater than 1. No such vertex can be turned into a \times -vertex or be adjacent to a \star -vertex in a \star -graph associated with Γ . This means that terms with different frames cannot lead to cancellations in the consistency equation. Therefore, a consistency equation naturally splits into multiple consistency equations, each one a frame invariant. This is summarized in the lemma below:

Lemma 7. *Any loopless 1-invariant is a linear combination of frame invariants.*

The proofs presented in Proposition 10 and 11 and Theorem 2 are directly applicable to frame invariants, from which we conclude:

Proposition 12. *Up to proportionality, any loopless frame invariant L is equal to the sum with unit coefficients of all plain-graphs that satisfy the following conditions:*

- (a) *The plain-graph has a frame $f(L)$.*
- (b) *If there is more than one connected component in the plain graph, then none of them is a tree.*

Note that condition (b) follows directly from Corollary 13. Proposition 12 effectively provides an equivalent definition for frame invariants. Classifying all non-minimal 1-invariants is thus reduced to classifying all non-minimal frame invariants. Furthermore, by Proposition 2, we can restrict our search to loopless frame invariants. In the following we will show that any loopless frame invariant is equal to an exact invariant up to total derivatives. We start with a useful lemma:

Lemma 8. *Let $\Gamma^{(\ell)} \in \mathcal{G}$ be an ℓ -looped exact 1-invariant, such that all vertices with loops have degree 2. Then $\rho^{(0)} \circ \theta(\Gamma^{(\ell)})$ is a loopless 1-invariant and is equal to $\Gamma^{(\ell)}$ up to a plain-relation.*

Proof. Label the loops in $\Gamma^{(\ell)}$ from 1 to ℓ . Note that $\rho \circ \theta_1(\Gamma^{(\ell)}) = \Gamma^{(\ell)} + \rho^{(\ell-1)} \circ \theta_1(\Gamma^{(\ell)})$. Since $\theta_1(\Gamma^{(\ell)})$ is a \star -ed plain graph, $\rho \circ \theta_1(\Gamma^{(\ell)})$ is a plain-relation. Hence $\rho^{(\ell-1)} \circ \theta_1(\Gamma^{(\ell)})$ is 1-invariant. Define

$$L_1 \equiv \rho^{(\ell-1)} \circ \theta_1(\Gamma^{(\ell)}) = \rho \circ \theta_1(\Gamma^{(\ell)}) - \Gamma^{(\ell)},$$

L_1 is by definition an exact 1-invariant up to a plain-relation $\rho \circ \theta_1(\Gamma^{(\ell)})$. Furthermore, all graphs in L_1 are $(\ell - 1)$ -looped. Therefore, $\rho \circ \theta_2(L_1) = L_1 + \rho^{(\ell-2)} \circ \theta_2(L_1)$. Define

$$L_2 \equiv \rho^{(\ell-2)} \circ \theta_2(L_1) = \rho \circ \theta_2(L_1) - L_1,$$

which is also an exact 1-invariant up to plain-relations and consists of graphs that are $(\ell - 2)$ -looped. Iterating ℓ times, we obtain

$$L_\ell = \rho^{(0)} \circ \theta_{\ell-1} \circ \dots \circ \rho^{(\ell-2)} \circ \theta_2 \circ \rho^{(\ell-1)} \circ \theta_1(\Gamma^{(\ell)}) = \rho^{(0)} \circ \theta(\Gamma^{(\ell)}),$$

which is an exact 1-invariant up to plain-relations. \square

Theorem 3. *A non-minimal frame invariant is an exact invariant up to a plain-relation.*

Proof. It is sufficient to consider any loopless non-minimal frame invariant $L^{(k)} \in \mathcal{L}_{N,\Delta}$, with k the number of empty vertices in $f(L^{(k)})$. Note that since $L^{(k)}$ is non-minimal, it is not a tree and therefore $k < N$. We prove the theorem by induction on k .

1. $k = 0$: In this case, $f(L^{(0)}) = L^{(0)}$. By construction, a vertex in a graph in $L^{(0)}$ is of degree no less than 2, and thus $L^{(0)}$ is already exactly invariant.
2. If any $L^{(k)}$ with $k < \alpha$ is an exact invariant plus a plain-relation: Consider any loopless non-minimal frame invariant $L^{(\alpha)}$. Form an ℓ -looped exact 1-invariant $\Gamma^{(\alpha)}$ from $f(L^{(\alpha)})$ by adding a loop to each empty vertex. By Lemma 8, $\rho^{(0)} \circ \theta(\Gamma^{(\alpha)})$ is a loopless 1-invariant, equal to $\Gamma^{(\alpha)}$ up to plain-relations. Using Lemma 7, $\rho^{(0)} \circ \theta(\Gamma^{(\alpha)}) = \sum_i F_i$, where each F_i is a frame invariant with a distinct frame. Provided $\alpha < n$, there is exactly one F_i , say \tilde{F} , with $f(\tilde{F}) = f(L^{(\alpha)})$, and all other F_i have fewer than α empty vertices in $f(F_i)$. Since all other F_i 's have fewer than α empty vertices in $f(F_i)$, they are exact 1-invariants up to a plain-relation, by the induction hypothesis. But this means that \tilde{F} is also an exact 1-invariant up to plain-relations. By Proposition 12, since \tilde{F} and $L^{(\alpha)}$ share the same frame, \tilde{F} is proportional to $L^{(\alpha)}$ and thus $L^{(\alpha)}$ is also an exact 1-invariant up to plain-relations.

By induction, $L^{(k)}$ is exactly 1-invariant up to plain-relations for any $0 \leq k < N$. \square

From the above discussion, we can conclude: The set of all exact 1-invariants with all looped vertices of degree 2 generates all non-minimal 1-invariants, up to plain-relations. An example of these graphs for $N = 3$ and $\Delta = 4$ is shown in Figure 3.B.3.

We end our discussion of the linear shift symmetry with a summary of the full classification of 1-invariants:

Theorem 4 (Classification of 1-invariants). *The sum with unit coefficients of all trees with n vertices is the unique 1-invariant with $\Delta = N - 1$ (up to proportionality and plain-relations). The set of all graphs consisting of N vertices, with all vertices of degree higher than 1 and any looped vertex of degree 2, generate all 1-invariants with $\Delta > N - 1$ (up to plain-relations). There are no invariants with $\Delta < N - 1$.*



Figure 3.B.3: All 1-invariant terms up to total derivatives, with $N = 3$, $\Delta = 4$ and $P = 1$.

3.B.4. Invariants from Superpositions

In this section, we describe a method of combining invariants to form other invariants. Therefore, we will need to keep track of the degree of the polynomial shifts under which the variation of various terms are taken. It is important to recall at this point that the variation map δ_P depends crucially on P . Therefore, all the different types of graphs depend on P as well. Until now, this dependence on P has been kept implicit. We will now make it explicit by referring to graphs as P -graphs.

The method of combining invariants involves the notion of superposition, defined below, which combines graphs with different values of P .

Definition 19 (Superposition of Graphs). *Given a P_A -graph Γ_A and a P_B -graph Γ_B , which each have the same value of N , the superposition of Γ_A and Γ_B is a P -graph formed by applying the the following procedure:*

1. *If there is a \times -vertex in Γ_B , replace the vertex in Γ_A that has the same label as the \times -vertex in Γ_B with a \times -vertex.*
2. *Add any \star -vertices in Γ_B to Γ_A .*
3. *Take all edges in Γ_B and add them to Γ_A , joining the same vertices as they do in Γ_B .*
4. *Identify the resulting graph as a null graph if $\deg(\times)$ is higher than P or there are two \times -vertices.*

The resulting graph is denoted by $\Gamma_A \cup \Gamma_B$.

Note that $\Gamma_A \cup \Gamma_B = \Gamma_B \cup \Gamma_A$. Note that the above definition of superposition depends on P . We will refer to such a superposition as a P -superposition.

Definition 20 (Superposition of Linear Combinations). *Given the linear combinations $L_A = \sum_{i=1}^{k_A} a_i \Gamma_i^A$ and $L_B = \sum_{i=1}^{k_B} b_i \Gamma_i^B$, where Γ_i^A, Γ_j^B are graphs with the same n , the superposition of L_A and L_B is defined as*

$$L_A \cup L_B \equiv \sum_{i=1}^{k_A} \sum_{j=1}^{k_B} a_i b_j \Gamma_i^A \cup \Gamma_j^B.$$

Superposition of a P -invariant and an Exact Invariant

This section involves the construction of new invariants by taking the superposition of a P -invariant with an exact invariant.

Lemma 9.

1. Given a P -graph $\Gamma \in \mathcal{L}_{N,\Delta}$ and a P_E -graph $\Gamma_E \in \mathcal{L}_{N,\Delta_E}$, where Γ_E is an exact P_E -invariant,

$$\Gamma_E \cup \delta_P(\Gamma) = \delta_{P+P_E+1}(\Gamma_E \cup \Gamma), \quad (3.47)$$

where \cup denotes $(P + P_E + 1)$ -superposition.

2. Given a P -graph $\Gamma^* \in \mathcal{L}_{N,\Delta}^*$ and a P_E -graph $\Gamma_E \in \mathcal{L}_{N,\Delta_E}$, where Γ_E is an exact P_E -invariant,

$$\Gamma_E \cup \rho(\Gamma^*) = \rho(\Gamma_E \cup \Gamma^*), \quad (3.48)$$

where \cup denotes $(P + P_E + 1)$ -superposition.

Proof.

1. Operationally, a graph in the LHS of (3.47) is given by substituting one \bullet -vertex, v , in Γ with a \times -vertex and then adding the edges in Γ_E to the result. Meanwhile, the RHS is given by adding the edges in Γ_E to Γ first before substituting v by a \times -vertex. Thus, (3.47) is violated only when a graph vanishes from one side and not the other. A graph vanishes from the RHS if and only if the degree of the vertex v in $\Gamma_E \cup \Gamma$ is greater than $P + P_E + 1$. If this condition holds, then the graph also vanishes from the LHS by the rules of $(P + P_E + 1)$ -superposition. A graph could also possibly vanish from the LHS if $\deg(v) > P$ in Γ . However, if $\deg(v) > P$ in Γ , then $\deg(v) > P + P_E + 1$ in $\Gamma_E \cup \Gamma$ since the degree of a vertex in Γ_E is at least $P_E + 1$ (by Corollary 4). Therefore, the conditions for the vanishing of a graph from either side of (3.47) are identical and thus the equation holds.
2. Once again, (3.48) is violated only when a graph vanishes from one side and not the other. A graph vanishes from the RHS if and only if the degree of the \times -vertex in $\rho(\Gamma_E \cup \Gamma^*)$ is greater than $P + P_E + 1$. If this condition holds, then the graph also vanishes from the LHS by the rules of $(P + P_E + 1)$ -superposition. A graph on the LHS could also possibly vanish if $\deg(\times) > P$ for a graph Γ^\times in $\rho(\Gamma^*)$. However, then $\deg(\times) > P + P_E + 1$ in $\Gamma_E \cup \Gamma^\times$, since the degree of a vertex in Γ_E is at least $P_E + 1$ (by Corollary 4). Therefore, the conditions for the vanishing of a graph from either side of (3.48) are identical and thus the equation holds. \square

Now we apply Lemma 9 to prove the main result:

Theorem 5. *For fixed N , the superposition of a P -invariant and an exact P_E -invariant is a $(P + P_E + 1)$ -invariant.*

Proof. Denote the P -invariant by $L = \sum_{i=1}^k b_i \Gamma_i$ and the exact P_E -invariant by $L_E = \sum_{i=1}^{k_E} a_i \Gamma_i^E$. By Corollary 4, all vertices in Γ_i^E have degree greater than P_E . Since L is a P -invariant, there exists a linear combination of \star -graphs, $L^* = \sum_{i=1}^{k^*} c_i \Gamma_i^*$, such that the following consistency equation holds:

$$\delta_P(L) = \rho(L^*). \quad (3.49)$$

Define $\tilde{L} \equiv L_E \cup L = \sum_{i,j} a_i b_j \Gamma_i^E \cup \Gamma_j$. Then, using Statement 1 of Lemma 9:

$$\begin{aligned} \delta_{P+P_E+1}(\tilde{L}) &= \sum_{i,j} a_i b_j \delta_{P+P_E+1}(\Gamma_i^E \cup \Gamma_j) \\ &= \sum_{i,j} a_i b_j \Gamma_i^E \cup \delta_P(\Gamma_j) = \sum_i a_i \Gamma_i^E \cup \delta_P(L) \end{aligned} \quad (3.50)$$

Furthermore, define $\tilde{L}^* \equiv \sum_{i,j} a_i c_j \Gamma_i^E \cup \Gamma_j^*$ using $(P + P_E + 1)$ -superposition. Using Statement 2 of Lemma 9:

$$\rho(\tilde{L}^*) = \sum_{i,j} a_i c_j \rho(\Gamma_i^E \cup \Gamma_j^*) = \sum_{i,j} a_i c_j \Gamma_i^E \cup \rho(\Gamma_j^*) = \sum_i a_i \Gamma_i^E \cup \rho(L^*) \quad (3.51)$$

Combining (3.49), (3.50) and (3.51) we have that $\delta_{P+P_E+1}(\tilde{L}) = \rho(\tilde{L}^*)$ and therefore $\tilde{L} \equiv L_E \cup L$ is a $(P + P_E + 1)$ -invariant. \square

Superposition of Minimal Loopless 1-invariants

In this section we show that the superposition of Q minimal loopless 1-invariants results in a $(2Q - 1)$ -invariant. To prove this statement, we need to construct a linear combination of Medusas in order to write down a valid consistency equation. This construction requires intermediate \star -graphs called ‘‘hyper-Medusas’’, which we now define:

Definition 21 (Hyper-Medusa). *A hyper-Medusa is a loopless \star -graph with all \star -vertices adjacent to the \times -vertex, such that the degree of the \times -vertex $\deg(\times)$ and the number of \star -vertices $N(\star)$ satisfy $\deg(\times) \geq P + 1 - N(\star)$.*

Lemma 10. *Given M_h a hyper-Medusa, there exists a linear combination of Medusas L_M that satisfies $\rho^{(0)}(M_h) = \rho^{(0)}(L_M)$.*

Proof. Within the action of $\rho^{(0)}$, we can delete $\deg(\times) + N(\star) - P + 1 \geq 0$ \star -vertices and then add the same number of edges in M_h , yielding a linear combination of \star -graphs with exactly $P + 1 - \deg(\times)$ \star -vertices. These resulting graphs are Medusas. \square

The following definition will allow us to construct the desired hyper-Medusas:

Definition 22. *Take Γ_1 to be any \times -graph or \star -graph and for each $i = 2, \dots, Q$, take T_i to be any tree, such that Γ_1 and T_i have the same value of n . Label the \times -vertex in Γ_1 by v^\times and define T_i^\times to be the graph formed from T_i by replacing the vertex that is labeled by v^\times with a \times -vertex. If v^\times is a leaf in T_i , then define \tilde{T}_i to be the unique $P = 1$ Medusa that is associated with T_i^\times , otherwise $\tilde{T}_i = T_i^\times$. Then we define:*

$$\chi(\Gamma_1 \cup T_2 \cup \dots \cup T_Q) \equiv \Gamma_1 \cup \tilde{T}_1 \cup \dots \cup \tilde{T}_Q.$$

Theorem 6. *For fixed N , the superposition of Q minimal loopless 1-invariants is a $(2Q - 1)$ -invariant.*

Proof. By Theorem 2, any minimal N -point loopless 1-invariant is equal to the sum with unit coefficients of all trees with N vertices, up to proportionality. Therefore, denote the Q copies of the minimal loopless 1-invariants by $L_n^{(c)} = \sum_{\alpha_c=1}^{N^{N-2}} T_{\alpha_c}^{(c)}$, for $c = 1, \dots, Q$. We add an additional structure to all graphs in this proof: We color all edges in all graphs in $L_N^{(c)}$ by a distinct color (c) . Throughout this proof, two graphs are equal if and only if they are the same graph and, in addition, their edges are the same colors. Taking into account this coloring, all of the plain-graphs in $L \equiv \bigcup_{c=1}^Q L_N^{(c)}$ now have unit coefficients, and the number of these plain-graphs is $(N^{N-2})^Q$. Moreover, L is the sum over $\alpha_1, \dots, \alpha_Q$ of all such $T_{\alpha_1}^{(1)} \cup T_{\alpha_2}^{(2)} \cup \dots \cup T_{\alpha_Q}^{(Q)}$'s with unit coefficients. By Theorem 2, there is a unique linear combination of Medusas $\sum_{\beta_c} M_{\beta_c}^{(c)}$ satisfying

$$\delta_1 \left(L_N^{(c)} \right) = \delta_1 \left(\sum_{\alpha_c=1}^{N^{N-2}} T_{\alpha_c}^{(c)} \right) = \rho^{(0)} \left(\sum_{\beta_c=1}^{N(N-1)^{N-3}} M_{\beta_c}^{(c)} \right),$$

where each $T_{\alpha_c}^{(c)}$ is a distinct tree and each $M_{\beta_c}^{(c)}$ is a distinct $P = 1$ Medusa, consisting of a subgraph tree and a disconnected subgraph $\star \text{---} \otimes$. In the following, we take the limit $P \rightarrow \infty$, so that no graph vanishes. Note that we have

$$\begin{aligned} \sum_{\alpha_1} \delta_\infty \left(T_{\alpha_1}^{(1)} \cup T_{\alpha_2}^{(2)} \cup \dots \cup T_{\alpha_Q}^{(Q)} \right) &= \sum_{\alpha_1} \left(\delta_\infty(T_{\alpha_1}^{(1)}) \right) \cup T_{\alpha_2}^{(2)} \cup \dots \cup T_{\alpha_Q}^{(Q)} \\ &= \sum_{\beta_1} \rho^{(0)} \left(M_{\beta_1}^{(1)} \right) \cup T_{\alpha_2}^{(2)} \cup \dots \cup T_{\alpha_Q}^{(Q)} + \sum_{\alpha_1} (\delta_\infty - \delta_1)(T_{\alpha_1}^{(1)}) \cup T_{\alpha_2}^{(2)} \cup \dots \cup T_{\alpha_Q}^{(Q)}. \end{aligned} \quad (3.52)$$

Define $X_L \equiv \sum_{\beta_1, \alpha_2, \dots, \alpha_Q} M_{\beta_1}^{(1)} \cup T_{\alpha_2}^{(2)} \cup \dots \cup T_{\alpha_Q}^{(Q)}$ and X_R to be the sum with unit coefficients of all distinct graphs contained in $\sum_{\beta_1, \alpha_2, \dots, \alpha_Q} \chi(M_{\beta_1}^{(1)} \cup T_{\alpha_2}^{(2)} \cup \dots \cup T_{\alpha_Q}^{(Q)})$. In the following, we show that

$$\rho^{(0)}(X_L) = \rho^{(0)}(X_R). \quad (3.53)$$

Since $T_{\alpha_c}^{(c)}$, $\alpha_c = 1, \dots, N^{N-2}$, and $M_{\beta_c}^{(c)}$, $\beta_c = 1, \dots, N(N-1)^{N-3}$, are all distinct from each other, all elements in X_L and X_R have unit coefficient. Therefore, it will suffice to show that any graph in $\rho^{(0)}(X_R)$ is also in $\rho^{(0)}(X_L)$, and vice versa.

RHS contains LHS: Let Γ^\times be a \times -graph in $\rho^{(0)}(X_L)$. Then, Γ^\times is contained in $\rho^{(0)}(M_{\beta_1}^{(1)} \cup T_{\alpha_2}^{(2)} \cup \dots \cup T_{\alpha_Q}^{(Q)})$ for some $\beta_1, \alpha_2, \dots, \alpha_Q$. The \star -graph, $M_{\beta_1}^{(1)} \cup T_{\alpha_2}^{(2)} \cup \dots \cup T_{\alpha_Q}^{(Q)}$ induces a unique $\chi(M_{\beta_1}^{(1)} \cup T_{\alpha_2}^{(2)} \cup \dots \cup T_{\alpha_Q}^{(Q)})$, such that all \times -graphs in $\rho^{(0)}(M_{\beta_1}^{(1)} \cup T_{\alpha_2}^{(2)} \cup \dots \cup T_{\alpha_Q}^{(Q)})$ (including Γ^\times) are contained in $\rho^{(0)} \circ \chi(M_{\beta_1}^{(1)} \cup T_{\alpha_2}^{(2)} \cup \dots \cup T_{\alpha_Q}^{(Q)})$. Therefore, Γ^\times is in $\rho^{(0)}(X_R)$ and $\rho^{(0)}(X_R)$ contains $\rho^{(0)}(X_L)$.

LHS contains RHS: Let Γ^\times be a \times -graph in $\rho^{(0)}(X_R)$. Then, Γ^\times is contained in $\rho^{(0)} \circ \chi(M_{\beta_1}^{(1)} \cup T_{\alpha_2}^{(2)} \cup \dots \cup T_{\alpha_Q}^{(Q)})$ for some $\beta_1, \alpha_2, \dots, \alpha_Q$. In particular, Γ^\times is contained in some $\rho^{(0)}(M_{\beta_1'}^{(1)} \cup T_{\alpha_2'}^{(2)} \cup \dots \cup T_{\alpha_Q'}^{(Q)})$ with $T_{\alpha_2'}^{(2)} \cup \dots \cup T_{\alpha_Q'}^{(Q)}$ in $\rho^{(0)} \circ \chi(T_{\alpha_2}^{(2)} \cup \dots \cup T_{\alpha_Q}^{(Q)})$. Since $M_{\beta_1'}^{(1)} \cup T_{\alpha_2'}^{(2)} \cup \dots \cup T_{\alpha_Q'}^{(Q)}$ is in X_L , Γ^\times is in $\rho^{(0)}(X_L)$ and $\rho^{(0)}(X_L)$ contains $\rho^{(0)}(X_R)$.

From (3.53) we obtain

$$\sum_{\beta_1, \dots, \alpha_Q} \rho^{(0)} \left(M_{\beta_1}^{(1)} \cup T_{\alpha_2}^{(2)} \cup \dots \cup T_{\alpha_Q}^{(Q)} \right) = \rho^{(0)} (X_R). \quad (3.54)$$

Similarly,

$$\sum_{\alpha_1, \dots, \alpha_Q} (\delta_\infty - \delta_1) T_{\alpha_1}^{(1)} \cup T_{\alpha_2}^{(2)} \cup \dots \cup T_{\alpha_Q}^{(Q)} = \rho^{(0)} (\tilde{X}_R), \quad (3.55)$$

with \tilde{X}_R given by the sum with unit coefficients of all graphs contained in

$$\sum_{\alpha_1, \dots, \alpha_Q} \chi \left((\delta_\infty - \delta_1) T_{\alpha_1}^{(1)} \cup T_{\alpha_2}^{(2)} \cup \dots \cup T_{\alpha_Q}^{(Q)} \right).$$

Therefore, by (3.52), (3.54) and (3.55), we conclude that

$$\delta_\infty(L) = \sum_{\alpha_1, \dots, \alpha_Q} \delta_\infty \left(T_{\alpha_1}^{(1)} \cup T_{\alpha_2}^{(2)} \cup \dots \cup T_{\alpha_Q}^{(Q)} \right) = \rho^{(0)} (X_R + \tilde{X}_R). \quad (3.56)$$

Finally, switch back to $P = 2Q - 1$. Then graphs with $\deg(\times) > 2Q - 1$ will vanish simultaneously on both sides of (3.56), and thus, in $P = 2Q - 1$:

$$\delta_{2Q-1}(L) = \rho^{(0)} (X_R + \tilde{X}_R). \quad (3.57)$$

Next we show that any graph, Γ , in $X_R + \tilde{X}_R$ is a hyper-Medusa. By construction, Γ results from the superposition of graphs with either a \times -vertex of degree 1 joined to a \star -vertex or a \times -vertex of degree larger than 1. Therefore, $\deg(\times)$ in Γ satisfies $\deg(\times) \geq N(\star) + 2(Q - N(\star))$. So, with $P = 2Q - 1$, $\deg(\times) \geq P + 1 - N(\star)$ and Γ is a hyper-Medusa. Hence, by Lemma 10, there exists a linear combination, L_M , of Medusas, such that $\rho^{(0)} (X_R + \tilde{X}_R) = \rho^{(0)} (L_M)$. Therefore, combined with (3.57), we obtain $\delta_{2Q-1}(L) = \rho^{(0)}(L_M)$, which proves that L is a $(2Q - 1)$ -invariant. \square

We end our search for P -invariants with a summary of all invariants that we found:

Theorem 7. *For fixed N , the superposition of any exact P_E -invariant with the superposition of Q minimal loopless 1-invariants results in a P -invariant, provided $P_E + 2Q \geq P$.⁴*

We conjecture that the above theorem captures all P -invariants, up to total derivatives. Since we have classified all exact invariants and all 1-invariants, it is straightforward to construct the P -invariants in the above theorem for any specific case.

Note that we have classified exact invariants and 1-invariants using the two parameters, N (number of vertices) and Δ (number of edges). Finite connected graphs can always be embedded on a Riemann surface of some genus, in which case Euler's theorem relates N ,

⁴This theorem applies even for $P_E < 0$. Recall that, by Corollary 5, an exact P -invariant for $P < 0$ is just any possible linear combination of plain-graphs. For example, the plain-graph consisting only of empty vertices is an exact P -invariant for any $P < 0$.

Δ and the number of faces F of the embedding to the genus g of the surface. Therefore, one could also use the parameters N and F instead to classify invariants⁵. Any finite graph that can be embedded into a 2-sphere can also be embedded into a plane, and is known as a planar graph. In particular, this is true for any graph with $N \leq 4$ and also for any tree. Furthermore, any superposition of planar graphs is again a planar graph. The number of faces of these planar graphs is exactly the number of “loops” when the graph is interpreted as a Feynman diagram⁶. One can check this statement for all of the examples in §3.3.4 since they were all generated by superposition of planar graphs. Note that, in §3.3.4, except for $P = 0$ (which is a trivial case), all superpositions involve trees, so that all superposed graphs are connected. For example, all of the graphs in Figure 3.3 have three faces when embedded into a plane. Indeed, when interpreted as Feynman diagrams, these graphs have three “loops”. In general, the superposition of Q minimal loopless 1-invariants yields graphs have F “loops” as Feynman diagrams, where F is given by $F = (Q-1)(N-1)$. Theorem 7 says that these superpositions will be P -invariant for $P \leq 2Q - 1$. For example, the superposition of three minimal loopless 1-invariants with $N = 4$ produces a 5-invariant with 6 faces.

3.B.5. Unlabeled Invariants

So far we have been dealing entirely with labeled graphs, which represent algebraic terms where each ϕ is given a distinct label. But we are primarily interested in invariants where all ϕ 's are the same. These are represented by *unlabeled* graphs, that is, where isomorphic graphs are identified with each other. One may wonder whether or not the labeled P -invariants capture all of the unlabeled ones. The following proposition addresses this question, and shows that our restriction to labeled P -invariants still allows us to find all unlabeled P -invariants.

Proposition 13. *Given an unlabeled P -invariant L_{unlab} , there exists a labeled P -invariant L_{lab} , such that L_{lab} reduces to an integer multiple of L_{unlab} once the labels are removed.*

Proof. Define $L_{\text{unlab}}^\times = \delta(L_{\text{unlab}})$, where $\delta(L_{\text{unlab}})$ contains $\delta(\Gamma_{\text{unlab}})$ for all Γ_{unlab} in L_{unlab} . Label L_{unlab}^\times (i.e., label the vertices from 1 to N) to form L_{lab} . This labeling is fiducial since we will eventually sum over all possible labelings. Do the same for L_{unlab}^\times to form L_{lab}^\times . Define $L_{\text{lab}'}^\times = \delta(L_{\text{lab}})$, which is a labeling of L_{unlab}^\times , possibly distinct from L_{lab}^\times . However, if $\Gamma_{\text{lab}}^\times$ in L_{lab}^\times and $\Gamma_{\text{lab}'}^\times$ in $L_{\text{lab}'}^\times$ reduce to the same $\Gamma_{\text{unlab}}^\times$ in L_{unlab}^\times once the labels are removed, then $\Gamma_{\text{lab}}^\times$ and $\Gamma_{\text{lab}'}^\times$ are simply related by a permutation. Therefore,

$$\sum_{\sigma \in S_N} \sigma \circ \delta(L_{\text{lab}}) = \sum_{\sigma \in S_N} \sigma(L_{\text{lab}}^\times) = \sum_{\sigma \in S_N} \sigma(L_{\text{lab}'}^\times), \quad (3.58)$$

where S_N is the group of permutations on the N vertices.

Since L_{unlab} is P -invariant, there exists L_{unlab}^* such that $\delta(L_{\text{unlab}}) = \rho(L_{\text{unlab}}^*)$. Label L_{unlab}^* to form L_{lab}^* and define $L_{\text{lab}''}^\times = \rho(L_{\text{lab}}^*)$. Generically, there can be cancellations between isomorphic graphs in $L_{\text{lab}''}^\times$, once the labels are removed, since one \times -graph can

⁵In principle, Δ and F could also be used, but this seems less natural.

⁶Thanks to Kurt Hinterbichler for bringing this issue to our attention at the 2014 BCTP Tahoe Summit.

be associated with more than one \star -graph. Therefore, L_{lab}^\times is not necessarily a labeling of L_{unlab}^\times . Nevertheless, if $\alpha \Gamma_{\text{unlab}}^\times$ appears in L_{unlab}^\times with $\alpha \neq 0$, then all of the graphs, $\Gamma_1^\times, \dots, \Gamma_k^\times$ in L_{lab}^\times which are isomorphic to $\Gamma_{\text{unlab}}^\times$ appear in L_{lab}^\times as a linear combination $\sum_{i=1}^k \alpha_i \Gamma_i^\times$ with $\sum_{i=1}^k \alpha_i = \alpha$. Conversely, if $\sum_{i=1}^k \alpha_i \Gamma_i^\times$ appears in L_{lab}^\times , but the graph, $\Gamma_{\text{unlab}}^\times$, to which Γ_i^\times reduces once the labels are removed, does not appear in L_{unlab}^\times , then $\sum_{i=1}^k \alpha_i = 0$. Therefore,

$$\sum_{\sigma \in S_N} \sum_{i=1}^k \alpha_i \cdot \sigma(\Gamma_i^\times) = \sum_{i=1}^k \alpha_i \sum_{\sigma \in S_N} \sigma(\Gamma_{\text{lab}}^\times) = \alpha \sum_{\sigma \in S_N} \sigma(\Gamma_{\text{lab}}^\times),$$

which implies

$$\sum_{\sigma \in S_N} \sigma \circ \rho(L_{\text{lab}}^\star) = \sum_{\sigma \in S_N} \sigma(L_{\text{lab}}^\times) = \sum_{\sigma \in S_N} \sigma(L_{\text{lab}}^\times). \quad (3.59)$$

Combining Eqs. (3.58) and (3.59) with the facts that $\sigma \circ \delta = \delta \circ \sigma$ and $\sigma \circ \rho = \rho \circ \sigma$ for each $\sigma \in S_N$, yields the desired labeled consistency equation:

$$\delta \left(\sum_{\sigma \in S_N} \sigma(L_{\text{lab}}) \right) = \rho \left(\sum_{\sigma \in S_N} \sigma(L_{\text{lab}}^\star) \right).$$

$\sum_{\sigma \in S_N} \sigma(L_{\text{lab}})$ is P -invariant and reduces to $N! L_{\text{unlab}}$ once the labels are removed. \square

3.C. Coset Construction

The standard technique for finding terms which are invariant under a nonlinear realization of a symmetry is to use a coset construction [67, 68, 69, 70]. In this appendix we explore the connection between our invariant Lagrangians and this construction. Although we find that the coset construction can reproduce some of the invariants that we have discovered, using this method is computationally difficult when compared to the graphical method introduced in this paper.

We first review the coset construction applied to the polynomial shift symmetry as presented in [71, 65]. In dimension D , consider the polynomial shift transformations of the Goldstone fields defined in (3.30), accompanied with space-time translations and spatial rotations. Denote the corresponding generators by $Z, Z^i, \dots, Z^{i_1 \dots i_P}$ for polynomial shifts, \mathcal{P}_i for spacial translations, \mathcal{P}_0 for temporal translations, and J^{ij} for spatial rotations. Note that there are no boost symmetries. For the nonlinear realization of space-time symmetry, the translation generators are treated as the broken generators [69, 70]. The Goldstone fields transform as

$$\delta_{\mathcal{P}_i} \phi = \partial_i \phi, \quad \delta_Z \phi = 1, \quad \delta_{Z^{i_1 \dots i_k}} \phi = \frac{1}{k!} x^{i_1} \dots x^{i_k}, \quad k = 1, \dots, P.$$

The commutators between the operators can be readily calculated,

$$[\mathcal{P}_i, Z] = 0, \quad [\mathcal{P}_i, Z^{i_1 \dots i_k}] = -i \sum_j \frac{1}{k} \delta_i^j Z^{i_1 \dots \hat{j} \dots i_k}, \quad [Z^{i_1 \dots i_k}, Z^{j_1 \dots j_\ell}] = 0,$$

where \hat{j} means that the index j is omitted.

The commutators above given by the generators $\mathcal{P}_0, \mathcal{P}_i, J^{ij}, Z$ and $Z^{i_1 \dots i_k}, k = 1, \dots, P$ define the Lie algebra of a Lie group G , and \mathcal{P}_0 and J^{ij} correspond to the unbroken normal subgroup H . Take left invariant differential N -forms on G/H to be N -cochains, and take the coboundary operator $d^{(k)}$ to be the exterior derivative of differential forms. Denote the group of N -cocycles by $\mathcal{Z}^k = \text{Ker } d^{(k)}$, and the group of k -coboundaries by $\mathcal{B}^k = \text{Im } d^{(k-1)}$. The Chevalley-Eilenberg cohomology group $\mathcal{E}^k(G/H)$ is defined to be

$$\mathcal{E}^k(G/H) = \mathcal{Z}^k / \mathcal{B}^k,$$

which is isomorphic to the Lie algebra cohomology $\mathcal{H}_0^k(G/H; \mathbb{Z})$. (See [72] for details.)

We associate the generator Z with the Goldstone field ϕ . To each generator $Z^{i_1 \dots i_k}, k = 1, \dots, P$ we associate a symmetric k -tensor field $\phi_{i_1 \dots i_k}$. Indices can be lowered or raised by Kronecker delta symbols. The coset space is parametrized by

$$g = \exp(i\mathcal{P}_i x^i) \exp\left(iZ\phi + i\sum_{k=1}^P Z^{i_1 \dots i_k} \phi_{i_1 \dots i_k}\right).$$

The Maurer-Cartan form is

$$-ig^{-1}dg = \mathcal{P}_i dx^i + Z(d\phi + \phi_i dx^i) + \sum_{n=1}^{P-1} Z^{i_1 \dots i_n} (d\phi_{i_1 \dots i_n} + \phi_{i_1 \dots i_n i} dx^i) + Z^{i_1 \dots i_P} d\phi_{i_1 \dots i_P}.$$

Therefore, the basis dual to the generators is

$$\begin{aligned} \omega_{\mathcal{P}}^i &= dx^i, & \omega_{i_1 \dots i_P} &= d\phi_{i_1 \dots i_P}, \\ \omega &= d\phi + \phi_i dx^i, & \omega_{i_1 \dots i_k} &= d\phi_{i_1 \dots i_k} + \phi_{i_1 \dots i_k i} dx^i, \quad k = 1, \dots, P-1. \end{aligned} \quad (3.60)$$

Moreover,

$$\begin{aligned} d\omega_{\mathcal{P}}^i &= 0, & d\omega_{i_1 \dots i_P} &= 0, \\ d\omega &= d\phi_i \wedge dx^i, & d\omega_{i_1 \dots i_k} &= d\phi_{i_1 \dots i_k i} \wedge dx^i, \quad k = 1, \dots, P-1. \end{aligned}$$

The inverse Higgs constraints [73, 74] imply the vanishing of ω and $\omega_{i_1 \dots i_k}$ ($k < P$) in (3.60):

$$\phi_{i_1 \dots i_k} = (-1)^k \partial_{i_1} \dots \partial_{i_k} \phi, \quad k = 1, \dots, P. \quad (3.61)$$

Having reviewed the coset construction, we now present examples for $P = 2$ and 3 (the $P = 1$ scenario is essentially the same as the Galileon case [71]).

$P=2$ Case: For $N = 3$, the cohomology group is trivial for $D < 2$. Therefore, let us start with the simplest nontrivial case, $D = 2$. We are looking for a closed form involving the wedge of three ω 's, which are not $\omega_{\mathcal{P}}$. There is one independent cohomology element, with the lowest number of indices on ω 's:

$$\Omega_3 = \epsilon_{ij} \omega_{ab} \wedge \omega_{ia} \wedge \omega_{jb} = d(\epsilon_{ij} \phi_{ab} d\phi_{ia} \wedge d\phi_{jb}) \equiv d\beta_2.$$

These expressions can be extended to $D \geq 2$:

$$\begin{aligned}\Omega_{D+1} &= \epsilon_{ijs_3\dots s_D} \omega_{ab} \wedge \omega_{ia} \wedge \omega_{jb} \wedge \omega_{\mathcal{P}}^{s_3} \wedge \dots \wedge \omega_{\mathcal{P}}^{s_D}, \\ \beta_D &= \epsilon_{ijs_3\dots s_D} \phi_{ab} d\phi_{ia} \wedge d\phi_{jb} \wedge dx^{s_3} \wedge \dots \wedge dx^{s_D}.\end{aligned}$$

Taking the pullback of β_D to the spacetime manifold and then applying the inverse Higgs constraints in (3.61) gives a term proportional to

$$\epsilon_{ijs_3\dots s_D} \epsilon_{kls_3\dots s_D} \partial_a \partial_b \phi \partial_i \partial_k \partial_a \phi \partial_j \partial_l \partial_b \phi,$$

which is already contained in [65]. One can verify that this is equivalent up to integration by parts and overall prefactor to the invariant in (3.27). That term was found to be invariant for $P = 3$, and is therefore also invariant for $P = 2$.

Next, consider $N = 4$. The simplest nontrivial case is $D = 3$. We seek a closed 4-form given as the wedge of four ω 's, which are not $\omega_{\mathcal{P}}$. There is one independent cohomology element, with the lowest number of indices on ω 's:

$$\begin{aligned}\Omega'_4 &= \epsilon_{ijk} \omega_a \wedge \omega_{ia} \wedge \omega_{jb} \wedge \omega_{kb} \\ &= d \left[\epsilon_{ijk} \phi_{ac} \left(\frac{1}{2} \phi_{ac} d\phi_{jb} + \phi_{bc} d\phi_{ja} \right) \wedge d\phi_{kb} \wedge dx_i \right] \equiv d\beta'_3\end{aligned}$$

These expressions can be extended to $D \geq 3$:

$$\begin{aligned}\Omega'_{D+1} &= \epsilon_{ijks_4\dots s_D} \omega_a \wedge \omega_{ia} \wedge \omega_{jb} \wedge \omega_{kb} \wedge \omega_{\mathcal{P}}^{s_4} \wedge \dots \wedge \omega_{\mathcal{P}}^{s_D}, \\ \beta'_D &= \epsilon_{ijks_4\dots s_D} \phi_{ac} \left(\frac{1}{2} \phi_{ac} d\phi_{jb} + \phi_{bc} d\phi_{ja} \right) \wedge d\phi_{kb} \wedge dx^i \wedge dx^{s_4} \wedge \dots \wedge dx^{s_D}.\end{aligned}$$

Taking the pullback of β'_D to the spacetime manifold and then applying the inverse Higgs constraints in (3.61) gives a term proportional to

$$\epsilon_{ijs_3\dots s_D} \epsilon_{kls_3\dots s_D} \partial_{(a} \partial_b \phi \partial_c) \partial_j \partial_l \phi \partial_a \partial_b \phi \partial_c \partial_i \partial_k \phi.$$

One can verify that this is equivalent up to integration by parts and an overall prefactor to the invariant in (3.24).

$P=3$ Case: Let us focus on $N = 3$. Again, we start with $D = 2$. There is one independent cohomology element:

$$\begin{aligned}\Omega_3 &= \epsilon_{ij} (\omega_{ab} \wedge \omega_{ia} \wedge \omega_{jb} + 2\omega_a \wedge \omega_{ib} \wedge \omega_{jab} - 2\omega_a \wedge \omega_{ia} \wedge \omega_{jbb} \\ &\quad - \omega \wedge \omega_{iab} \wedge \omega_{jab} + \omega \wedge \omega_{iaa} \wedge \omega_{jbb}).\end{aligned}$$

It is quite a challenge to determine the potential, β_2 , for this Ω_3 . One can appreciate the power of the graphical method at this point: We have already determined that there is one independent 3-invariant with $N = 3$. Therefore, we can immediately conclude without calculation that the pullback of β_2 must be proportional to the invariant in (3.20) up to total derivatives. Again, Ω_3 can be generalized to $D \geq 2$ by wedging the appropriate number of $\omega_{\mathcal{P}}$'s on the end:

$$\begin{aligned}\Omega_{D+1} &= \epsilon_{ijs_3\dots s_D} (\omega_{ab} \wedge \omega_{ia} \wedge \omega_{jb} + 2\omega_a \wedge \omega_{ib} \wedge \omega_{jab} - 2\omega_a \wedge \omega_{ia} \wedge \omega_{jbb} \\ &\quad - \omega \wedge \omega_{iab} \wedge \omega_{jab} + \omega \wedge \omega_{iaa} \wedge \omega_{jbb}) \wedge \omega_{\mathcal{P}}^{s_3} \wedge \dots \wedge \omega_{\mathcal{P}}^{s_D}.\end{aligned}$$

Chapter 4

Cascading Multicriticality in Spontaneous Symmetry Breaking

Without Lorentz invariance, spontaneous global symmetry breaking can lead to multicritical Nambu-Goldstone modes with a higher-order low-energy dispersion $\omega \sim k^n$ ($n = 2, 3, \dots$), whose naturalness is protected by polynomial shift symmetries. Here we investigate the role of infrared divergences and the nonrelativistic generalization of the Coleman-Hohenberg-Mermin-Wagner (CHMW) theorem. We find novel cascading phenomena with large hierarchies between the scales at which the value of n changes, leading to an evasion of the “no-go” consequences of the relativistic CHMW theorem.

4.1. Introduction

Some of the most pressing questions about the fundamental laws of the Universe (such as the cosmological constant problem, or the hierarchy between the Higgs mass and the Planck scale) can be viewed as puzzles of technical naturalness [26]. In this chapter, we study the interplay of technical naturalness with spontaneous symmetry breaking (SSB) in nonrelativistic systems.

SSB is ubiquitous in Nature. For relativistic systems and global continuous internal symmetries, the universal features of SSB are controlled by the Goldstone theorem. Much progress in SSB has also been achieved in the nonrelativistic cases, where the reduced spacetime symmetries allow a much richer behavior, still very much the subject of active research (see e.g. [21, 22, 75, 76, 77, 78, 79] and references therein). Important novelties emerge already in the simplest case of theories in the flat nonrelativistic spacetime \mathbf{R}^{D+1} (covered with Cartesian coordinates (t, \mathbf{x}) , $\mathbf{x} \equiv (x^i, i = 1, \dots, D)$) and with the Lifshitz symmetries of spatial rotations and spacetime translations. In such theories, the Nambu-Goldstone (NG) modes can be of two distinct types: Type A, effectively described by a single real scalar $\phi(t, \mathbf{x})$ with a kinetic term quadratic in the time derivatives; or Type B, described by *two* scalar fields $\phi_{1,2}(t, \mathbf{x})$ which have a first-order kinetic term and thus form a canonical pair.

In [21, 22], we showed that this Type A-B dichotomy is further refined into two discrete families, labeled by a positive integer n : Type A_n NG modes are described by a single scalar

with dispersion $\omega \sim k^n$ (and dynamical critical exponent $z = n$), while Type B_{2n} modes are described by a canonical pair and exhibit the dispersion relation $\omega \sim k^{2n}$ (and dynamical exponent $z = 2n$). These two families are technically natural, and therefore stable under renormalization in the presence of interactions [21]. As usual, such naturalness is explained by a new symmetry. For $n = 1$, the NG modes are protected by the well-known constant shift symmetry $\delta\phi(t, \mathbf{x}) = b$. The $n > 1$ theories enjoy shift symmetries by a degree- P polynomial in the spatial coordinates [21],

$$\delta\phi(t, \mathbf{x}) = b + b_i x^i + \cdots + b_{i_1 \dots i_P} x^{i_1} \cdots x^{i_P}, \quad (4.1)$$

with suitable P . Away from the Type A_n and B_{2n} Gaussian fixed points, the polynomial shift symmetry is generally broken by most interactions. The lowest, least irrelevant interaction terms invariant under the polynomial shift were systematically discussed in [22] (see also [65]). Such terms are often highly irrelevant compared to all the other possible interactions that break the symmetry.

Having established the existence of the multicritical Type A and B families of NG fixed points, in this chapter we study the dynamics of flows between such fixed points in interacting theories. We uncover a host of novel phenomena, involving large, technically natural hierarchies of scales, protected again by the polynomial shift symmetries. As a given theory flows between the short-distance and the long-distance regime, it can experience a natural cascade of hierarchies, sampling various values of the dynamical critical exponent z in the process. Such cascades represent an intriguing mechanism for evading some of the consequences of the relativistic Coleman-Hohenberg-Mermin-Wagner (CHMW) Theorem.

4.2. The Relativistic CHMW Theorem

Recall that in relativistic systems, all NG bosons are of Type A_1 , assuming that they exist as well-defined quantum objects. Whether or not they exist, and whether or not the corresponding symmetry can be spontaneously broken, depends on the spacetime dimension. This phenomenon is controlled by a celebrated theorem, discovered independently in condensed matter by Mermin and Wagner [63] and by Hohenberg [62], and in high-energy physics by Coleman [61]. We therefore refer to this theorem, in the alphabetical order, as the CHMW theorem.

The relativistic CHMW theorem states that the spontaneous breaking of global continuous internal symmetries is not possible in $1 + 1$ spacetime dimensions. The proof is beautifully simple. $1 + 1$ is the “lower critical dimension,” where ϕ is formally dimensionless at the Gaussian fixed point. Quantum mechanically, this means that its propagator is logarithmically divergent, and we must regulate it by an infrared (IR) regulator μ_{IR} :

$$\begin{aligned} \langle \phi(x)\phi(0) \rangle &= \int \frac{d^2k}{(2\pi)^2} \frac{e^{ik \cdot x}}{k^2 + \mu_{\text{IR}}^2} \\ &\approx -\frac{1}{2\pi} \log(\mu_{\text{IR}}|x|) + \text{const.} + \mathcal{O}(\mu_{\text{IR}}|x|). \end{aligned} \quad (4.2)$$

The asymptotic expansion in (4.2), valid for $\mu_{\text{IR}}|x| \ll 1$, shows that as we take $\mu_{\text{IR}} \rightarrow 0$, the propagator stays sensitive at long length scales to the IR regulator. We can still construct

various composite operators from the derivatives and exponentials of ϕ , with consistent and finite renormalized correlation functions in the $\mu_{\text{IR}} \rightarrow 0$ limit, but the field ϕ itself does not exist as a quantum object. Since the candidate NG mode ϕ does not exist, the corresponding symmetry could never have been broken in the first place, which concludes the proof.

4.3. Nonrelativistic CHMW Theorem

For nonrelativistic systems with Type A_n NG modes, we find an intriguing nonrelativistic analog of the CHMW theorem. The scaling dimension of $\phi(t, \mathbf{x})$ at the A_n Gaussian fixed point, measured in the units of spatial momentum, is

$$[\phi(t, \mathbf{x})]_{A_n} = (D - n)/2. \quad (4.3)$$

The Type A_n field ϕ is at its lower critical dimension when $D = n$. Its propagator then requires an IR regulator. There are many ways how to introduce μ_{IR} ; for example, by modifying the dispersion relation of ϕ , as in

$$\langle \phi(t, \mathbf{x}) \phi(0) \rangle = \int \frac{d\omega d^D \mathbf{k}}{(2\pi)^{D+1}} \frac{e^{i\mathbf{k}\cdot\mathbf{x} - i\omega t}}{\omega^2 + |\mathbf{k}|^{2D} + \mu_{\text{IR}}^{2D}}, \quad (4.4)$$

or

$$\langle \phi(t, \mathbf{x}) \phi(0) \rangle = \int \frac{d\omega d^D \mathbf{k}}{(2\pi)^{D+1}} \frac{e^{i\mathbf{k}\cdot\mathbf{x} - i\omega t}}{\omega^2 + (|\mathbf{k}|^2 + \mu_{\text{IR}}^2)^D}. \quad (4.5)$$

Regardless of how μ_{IR} is implemented, as we take $\mu_{\text{IR}} \rightarrow 0$, the propagator again behaves logarithmically, both in space

$$\langle \phi(t, \mathbf{x}) \phi(0) \rangle \approx -\frac{1}{(4\pi)^{D/2} \Gamma(D/2)} \log(\mu_{\text{IR}} |\mathbf{x}|) + \dots \quad (4.6)$$

for $|\mathbf{x}|^D \gg t$, and in time,

$$\langle \phi(t, \mathbf{x}) \phi(0) \rangle \approx -\frac{1}{(4\pi)^{D/2} D \Gamma(D/2)} \log(\mu_{\text{IR}}^D t) + \dots \quad (4.7)$$

for $|\mathbf{x}|^D \ll t$. The propagator remains sensitive to the IR regulator μ_{IR} . Consequently, we obtain the *nonrelativistic multicritical CHMW theorem for Type A modes*:

The propagator of the Type A_n would-be NG mode $\phi(t, \mathbf{x})$ at its lower critical dimension $D = n$ is logarithmically sensitive to μ_{IR} , and therefore $\phi(t, \mathbf{x})$ does not exist as a quantum mechanical object. Consequently, no spontaneous symmetry breaking with Type A_n NG modes is possible in $D = n$ spatial dimensions.

By extension, this invalidates all Type A_n would-be NG modes with $n > D$, whose propagator would also be pathological at long distances.

In contrast, the scaling dimension of the Type B_{2n} fields is ¹

$$[\phi_{1,2}(t, \mathbf{x})]_{B_{2n}} = D/2, \quad (4.8)$$

¹Here we have assumed that both components of the canonical Type B pair $\phi_{1,2}$ carry the same dimension. The more general case would only require the sum of their dimensions to equal D , still preventing a logarithmic IR divergence in $\langle \phi_1 \phi_2 \rangle$.

and the lower critical dimension is $D = 0$. Hence, in all spatial dimensions $D > 0$, the Type B_{2n} NG modes are free of IR divergences and well-defined quantum mechanically for all $n = 1, 2, \dots$. The *nonrelativistic multicritical CHMW theorem for Type B modes* then simply states that *the Type B_{2n} symmetry breaking is possible in any $D > 0$ and for any $n = 1, 2, \dots$*

In the special cases for Type A_2 and Type B_2 NG modes, the multicritical CHMW theorems stated above reproduce the results reported in [80].

4.4. Cascading Multicriticality

Whereas in the relativistic case, all NG modes must always be of Type A_1 , in nonrelativistic systems the existence of the Type A_n and B_{2n} families allows a much richer dynamical behavior.

For example, with the changing momentum or energy scales, a given NG mode can change from Type A_n (or B_{2n}) to Type $A_{n'}$ (or $B_{2n'}$) with $n \neq n'$, or it could change from Type A to Type B. The hierarchies of scales that open up in this process are naturally protected by the corresponding polynomial symmetries. One of the simplest cases is the Type A_n scalar with $n > 1$, whose polynomial shift symmetry of degree P is broken at some momentum scale μ to the polynomial shift symmetry of degree $P - 2$, by some small amount $\varepsilon \ll 1$. This breaking modifies the dispersion relation to $\omega^2 \approx k^{2n} + \zeta_{n-1}^2 k^{2n-2}$, with $\zeta_{n-1}^2 \approx \varepsilon \mu^2$. Here, as in [26], we identify μ as the scale of naturalness. At a hierarchically much smaller scale, $\mu_\times \equiv \mu\sqrt{\varepsilon}$, the system exhibits a crossover, from Type A_n above μ_\times to Type A_{n-1} below μ_\times . The technical naturalness of the large hierarchy $\mu_\times \ll \mu$ is protected by the restoration of the polynomial shift symmetry of degree P as $\varepsilon \rightarrow 0$.

In the special case of $n = D$, this crossover from Type A_D to Type A_{D-1} yields an intriguing mechanism for evading the naive conclusion of our CHMW theorem. For a large range of scales close to μ , the would-be NG mode can exhibit a logarithmic propagator. The hierarchically smaller scale $\mu_\times \ll \mu$ then serves as a natural IR regulator, allowing the NG mode to cross over to Type A_{D-1} at very long distances. Therefore, the mode is well-defined as a quantum mechanical object, despite the large hierarchy across which it behaves effectively logarithmically.

An interesting refinement of this scenario comes from breaking the polynomial symmetries hierarchically, in a sequence of partial breakings, from a higher polynomial symmetry of degree P to symmetries with degrees $P' < P$, $P'' < P'$, \dots , all the way to constant shift. This gives rise to a cascading phenomenon, with a hierarchy of crossover scales $\mu \gg \mu' \gg \mu'' \gg \dots$, separating plateaux governed by the fixed points with the dynamical exponent taking the corresponding different integer values. Again, such cascading hierarchies are technically natural, and protected by the underlying breaking pattern of the polynomial symmetries.

Before we illustrate this behavior in a series of examples, it is worth pointing out one very simple yet important feature of large hierarchies in nonrelativistic theories. Consider a theory dominated over some range of scales by the dispersion relation $\omega \approx k^n$, with $n > 1$. If we open up a large hierarchy of momentum scales $\mu \gg \mu'$ (say by N orders of magnitude), this hierarchy of momentum scales gets magnified into an even larger hierarchy in energy

scales (by nN orders of magnitude).

4.5. Examples

First, we will demonstrate an example of the hierarchy with a system that starts out near the $z = 2$ fixed point at high energies and flows towards the $z = 1$ fixed point. Next, we show a bona fide cascade from $z = 3$ to $z = 2$ and then to $z = 1$. Finally, we describe a system which exhibits a hierarchy between Type A and Type B.

4.5.1. Type-A Hierarchy

The first model that we use to illustrate the hierarchy is a relatively well-known system in $2 + 1$ dimensions: the $z = 2$ Gaussian model of a single Lifshitz scalar field $\phi(t, \mathbf{x})$, with a derivative 4-point self-interaction turned on [81, 82]:

$$S_2 = \frac{1}{2} \int dt d^2 \mathbf{x} \left\{ \dot{\phi}^2 - (\partial^2 \phi)^2 - c^2 \partial_i \phi \partial_i \phi - g (\partial_i \phi \partial_i \phi)^2 \right\}.$$

This action contains all the marginal and relevant terms of the $z = 2$ fixed point consistent with the constant shift symmetry and the reflection symmetry $\phi \rightarrow -\phi$. At the $z = 2$ Gaussian fixed point, g is classically marginal, and breaks the polynomial shift symmetry of this fixed point to constant shift. Quantum corrections at one loop turn g marginally irrelevant [81].

This system allows a natural hierarchy of scales, stable under quantum corrections. At the naturalness scale μ , we can break the polynomial shift symmetry of the $z = 2$ fixed point to constant shifts by a small amount $\varepsilon_1 = 0 \ll 1$. This implies $g \sim \varepsilon_0$ and $c^2 \sim \varepsilon_0 \mu^2$, relations which can be shown to be respected by the loop corrections. In particular, c^2 can stay naturally small, much less than μ^2 . The dispersion relation changes from $z = 2$ close to the high scale μ , to $z = 1$ around the much lower scale $\mu_1 \equiv \mu \sqrt{\varepsilon_0} \ll \mu$.

4.5.2. Type-A Cascade

Our next example is a new model, which not only illustrates the cascading hierarchy with multiple crossovers, but also exhibits additional intriguing renormalization properties of independent interest.

We start with the Gaussian $z = 3$ fixed point of a single scalar $\Phi(t, \mathbf{x})$ in $3 + 1$ dimensions, and turn on derivative self-interactions and relevant terms as in our previous example. The free theory is

$$S_3 = \frac{1}{2} \int dt d^3 \mathbf{x} \left\{ \dot{\Phi}^2 - \zeta_3^2 (\partial_i \partial_j \partial_k \Phi) (\partial_i \partial_j \partial_k \Phi) - \zeta_2^2 (\partial^2 \Phi)^2 - c^2 \partial_i \Phi \partial_i \Phi \right\}. \quad (4.9)$$

At the classical level we can set $\zeta_3^2 = 1$ by the rescaling of space. The terms on the second line represent relevant Gaussian deformations away from the $z = 3$ fixed point. The spectrum of available self-interaction operators that are classically marginal or relevant at the $z = 3$ Gaussian fixed point is much richer than in our $2 + 1$ dimensional example. We

shall again restrict our attention only to the operators even under $\Phi \rightarrow -\Phi$, and invariant at least under the constant shift. Up to total derivatives, which we ignore, there are three independent marginal 4-point operators $\mathcal{O}_4^{(a)}$, $a = 1, 2, 3$, one marginal 6-point operator $\mathcal{O}_6 = (\partial_i \Phi \partial_i \Phi)^3$, and one relevant 4-point operator

$$\mathcal{W} = (\partial_i \Phi \partial_i \Phi)^2. \quad (4.10)$$

Among them, there is one unique operator \mathcal{O} invariant under the linear shift symmetry up to a total derivative:

$$\begin{aligned} \mathcal{O} &= 4\partial_i \partial_j \partial_k \Phi \partial_i \Phi \partial_j \Phi \partial_k \Phi + 12\partial_i \Phi \partial_i \partial_j \Phi \partial_j \partial_k \Phi \partial_k \Phi \\ &= 4 \begin{array}{c} \bullet \\ | \\ \bullet \\ | \\ \bullet \end{array} \begin{array}{c} \bullet \\ / \\ \bullet \\ | \\ \bullet \end{array} + 12 \begin{array}{c} \bullet \\ | \\ \bullet \\ | \\ \bullet \end{array} \begin{array}{c} \bullet \\ | \\ \bullet \\ | \\ \bullet \end{array}, \end{aligned} \quad (4.11)$$

cf. Fig.(3.1a). This operator is classically marginal.

To construct our model, we start with the free theory S_3 and turn on just the unique linear-shift invariant self-interaction \mathcal{O} , with coupling λ . The Feynman rules of this model involve one 4-vertex, which can be simplified using the condition of momentum conservation $\mathbf{k}_4 = -\mathbf{k}_1 - \mathbf{k}_2 - \mathbf{k}_3$ to

$$\begin{array}{c} \omega_4, \mathbf{k}_4 \\ \swarrow \quad \searrow \\ \omega_1, \mathbf{k}_1 \quad \omega_2, \mathbf{k}_2 \\ \nearrow \quad \nwarrow \\ \omega_3, \mathbf{k}_3 \end{array} = \begin{aligned} &-i\lambda [k_1^2 k_2^2 k_3^2 + 2(\mathbf{k}_1 \cdot \mathbf{k}_2)(\mathbf{k}_2 \cdot \mathbf{k}_3)(\mathbf{k}_3 \cdot \mathbf{k}_1) \\ &- k_1^2 (\mathbf{k}_2 \cdot \mathbf{k}_3)^2 - k_2^2 (\mathbf{k}_3 \cdot \mathbf{k}_1)^2 - k_3^2 (\mathbf{k}_1 \cdot \mathbf{k}_2)^2]. \end{aligned} \quad (4.12)$$

Note that in this vertex, each momentum appears quadratically, with no subleading terms. We can write it even more compactly with the use of the fully antisymmetric ϵ_{ijk} tensor: if for any three momenta $\mathbf{k}, \mathbf{p}, \mathbf{q}$ we define $[\mathbf{k}\mathbf{p}\mathbf{q}] \equiv \epsilon_{ijk} k_i p_j q_k$, our vertex becomes simply

$$-i\lambda [\mathbf{k}_1 \mathbf{k}_2 \mathbf{k}_3]^2. \quad (4.13)$$

This simple vertex structure is intimately related to the underlying symmetries: When translated into momentum space, the linear shift symmetry $\delta\phi(t, \mathbf{x}) = b_i x^i + b$ becomes a shift of the Fourier modes $\phi(t, \mathbf{k})$ by $b_i (\partial/\partial \mathbf{k}_i) \delta(\mathbf{k}) + b \delta(\mathbf{k})$. Acting with this symmetry on any of the legs of the vertex produces zero, as the vertex is purely quadratic in each of the outside momenta.

Quantum properties. This model has intriguing renormalization group properties, which will be discussed in the next chapter. First, note that λ satisfies a non-renormalization theorem: Consider the $2N$ -point function of Φ , with $N > 1$, and with external momenta $\mathbf{k}_1, \dots, \mathbf{k}_{2N}$. Any 1PI diagram will be of the form $k_1^{i_1} k_1^{j_1} \dots k_{2N}^{i_{2N}} k_{2N}^{j_{2N}} \cdot \mathcal{I}_{i_1 j_1 \dots i_{2N} j_{2N}}(\mathbf{k}_1, \dots, \mathbf{k}_{2N})$. The factor \mathcal{I} has no ultraviolet divergences, and with $c^2 \neq 0$ or $\zeta_2^2 \neq 0$ it approaches a finite value at $\mathbf{k}_1 = \dots = \mathbf{k}_{2N} = 0$. The special case of $N = 2$ implies that λ does not get renormalized, at any loop order. Note also that none of the operators \mathcal{W} , \mathcal{O}_6 or $\mathcal{O}_4^{(a)}$ that would break the linear shift symmetry is generated by the loop corrections.

The remarkable non-renormalization of λ does not imply that the effective strength of the self-interaction would be independent of scale: There is a non-trivial renormalization

of the 2-point function. While the one-loop diagram $\underline{\bigcirc}$ is identically zero, the two-loop diagram $\text{---}\bigcirc\text{---}$ gives the generic behavior which persists at higher loops: There is no wave-function renormalization, no renormalization of c^2 , the loop corrections to ζ_2^2 are quadratically divergent, and those to ζ_3^2 diverge logarithmically [24]. This log divergence effectively corrects the dynamical exponent of the ultraviolet fixed point away from the classical value $z = 3$. The modified scaling in turn implies that the theory becomes effectively strongly coupled at some finite scale μ_s .

Having understood the quantum corrections, we can now study cascading hierarchies of symmetry breaking in this model, and confirm their technical naturalness. At some high scale μ , which will be our naturalness scale, and which we keep below μ_s , consider the following hierarchical breaking of polynomial symmetries: First, break the $P = 4$ symmetry of the $z = 3$ Gaussian fixed point to the $P = 2$ symmetry of the $z = 2$ fixed point by some small amount $\varepsilon_2 \ll 1$. Then break $P = 2$ to $P = 1$ by an even smaller amount $\varepsilon_1 \ll \varepsilon_2$. This pattern corresponds to

$$\zeta_3^2 \approx 1, \quad \zeta_2^2 \approx \mu^2 \varepsilon_2, \quad c^2 \approx \mu^4 \varepsilon_1, \quad \lambda \approx \varepsilon_1. \quad (4.14)$$

The dispersion relation cascades from $z = 3$ at high energy scales, to $z = 2$ at intermediate scales, to $z = 1$ at low scales.² Both the large hierarchies in (4.14) and the cascading behavior of the dispersion relation are respected by all loop corrections, and therefore are technically natural. This follows by inspection from the properties of the quantum corrections discussed above.

4.5.3. Type-A/Type-B Hierarchy

So far, we focused on the cascading mechanism in the Type A case. Type B systems can form their own hierarchies, in the obvious generalization of the Type A cascades exemplified above. There is no analog of the lower critical dimension and the CHMW limit on n . Type A NG modes can also exhibit a flow to Type B. This behavior, albeit not new (see e.g. [83]), can be embedded as one step into the more general technically natural hierarchies of Type A or B as discussed above. In particular, the crossover to Type B can provide a new IR regulator of the Type A cascade at the lower critical dimension.

We shall illustrate this on the simplest Type A₁ example, although the full story is, of course, more general. Consider two would-be Type A NG fields, $\phi_{1,2}(t, \mathbf{x})$, in the vicinity of the $z = 1$ Gaussian fixed point

$$S_1 = \frac{1}{2} \int dt d^D \mathbf{x} \left\{ \dot{\phi}_1^2 + \dot{\phi}_2^2 - c_1^2 (\partial_i \phi_1)^2 - c_2^2 (\partial_i \phi_2)^2 \right\}.$$

For simplicity, we will set $c_1 = c_2 = 1$, although this is not necessary for our argument. Besides the rotations and translations of the two scalars, note two independent \mathbf{Z}_2 symmetries – the field reflection $R: (\phi_1, \phi_2) \rightarrow (\phi_1, -\phi_2)$, and the time reversal $\mathcal{T}: t \rightarrow -t$,

²We can also break the linear shift symmetry to constant shifts, by some amount $\varepsilon_0 \ll \varepsilon_1$. This would generate the remaining classically marginal operators $\mathcal{O}_4^{(a)}$, \mathcal{O}_6 and the relevant operator \mathcal{W} , with coefficients of order ε_0 in the units of μ .

$\phi_{1,2}(t, \mathbf{x}) \rightarrow \phi_{1,2}(-t, \mathbf{x})$. We can now turn on the Type B kinetic term,

$$S' = S_1 + \frac{\Omega}{2} \int dt d^D \mathbf{x} \left(\phi_1 \dot{\phi}_2 - \phi_2 \dot{\phi}_1 \right). \quad (4.15)$$

Ω now provides an IR regulator for the propagator. At that scale, the field reversal R and the time reversal \mathcal{T} are broken to their diagonal subgroup. At energy scales below Ω , one of the would-be Type A NG modes survives and turns into the Type B NG mode, while the other would-be Type A mode develops a gap set by Ω (see Appendix 4.A). Note that in $1+1$ dimensions, the “no-go” consequences of the relativistic CHMW theorem are again naturally evaded by this hierarchy: a NG mode exists quantum mechanically after all, and symmetry breaking is possible, despite the fact that above the scale Ω , the two would-be Type A modes exhibit the logarithmic two-point function suggesting that symmetry breaking may not be possible.

The hierarchy between the Type A and Type B behavior is also protected by symmetries. In fact, the system has multiple symmetries that can do this job. One can rely on the breaking pattern of the discrete symmetries R and \mathcal{T} mentioned above. If the Type A system is Lorentz invariant, one can use Lorentz symmetry breaking to protect small Ω . More interestingly, without relying on the discrete or Lorentz symmetries, one can introduce a shift symmetry linear in time, $\delta\phi_{1,2} = b_{1,2}t$. While the Type A kinetic term is invariant under this symmetry, the Type B kinetic term is not. Breaking the linear shift symmetry to constant shifts allows the Type-A/Type-B crossover scale to be hierarchically smaller than the naturalness scale.

4.6. Outlook

We have seen that the multicritical Type A_n and B_{2n} NG modes can experience technically natural cascading hierarchies of scales, protected by a hierarchy of polynomial shift symmetries. Perhaps the most interesting case is Type A with $n = D$, which according to our CHMW theorem exhibits logarithmic sensitivity to the IR regulator. In the relativistic case, this would prevent the symmetry breaking. We have shown that the Type A_D modes can experience a cascade to Type A_n with $n < D$ (or to Type B), which provides a natural IR regulator, thus making the symmetry breaking possible after all.

Our original motivation for this study of technical naturalness and hierarchies in SSB came from quantum gravity and high-energy physics [21, 22]. Besides extending our understanding of the general “landscape of naturalness,” we expect that our results could find their most immediate applications in two other areas: In condensed matter physics, and in effective field theory of inflationary cosmology [84, 85, 86]. Both areas treat systems with nonrelativistic, Lifshitz-like symmetries similar to ours. In condensed matter, the multicriticality of NG modes will affect their thermodynamic and transport properties; for example, the Type A_D modes at the lower critical dimension will exhibit specific heat linear in temperature T over the range of T dominated by the $z = D$ dispersion (up to $\log T$ corrections due to self-interactions). In the context of inflation, our self-interacting scalar field theories represent a new nonrelativistic variation on the theme of the Galileon [60], an extension of the $z = 2$ ghost condensate [87], and of the $z = 3$ cosmological scalar theory [12, 88].

Appendix

4.A. A Flow from Type-A to Type-B

In this appendix, we will show the explicit calculation demonstrating the flow between two would-be gapless Type-A modes at high energies to one gapped Type-A mode and one gapless Type-B mode at low energies.

Let the two would-be Type A NG fields be $\phi_{1,2}(t, \mathbf{x})$. The most general form of the quadratic Lagrangian in the vicinity of the $z = 1$ Gaussian fixed point compatible with Lifshitz symmetries would consist of the terms $\Omega_{IJ}\phi_I\dot{\phi}_J$, $g_{IJ}\dot{\phi}_I\dot{\phi}_J$ and $h_{IJ}\partial_i\phi_I\partial_i\phi_J$, where Ω_{IJ} , g_{IJ} and h_{IJ} are constant in spacetime, two-forms in the two-dimensional space of fields, and Ω_{IJ} is antisymmetric and g_{IJ} and h_{IJ} are symmetric. One can use the $GL(2, \mathbf{R})$ symmetry group of arbitrary linear reparametrizations in field space to set $g_{IJ} = \delta_{IJ}$. The $SO(2)$ subgroup remains under which δ_{IJ} is unchanged. One can use this residual symmetry to diagonalize h_{IJ} . Furthermore, due to its antisymmetry, Ω_{IJ} takes the general form $\Omega\epsilon_{IJ}$, where ϵ_{IJ} is the Levi-Civita symbol, in *any* basis in field space. Therefore, without loss of generality, we take the action to be

$$S = \frac{1}{2} \int dt d^D \mathbf{x} \left\{ \delta_{IJ} \dot{\phi}_I \dot{\phi}_J - c_I^2 \delta_{IJ} \partial_i \phi_I \partial_i \phi_J + \Omega \epsilon_{IJ} \phi_I \dot{\phi}_J \right\}. \quad (4.16)$$

In fact, we have enough freedom in rescaling space to set one of the speed parameters equal to unity. In addition, as far as the Type-A/Type-B hierarchy is concerned, there is no particular loss in generality in setting $c_1 = c_2 = 1$. However, in this appendix, we will keep these parameters general.

In Fourier space, one finds

$$S = \frac{1}{2} \int \frac{d\omega}{2\pi} \frac{d^D k}{(2\pi)^D} \left\{ (\omega^2 - c_I^2 k^2) \delta_{IJ} + i\Omega\omega\epsilon_{IJ} \right\} \tilde{\phi}_I(\omega, \mathbf{k}) \tilde{\phi}_J(-\omega, -\mathbf{k}). \quad (4.17)$$

Setting to zero the eigenvalues of the matrix multiplying the two fields yields the dispersion relations of the two independent physical modes. The small momentum expansions of these dispersion relations are

$$\omega^2 = \Omega^2 + (c_1^2 + c_2^2)k^2, \quad (4.18a)$$

$$\omega^2 = \frac{c_1^2 c_2^2}{\Omega^2} k^4. \quad (4.18b)$$

Hence, we observe that one would-be Type-A₁ NG mode develops a gap equal to Ω and keeps the $z = 1$ scaling behavior, whereas the other turns into a true gapless NG mode that is Type-B₂.

Chapter 5

The $z=3$ Scalar Field with a Linear-Shift Invariant Interaction

We revisit the theory considered in §4.5.2 of a scalar field theory in the vicinity of the $z = 3$ fixed point with a four-point linear-shift invariant interaction. We previously studied this theory for the Type A cascade that it exhibits. However, this theory also exhibits very interesting properties under renormalization group flow. The purpose of this chapter is to bring these properties to light. Although the techniques described herein are not new, this chapter represents a significant step forward by applying the main renormalization methods to theories with Lifshitz scaling and demonstrating their mutual consistency. Furthermore, we show that, in fact, there exists a continuum of different, but consistent, interpretations of the behavior of such theories under renormalization.

5.1. Introduction

In the previous chapter, we demonstrated a Type A cascade in a theory of a single scalar field in the vicinity of the $z = 3$ Gaussian fixed point at high energies, to the $z = 2$ fixed point at intermediate energies, and finally to the $z = 1$ fixed point at low energies. The renormalization of the theory is driven by the one four-point interaction which is invariant under the linear shift. We are met with some interesting subtleties in applying the standard techniques of renormalization to this theory.

The theory, including counterterms, and Wick-rotated to Euclidean signature, is

$$S = \frac{1}{2} \int dt d^3x \left\{ (1 + \delta) \dot{\phi}^2 + (1 + \delta_\zeta) \zeta^2 \partial^2 \partial_i \phi \partial^2 \partial_i \phi + \dots \right. \\ \left. + (1 + \delta_\lambda) \frac{\lambda}{12} \varepsilon^{ijk} \varepsilon^{lmn} \partial_i \phi \partial_\ell \phi \partial_j \partial_m \phi \partial_k \partial_n \phi \right\}, \quad (5.1)$$

where \dots refers to relevant lower- z deformations, which we will ignore. δ , δ_{ζ^2} and δ_λ are counterterms. By default, we set the engineering dimension of the spatial coordinates x^i to -1 . It follows that the engineering dimensions of ϕ , ζ and λ are respectively

$$[\phi] = \frac{1}{2} (3 - z), \quad [\zeta] = z - 3, \quad [\lambda] = 3(z - 3). \quad (5.2)$$

Classically, the dynamical exponent z equals 3, in which case the classical engineering dimensions of ϕ , ζ and λ all vanish. Unsurprisingly, this property is not preserved under renormalization.

5.2. Feynman Rules and Diagrams

The tree level propagator is

$$D(\omega, \mathbf{p}) \equiv \overrightarrow{\omega, \mathbf{p}} = \frac{1}{\omega^2 + \zeta^2 p^6 + \mu_{\text{IR}}^6}, \quad (5.3a)$$

where we have introduced a gap μ_{IR} as an IR regulator.

The 4-point vertex is

$$\begin{array}{c} p_2 \quad p_3 \\ \diagdown \quad / \\ \diagup \quad \diagdown \\ p_1 \quad p_4 \end{array} = -i^6 \lambda [p_1 p_3 p_4] [p_2 p_3 p_4] = \lambda [p_1 p_3 p_2] [p_2 p_3 p_1] = -\lambda [p_1 p_2 p_3]^2, \quad (5.4)$$

where

$$[p_1 p_2 p_3] = \varepsilon^{ijk} p_1^i p_2^j p_3^k. \quad (5.5)$$

The form of the vertex implies that any diagram that contains a cactus subgraph vanishes identically. The only 1-loop contribution to the 2-point Green's function is a cactus diagram, which therefore vanishes:

$$\begin{array}{c} \text{---} \text{---} \\ \text{---} \text{---} \end{array} = 0. \quad (5.6)$$

The 1-loop contribution to the vertex is

$$\begin{array}{c} \diagdown \quad / \\ \text{---} \text{---} \\ \diagup \quad \diagdown \end{array} \quad (5.7)$$

The form of the vertex implies that this diagram does not contribute to the λ term in the Lagrangian, which has four ϕ 's and six spatial derivatives. Instead, the first nontrivial contribution is to a term with four ϕ 's and eight spatial derivatives, which is irrelevant. In addition, the contribution of this diagram to this latter term is finite.

The only non-cactus 2-loop diagram contributing to the 2-point Green's function is the sunset diagram:

$$\mathcal{I} = \begin{array}{c} \nu_1, \mathbf{k}_1 \\ \text{---} \text{---} \\ \text{---} \text{---} \\ \nu_2, \mathbf{k}_2 \end{array} \omega, \mathbf{p} \quad (5.8)$$

This diagram evaluates to

$$\mathcal{I} = \frac{1}{3!} \int \frac{d\nu_{1,2} d^3 k_{1,2}}{(2\pi)^8} (-\lambda [p k_1 k_2]^2)^2 D(\nu_1, \mathbf{k}_1) D(\nu_2, \mathbf{k}_2) D(\nu + \omega, \mathbf{k} + \mathbf{p}), \quad (5.9)$$

where $\nu = \nu_1 + \nu_2$ and $\mathbf{k} = \mathbf{k}_1 + \mathbf{k}_2$.

The numerator of this integral already contains a factor of p^4 and therefore the contributions to the operators $\dot{\phi}^2$ and $(\partial\phi)^2$ vanish. One can check that the contribution to the operator $(\partial^2\phi)^2$ has a quadratic superficial degree of divergence.

To extract the quantum corrections to ζ^2 , we need the piece proportional to p^6 . This requires the order p^2 term in the final propagator in (5.9):

$$D(\nu + \omega, \mathbf{k} + \mathbf{p}) = D(\nu, \mathbf{k}) - \frac{\zeta^2(3p^2k^4 + 12(\mathbf{p} \cdot \mathbf{k})^2k^2) + \dots}{(\nu^2 + \zeta^2k^6 + \mu_{\text{IR}}^6)^2} + \mathcal{O}(p^4). \quad (5.10)$$

The terms proportional to ζ^2p^2 have a logarithmic superficial degree of divergence. The terms in \dots would be present if we included the operators $(\partial^2\phi)^2$ and $(\partial\phi)^2$ from the start. However, they involve fewer powers of the internal momenta and are thus finite.

Let $\mathcal{I}^{(6)}$ denote the contribution of (5.9) that is of order p^6 . By power counting, $\mathcal{I}^{(6)}$ is logarithmically divergent. A priori, it could contain multi-logs if, for example, the integral over ν_2 and \mathbf{k}_2 were itself divergent. However, this latter integral is of the same type as the 1-loop diagram in (5.7), which is finite. Therefore, $\mathcal{I}^{(6)}$ contains logs but no multi-logs.

To extract the high-energy behavior of the integral \mathcal{I} , we can take a UV momentum cutoff Λ . Since the integrand in \mathcal{I} is positive and the expansion of the propagator in (5.10) generates a minus sign, $\mathcal{I}^{(6)}$ is proportional to $-\log \Lambda^2$. Furthermore, rotational symmetry in the external momentum \mathbf{p} implies that $\mathcal{I}^{(6)}$ is proportional to p^6 . Therefore,

$$\mathcal{I}^{(6)} = -B\lambda^2\zeta^2p^6 \log\left(\frac{\Lambda^2}{\mu^2}\right), \quad (5.11)$$

where B is a positive coefficient and μ is some parameter that absorbs the dimension of Λ . Since the theory under consideration is gapless, μ is a function of the frequency ω and the momentum \mathbf{p} (actually, of p^2 , due to rotation symmetry).

In the $\omega = 0$ limit, the random phase approximation (RPA) result for the 2-point Green's function is

$$G^{(2)}(\omega = 0, \mathbf{p}) = \frac{1}{\zeta^2p^6} + \left(\frac{1}{\zeta^2p^6}\right)^2 \Sigma + \dots + \left(\frac{1}{\zeta^2p^6}\right)^{n+1} \Sigma^n + \dots = \frac{1}{\zeta^2p^6 - \Sigma}, \quad (5.12)$$

with

$$\Sigma = \mathcal{I} - \delta_{\zeta^2} + \mathcal{O}(\lambda^3). \quad (5.13)$$

Hence, the inverse propagator is

$$\Gamma(\omega, \mathbf{p}) = (1 + \delta)\omega^2 + \zeta^2p^6 \left[1 + B\lambda^2 \log\left(\frac{\Lambda^2}{\mu^2}\right) + \delta_{\zeta^2} + \mathcal{O}(\lambda^3) \right]. \quad (5.14)$$

Next, we consider the correction to the 4-point Green's function. There is no contribution to the vertex factor itself. We can generalize the argument we gave to show that the diagram (5.7) does not contribute to λ . Any diagram with n external legs contributes to Lagrangian terms involving n ϕ 's and at least $2n$ spatial derivatives. Immediately, we can conclude that no diagram can contribute to the operators $\dot{\phi}^2$, $(\partial\phi)^2$ or to the λ interaction

term. However, the 4-point Green's function is not amputated – the 2-loop contribution to it is

$$\mathcal{T} = \begin{array}{c} \diagup \\ \diagdown \\ \circ \end{array} + \text{permutations}, \quad (5.15)$$

which is logarithmically divergent.

Omitting the IR regulator, the diagram at zero frequency is

$$\begin{aligned} \mathcal{T} &= \left[-B\lambda^2 \zeta^2 p_1^6 \log\left(\frac{\Lambda^2}{\mu^2}\right) \right] \left(\frac{1}{\zeta^2 p_1^6} \right) (-\lambda [p_1 p_2 p_3]^2) \prod_{\alpha=1}^4 \frac{1}{\zeta p_\alpha^6} + \text{permutations} \\ &= 4B\lambda^3 \log\left(\frac{\Lambda^2}{\mu^2}\right) [p_1 p_2 p_3]^2 \prod_{\alpha=1}^4 \frac{1}{\zeta p_\alpha^6}, \end{aligned} \quad (5.16)$$

Therefore, the 4-point Green's function is

$$\begin{aligned} G^{(4)}(\omega = 0, \mathbf{p}) &= \left([p_1 p_2 p_3]^2 \prod_{\alpha=1}^4 \frac{1}{\zeta p_\alpha^6} \right) \\ &\times \left[-\lambda + 4\lambda \left(B\lambda^2 \log\left(\frac{\Lambda^2}{\mu^2}\right) + \delta_{\zeta^2} \right) + \delta_\lambda + \mathcal{O}(\lambda^4) \right]. \end{aligned} \quad (5.17)$$

5.3. The Renormalization Group

We will now perform the analysis of the renormalization group flow of this theory. Since some interesting subtleties arise, we will perform the analysis using the Wilsonian approach, the Callan-Symanzik equation, and the methods of dimensional regularization and the $\overline{\text{MS}}$ renormalization scheme. We will explicitly show the consistency among these standard techniques and demonstrate the existence of a continuum of different, but mutually consistent, physical interpretations of the renormalization group flow.

5.3.1. Renormalization Conditions

In the action (5.1) we have the freedom to rescale space and time such that $\zeta = 1$ classically. We then take the renormalization conditions for the inverse propagator Γ as

$$\left. \frac{\partial \Gamma(\omega, \mathbf{p})}{\partial (\omega^2)} \right|_{\omega=0, \mu=M} = 1, \quad (5.18a)$$

$$\left. \frac{\partial \Gamma(\omega, \mathbf{p})}{\partial (p^6)} \right|_{\omega=0, \mu=M} = 1. \quad (5.18b)$$

Here M sets the renormalization group scale. Furthermore, since there is no renormalization to the coupling λ , we have no need to introduce the counterterm δ_λ in the first place. Since μ is a function of ω and \mathbf{p} , the renormalization conditions are evaluated at $\mu(\omega = 0, \mathbf{p}) = M$.

We apply the above renormalization group conditions to (5.14). From (5.18a) we obtain $\delta = 0 + \mathcal{O}(\lambda^3)$. From (5.18b) we obtain

$$\left. \frac{\partial \Gamma(\omega, \mathbf{p})}{\partial (p^6)} \right|_{\omega=0, \mu=M} = \zeta^2 \left[1 + B\lambda^2 \log \left(\frac{\Lambda^2}{M^2} \right) + \delta_{\zeta^2} + \mathcal{O}(\lambda^3) \right] = 1, \quad (5.19)$$

i.e.,

$$\delta_{\zeta^2} = -B\lambda^2 \log \left(\frac{\Lambda^2}{M^2} \right) + \mathcal{O}(\lambda^3). \quad (5.20)$$

Note that ζ has been set to 1 at the renormalization group scale.

Therefore, the renormalized inverse propagator is

$$\Gamma(\omega, \mathbf{p}) = \omega^2 + p^6 \left[1 + B\lambda^2 \log \left(\frac{M^2}{\mu^2} \right) + \mathcal{O}(\lambda^3) \right]. \quad (5.21)$$

This in turn gives the 4-point Green's function:

$$G^{(4)}(\omega = 0, \mathbf{p}) = \left([p_1 p_2 p_3]^2 \prod_{\alpha=1}^4 \frac{1}{\zeta p_\alpha^6} \right) \left[-\lambda + 4B\lambda^3 \log \left(\frac{M^2}{\mu^2} \right) + \mathcal{O}(\lambda^4) \right]. \quad (5.22)$$

On the other hand, since the scaling between space and time need not be fixed any more, we have the freedom to introduce an arbitrary deviation for the dynamical exponent z away from its classical value of 3. This deviation is of order λ^2 since the quantum corrections only kick in at this order. Thus we can write

$$z = 3 - A\lambda^2 + \mathcal{O}(\lambda^3), \quad (5.23)$$

where A is some real number.

5.3.2. The Wilsonian Approach

In the Wilsonian approach, we integrate out the high-momentum modes lying in a thin momentum shell $\delta\Lambda$ around the cut-off Λ . Formally, the couplings will change, as a result.

$$S_{\text{eff}} = \frac{1}{2} \int dt d^3x \left[\dot{\phi}^2 - (\zeta^2 + \delta\zeta^2) \partial^2 \partial_i \phi \partial^2 \partial_i \phi - \dots \right. \\ \left. - \frac{1}{2} (\lambda + \delta\lambda) \varepsilon^{ijk} \varepsilon^{\ell mn} \partial_i \phi \partial_\ell \phi \partial_j \partial_m \phi \partial_k \partial_n \phi \right]. \quad (5.24)$$

As previously argued, $\delta\lambda = 0$ to all orders. From (5.14), we obtain

$$\delta\zeta^2 = \delta\Lambda \frac{\delta}{\delta\Lambda} \left[\zeta^2 B\lambda^2 \log \left(\frac{\Lambda^2}{\mu^2} \right) \right] = 2\zeta^2 B\lambda^2 \frac{\delta\Lambda}{\Lambda}. \quad (5.25)$$

To compare with the theory prior to integrating out the high-momentum modes, we rescale spacetime according to

$$t' = b^z t, \quad x' = bx, \quad (5.26)$$

with

$$b = e^{-\delta t}, \quad \delta t = \frac{\delta \Lambda}{\Lambda}. \quad (5.27)$$

We define the rescaling of the field ϕ according to

$$\phi' = b^{-h} \phi. \quad (5.28)$$

In terms of the rescaled variable t' and x' , the effective action (5.24) becomes

$$S_{\text{eff}} = \frac{1}{2} \int dt' d^3 x' b^{-z-3} \left[b^{2h+2z} (\dot{\phi}')^2 - (\zeta^2 + \delta \zeta^2) b^{2h+6} \partial^2 \partial_i \phi' \partial^2 \partial_i \phi' - \dots \right. \\ \left. - \frac{1}{12} \lambda b^{4h+6} \varepsilon^{ijk} \varepsilon^{\ell mn} \partial_i \phi' \partial_\ell \phi' \partial_j \partial_m \phi' \partial_k \partial_n \phi' \right], \quad (5.29)$$

where all derivatives are now with respect to the primed coordinates.

The requirement that the time derivative piece have unit coefficient translates to the condition

$$h = \frac{1}{2} (3 - z). \quad (5.30)$$

This parameter is the anomalous dimension of the field ϕ . Recalling (5.23), this gives

$$\gamma_\phi = h = \frac{1}{2} A \lambda^2 + \mathcal{O}(\lambda^3). \quad (5.31)$$

The effective action is then

$$S_{\text{eff}} = \frac{1}{2} \int dt' d^3 x' \left[(\dot{\phi}')^2 + \zeta'^2 \partial^2 \partial_i \phi' \partial^2 \partial_i \phi' + \frac{1}{12} \lambda' \varepsilon^{ijk} \varepsilon^{\ell mn} \partial_i \phi' \partial_\ell \phi' \partial_j \partial_m \phi' \partial_k \partial_n \phi' \right],$$

with

$$\zeta'^2 = (\zeta^2 + \delta \zeta^2) b^{-z+3+2h} = \zeta^2 [1 + 2(B - A) \lambda^2 \delta t + \mathcal{O}(\lambda^3)], \quad (5.32)$$

where use was made of $\delta \zeta^2$ given in (5.25), and

$$\lambda' = \lambda b^{-z+3+4h} = \lambda - 3A \lambda^3 \delta t + \mathcal{O}(\lambda^4). \quad (5.33)$$

(5.32) indicates that ζ slowly increases if $B - A > 0$ (or decreases if $B - A < 0$) as we integrate out high-momentum degrees of freedom, i.e.,

$$\gamma_\zeta \equiv \frac{d \log \zeta}{d \log M} = (A - B) \lambda^2 + \mathcal{O}(\lambda^3). \quad (5.34)$$

On the other hand, (5.33) implies that λ slowly increases if $A < 0$ (or decreases if $A > 0$) as we integrate out high-momentum degrees of freedom, i.e.,

$$\beta_\lambda = \frac{d \lambda}{d \log M} = 3A \lambda^3 + \mathcal{O}(\lambda^4). \quad (5.35)$$

In summary,

$$z = 3 - A \lambda^2 + \mathcal{O}(\lambda^3), \quad (5.36a)$$

$$\gamma_\phi = \frac{1}{2} A \lambda^2 + \mathcal{O}(\lambda^3), \quad (5.36b)$$

$$\gamma_\zeta = (A - B) \lambda^2 + \mathcal{O}(\lambda^3), \quad (5.36c)$$

$$\beta_\lambda = 3A \lambda^3 + \mathcal{O}(\lambda^4). \quad (5.36d)$$

5.3.3. The Callan-Symanzik Equation

In contrast to the Wilsonian approach, the Callan-Symanzik equation is derived from the requirement that the physics be insensitive to the renormalization group scale, M . We will generalize the Callan-Symanzik equation to account for the renormalization of the dynamical exponent z .

The n -point Green's function in position space is defined as

$$G^{(n)}(t_1, \dots, t_n, \mathbf{x}_1, \dots, \mathbf{x}_n) = \langle 0 | \phi(t_1, \mathbf{x}_1) \cdots \phi(t_n, \mathbf{x}_n) | 0 \rangle. \quad (5.37)$$

The n -point Green's function in momentum space is defined to be

$$G^{(n)}(\omega_i, \mathbf{p}_i) = \int \left(dt d^3 \mathbf{x} e^{i(\omega t - \mathbf{k} \cdot \mathbf{x})} \right)^{n-1} \langle 0 | \phi \cdots \phi | 0 \rangle, \quad (5.38)$$

where the coordinates t and \mathbf{x} denote collectively the spacetime coordinates. The power $n-1$ in $(d^3 t d^3 x)^n$ represents that there are in total $n-1$ spacetime integrals. Naively, there are in total n pairs of independent spacetime integrals to do in order to obtain the Green's function in the Fourier space, but we should note that there also exist conservation laws of the overall frequency and momentum,

$$\sum_i \omega_i = 0, \quad \sum_i \mathbf{k}_i = 0, \quad (5.39)$$

which leave only $n-1$ pairs of independent spacetime integrals.

In relativistic theories, the bare Green's function $G_0^{(n)}$ and the physical Green's function $G^{(n)}$ differ by the field redefinition. More precisely, the relationship between the bare and physical field is

$$\phi_0 = Z_\phi^{1/2} \phi, \quad (5.40)$$

implying that

$$G_0^{(n)} = Z_\phi^{n/2} G^{(n)} \quad (5.41)$$

Here Z_ϕ determines the anomalous dimension of ϕ

$$\gamma_\phi = \frac{1}{2} \frac{d \log Z_\phi}{d \log M}. \quad (5.42)$$

This is not the entire story for Lifshitz theories. In the presence of the running dynamical exponent z given by (5.23), the temporal coordinate gains an anomalous dimension

$$\gamma_t = (-z) - (-3) = A\lambda^2 + \mathcal{O}(\lambda^3). \quad (5.43)$$

Note that we are sticking to the convention in which the dimension of each spatial coordinate is -1 . Furthermore, the anomalous dimension of the temporal coordinate can be interpreted as the rescaling of time:

$$t_0 = Z_t t, \quad (5.44)$$

where Z_t determines the anomalous dimension via

$$\gamma_t = \frac{d \log Z_t}{d \log M}. \quad (5.45)$$

This additional rescaling implies that

$$\begin{aligned} G_0^{(n)} &= \int \left(dt_0 d^3 \mathbf{x}_0 e^{i\omega_0 t_0 - i\mathbf{k}_0 \cdot \mathbf{x}_0} \right)^{n-1} \langle 0 | \phi_0 \dots \phi_0 | 0 \rangle \\ &= Z_t^{n-1} Z_\phi^{\frac{n}{2}} \int \left(dt d^3 \mathbf{x} e^{i(\omega t - \mathbf{k} \cdot \mathbf{x})} \right)^{n-1} \langle 0 | \phi \dots \phi | 0 \rangle \\ &= Z_t^{n-1} Z_\phi^{\frac{n}{2}} G^{(n)}. \end{aligned}$$

The renormalization condition (5.18a) implies

$$\int dt_0 d^3 x_0 \left(\frac{\partial \phi_0}{\partial t_0} \right)^2 = \int dt d^3 x \left(\frac{\partial \phi}{\partial t} \right)^2. \quad (5.46)$$

This implies

$$Z_t^{-1} Z_\phi = 1 + \mathcal{O}(\lambda^3) \quad \implies \quad Z_\phi = Z_t + \mathcal{O}(\lambda^3), \quad (5.47)$$

i.e., using (5.43),

$$\gamma_\phi = \frac{1}{2} \gamma_t = \frac{1}{2} A \lambda^2 + \mathcal{O}(\lambda^3). \quad (5.48)$$

A shift δM in the renormalization group scale M generates a corresponding shift in the temporal coordinate, the coupling constant and the field strength such that the bare Green's functions remain fixed:

$$0 = \frac{dG_0^{(n)}}{d \log M} = \left(\frac{\partial}{\partial \log M} + \frac{d\lambda}{d \log M} \frac{\partial}{\partial \lambda} + \gamma_\zeta \zeta \frac{\partial}{\partial \zeta} + (n-1) \frac{dZ_t}{d \log M} + \frac{n}{2} \frac{dZ_\phi}{d \log M} \right) G^{(n)},$$

i.e.,

$$\left(M \frac{\partial}{\partial M} + \beta_\lambda \frac{\partial}{\partial \lambda} + \gamma_\zeta \zeta \frac{\partial}{\partial \zeta} + (n-1) \gamma_t + n \gamma_\phi \right) G^{(n)}(\omega, \mathbf{p}; M, \lambda) = 0. \quad (5.49)$$

Using (5.21), the $n = 2$ Callan-Symanzik equation is derived:

$$-2B\lambda^2 - 2B\lambda\beta_\lambda \log\left(\frac{M^2}{\mu^2}\right) - 2\gamma_\zeta + 2A\lambda^2 + \mathcal{O}(\lambda^3) = 0, \quad (5.50)$$

i.e.,

$$\begin{aligned} \beta_\lambda &= 0 + \mathcal{O}(\lambda^2), \\ \gamma_\zeta &= (A - B)\lambda^2 + \mathcal{O}(\lambda^3). \end{aligned}$$

Using (5.22), the $n = 4$ Callan-Symanzik equation is derived:

$$8B\lambda^3 - \beta_\lambda + 8\gamma_\zeta \lambda - 5A\lambda^3 + \mathcal{O}(\lambda^4) = 0, \quad (5.51)$$

i.e.,

$$\beta_\lambda = 3A\lambda^3 + \mathcal{O}(\lambda^4). \quad (5.52)$$

Therefore, we have reproduced the results of the Wilsonian approach in (5.36).

5.3.4. Modified Minimal Subtraction in $3 - \epsilon$ Spatial Dimensions

In this section we will use dimensional regularization and the $\overline{\text{MS}}$ renormalization scheme. In general, the direct evaluation of the integral in (5.9) in $3 - \epsilon$ spatial dimensions results in the expression

$$\begin{aligned} \mathcal{I}^{(6)} = & -\lambda^2 \zeta^2 p^6 \left[\frac{a_1}{\epsilon} + b_1 \log \left(\frac{M^2}{\mu^2} \right) \right. \\ & \left. + \frac{a_2}{\epsilon^2} + b_2 \log^2 \left(\frac{M^2}{\mu^2} \right) + \frac{c_1}{\epsilon} \log \left(\frac{M^2}{\mu^2} \right) + \dots \right], \end{aligned} \quad (5.53)$$

where M is the “fake” scale introduced formally in dimensional regularization to absorb the engineering dimensions of the coupling constants, and can be identified with the renormalization group scale introduced previously. We keep only the most interesting piece in \mathcal{I} , which is proportional to p^6 . We also keep all possible terms involving multi-logs and higher powers in ϵ^{-1} . Such terms should vanish for consistency with our previous results, but it will be interesting to see how this consistency is directly imposed by the renormalization group equations. The renormalized inverse propagator is then

$$\Gamma(\omega, \mathbf{p}) = \omega^2 + \zeta^2 p^6 \left[1 - \frac{\mathcal{I}^{(6)}}{\zeta^2 p^6} + \delta_{\zeta^2} + \mathcal{O}(\lambda^3) \right]. \quad (5.54)$$

The choice of the $\overline{\text{MS}}$ scheme requires

$$\delta_{\zeta^2} = -\lambda^2 \left\{ \frac{1}{\epsilon} \left[a_1 + c_1 \log \left(\frac{M^2}{\mu^2} \right) \right] + \frac{a_2}{\epsilon^2} + \dots \right\} + \mathcal{O}(\lambda^3). \quad (5.55)$$

In terms of bare fields and parameters, the theory is given by

$$S = \frac{1}{2} \int dt_0 d^D x_0 \left[\left(\frac{\partial \phi_0}{\partial t_0} \right)^2 + \zeta_0^2 \left(\frac{\partial^3 \phi_0}{\partial x_0^2 \partial x_0^i} \right)^2 + \frac{\lambda_0}{12} \varepsilon^{ijk} \varepsilon^{\ell mn} \frac{\partial \phi_0}{\partial x_0^i} \frac{\partial \phi_0}{\partial x_0^j} \frac{\partial^2 \phi_0}{\partial x_0^k \partial x_0^m} \frac{\partial^2 \phi_0}{\partial x_0^l \partial x_0^n} \right].$$

In terms of the physical (or renormalized) fields and parameters, the theory is given by

$$S = \frac{1}{2} \int dt d^D x \left[Z (\partial_t \phi)^2 + Z_{\zeta^2} \zeta^2 (\partial^2 \partial_i \phi)^2 + \frac{Z_\lambda \lambda M^\epsilon}{12} \varepsilon^{ijk} \varepsilon^{\ell mn} \partial_i \phi \partial_\ell \phi \partial_j \partial_m \phi \partial_k \partial_n \phi \right].$$

Comparing this physical action to (5.1), we can read out

$$Z = 1 + \delta, \quad Z_{\zeta^2} = 1 + \delta_{\zeta^2}, \quad Z_\lambda = 1 + \delta_\lambda. \quad (5.56)$$

We further introduce the “physical” time and space, respectively,

$$t_0 = Z_t t, \quad x_0 = x. \quad (5.57)$$

We then have, collectively,

$$\begin{aligned}\phi_0 &= Z_\phi^{\frac{1}{2}} \phi, \\ 1 &= Z_t Z_\phi^{-1} Z, \\ \zeta_0 &= Z_t^{-\frac{1}{2}} Z_\phi^{-\frac{1}{2}} Z_{\zeta^2}^{\frac{1}{2}} \zeta, \\ \lambda_0 &= Z_t^{-1} Z_\phi^{-2} Z_\lambda \lambda M^\epsilon.\end{aligned}$$

Further note that

$$\begin{aligned}Z &= 1 + \mathcal{O}(\lambda^3), \\ Z_{\zeta^2} &= 1 + \delta_{\zeta^2}, \\ Z_\lambda &= 1.\end{aligned}$$

Here δ_{ζ^2} is given by (5.55). Then,

$$\begin{aligned}Z_t &= Z_\phi + \mathcal{O}(\lambda^3), \\ \zeta_0 &= Z_t^{-\frac{1}{2}} Z_\phi^{-\frac{1}{2}} \left[1 - \frac{\lambda^2}{2} \left\{ \frac{1}{\epsilon} \left[a_1 + c_1 \log \left(\frac{M^2}{\mu^2} \right) \right] + \frac{a_2}{\epsilon^2} + \dots \right\} + \mathcal{O}(\lambda^3) \right] \zeta, \\ \lambda_0 &= Z_t^{-1} Z_\phi^{-2} \lambda M^\epsilon.\end{aligned}$$

The last two expressions will generate the β -functions due to the fact that the bare couplings ζ_0 and λ_0 are constants that do not run under renormalization. Now we have three formulae to determine four unknown quantities, Z_t , Z_ϕ , ζ and λ . This suggests that there is some room left in the choice of Z_t . In general, we can take a Laurent expansion of Z_t with respect to ϵ^{-1} :

$$Z_t = 1 - \lambda^2 \left(\frac{d_1}{\epsilon} + \frac{d_2}{\epsilon^2} + \frac{e_1}{\epsilon} \log \left(\frac{M^2}{\mu^2} \right) + \dots \right) + \mathcal{O}(\lambda^3), \quad (5.58)$$

where we keep all terms up to order of λ^2 .

Then,

$$\log \lambda_0 = 3 \left[\lambda^2 \left(\frac{d_1}{\epsilon} + \frac{d_2}{\epsilon^2} + \frac{e_1}{\epsilon} \log \left(\frac{M^2}{\mu^2} \right) + \dots \right) + \mathcal{O}(\lambda^3) \right] + \log \lambda + \epsilon \log M. \quad (5.59)$$

Taking the derivative with respect to $\log M$ of both sides of the above equation gives

$$0 = \frac{d \log \lambda_0}{d \log M} = 6\lambda\lambda' \left[\left(\frac{d_1}{\epsilon} + \frac{d_2}{\epsilon^2} + \frac{e_1}{\epsilon} \log \left(\frac{M^2}{\mu^2} \right) + \dots \right) + \mathcal{O}(\lambda^3) \right] + 6\lambda^2 \frac{e_1}{\epsilon} + \frac{\lambda'}{\lambda} + \epsilon, \quad (5.60)$$

where

$$\lambda' \equiv \frac{d\lambda}{d \log M}. \quad (5.61)$$

Plug in the ansatz

$$\lambda' = -\epsilon\lambda + \beta_\lambda, \quad (5.62)$$

where β_λ is independent of ϵ and M .

Then, keeping only up to order λ^3 , the order ϵ^0 and ϵ^{-1} equations read, respectively,

$$\beta_\lambda - 6d_1\lambda^3 - 6e_1\lambda^3 \log\left(\frac{M^2}{\mu^2}\right) = 0, \quad (5.63a)$$

$$d_1\beta_\lambda - d_2 + e_1 + e_1\beta_\lambda \log\left(\frac{M^2}{\mu^2}\right) = 0. \quad (5.63b)$$

These equations immediately imply

$$d_2 = e_1 = 0.$$

Similarly, all higher order coefficients are zero. Hence,

$$\begin{aligned} Z_t &= 1 - \lambda^2 \frac{d_1}{\epsilon} + \mathcal{O}(\lambda^3), \\ \beta_\lambda &= 6d_1\lambda^3 + \mathcal{O}(\lambda^4). \end{aligned}$$

Then the anomalous dimension of the temporal coordinate is

$$\gamma_t = \frac{d \log Z_t}{d \log M} = -2\lambda\lambda' \frac{d_1}{\epsilon} + \mathcal{O}(\lambda^3) = 2d_1\lambda^2 + \mathcal{O}(\lambda^3). \quad (5.64)$$

Comparing to (5.43), we obtain

$$d_1 = \frac{A}{2}, \quad (5.65)$$

and thus

$$\begin{aligned} z &= 3 - A\lambda^2 + \mathcal{O}(\lambda^3), \\ \beta_\lambda &= 3A\lambda^3 + \mathcal{O}(\lambda^4). \end{aligned}$$

Finally, from the equation

$$\zeta_0 = Z_t^{-\frac{1}{2}} Z_\phi^{-\frac{1}{2}} \left[1 - \frac{\lambda^2}{2} \left\{ \frac{1}{\epsilon} \left[a_1 + c_1 \log\left(\frac{M^2}{\mu^2}\right) \right] + \frac{a_2}{\epsilon^2} + \dots \right\} + \mathcal{O}(\lambda^3) \right] \zeta, \quad (5.66)$$

we obtain

$$\begin{aligned} 0 &= -\lambda\lambda' \left\{ \frac{1}{\epsilon} \left[a_1 - A + c_1 \log\left(\frac{M^2}{\mu^2}\right) \right] + \frac{a_2}{\epsilon^2} + \dots \right\} + \frac{1}{\zeta} \frac{d\zeta}{d \log M} + \mathcal{O}(\lambda^3) \\ &= \lambda^2 \left[a_1 - A + c_1 \log\left(\frac{M^2}{\mu^2}\right) - 2\lambda \frac{a_2}{\epsilon} + \dots \right] + \gamma_\zeta + \mathcal{O}(\lambda^3). \end{aligned} \quad (5.67)$$

This implies

$$\begin{aligned} c_1 &= a_2 = 0, \\ \gamma_\zeta &= \lambda^2 (A - a_1) + \mathcal{O}(\lambda^3). \end{aligned}$$

Similarly, all higher coefficients are zero. Comparing the second equation to (5.34), gives

$$a_1 = B, \quad (5.68)$$

i.e.,

$$\gamma_\zeta = (A - B)\lambda^2 + \mathcal{O}(\lambda^3). \quad (5.69)$$

Therefore, consistency of the renormalization group equations constrains $\mathcal{I}^{(6)}$ to be

$$\mathcal{I}^{(6)} = -\lambda^2 \zeta^2 p^6 \left[\frac{B}{\epsilon} + b_1 \log \left(\frac{M^2}{\mu^2} \right) \right]. \quad (5.70)$$

By comparison with (5.11) with the counterterm δ_{ζ^2} included, we obtain

$$b_1 = B. \quad (5.71)$$

Hence,

$$\mathcal{I}^{(6)} = -\lambda^2 \zeta^2 p^6 B \left[\frac{1}{\epsilon} + \log \left(\frac{M^2}{\mu^2} \right) \right]. \quad (5.72)$$

The absence of the double-logs and the $1/\epsilon^2$ terms (and their cross terms) is a result of the very special form of the vertex (5.4). By naive power counting, the 1-loop diagrams are logarithmically divergent. However, since the vertex contains a factor in which there are three momenta contracted by a Levi-Civita symbol, the 1-loop contribution to ζ^2 and λ both vanish. Moreover, at the two loop level, the sunset digram has nonzero contribution to ζ^2 , and thus by power counting it will contain a nonzero logarithmic divergence, i.e., $B \neq 0$. This completes our consistency check for the poles of the sunset diagram.

Note that the cancellation of the nonlocal terms given by mixtures of $1/\epsilon$'s and \log 's is also required in the Bogoliubov-Parasiuk-Hepp-Zimmermann (BPHZ) prescription, after taking into account of the relevant diagrams containing counterterm vertices. Here the vanishing of the nonlocal contribution is due to the vanishing of the diagram

$$\begin{array}{c} \text{---} \circlearrowleft \text{---} \\ \text{---} \otimes \text{---} \end{array} = 0. \quad (5.73)$$

Here \otimes denotes the counterterm vertex $-\delta_\lambda [k_1 k_2 k_3]^2$.

5.3.5. Physical Interpretations of the RG Flow

By solving the renormalization group equations, we obtain

$$\begin{aligned} z &= 3 - A\lambda^2 + \mathcal{O}(\lambda^3), \\ \gamma_\phi &= \frac{1}{2}A\lambda^2 + \mathcal{O}(\lambda^3), \\ \gamma_\zeta &= (A - B)\lambda^2 + \mathcal{O}(\lambda^3), \\ \beta_\lambda &= 3A\lambda^3 + \mathcal{O}(\lambda^4), \end{aligned}$$

where $B > 0$.

On one hand, we can turn off the rescaling of time by setting $A = 0$. Then

$$\gamma_\phi = 0, \quad \beta_\lambda = 0, \quad \gamma_\zeta = -B\lambda^2 + \mathcal{O}(\lambda^3).$$

Flowing towards the IR regime, the lightcone opens up and the theory eventually flows to lower values of z . In the UV, the lightcone gradually closes and finally the theory ceases to be sensible.

However, alternatively, we also have the freedom to fix the coupling ζ by demanding $\gamma_\zeta = 0$. Then

$$A = B, \quad (5.74)$$

and

$$\begin{aligned} z &= 3 - B\lambda^2 + \mathcal{O}(\lambda^3), \\ \gamma_\phi &= \frac{1}{2}B\lambda^2 + \mathcal{O}(\lambda^3), \\ \beta_\lambda &= 3B\lambda^3 + \mathcal{O}(\lambda^4). \end{aligned}$$

In this description, z increases in the IR and exceeds the dimension D of space, which will force the theory to cascade into lower values of z by turning on relevant deformations. Meanwhile, λ decreases and the theory becomes free in the IR. In the UV regime, z gradually decreases such that $z < D$ and the theory recovers a physical propagator. Meanwhile, the coupling λ keeps increasing and eventually the theory becomes non-perturbative. This is also consistent with the instability of the theory in the UV, as seen by the decay rate, which scales as

$$\Gamma_{\text{decay}} \sim \lambda^2 p^3, \quad (5.75)$$

with \mathbf{p} the incoming momentum.

We have described here two special choices of physical interpretation of the renormalization group flow – the first in which time is not rescaled, and the second in which ζ is not renormalized. Clearly, there exists a continuum of choices of parametrization of the RG flow. The physical interpretations of these parametrizations will involve mixtures, by various degrees, of the behaviors described above.

5.4. $O(N)$ Extension and the Large N Limit

Now we generalize the action (5.1) to a theory consisting of N field components, Φ^I , $I = 1, \dots, N$, with $O(N)$ symmetry:

$$S = \frac{1}{2} \int dt d^3x \left(\dot{\Phi}^2 + \zeta^2 \partial^2 \partial_i \Phi^I \partial^2 \partial_i \Phi^I + \dots + \frac{\lambda}{12} \varepsilon^{ijk} \varepsilon^{lmn} \partial_i \Phi^I \partial_\ell \Phi^I \partial_j \partial_m \Phi^J \partial_k \partial_n \Phi^J \right).$$

Note that $\varepsilon^{ijk} \varepsilon^{lmn} \partial_i \Phi^I \partial_\ell \Phi^J \partial_j \partial_m \Phi^I \partial_k \partial_n \Phi^J$ is equivalent to the interaction term given above up to integration by parts.

The 4-point vertex takes the form

$$\begin{array}{ccc} J, p_2 & \diagdown & K, p_3 \\ & \times & \\ I, p_1 & \diagup & L, p_4 \end{array} = -\frac{1}{3} \lambda [p_1 p_2 p_3]^2 (IJKL), \quad (5.76)$$

where

$$(IJKL) = \delta^{IJ} \delta^{KL} + \delta^{IL} \delta^{JK} + \delta^{IK} \delta^{JL}. \quad (5.77)$$

The integral (5.11) from the sunset diagram is now

$$I_6 = -B\lambda^2 \zeta^2 p^6 (IABC)(ABCJ) = -\frac{1}{3}(N+2)B\lambda^2 \zeta^2 p^6. \quad (5.78)$$

The only modification to the previous results is that B is now multiplied by $\frac{N+2}{3}$. If we take the perspective in which ζ does not run, then the β -function for the coupling λ is

$$M \frac{d\lambda}{dM} = (N+2)B\lambda^3 + \mathcal{O}(\lambda^4), \quad (5.79)$$

This becomes infinitely steep in the large N limit for fixed λ . Instead, let us define the 't Hooft coupling

$$g = \lambda N, \quad (5.80)$$

such that

$$M \frac{dg}{dM} = \frac{N+2}{3N^2} Bg^3 + \mathcal{O}(g^4) \xrightarrow{N \rightarrow \infty} \frac{1}{3N} Bg^3 + \mathcal{O}(g^4), \quad (5.81)$$

which vanishes in the large N limit up to this order. In fact, we can argue that this vanishing of the β -function for g holds to all orders. To demonstrate this, we rescale Φ^I by dividing it by \sqrt{N} . The action now reads

$$\mathcal{S} = \frac{N}{2} \int dt d^3x \left[\dot{\Phi} \cdot \dot{\Phi} + \partial^2 \partial_i \Phi \cdot \partial^2 \partial_i \Phi + \frac{g}{2} \varepsilon_{ijk} \varepsilon_{lmn} (\partial_i \Phi \cdot \partial_l \Phi) (\partial_j \partial_m \Phi \cdot \partial_k \partial_n \Phi) \right].$$

Now, the propagator is

$$\frac{1}{N} \frac{1}{\omega^2 + p^6}, \quad (5.82)$$

and the vertex is

$$-N\lambda [k_1 k_2 k_3]^2 (IJKL). \quad (5.83)$$

Hence, in a specific Feynman diagram, each internal propagator contributes a factor $1/N$ and each vertex contributes a factor N . Moreover, summing over N fields in a loop contributes a factor N . Let us assume the following notation:

- L : number of loops;
- I : number of internal legs (edges);
- V : number of vertices;
- $\ell \leq L$: power of N from summing over fields.
- s : overall power of N in a diagram.

Filling each loop with a 2-cell associates to each Feynman diagram a Riemann surface “triangulated” by L faces. The Euler characteristic χ of this surface is

$$V - I + L = \chi = 2 - 2h - n_b - n_c, \quad (5.84)$$

where h is the number of handles, n_b is the number of boundaries and n_c is the number of cross caps. Note that $n_b \geq 1$ and thus $\chi \leq 1$. Therefore,

$$s = V - I + \ell = \chi - L + \ell \leq 1 - L + \ell \leq 1. \quad (5.85)$$

Since the tree level 4-point vertex is of order Ng , diagrams of order lower than N are suppressed by $1/N$. Hence, only the Feynman diagrams with $s = 1$ contribute to the β -functions. In (5.85), the first “ \leq ” sign becomes “ $=$ ” if and only if $\chi = 1$, i.e., the graph is planar; the second “ \leq ” sign becomes “ $=$ ” if and only if $\ell = L$, i.e., each loop sums over all N fields and contributes a factor N . However, each pair of overlapping loops will lower ℓ by 1, and thus any diagram scaling as N cannot contain any overlapping subgraphs. The remaining diagrams are all cactus diagrams, which vanish identically due to the special structure of the vertices. In conclusion, all loop contributions vanish in the large N limit.

The theory is formally stable in the UV regime in the large N limit. The decay rate scales as

$$\Gamma_{\text{decay}} \sim N\lambda^2 p^3 = \frac{1}{N} g^2 p^3, \quad (5.86)$$

which vanishes for finite incoming momentum \mathbf{p} in the limit $N \rightarrow \infty$. The factor N in the second formula comes from summing over all possible outgoing channels.

5.5. Outlook

In this chapter, we have explicitly carried out the renormalization group analysis of a specific Lifshitz scalar field theory. We demonstrated the mutual consistency of the Wilsonian approach, the Callan-Symanzik equation, and the $\overline{\text{MS}}$ scheme with dimensional regularization. Furthermore, we showed that there is a continuum of distinct, but mutually consistent physical interpretations of the renormalization group flow in terms of the widening or narrowing of the lightcone or the existence of a strong coupling regime in the UV. These RG properties, particularly, the existence of multiple interpretations is generic in Lifshitz field theories and arise from the possibility of a changing dynamical critical exponent.

A number of directions of inquiry related to this present work naturally open up. For example, it would be interesting to look for new IR fixed points in $3 - \epsilon$ spatial dimensions in the large N limit, in the same vein as Wilson and Fisher [89]. The interest here would be to take the $\epsilon \rightarrow 1$ limit to describe a new Wilson-Fisher fixed point in $2 + 1$ dimensions. For the theory studied in this chapter, this procedure would not yield anything interesting since the interaction term vanishes identically in $2 + 1$ dimensions. However, other scenarios may exist that exhibit bona fide Wilson-Fisher fixed points with Lifshitz scaling.

In addition, one could consider extending the field content. For example, one could consider a matrix extension as well as gauge field extensions. In any case, the latter would be necessary to achieve the goal of applying the present work to quantum gravity.

Perhaps the most interesting topic for future research relates to the observation that the interacting $O(N)$ relativistic ϕ^4 theory is dual to a Vasiliev-type higher spin gravity theory in anti-de Sitter (AdS) spacetime [90, 91]. This motivates the conjecture that there ought to exist a higher spin gravity theory in an asymptotically Lifshitz spacetime dual to the CFT considered in §5.4 in the large- N limit. Lifshitz holography usually employs relativistic bulk gravity coupled to matter in order to ensure asymptotic Lifshitz scaling [49, 92]. This may not be the most natural approach in our present scenario; Instead, it may be more reasonable to start with a nonrelativistic gravity theory in the bulk, such as Hořava-Lifshitz gravity, as suggested in [18]. This intuition is supported by the fact that higher spin gauge theories are highly restrictive and one generally does not have the freedom to introduce extra matter fields. Furthermore, the cascading phenomenon described in §4 would seem to imply that this hypothetical higher-spin gravity theory must support spacetimes which exhibit hierarchies of asymptotics of Lifshitz scaling with arbitrary values of the dynamical exponent z (or integer values, at least). This is a rather remarkable property indeed. An explicit construction of such a theory would be fascinating.

Chapter 6

Multicritical Phonon-Electron Interactions in Metals

Nambu-Goldstone modes produced by nonrelativistic spontaneous symmetry breaking can exhibit naturally higher-order dispersion relations over a large hierarchy of scales. In flat noncompact space, the naturalness of this behavior is protected by a polynomial shift symmetry. Here we continue our study of such multicritical NG modes. First we show how to generalize the polynomial symmetry when some spatial dimensions are compactified on a torus or replaced by a periodic finite lattice. Then we consider the case in which the multicritical NG bosons play the role of acoustic phonons, associated with spontaneous breaking of spatial Euclidean symmetries. We couple the multicritical acoustic phonons to a Fermi liquid of nonrelativistic electrons, and study the physical properties of such “multicritical metals” in the simplest, isotropic case. Both thermodynamic and transport properties depend on the degree of multicriticality of the phonon sector and the dimension of space. We calculate the resistivity of the metal as a function of temperature T , at the leading order in the Bloch-Boltzmann transport theory. In particular, we point out that the system of $z = 3$ phonons in $3 + 1$ dimensions (which is their lower critical dimension), minimally coupled to the Fermi surface, gives resistivity linear in T over a naturally large hierarchy of scales.

6.1. Introduction

Some of the most fascinating puzzles of modern theoretical physics can be viewed as puzzles of naturalness. This is true of high-energy particle physics, and in gravitational and cosmological physics. It is also true in some areas of condensed matter physics, as in high- T_c superconductivity [93]. The surprising robustness with which the strange metals exhibit resistivity linear in temperature over a remarkable range of scales is begging for an explanation in terms of a mechanism (or mechanisms) which would naturally protect this observed hierarchy of scales. Novel ideas seem to be needed, in view of which, we turn our attention to the question of naturalness in a specific class of non-relativistic systems, with Lifshitz symmetries. It is our hope that the basic pairing mechanism provided by electron-phonon interactions might still be capable of describing the electronic properties of strange metals

as long as one is willing to make the phonons multicritical. Appendix 6.A provides a review of the standard picture of superconductivity.

One of the classic phenomena, spectacularly successful across a broad range of disciplines, is the phenomenon of spontaneous global symmetry breaking and its prediction of the existence of gapless Nambu-Goldstone (NG) excitations. Typically, the NG modes are either linearly dispersing (as in relativistic systems, or in antiferromagnets), or quadratically dispersing (as in ferromagnets). Assuming Lifshitz symmetries for simplicity, we have refined the classification of such NG modes in Chapter 2. We found towers of new universality classes. The stability of these classes under fluctuations is protected by a shift symmetry by a polynomial $f(\mathbf{x})$ of appropriate degree in the spatial Cartesian coordinates $\mathbf{x} = \{x^i, i = 1, \dots, D\}$. This symmetry implies the naturalness of new and perhaps surprising hierarchies, between scales at which various subgroups of the polynomial shift symmetry group are explicitly broken.

6.2. Polynomial Shifts, Compactifications and the Lattice

Having established the possibility of a new symmetry in the continuum theory, one can naturally ask whether there is a discretized version of this symmetry, such that it can be implemented on the lattice and reproduce the continuous polynomial symmetry as the continuum infinite-volume limit is taken.

There are several reasons why to ask this question. First, especially with condensed matter applications in mind, it is useful to know whether lattice systems exist in which the analog of the polynomial shift can be realized as an exact symmetry at the microscopic level, at least in principle. Secondly, even if one is only interested in the continuum limit itself, it is useful to know whether there is a lattice regularization of the theory which maintains the lattice version of the polynomial shift symmetry before the continuum limit is taken. Besides, one might be interested in taking continuum limits other than the infinite volume limit, for example the limit in which the radius of the periodic lattice in one or more dimensions is held fixed as the number of sites goes to infinity. Having a lattice version of the polynomial shift symmetry will then yield automatically a natural continuum symmetry that works on toroidal spatial compactifications.

6.2.1. Bosons on a finite periodic lattice

One spatial dimension

To begin with, consider the theory in one spatial dimension, on a finite, periodic lattice of N sites, labeled by the site index $j = 0, \dots, N - 1$. We are interested in the dynamics of a single scalar field, represented by the real-valued ϕ_j at each site j of the lattice, with periodic boundary conditions (i.e., we define $\phi_{j+N} \equiv \phi_j$ for all $j \in \mathbf{Z}$). We also introduce the uniform lattice spacing a , which represents a natural microscopic scale in the theory: The lattice sites are located at $X = X_j \equiv aj$. Similarly, N serves as an infrared cutoff, and the radius of the spatial circle is given by $R = Na/(2\pi)$: We have $X = X + 2\pi R$.

The dual momentum lattice consists of N points, labeled by integers $k = 0, \dots, N - 1$, arranged uniformly on a circle with periodic boundary conditions. Since the momentum K

dual to X is naturally quantized in the units of $1/R = 2\pi/(Na)$, the lattice sites of the dual lattice are at $K_k \equiv 2\pi k/(Na)$, implying that $K = K + 2\pi/a$: The radius of the momentum circle is $1/a$. For now, we will set $a = 1$ for simplicity. We will restore it again only when we are ready to take the continuum limit with R fixed.

The momentum modes $\tilde{\phi}_k$ associated with the scalar field ϕ_j are given by the discrete Fourier transform,

$$\tilde{\phi}_k = \sum_{j=0}^{N-1} \phi_j e^{2\pi i j k / N}, \quad (6.1)$$

with the inverse given by

$$\phi_j = \frac{1}{N} \sum_{k=0}^{N-1} \tilde{\phi}_k e^{-2\pi i j k / N}. \quad (6.2)$$

The constant shift symmetry is easily realized by the lattice degrees of freedom ϕ_j : The simplest textbook example of a nearest-neighbor Hamiltonian describing lattice vibrations,

$$H = \sum_{j=0}^{N-1} (\phi_{j+1} - \phi_j)^2, \quad (6.3)$$

is indeed manifestly invariant under the constant shift, $\phi_j \rightarrow \phi_j + \alpha$, with $\alpha \in \mathbf{R}$.

Moving on to polynomial shift symmetries of degree $P > 0$, we are facing our first issue: The polynomial functions of the spatial coordinate X , even when discretized and evaluated at the lattice sites $X_j = aj$, are not well-defined as uni-valued functions on the periodic lattice. To find our way out, let us consider the action of our symmetries as they act in the momentum space. In the continuum theory in $D + 1$ dimensions, the constant shift symmetry $\phi(\mathbf{x}) \rightarrow \phi(\mathbf{x}) + \alpha$ acts on the momentum modes via $\phi(\mathbf{k}) \rightarrow \phi(\mathbf{k}) + \alpha \delta^{(D)}(\mathbf{k})$. The polynomial shift symmetries of degree P similarly act on the momentum modes as shifts by derivatives of degree P of $\delta^{(D)}(\mathbf{k})$. Thus, the textbook Hamiltonian (6.3), when rewritten in momentum space,

$$H = \sum_{k=0}^{N-1} \sin^2\left(\frac{\pi k}{N}\right) \tilde{\phi}_k^* \tilde{\phi}_k, \quad (6.4)$$

is invariant under the shift of $\tilde{\phi}_k$ by the lattice delta-function δ_k at the origin,

$$\delta_k = \begin{cases} 1, & k = 0 \\ 0, & k \neq 0, \end{cases} \quad (6.5)$$

simply because the coefficient $\sin^2(\pi k/N)$ vanishes at $k = 0$, the only place where the delta function δ_k is non-zero. The idea now is to extend this picture to higher polynomial symmetries, and to simply define our lattice analog of the ‘‘polynomial shift symmetry of degree P ’’ in its momentum space representation as a shift of the momentum modes by the properly discretized P -th order derivative of the momentum-space delta function.

As an example, consider the quadratic shift $\phi(\mathbf{x}) \rightarrow \phi(\mathbf{x}) + \alpha \mathbf{x}^2$ of the continuum theory, which translates in momentum space into $\phi(\mathbf{k}) \rightarrow \phi(\mathbf{k}) + \alpha \Delta \delta^{(D)}(\mathbf{k})$ (Δ here denotes the

Laplacian in the \mathbf{k} -space). We now *define* our lattice analog of this symmetry (in the one-dimensional case) via

$$\tilde{\phi}_k \rightarrow \tilde{\phi}_k + \alpha(\delta_{k+1} + \delta_{k-1} - 2\delta_k), \quad (6.6)$$

a shift by the discretized lattice version of the second derivative of the momentum-space delta function at $k = 0$.

In order to construct a Hamiltonian invariant under (6.6), we just need to make sure that the coefficient of $\tilde{\phi}_k^* \tilde{\phi}_k$ vanishes not only at $k = 0$, but also at $k = \pm 1$. One natural way to accomplish this is to write

$$H = \sum_k \sin^2 \left(\frac{\pi k}{N} \right) \sin \left(\frac{\pi(k+1)}{N} \right) \sin \left(\frac{\pi(k-1)}{N} \right) \tilde{\phi}_k^* \tilde{\phi}_k. \quad (6.7)$$

This is manifestly real, invariant under $k \rightarrow -k$, and invariant under the lattice $P = 2$ shift symmetry defined in (6.6).

In the continuum infinite-volume limit $a \rightarrow 0$ and $R \rightarrow \infty$, we find $\sin^2(2\pi k/N) \rightarrow K^2$, as well as $\sin(2\pi(k \pm 1)/N) \rightarrow K$. Thus, this limit correctly reproduces the $z = 2$ Hamiltonian of the continuum theory on the decompactified spatial dimension,

$$H = \int dK K^4 \phi^*(K) \phi(K), \quad (6.8)$$

known to be invariant under the quadratic shift symmetry $\phi(X) \rightarrow \phi(X) + \alpha X^2$ (which acts via $\phi(K) \rightarrow \phi(K) + \alpha \delta''(K)$ in the momentum-space picture).

Note that (6.7) is of course not the only lattice Hamiltonian with the exact symmetry (6.6) which gives this continuum limit. For example, the lattice Hamiltonian

$$H' = \sum_k \sin^2 \left(\frac{\pi k}{N} \right) \left\{ \sin^2 \left(\frac{\pi k}{N} \right) - \sin^2 \left(\frac{\pi}{N} \right) \right\} \tilde{\phi}_k^* \tilde{\phi}_k \quad (6.9)$$

is also invariant under (6.6). It gives the same continuum infinite-volume limit as (6.7), but differs from (6.7) on the lattice by terms that are technically irrelevant in the limit.

Higher-degree shift symmetries

The generalization for arbitrary polynomial shift symmetry of degree $2n - 2$, with $n \in \mathbf{N}$, is straightforward. The symmetry is defined as a shift in momentum space by the corresponding $2n - 2$ -th lattice derivative of δ_k at $k = 0$. The important point is that any such $2n - 2$ -th order derivative has its support on sites in the range ¹

$$-n + 1 \leq k \leq n - 1 \quad (6.10)$$

around the origin in momentum space.

¹This is more obvious for the more interesting case considered here, with the shift symmetries of even degree, since an even-degree lattice derivative of any function f_k defined on the sites k is again naturally a function on these sites. Odd-degree shift symmetries would be implemented via odd-degree derivatives of δ_k . It is more accurate to think of the odd-degree derivative of any function f_k as a function on the links between neighboring sites k and $k+1$, and label the link by the half-integer $k+1/2$. With this interpretation, Eqn. (6.10) is correct also for shift symmetries represented by the odd-degree derivatives of δ_k .

Our Hamiltonian (6.7) generalizes to

$$H_n = \sum_k \sin^2 \left(\frac{\pi k}{N} \right) \prod_{\ell=1}^{n-1} \left[\sin \left(\frac{\pi(k+\ell)}{N} \right) \sin \left(\frac{\pi(k-\ell)}{N} \right) \right] \tilde{\phi}_k^* \tilde{\phi}_k, \quad (6.11)$$

and H' of (6.9) to

$$H'_n = \sum_k \sin^2 \left(\frac{\pi k}{N} \right) \prod_{\ell=1}^{n-1} \left\{ \sin^2 \left(\frac{\pi k}{N} \right) - \sin^2 \left(\frac{\pi \ell}{N} \right) \right\} \tilde{\phi}_k^* \tilde{\phi}_k. \quad (6.12)$$

Both H_n and H'_n are invariant under the lattice version of the shift symmetry of degree $2n-2$, and they both give the same continuum infinite-volume limit

$$H = \int dK K^{2n} \phi^*(K) \phi(K). \quad (6.13)$$

It is straightforward to generalize the above construction to a D -dimensional square lattice and to demonstrate the emergence of rotational symmetry at low energies.

6.3. Multicritical Phonons

We are interested in coupling the multicritical phonons to the Fermi surface associated with the electron gas in a metal. Our intention is to examine how the standard physical properties of metals change when the acoustic phonons develop a higher-order dispersion relation over some natural hierarchy of scales. For simplicity, we will consider the rotationally invariant case, with

$$\omega_{\mathbf{k}} \equiv \omega_k = \zeta_n k^n. \quad (6.14)$$

6.3.1. Hydrodynamics with Lifshitz Symmetries

This exposition follows closely the logic of Landau-Lifshitz, Vol. 9, §24, as well as the early chapters of Abrikosov-Gorkov-Dzyaloshinski [94, 95].

Model the phonon system by an isotropic dissipationless Bose liquid described by sound waves in a hydrodynamical system. Such an ideal fluid is described the pressure distribution p , density function f , and the velocity distribution v . We will split the total density $f(\mathbf{x}, t)$ into an equilibrium background density $f_0(\mathbf{x}, t)$ plus the deviation from equilibrium which we denote by $Q(\mathbf{x}, t)$,

$$f(\mathbf{x}, t) = f_0(\mathbf{x}, t) + Q(\mathbf{x}, t). \quad (6.15)$$

From now on, we will assume that $f_0(\mathbf{x}, t) = f_0$ is uniform in space and time, and that $Q(\mathbf{x}, t)$ is small and slowly varying.

We will assume that the flow is a potential flow,

$$\mathbf{v} = \nabla \phi. \quad (6.16)$$

This assumption can be related to several things: First, it may be a consequence of some thermodynamic requirement about the behavior of entropy under the flow. Secondly, for

isotropic fluids, having \mathbf{v} be the gradient of a potential function leads to purely longitudinal phonons – hence, the condition that the flow be a potential flow eliminates the transverse polarizations of the phonons.

The system is assumed to satisfy the continuity equation for mass, which in the linearized approximation is

$$\dot{Q} \approx -f_0 \nabla \cdot \mathbf{v} = -f_0 \Delta \phi. \quad (6.17)$$

Note that we are not proposing to replace the conventional continuity equation with a multicritical version (such as, for example, $\dot{Q} \sim \nabla \cdot \Delta \mathbf{v}$).

In terms of the velocity potential, the Euler equation becomes a wave equation,

$$\ddot{\phi} + \zeta_1^2 \Delta \phi = 0, \quad (6.18)$$

where ζ_1 is the speed of sound, given by

$$\zeta_1 = \sqrt{\left(\frac{\partial p}{\partial f}\right)_s}. \quad (6.19)$$

The subscript “s” denotes “constant entropy”. The Hamiltonian of the system, in the Gaussian approximation, is

$$H = \frac{1}{2f_0} \int d^3\mathbf{x} \left((f_0 v)^2 + (\zeta_1 Q)^2 \right). \quad (6.20)$$

If higher polynomial shift symmetries are applied to Q , the speed of sound ζ_1 will be protected to be close to zero. In this case, higher order operators dominate and need be considered in the derivative expansion of the theory, which will now be described near a Gaussian fixed point with a dynamical critical exponent $z > 1$. In general, the expression for the total energy will be modified to

$$H = \frac{1}{2f_0} \int d^3\mathbf{x} \left((f_0 v)^2 + (\zeta_z \partial^{z-1} Q)^2 \right). \quad (6.21)$$

That is, in order to obtain phonons with the higher-order dispersion relation $\omega_{\mathbf{k}} = \zeta_z k^z$, we must impose the polynomial shift symmetry of degree $2z - 4$ on the field Q .

Assuming the standard microphysics interpretation of f (or \mathbf{v}) as the coarse graining of the sum, over all particles, of the spatial delta functions weighted by m (or \mathbf{k}/m), one finds that Q and ϕ form a canonical pair, with Q a generalized coordinate and ϕ its canonical momentum,

$$[\phi(\mathbf{x}), Q(\mathbf{x}')] = -i\delta(\mathbf{x} - \mathbf{x}'). \quad (6.22)$$

The mode expansions for $\phi(\mathbf{x})$ and $Q(\mathbf{x}')$ are, respectively,

$$\phi(\mathbf{x}) = \sqrt{\frac{\rho_0}{2V}} \sum_{\mathbf{k}} \frac{\sqrt{\omega_{\mathbf{k}}}}{k} (a_{\mathbf{k}} e^{i(\mathbf{k}\cdot\mathbf{x} - \omega_{\mathbf{k}}t)} + a_{\mathbf{k}}^\dagger e^{-i(\mathbf{k}\cdot\mathbf{x} - \omega_{\mathbf{k}}t)}), \quad (6.23a)$$

$$Q(\mathbf{x}) = \frac{1}{\sqrt{2\rho_0 V}} \sum_{\mathbf{k}} \frac{ik}{\sqrt{\omega_{\mathbf{k}}}} \left(a_{\mathbf{k}} e^{i(\mathbf{k}\cdot\mathbf{x} - \omega_{\mathbf{k}}t)} - a_{\mathbf{k}}^\dagger e^{i(\mathbf{k}\cdot\mathbf{x} - \omega_{\mathbf{k}}t)} \right), \quad (6.23b)$$

where the modes satisfy the canonical commutation relation

$$[a_{\mathbf{k}}, a_{\mathbf{k}'}^\dagger] = \delta_{\mathbf{k}\mathbf{k}'}. \quad (6.24)$$

The Hamiltonian of the liquid thus takes the form

$$H = \sum_{\mathbf{k}} \omega_{\mathbf{k}} \left(a_{\mathbf{k}}^\dagger a_{\mathbf{k}} + \frac{1}{2} \right), \quad (6.25)$$

The free propagator for Q will be

$$D(\mathbf{k}, \omega) \sim \frac{k^2}{\omega^2 - \omega_{\mathbf{k}}^2 + i\epsilon}. \quad (6.26)$$

In the linearized approximation, we have expanded our theory around a fixed uniform density f_0 , and obtained a description of the multicritical liquid in terms of the fluctuations Q around this equilibrium density. Such a non-interacting limit defines a Gaussian fixed point, with polynomial shift symmetry protecting the scaling with the dynamical exponent z . When interactions are restored, generically they explicitly break the polynomial shift symmetry. Indeed, in the full non-linear theory, we expect self-interaction terms to come from $f_0 \rightarrow f$. While f_0 is not acted on by the polynomial shift, f is.

The fixed point scaling is defined as follows: $[\partial_i] = 1$, $[\partial_t] = z$, $[Q] = (D - z)/2$, holding f_0 fixed (and hence of $[f_0] \equiv 0$). Thus, we scale *towards the state with uniform fixed density* $f = f_0$, and not towards the naive empty state with $f = 0$. This interplay between the nonlinear structure of the theory versus the renormalization group (RG) scaling near one of its fixed points is somewhat reminiscent of a similar split in the theory of gravity, where, in order to define the Gaussian fixed point that describes free gravitons, one splits the spacetime metric into the sum of a non-zero background, which defines the inertia, and the fluctuations describing the propagating gravitons with the appropriate, background-dependent dispersion relation.

6.3.2. Multicriticality in the Debye model

In a realistic crystal, there will be a finite number of oscillation modes. In the simplest Debye model description of the crystal, one assumes homogeneity and isotropy as in our discussion of multicritical hydrodynamics, and implements the finiteness of the total number of degrees of freedom by cutting off the spatial momenta at the appropriate value $k = k_D$, so that the total number of states reproduces the number of degrees of freedom.² Since the counting of states, \tilde{N} , inside the sphere of radius k_D is the same as the number, N , in the standard Debye model of linearly dispersing phonons, k_D is the standard Debye momentum of the crystal.³ The cutoff on k translates into a natural cutoff $\tilde{\omega}_D$ on phonon frequencies, and

²We will often want to compare our multicritical version of the Debye model to the standard one, with the linearly dispersing acoustic phonons of constant velocity c_s .

³One can easily relax this condition, and allow $\tilde{N} \neq N$. Consequently, the value of the Debye momentum would also change, to $\tilde{k}_D = (\tilde{N}/N)^{1/D} k_D$. In this paper, for simplicity, we will focus on $\tilde{N} = N$ and hence $\tilde{k}_D = k_D$.

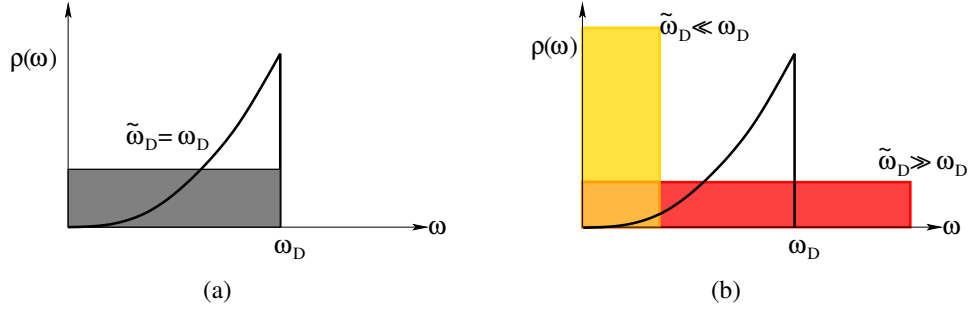


Figure 6.1: The density of states $\varrho(\omega)$ as a function of frequency in the multicritical Debye model at the lower critical dimension, compared to the density of states in the standard Debye model. **(a)**: the case of $\tilde{\omega}_D = \omega_D$; **(b)**: the regimes with $\tilde{\omega}_D \ll \omega_D$ and $\tilde{\omega}_D \gg \omega_D$, assuming fixed k_D .

the existence of the characteristic temperature $\tilde{\Theta}_D$ of the system. Due to the higher-order nature of the dispersion relation,

$$\tilde{\omega}_D = \omega_{k_D} \equiv \zeta_n k_D^n, \quad (6.27)$$

and $\tilde{\Theta}_D = \tilde{\omega}_D$, in the units of $\hbar = 1 = k_B$, are not the standard Debye frequency and Debye temperature, but depend on the order n of the dispersion relation. In our comparison to the standard Debye model with the same Debye momentum k_D , we have

$$\frac{\tilde{\omega}_D}{\omega_D} = \frac{\zeta_n}{c_s} k_D^{n-1}. \quad (6.28)$$

Similarly, the density of states $\varrho(\omega)$, defined via

$$\int_0^{\omega_k} \varrho(\omega) d\omega = \int_0^{|\mathbf{k}|=k} \frac{d^D \mathbf{k}}{(2\pi)^D}, \quad (6.29)$$

is not proportional to ω^{D-1} as in the standard Debye model, but given instead by

$$\varrho(\omega) \propto \omega^{(D-n)/n}. \quad (6.30)$$

Note that when the phonons with the n -th order dispersion are at their lower critical dimension, $D = n$, then the density of states is a constant across all values of ω . Consequently, there are many more phonon states available near $\omega = 0$ than in the standard Debye model of linearly dispersing phonons. In this simple case, we now have three qualitatively distinct regimes that we could consider: (a) $\tilde{\omega}_D \approx \omega_D$; (b) $\tilde{\omega}_D \ll \omega_D$; and (c) $\tilde{\omega}_D \gg \omega_D$. In all three cases, very low frequency phonon modes proliferate in comparison to the standard Debye model. However, this behavior is more pronounced in case (b).

6.4. Electron-Phonon Transport Properties

Now we consider the interaction of the multicritical phonon system with a Fermi liquid of nonrelativistic electrons. In order to illustrate the main robust features caused by the

multicriticality of the phonons, we consider the simplest model, with the electrons modelled by a Fermi liquid of spinless screened quasiparticles with a spherical Fermi surface, coupled to the multicritical Debye model of phonons characterized by their dispersion exponent n . Thus, we are assuming that the range of length and time scales is such that the phonons are well-approximated by a fixed value of n . Once such a hierarchy of scales opens up, across which the phonon dispersion is characterized by fixed $n > 1$, the hierarchy can be naturally protected by the corresponding polynomial shift symmetry.

6.4.1. Minimal coupling to the Fermi surface

The coupling between electrons and our phonon liquid is minimal,⁴

$$H_{\text{int}} = g \int d^D \mathbf{x} Q \Psi^\dagger \Psi. \quad (6.31)$$

This coupling breaks the polynomial shift symmetry in the phonon field Q , generates relevant deformations, and produces a natural pairing mechanism for the electrons.

Plugging in the mode expansion (6.23b) for Q , one finds that the electron-phonon vertex is given by

$$g_{\mathbf{k}} = g \frac{k}{\sqrt{\omega_{\mathbf{k}}}}. \quad (6.32)$$

Using the Boltzmann-Bloch transport theory, one computes an estimate of the resistivity via the relaxation time $\tau(\mathbf{k})$ between electron-phonon collisions [96],

$$\rho \sim \frac{1}{\tau(k_F)} \sim \int_0^{k_F} |g_{\mathbf{k}}|^2 n(k) k^2 d^D \mathbf{k}, \quad (6.33)$$

where $n(k)$ is the phonon distribution function, which at equilibrium is simply the Bose-Einstein distribution function,

$$n(k) = \frac{1}{e^{\omega_{\mathbf{k}}/T} - 1}.$$

Switching integration variable to energy appropriately undimensionalized by dividing by the temperature, one derives the temperature dependence of the resistivity:

$$\rho \sim T^{\frac{3+D-z}{z}}. \quad (6.34)$$

Indeed, this immediately reproduces the standard result that in $D = 3$ and when $z = 1$, the temperature dependence of the resistivity is $\rho \sim T^5$.

It turns out that this simple derivation can be slightly naive and potentially misses crucial low-energy physics and, in particular, infrared divergences. These we will capture using a more sophisticated analysis of a microscopic model for the interaction between the Fermi liquid and the multicritical phonons.

⁴As an alternative, we could also consider non-minimal couplings, for example the shift-symmetry-preserving coupling, of the form $\Psi^\dagger \Psi \Delta^\# Q$, with the appropriate power $\#$. What is the appropriate $\#$? If we want an exact invariant, we need $\Psi^\dagger \Psi \Delta^{2z-2} Q$. Intriguingly, if we allow the polynomial shift to act on the chemical potential by a shift, we can have $\Psi^\dagger \Psi \Delta^{2z-4} Q$, whose variation under the shift of degree $2z - 4$ is a constant which can be compensated for by the shift of the chemical potential.

6.4.2. Generalized Bloch-Grüneisen Formula

In the language of the “lattice displacement field” \mathbf{P} , which describes the displacement of the lattice points away from their equilibrium position, we anticipate that $Q = \nabla \cdot \mathbf{P}$. From the mode expansion for Q in (6.23b), we then derive the mode expansion for \mathbf{P} :

$$\mathbf{P} = \frac{1}{\sqrt{2\rho_0 V}} \sum_{\mathbf{k}} \frac{\hat{\mathbf{k}}}{\sqrt{\omega_{\mathbf{k}}}} \left(a_{\mathbf{k}} e^{i(\mathbf{k} \cdot \mathbf{x} - \omega_{\mathbf{k}} t)} - a_{\mathbf{k}}^\dagger e^{i(\mathbf{k} \cdot \mathbf{x} - \omega_{\mathbf{k}} t)} \right). \quad (6.35)$$

Indeed, with the identification of ρ_0 as the mass M of the lattice ions, one would interpret this \mathbf{P} as the displacement field of the ions themselves. The interaction can then be “derived” from a simple microscopic model which is just the standard electrostatic interaction between the electron fluid and the electric dipole moment density produced by the displacement field of the heavy positive ions in the metal.

The interaction energy is

$$H_{\text{int}} = \int d^D \mathbf{x} d^D \mathbf{x}' \rho(\mathbf{x}) \mathbf{P}(\mathbf{x}') \cdot \nabla_{\mathbf{x}'} \frac{1}{|\mathbf{x} - \mathbf{x}'|}. \quad (6.36)$$

Second quantization promotes the classical charge density $\rho(\vec{x})$ to an operator given by $\rho(\mathbf{x}) = e\psi^\dagger(\mathbf{x})\psi(\mathbf{x})$, where $\psi(\mathbf{x})$ is the field operator for the electron-hole system. For metals, with itinerant electrons, one must take screening effects into account. This amounts to replacing the Coulomb potential with a Yukawa potential with screening strength λ . In the limit of very effective screening, $\lambda \rightarrow \infty$, one may take the following replacement

$$\frac{1}{|\mathbf{x} - \mathbf{x}'|} \rightarrow \frac{2\pi^{\frac{D}{2}} \Gamma(D-1)}{\Gamma(\frac{D}{2}) \lambda^{D-1}} \delta(\mathbf{x} - \mathbf{x}'). \quad (6.37)$$

Of course, one need not take this approximation and may consider more general potentials. Such generalizations are beyond the scope of the present work.

Expand $\psi(\mathbf{x})$ and $\mathbf{P}(\mathbf{x})$ as follows

$$\psi(\mathbf{x}) = \frac{1}{\sqrt{V}} \sum_{\mathbf{k}} c_{\mathbf{k}} e^{i\mathbf{k} \cdot \mathbf{x}}, \quad \mathbf{P}(\mathbf{x}) = \frac{1}{\sqrt{2MV}} \sum_{\mathbf{k}} \frac{\hat{\mathbf{k}}}{\sqrt{\omega_{\mathbf{k}}}} \left(a_{\mathbf{k}} e^{i\mathbf{k} \cdot \mathbf{x}} + \text{h.c.} \right), \quad (6.38)$$

where V is the D -dimensional volume of the system, $c_{\mathbf{k}}$ and $a_{\mathbf{k}}$ are modes for $\psi(\mathbf{x})$ and $\mathbf{P}(\mathbf{x})$, respectively, and M is the mass of the lattice ion. Note that $\mathbf{P}(\mathbf{x})$ is manifestly real. Then, (6.36) turns into the Fröhlich interaction

$$H_{\text{int}} = \sum_{\mathbf{k}, \mathbf{q}} g_{\mathbf{q}} c_{\mathbf{k}+\mathbf{q}}^\dagger c_{\mathbf{k}} a_{\mathbf{q}} + \text{h.c.}, \quad (6.39)$$

where

$$g_{\mathbf{q}} = -i \frac{2\pi^{\frac{D}{2}}}{\sqrt{2MV}} \frac{\Gamma(D-1)}{\Gamma(\frac{D}{2})} \frac{e}{\lambda^{D-1}} \frac{q}{\sqrt{\omega_{\mathbf{q}}}}. \quad (6.40)$$

This can be compared with (6.32). The entire prefactor of $q/\sqrt{\omega_{\mathbf{q}}}$ is just a microscopic model for the parameter g introduced at the effective level.

Suppose that the phonon system is close to a Gaussian fixed point characterized by the dynamical exponent z . Then, the phonon dispersion relation is approximately

$$\omega_{\mathbf{q}} = \zeta_z q^z, \quad (6.41)$$

where ζ_z is a constant, which can be set to unity if the system remains in the vicinity of this fixed point. Then, the coupling constant becomes

$$g_{\mathbf{q}} = -i \frac{2\pi^{\frac{D}{2}}}{\sqrt{2\zeta_z} MV} \frac{\Gamma(D-1)}{\Gamma(\frac{D}{2})} \frac{e}{\lambda^{D-1}} q^{1-\frac{z}{2}}. \quad (6.42)$$

Expand the electron distribution function $n(\mathbf{x}, \mathbf{k})$ as

$$n(\mathbf{x}, \mathbf{k}) = n_0(\varepsilon) + \frac{\partial n_0}{\partial \varepsilon} \Phi(\mathbf{x}, \mathbf{k}), \quad (6.43)$$

where ε is the dressed electron (quasi-particle) energy and

$$n_0(\varepsilon) = \frac{1}{e^{\varepsilon/T} + 1} \quad (6.44)$$

is the equilibrium, Fermi-Dirac distribution. Plugging (6.44) into (6.43) gives

$$n(\mathbf{x}, \mathbf{k}) = n_0(\varepsilon) + \frac{n_0(\varepsilon)(1 - n_0(\varepsilon))}{T} \Phi(\mathbf{x}, \mathbf{k}) \quad (6.45)$$

In principle, one should perform a similar expansion for the phonon distribution function $N(\mathbf{x}, \mathbf{k})$. However, we will assume that the phonon system is always in thermal equilibrium: $N(\mathbf{x}, \mathbf{k}) = N_0(\omega)$, where

$$N_0(\omega) = \frac{1}{e^{\omega/T} - 1}, \quad (6.46)$$

and ω is the phonon frequency.

In terms of these distribution functions, the resistivity of metals is given by the Bloch-Boltzmann theory as

$$\rho = \frac{\int \frac{d^D k}{(2\pi)^D} \frac{d^D k'}{(2\pi)^D} \frac{d^D q}{(2\pi)^D} (\Phi_{\mathbf{k}} - \Phi_{\mathbf{k}'})^2 \left(\mathcal{P}_{\mathbf{k}}^{\mathbf{k}', \mathbf{q}} + \mathcal{P}_{\mathbf{k}, \mathbf{q}}^{\mathbf{k}'} \right)}{4T \left| \int \frac{d^D k}{(2\pi)^D} e^{\mathbf{v}} \Phi \frac{\partial n_0}{\partial \varepsilon} \right|^2}, \quad (6.47)$$

where \mathbf{v} is the quasi-particle velocity, $\mathcal{P}_{\mathbf{k}}^{\mathbf{k}', \mathbf{q}}$ is the equilibrium transition rate for the process

$$\mathbf{k}_{\text{electron}} \rightleftharpoons \mathbf{k}'_{\text{electron}} + \mathbf{q}_{\text{phonon}},$$

and $\mathcal{P}_{\mathbf{k}, \mathbf{q}}^{\mathbf{k}'}$ is the equilibrium transition rate for the process

$$\mathbf{k}_{\text{electron}} + \mathbf{q}_{\text{phonon}} \rightleftharpoons \mathbf{k}'_{\text{electron}},$$

where we ignored the contributions from Umklapp processes [97]. The transition rates are given by Fermi's Golden rule as

$$\mathcal{P}_{\mathbf{k}}^{\mathbf{k}',\mathbf{q}} = 2\pi|g_{\mathbf{q}}|^2 n_0(1 - n'_0)(1 + N_0)\delta(\varepsilon_{\mathbf{k}} - \varepsilon_{\mathbf{k}'} - \omega_{\mathbf{q}})\delta_{\mathbf{b},\mathbf{k}-\mathbf{k}'-\mathbf{q}}, \quad (6.48a)$$

$$\mathcal{P}_{\mathbf{k},\mathbf{q}}^{\mathbf{k}'} = 2\pi|g_{\mathbf{q}}|^2 n_0(1 - n'_0)N_0\delta(\varepsilon_{\mathbf{k}} - \varepsilon_{\mathbf{k}'} + \omega_{\mathbf{q}})\delta_{\mathbf{b},\mathbf{k}-\mathbf{k}'+\mathbf{q}}. \quad (6.48b)$$

Then, (6.47) becomes

$$\rho = \frac{1}{12\sqrt{\pi}e^2 k_F^2 v_F^2} \frac{D}{(2\pi)^{2D-1}} \frac{\Gamma\left(\frac{D}{2}\right)}{\Gamma\left(\frac{D-1}{2}\right)} \int_0^{2k_F} \frac{dq q^D |g_{\mathbf{q}}|^2 \omega}{\sinh^2\left(\frac{\omega}{2T}\right)} \left(1 - \frac{q^2}{4k_F^2}\right)^{\frac{D-3}{2}}, \quad (6.49)$$

where e is the effective electric charge, k_F is the Fermi momentum, v_F is the Fermi speed, and $g_{\mathbf{q}}$ is the coupling of the electron-phonon interaction. We have relegated the details in the derivation of the formula for resistivity (6.47) as well as the subsequent computation of (6.49) to Appendices 6.B and 6.C.

To go any further, one must invoke a specific physical model for the electron-phonon interaction to obtain an explicit expression for $g_{\mathbf{q}}$. We use the model (6.42), together with (6.41) and (6.49). We evaluate the expression in the limit $T \ll \Theta_D \ll \frac{1}{2}(2k_F)^z$, where Θ_D is the Debye temperature. Then, one obtains the generalized Bloch-Grüneisen formula

$$\begin{aligned} \rho &= \frac{T^{\frac{D+3}{z}-1}}{\lambda^{2D-2} M V k_F^2 v_F^2} \frac{\Gamma(D-1)}{2^{\frac{3+D}{z}+1-D} \pi^D} \int_0^\infty \frac{dx x^{\frac{D+3}{z}-1}}{\sinh^2(x)} \\ &= \alpha \mathcal{I} T^{\frac{D+3}{z}-1}, \end{aligned} \quad (6.50)$$

where

$$\alpha = \frac{\Gamma(D-1)}{2^{2-D} \pi^D \lambda^{2D-2} M V k_F^2 v_F^2}, \quad (6.51)$$

and

$$\mathcal{I} = \int_0^\infty \frac{dx \left(\frac{x}{2}\right)^{\frac{D+3}{z}-1}}{\sinh^2(x)} = \frac{1}{4^{\frac{D+3}{z}-1}} \Gamma\left(\frac{D+3}{z}\right) \zeta\left(\frac{D+3}{z} - 1\right). \quad (6.52)$$

6.4.3. Resistivity for Various Values of D and z

Nominally, (6.50) gives $\rho \sim T^{\frac{D+3}{z}-1}$. For example, this immediately reproduces the standard result that for $z = 1$ acoustic phonons in $D = 3$, we have $\rho \sim T^5$. However, one must take care of possible singularities in the coefficient A , which arise when $D = 1$, when $\Gamma(D-1)$ is singular, and $D+3 = 2z$, when $\zeta\left(\frac{D+3}{z} - 1\right)$ is singular.

Assuming integer values for D and z , the first interesting case of the latter singularity is $D = z = 3$. In this case, one can regulate the singularity by an infrared cut-off μ , replacing the lower bound of the integral with μ/T . The integral \mathcal{I} in (6.52) becomes

$$\begin{aligned} \mathcal{I} &= \frac{1}{2} \int_{\mu/T}^\infty \frac{dx x}{\sinh^2(x)} = \frac{\mu}{T} \coth\left(\frac{\mu}{T}\right) - \log\left[2 \sinh\left(\frac{\mu}{T}\right)\right] \\ &= \frac{1}{2} \left[1 - \log 2 + \log\left(\frac{T}{\mu}\right)\right] T + \mathcal{O}\left(\frac{\mu}{T}\right)^2. \end{aligned} \quad (6.53)$$

Therefore, the resistivity in this case picks up a $T \log T$ dependence in addition to a T dependence. It is interesting to note that the coupling given in (6.42) now scales as

$$g_{\mathbf{q}} \sim q^{-\frac{1}{2}}, \quad (6.54)$$

which blows up in the far infrared when $q \rightarrow 0$ and the theory becomes strongly coupled. However, we have the option of softly breaking the polynomial shift symmetry, letting the theory cascade to the $z = 2$ fixed point at the energy scale μ and then cascade to the $z = 1$ fixed point at the energy scale μ' , with $0 < \mu' < \mu \ll T$. In this case, the resistivity is given by

$$\begin{aligned} \rho &= \alpha \left(\frac{1}{32} \zeta_1^6 T^5 \int_0^{\frac{\mu'}{T}} \frac{dx x^5}{\sinh^2(x)} + \frac{1}{4} \zeta_2^3 T^2 \int_{\frac{\mu'}{T}}^{\frac{\mu}{T}} \frac{dx x^2}{\sinh^2(x)} + \frac{1}{2} \zeta_3^2 T \int_{\frac{\mu}{T}}^{\infty} \frac{dx x}{\sinh^2(x)} \right) \\ &= c_0 T + c_1 T \log \left(\frac{T}{\mu} \right) + \mathcal{O} \left(\frac{\mu}{T}, \frac{\mu'}{T} \right), \end{aligned} \quad (6.55)$$

where

$$c_0 = \frac{\alpha}{2} \left[\frac{\zeta_1^6}{64} (\mu')^4 + \frac{\zeta_2^3}{2} (\mu - \mu') + (1 - \log 2) \zeta_3^2 \right], \quad c_1 = \frac{\alpha}{2}. \quad (6.56)$$

By tuning various parameters, this theory can support a temperature dependence of the resistivity that is very close to being linear over a broad range of energy scales. This tuning of parameters is in principle achieved by tuning various physical characteristics of actual condensed matter systems (e.g., doping, etc.)

6.4.4. Heat Capacity for Various Values of D and z

Famously, the electronic contribution to the heat capacity behaves linearly with temperature at low temperatures, independent of the spatial dimension. On the other hand, standard linearly-dispersing phonons in D spatial dimensions contribute a heat capacity which scales as T^D . For multicritical phonons, with a dynamical exponent z , this is modified to $T^{D/z}$. The one-loop phonon correction to the phonon propagator is finite and immaterial unless $z \geq D$. At $z = D$, the correction is logarithmically divergent and contributes a $\log T$ correction to the heat capacity.

To calculate the effect of the electron-phonon interaction on the heat capacity, we will follow the techniques in [98], wherein the one-loop contribution to the entropy is given by

$$S^{(1)} \propto -\frac{nN|g|^2}{4M} \int_{-\infty}^{\infty} d\omega \frac{\partial n_B(\omega)}{\partial T} \int d^D q \frac{\omega}{qv_F} \theta \left(1 - \left| \frac{\omega}{qv_F} \right| \right) \frac{q^2}{\omega^2 - \omega_q^2}, \quad (6.57)$$

where n is the number of ions per unit volume, M is the ion mass, N is the bare electron density of states at the Fermi surface, v_F is the Fermi speed, g is the electron-phonon coupling constant, and n_B is the Bose-Einstein distribution function. Note that the final piece in the integrand is nothing but the multicritical phonon bare propagator. The temperature

dependence of this integral is straightforward to extract in the low-temperature regime and is given by

$$S^{(1)} \propto T^{\frac{D+1}{z}-1}. \quad (6.58)$$

Therefore, the interaction contribution to the heat capacity, which is given by $C = T \frac{\partial S}{\partial T}$, has the same temperature dependence:

$$C_{\text{int}} \propto T^{\frac{D+1}{z}-1}. \quad (6.59)$$

When $z = D$, this gives $C_{\text{int}} \propto T^{1/z}$, which, for $z = 3$ gives $T^{1/3}$. Indeed, one can derive rather unorthodox power law dependence in the heat capacity via the coupling of multicritical phonons with electrons. However, one should note that there does exist interesting power law dependence in the heat capacity of certain exotic materials, particularly in organic superconductors. For example, in one particular compound, it is found that $C \sim T^{1/z}$, but with $z = 3/2$, rather than an integer value [99].

6.4.5. Coupling Systems with Different Scalings

One must keep in mind one critical assumption that has entered into the derivation of the generalized Bloch-Grüneisen formula. Here, we are coupling two systems – the electron system and the phonon system. We assume that both systems are close to Gaussian fixed points, but that they are characterized by *different* dynamical exponents: unity for the electrons and z for the phonons. This is manifest in the limit that we are taking: $T \ll \Theta_D \ll \frac{1}{2} (2k_F)^z$. In the standard case, where the acoustic phonons have a linear dispersion relation, this limit is perfectly intuitive. Most metals are rigid and stable at the temperatures in which we deal with them experimentally (this is particularly true in superconductive cases, which still only occur at very low temperatures). Therefore, it should certainly be true that the Debye temperature be much greater than the physical temperature. However, and in addition, the solid formed by the lattice ions is usually far more compressible than the fluid formed by the electrons, which is just the statement that the Fermi temperature is much greater than the Debye temperature. Note that we are comparing one temperature associated with electrons to another associated with phonons. There is no subtlety when both have the same scaling. However, one must keep in mind that what we really mean here is that phononic excitations with momenta of order, or greater than, the Fermi momentum are extremely suppressed. When the phonon system has a dynamical exponent z , then these excitations are characterized by a temperature of order k_F^z , not k_F , which explains the limit that we are taking.

One way to think about our assumption here is to make an analogy with the sudden or impulse approximation. If a charged object with a large linear momentum is deflected slightly by a magnetic field, one can approximate the deflection by a small impulse keeping the original linear momentum fixed. Clearly, this is incorrect since it violates momentum conservation, but the violation is sufficiently small that one is able to extract the dominant physical behavior of the system in question. Likewise, we assume that the electron-phonon coupling is sufficiently weak or transitory that we may extract the main physics in the system without significantly perturbing each subsystem away from each ones respective Gaussian fixed point.

Of course, properly, once the two systems are allowed to interact, a hypothetical fixed point for the combined system must be described by a single dynamical exponent. How this comes about in detail is not at all clear and is beyond the scope of the present work.

6.5. One Loop Effects

We now turn our attention to the question of the stability of the multicritical phonons. Our main concern is the stability of these phonons against decay into electron-hole pairs.⁵ Properly, we will need to study these effects at finite temperature. However, we will perform the analysis at zero temperature first as a warmup since it is technically simpler.

We ought to be concerned about loop corrections to the interaction vertex itself. That is, we should check that the Migdal theorem continues to hold for multicritical phonons as it does for ordinary ones (i.e., that quantum corrections to the vertex are suppressed by a naturally small ratio of scales, which in the usual case is the ratio of the electron mass to the ion mass) [100]. The one-loop correction to the electron-phonon vertex is given by an additional phonon exchange between the outgoing electrons. Migdal's theorem will apply to this diagram as long as the population of phonons near the “low-energy” states of the intermediate electrons is suppressed. This is essentially always the case since the low-energy electronic excitations lie around the Fermi surface, which has a very high momentum. As stated in the previous section, we assume that phononic excitations with momenta of order the Fermi momentum are extremely suppressed. Hence, we need only consider the one-loop correction to the phonon propagator in detail.

6.5.1. Feynman Rules

The free Fermion Lagrangian is

$$\mathcal{L}_{\text{ff}} = i\psi^\dagger \dot{\psi} - \frac{1}{2m} \partial_i \psi^\dagger \partial_i \psi. \quad (6.60)$$

In Fourier space, this reads

$$\mathcal{L}_{\text{ff}}^{(q)} = \psi^\dagger \left[i(-i\varepsilon) - \frac{1}{2m} (-i\mathbf{q}) \cdot (i\mathbf{q}) \right] \psi = \psi^\dagger \left(\varepsilon - \frac{q^2}{2m} \right) \psi. \quad (6.61)$$

We split the Fermion propagator up into two pieces depending on whether $q > k_F$ (electron) or $q < k_F$ (hole). The bare electron propagator is

$$\overrightarrow{\text{---}(\mathbf{q}, \varepsilon)} = iG_0^+(\mathbf{q}, \varepsilon) = \frac{i}{\varepsilon - \varepsilon_{\mathbf{q}} + i0^+}, \quad (6.62)$$

where we have defined

$$\varepsilon_{\mathbf{q}} = \frac{q^2}{2m}. \quad (6.63)$$

⁵We might also be concerned with decays into softer phonons. However, these are suppressed by additional electron-phonon interaction vertices.

The bare hole propagator is

$$\overleftarrow{\text{---}}^{(\mathbf{q}, \varepsilon)} = iG_0^-(\mathbf{q}, \varepsilon) = \frac{i}{\varepsilon - \varepsilon_{\mathbf{q}} - i0^+}. \quad (6.64)$$

The free Boson Lagrangian is written in terms of the displacement field \mathbf{P} as

$$\mathcal{L}_{\text{fb}} = \frac{1}{2}\dot{P}^2 - \frac{\xi^2}{2}(\partial^2 \partial_i P)^2. \quad (6.65)$$

As usual, one would Fourier expand \mathbf{P} such that

$$\mathbf{P}_{\mathbf{k}} = \frac{\hat{\mathbf{k}}}{\sqrt{\omega_{\mathbf{k}}}} (a_{\mathbf{k}} e^{-i(\omega t - \mathbf{k} \cdot \mathbf{x})} + a_{\mathbf{k}}^\dagger e^{i(\omega t - \mathbf{k} \cdot \mathbf{x})}), \quad (6.66)$$

where

$$\omega_{\mathbf{k}}^2 = \xi^2 k^6. \quad (6.67)$$

Note that we only keep the longitudinal component since only this component contributes to the interaction. Plugging this into \mathcal{L}_{fb} gives

$$\mathcal{L}_{\text{fb}}^{(k)} = \frac{1}{2} \left(\frac{-\omega^2 + \omega_{\mathbf{k}}^2}{\omega_{\mathbf{k}}} \right) (a_{\mathbf{k}} e^{-i(\omega t - \mathbf{k} \cdot \mathbf{x})} + a_{\mathbf{k}}^\dagger e^{i(\omega t - \mathbf{k} \cdot \mathbf{x})})^2. \quad (6.68)$$

Therefore, if we take the convention of [101], where the phonon is created by $a_{\mathbf{k}}^\dagger$ (with no prefactors), then the bare phonon propagator is

$$\overline{\text{-----}}^{(\mathbf{k}, \omega)} = iD_0(\mathbf{k}, \omega) = \frac{2i\omega_{\mathbf{k}}}{\omega^2 - \omega_{\mathbf{k}}^2 + i0^+}. \quad (6.69)$$

The interaction term is

$$\mathcal{L}_{\text{int}} = -g\psi^\dagger \psi (\nabla \cdot \mathbf{P}) = \psi^\dagger \psi \left(V_{\mathbf{k}} a_{\mathbf{k}} e^{-i(\omega t - \mathbf{k} \cdot \mathbf{x})} + V_{\mathbf{k}}^* a_{\mathbf{k}}^\dagger e^{i(\omega t - \mathbf{k} \cdot \mathbf{x})} \right), \quad (6.70)$$

where

$$V_{\mathbf{k}} = -\frac{igk}{\sqrt{\omega_{\mathbf{k}}}}. \quad (6.71)$$

Note that the phonon line is created by $a_{\mathbf{k}}^\dagger$ (with no prefactors) and annihilated by $a_{\mathbf{k}}$, the Feynman rule for the vertex factor is

$$\begin{array}{c} \mathbf{k} \\ \rightarrow \\ \overline{\text{-----}} \\ \swarrow \nearrow \\ \text{---} \end{array} = -iV_{\mathbf{k}} = -\frac{gk}{\sqrt{\omega_{\mathbf{k}}}}, \quad \begin{array}{c} \mathbf{k} \\ \leftarrow \\ \overline{\text{-----}} \\ \swarrow \nearrow \\ \text{---} \end{array} = -iV_{\mathbf{k}}^* = \frac{gk}{\sqrt{\omega_{\mathbf{k}}}}. \quad (6.72)$$

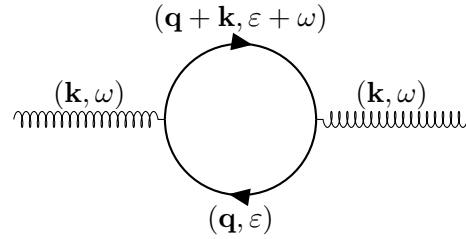
We summarize the Feynman rules below for convenience:

Quantity	Diagram	Feynman Rule
Electron propagator	$\xrightarrow{(\mathbf{q}, \varepsilon)}$	$iG_0^+(\mathbf{q}, \varepsilon) = \frac{i}{\varepsilon - \varepsilon_{\mathbf{q}} + i0^+}$
Hole propagator	$\xleftarrow{(\mathbf{q}, \varepsilon)}$	$iG_0^-(\mathbf{q}, \varepsilon) = \frac{i}{\varepsilon - \varepsilon_{\mathbf{q}} - i0^+}$
Phonon propagator	~~~~~	$iD_0(\mathbf{k}, \omega) = \frac{2i\omega_{\mathbf{k}}}{\omega^2 - \omega_{\mathbf{k}}^2 + i0^+}$
Absorption Vertex		$-iV_{\mathbf{k}} = \frac{-gk}{\sqrt{\omega_{\mathbf{k}}}}$
Emission Vertex		$-iV_{\mathbf{k}}^* = \frac{gk}{\sqrt{\omega_{\mathbf{k}}}}$

6.5.2. Phonon Propagator

Zero-Temperature Case

The diagram we wish to calculate is



The one-loop correction to the inverse phonon propagator is

$$(-1) \frac{1}{2} (2)(2) (-iV_{\mathbf{k}}) (-iV_{\mathbf{k}}^*) \overbrace{\int \frac{d\varepsilon d^3q}{(2\pi)^4} [iG_0^-(\mathbf{q}, \varepsilon)] [iG_0^+(\mathbf{q} + \mathbf{k}, \varepsilon + \omega)]}^{\mathcal{I}}. \quad (6.73)$$

The factor of (-1) is due to the fermion loop. The first factor of 2 is due to the sum over two diagrams with the electron and the hole exchanged; the second factor of 2 is due to the sum over spins. Since the vertex factor can depend only on the momentum of the phonon, it can be pulled out of the integral over the fermion degrees of freedom, which is why we do not actually need the exact form of the vertex until the end, when we will examine the behavior of the result as a function of \mathbf{k} .

$$\mathcal{I} = \frac{1}{(2\pi)^4} \int d^3q \int_{-\infty}^{\infty} d\varepsilon \frac{i}{\varepsilon - \varepsilon_{\mathbf{q}} - i0^+} \frac{i}{(\omega + \varepsilon) - \varepsilon_{\mathbf{q}+\mathbf{k}} + i0^+}. \quad (6.74)$$

Expand out the propagators as usual:

$$\frac{1}{x - i0^+} = \mathcal{P} \frac{1}{x} + i\pi\delta(x). \quad (6.75)$$

In a shortcut notation, we denote

$$\frac{1}{\varepsilon - \varepsilon_{\mathbf{q}} - i0^+} = \mathcal{P}_{\mathbf{q}} + i\pi\delta_{\mathbf{q}}, \quad \frac{1}{\varepsilon - \varepsilon_{\mathbf{q}+\mathbf{k}} + \omega + i0^+} = \mathcal{P}_{\mathbf{k}} - i\pi\delta_{\mathbf{k}}. \quad (6.76)$$

Therefore,

$$\text{Re} \mathcal{I} \sim \int \mathcal{P}_{\mathbf{q}} \mathcal{P}_{\mathbf{k}} + \pi^2 \delta_{\mathbf{q}} \delta_{\mathbf{k}}, \quad \text{Im} \mathcal{I} \sim \int \pi (\mathcal{P}_{\mathbf{k}} \delta_{\mathbf{q}} - \mathcal{P}_{\mathbf{q}} \delta_{\mathbf{k}}). \quad (6.77)$$

Note that

$$0 = \text{Re} \int \frac{1}{\dots - i0^+} \frac{1}{\dots - i0^+} = \int \mathcal{P}_{\mathbf{q}} \mathcal{P}_{\mathbf{k}} - \pi^2 \delta_{\mathbf{q}} \delta_{\mathbf{k}}. \quad (6.78)$$

Therefore,

$$\text{Re} \mathcal{I} \sim \int 2\pi^2 \delta_{\mathbf{q}} \delta_{\mathbf{k}}. \quad (6.79)$$

Hence,

$$\text{Re} \mathcal{I} = -\frac{2}{(2\pi)^4} \int d^3q \int_{-\infty}^{\infty} d\varepsilon \pi^2 \delta(\varepsilon - \varepsilon_{\mathbf{q}}) \delta(\varepsilon - \varepsilon_{\mathbf{q}+\mathbf{k}} + \omega).$$

and

$$\begin{aligned} \text{Im} \mathcal{I} &= -\frac{1}{(2\pi)^4} \int d^3q \int_{-\infty}^{\infty} d\varepsilon \left[\frac{\pi\delta(\varepsilon - \varepsilon_{\mathbf{q}})}{\varepsilon - \varepsilon_{\mathbf{q}+\mathbf{k}} + \omega} + \frac{-\pi\delta(\varepsilon - \varepsilon_{\mathbf{q}+\mathbf{k}} + \omega)}{\varepsilon - \varepsilon_{\mathbf{q}}} \right] \\ &= -\frac{1}{(2\pi)^3} \int d^3q \frac{1}{\varepsilon_{\mathbf{q}} - \varepsilon_{\mathbf{q}+\mathbf{k}} + \omega}. \end{aligned}$$

Here

$$\varepsilon_{\mathbf{q}} - \varepsilon_{\mathbf{q}+\mathbf{k}} = -\frac{qk \cos \theta}{m} - \frac{k^2}{2m}, \quad (6.80)$$

where θ is the angle between \mathbf{q} and \mathbf{k} .

Finite Temperature Case

Although we are only concerned with the zero temperature limit, it turns out to be necessary to consider the finite temperature Green's function when dealing with the real part of \mathcal{I} . After summing over the Matsubara frequencies, the temperature dependent part of the Green's function contributes a factor $\tanh(\varepsilon/2T)$ to the integrand of \mathcal{I} . Therefore,

$$\mathcal{I} = \frac{1}{(2\pi)^4} \int d^3q \int_{-\infty}^{\infty} d\varepsilon \frac{i}{\varepsilon - \varepsilon_{\mathbf{q}} - i0^+} \frac{i}{\varepsilon - \varepsilon_{\mathbf{q}+\mathbf{k}} + \omega + i0^+} \tanh \frac{\varepsilon}{2T}.$$

Hence,

$$\begin{aligned} \text{Re} \mathcal{I} &= -\frac{1}{16\pi^2} \int_{-\infty}^{\infty} d\varepsilon \int d^3q \delta(\varepsilon - \varepsilon_{\mathbf{q}}) \delta(\varepsilon - \varepsilon_{\mathbf{q}+\mathbf{k}} + \omega) \left(\tanh \frac{\varepsilon}{2T} - \tanh \frac{\varepsilon - \omega}{2T} \right), \\ \text{Im} \mathcal{I} &= -\frac{1}{8\pi^3} \int d^3q \frac{1}{\varepsilon_{\mathbf{q}} - \varepsilon_{\mathbf{q}+\mathbf{k}} + \omega} \tanh \frac{\varepsilon_{\mathbf{q}}}{2T}. \end{aligned}$$

Real Part of \mathcal{I}

Let us focus on the real part of \mathcal{I} first. Define $\mathbf{q}_1 = \mathbf{q} + \mathbf{k}$. Note that $q_1^2 = q^2 + k^2 + 2qk \cos \theta$ and $2q_1 dq_1 = 2qk d \cos \theta$. Moreover, the integral over the azimuthal angle in Eqn. (6.80) just gives a factor of 2π . We cut off the integral over q by a upper bound p_0 . Then,

$$\text{Re } \mathcal{I} = -\frac{1}{8\pi k} \int_{-\infty}^{\infty} d\varepsilon \int dq dq_1 q q_1 \delta\left(\varepsilon - \frac{q^2}{2m}\right) \delta\left(\varepsilon - \frac{q_1^2}{2m} + \omega\right) \left(\tanh \frac{\varepsilon}{2T} - \tanh \frac{\varepsilon - \omega}{2T}\right).$$

The q_1 integral pulls out a factor of m as well as imposing the condition

$$|a| \leq 1,$$

where

$$a \equiv \frac{k}{2p_0} - \frac{m\omega}{k p_0}.$$

Subsequently, the q integral once again just pulls out a factor of m and imposes the upper bound p_0^2/m on the ε integral. However, after removing dimensions by pulling out the temperature dependence, the upper limit of the resulting integral goes to ∞ in the low temperature limit anyway. The result is

$$\text{Re } \mathcal{I} = -\frac{m^2 \omega}{8\pi k} \theta(1 - a^2). \quad (6.81)$$

Imaginary Part of \mathcal{I}

At zero temperature, the T dependence will drop out in $\text{Im } \mathcal{I}$. The integral over θ is easily done giving the result

$$\begin{aligned} i \text{Im } \mathcal{I} &= -\frac{i}{(2\pi)^2} \int_0^{p_0} dq q^2 \left(-\frac{m}{qk}\right) \left(\ln \left| -\frac{qk \cos \theta}{m} - \frac{k^2}{2m} + \omega \right| \right)_{\theta=\pi}^{\theta=0} \\ &= \frac{i}{(2\pi)^2} \frac{m p_0^2 a}{k} h(a), \end{aligned} \quad (6.82)$$

where we defined

$$h(a) \equiv a \int_0^{-1/a} dx x \ln \left| \frac{1-x}{1+x} \right|. \quad (6.83)$$

Furthermore,

$$\begin{aligned} h(a) &= a \int_0^{\frac{1}{a}} dx x \ln \left| \frac{1+x}{1-x} \right| \\ &= a \int_0^1 dx x \ln \left(\frac{1+x}{1-x} \right) + a^2 \int_1^{\frac{1}{a}} dx x \ln \left(\frac{1+x}{x-1} \right) \\ &= a(I_1 + I_2). \end{aligned}$$

Note that the above expression is valid for $|a| > 1$. Here,

$$\begin{aligned} I_1 &= \int_0^\infty d(\tanh^2 v)v = \lim_{M \rightarrow \infty} \left(v \tanh^2 v \Big|_0^M - \int_0^M dv \frac{\cosh^2 v - 1}{\cosh^2 v} \right) \\ &= \tanh v \Big|_0^\infty + \lim_{M \rightarrow \infty} M(\tanh^2 M - 1) = 1, \end{aligned}$$

and

$$\begin{aligned} I_2 &= \int_\infty^{\operatorname{arctanh} a} d(\coth^2 v)v = \lim_{M \rightarrow \infty} \left(v \coth^2 v \Big|_M^{\operatorname{arctanh} a} - \int_M^{\operatorname{arctanh} a} dv \frac{1 + \sinh^2 v}{\sinh^2 v} \right) \\ &= \left(\frac{1}{a^2} - 1 \right) \operatorname{arctanh} a - \left(-\coth v \Big|_\infty^{\operatorname{arctanh} a} \right) + \lim_{M \rightarrow \infty} [-M(\coth^2 M - 1)] \\ &= -1 + \frac{1}{a} + \left(\frac{1}{a^2} - 1 \right) \operatorname{arctanh} a. \end{aligned}$$

Therefore,

$$h(a) = 1 + \frac{1 - a^2}{a} \operatorname{arctanh} a = -2a \sum_{n=0}^{\infty} \frac{a^{2n}}{4n^2 - 1}. \quad (6.84)$$

For $|a| < 1$, Eqn. (6.83) yields

$$h(a) = a \int_0^{\operatorname{arctanh} \frac{1}{a}} d(\tanh^2 v)v = 1 + \frac{1 - a^2}{a} \operatorname{arctanh} \frac{1}{a}.$$

Generically, we have

$$h(a) = 1 + \frac{1 - a^2}{2a} \ln \left| \frac{1 + a}{1 - a} \right|. \quad (6.85)$$

This reproduces Eqn. 21.14 in [95].

One-Loop Correction to the Phonon Propagator

Combining (6.81) and (6.82), we obtain the random phase approximation (RPA) form of the exact phonon propagator:

$$\begin{aligned} & iD_{\text{phonon}}(\mathbf{k}, \omega) \\ &= \frac{2i\omega_{\mathbf{k}}}{\omega^2 - \omega_{\mathbf{k}}^2} + \left(\frac{2i\omega_{\mathbf{k}}}{\omega^2 - \omega_{\mathbf{k}}^2} \right)^2 \frac{2g^2 k^2}{\omega_{\mathbf{k}}} \left[\frac{i}{(2\pi)^2} \frac{mp_0^2 a}{k} h(a) - \frac{m^2 \omega}{8\pi k} \theta(1 - a^2) \right] + \dots \\ &\approx \frac{2i\omega_{\mathbf{k}}^2}{\omega^2 - \omega_{\mathbf{k}}^2} \sum_{n=0}^{\infty} \left[\frac{2i\omega_{\mathbf{k}}}{\omega^2 - \omega_{\mathbf{k}}^2} \left(\frac{ig^2 mp_0^2 k}{2\pi^2 \omega_{\mathbf{k}}} a h(a) - \frac{g^2 m^2 \omega k}{4\pi \omega_{\mathbf{k}}} \theta(1 - a^2) \right) \right]^n \\ &= \frac{2i\omega_{\mathbf{k}}}{\omega^2 - \omega_{\mathbf{k}}^2 - \Pi}, \end{aligned}$$

where

$$\Pi = -\frac{g^2 m p_0^2 k}{\pi^2} a h(a) - \frac{i g^2 m^2 \omega k}{2\pi} \theta(1 - a^2). \quad (6.86)$$

In the regime where $\omega \ll \frac{k^2}{m}$, we have

$$\begin{aligned} \Pi &= -\frac{g^2 p_0 m k^2}{2\pi^2} h\left(\frac{k}{2p_0}\right) - \frac{i g^2 m^2 \omega k}{2\pi} \theta(2p_0 - k) \\ &= -\frac{g^2 p_0 m}{\pi^2} \left(k^2 - \frac{1}{12} \frac{k^4}{p_0^2} - \frac{1}{240} \frac{k^6}{p_0^4} + \dots \right) - \frac{i g^2 m^2 \omega k}{2\pi} \theta(2p_0 - k). \end{aligned}$$

The correction to $\omega_{\mathbf{k}}$ is thus

$$\omega_{\mathbf{k}}^2 \rightarrow \omega_{\mathbf{k}}^2 - \frac{g^2 p_0 m}{\pi^2} \left(k^2 - \frac{1}{12} \frac{k^4}{p_0^2} - \frac{1}{240} \frac{k^6}{p_0^4} + \dots \right) - \frac{i g^2 m^2 \omega k}{2\pi} \theta(2p_0 - k),$$

i.e.,

$$\omega_{\mathbf{k}}^2 \rightarrow k^2 \left[\frac{\omega_{\mathbf{k}}^2}{k^2} - \eta h\left(\frac{k}{2p_0}\right) - \eta \frac{i\pi m \omega}{p_0 k} \theta(2p_0 - k) \right], \quad (6.87)$$

where

$$\eta = \frac{g^2 p_0 m}{2\pi^2}.$$

Note that $[\eta] = T^{-2} L^2$, which is customarily dimensionless near a $z = 1$ fixed point. Furthermore, (6.87) is identical to the results in [95, 100].

Small k and ω Regime

We study the behavior of the real part of (6.86) at small k and ω . We define

$$\nu = \frac{m\omega}{p_0 k}, \quad \kappa = \frac{k}{2p_0}.$$

We can then write

$$\Pi = \frac{2g^2 m p_0^3}{\pi} \kappa (\kappa - \nu) \left(1 + \frac{1 - (\kappa - \nu)^2}{2(\kappa - \nu)} \ln \left| \frac{1 + \kappa - \nu}{1 - \kappa + \nu} \right| \right).$$

It is convenient to define

$$f(k, \omega) = \kappa (\kappa - \nu) \left(1 + \frac{1 - (\kappa - \nu)^2}{2(\kappa - \nu)} \ln \left| \frac{1 + \kappa - \nu}{1 - \kappa + \nu} \right| \right). \quad (6.88)$$

If we approach $(k, \omega) \rightarrow 0$ along the direction $\omega = 0$, i.e., $\nu = 0$, we obtain

$$f(k, \omega) = \kappa^2 \left(1 + \frac{1 - \kappa^2}{2\kappa} \ln \left| \frac{1 + \kappa}{1 - \kappa} \right| \right) \rightarrow \kappa^2 = \frac{k^2}{4p_0^2}.$$

This is known as the static limit. The decay rate stays at 0 in this case.

Along the direction $k \rightarrow 0$, $f(k, \omega)$ is divergent. This case is referred to as the dynamical long-wavelength limit. For large $\nu > 0$, we have

$$f(k, \omega) \rightarrow \kappa \nu \left[1 - \frac{1 - \nu^2}{2\nu} \ln \left(\frac{1 - \frac{1}{\nu}}{1 + \frac{1}{\nu}} \right) \right] \rightarrow \frac{\kappa}{\nu} = \frac{k^2}{2m\omega}.$$

Note that at $\nu \rightarrow \infty$, the real part goes to 0 and the imaginary part of Π goes to infinity, and thus the phonons decay quickly into electron-hole pairs.

What if $\nu \rightarrow 1$? This seemingly divergent point is not singular at all. We denote $\nu = 1 - z$. Then

$$f(k, \omega) \rightarrow -\kappa(1 - z) \left[1 - \frac{1 - (1 - z)^2}{2(1 - z)} \ln \left(\frac{z}{2 - z} \right) \right] \rightarrow -\kappa [1 + (\ln 2 - 1 - \ln z) z].$$

For small z , we have

$$\lim_{z \rightarrow 0} z \ln z = -\lim_{z \rightarrow 0} z = 0.$$

Therefore,

$$f(k, \omega) \rightarrow -\kappa(1 + z \ln 2) \rightarrow -\frac{k}{2p_0}.$$

For $z > 1$, the parameter ν approaches 0 as k approaches 0. Therefore, the static limit is the appropriate one in this case, and, indeed, we find that the multicritical phonons are indeed stable against decay.

6.6. Discussion

In this chapter, we applied the lessons that we have learned in the previous chapters to the naturalness problem of the linear dependence in temperature of the heat capacity of some materials, namely strange metals. We demonstrated that this behavior may be described within the standard picture of electron-phonon interactions, as long as one allows the phonons to be multicritical and, in particular, near their lower critical dimension. Furthermore, we are clear in pointing out that these phonons need not be of the usual type of lattice vibrations – they are bosonic degrees of freedom, which interact with the electrons. This is their universal description and we have not speculated as to their exact nature and microscopic origin. In addition, we do not go so far as to suggest that this mechanism is indeed the one in play in all known high- T_c superconductors. However, the mechanism is available and there may very well be physical systems in which it comes to play.

In the context of this thesis, we highlight one main virtue of this model of multicritical phonons interacting with electrons – it is technically natural and protected by the polynomial shift symmetry. This addresses the main theoretical conundrum raised in [93], which demonstrates that attempts at modeling the behavior of the resistivity are almost certainly doomed to be technically unnatural. The Lifshitz scaling in our model represents one way around this problem. However, as mentioned earlier, the question of how two interacting subsystems with different scalings settle into one overall dynamical exponent remains open and represents an intriguing direction for future research.

Appendix

6.A. The Standard Model of Superconductivity

6.A.1. The Phonon-Electron Interaction

In this appendix, we outline the standard model of superconductivity in which an electron-phonon interaction produces an attractive effective electron-electron interaction. A phase transition occurs when this interaction overwhelms the repulsive electromagnetic interaction. Electrons form Bosonic Cooper pairs, which condense. This discussion follows closely *Solid State Theory* by Zheng-Zhong Li [102].

The Classical Theory of Phonon-Electron Interaction

For simple crystal lattices we can focus on the acoustic oscillations. Suppose that the interaction potential between an ion at lattice ℓ and an electron at \mathbf{r}_i is $V(\ell - \mathbf{r}_i)$. For static ions, the interaction between electrons and ions can be obtained by summing over all lattices and electrons as follows:

$$\sum_{i,\ell} V(\mathbf{r}_i - \ell). \quad (6.89)$$

To take into account of the vibrations of the ions, we introduce a relative time-dependent displacement $\mathbf{u}_\ell(t)$ to ℓ , which describes a small deviation of an ion from its equilibrium position:

$$\sum_{i,\ell} V[\mathbf{r}_i - (\ell + \mathbf{u}_\ell)] \quad (6.90)$$

Then the interaction between electrons and the lattice vibrations is simply the discrepancy between the Hamiltonian :

$$H_{\text{el-ph}} = \sum_{i,\ell} \left(V[\mathbf{r}_i - (\ell + \mathbf{u}_\ell)] - V(\mathbf{r}_i - \ell) \right) = - \sum_{i,\ell} \mathbf{u}_\ell \cdot \nabla V(\mathbf{r}_i - \ell). \quad (6.91)$$

For a monovalent metal, we have

$$V(\mathbf{r}_i - \ell) = - \frac{4\pi e^2}{|\mathbf{r}_i - \ell|} e^{-\lambda|\mathbf{r}_i - \ell|}, \quad (6.92)$$

where λ is the Coulomb screening factor.

The Bloch Representation

Define $\psi_{n,\mathbf{k}}(\mathbf{r})$ as the Bloch function, which represents the energy eigenfunctions of the Hamiltonian of a single electron in the ideal lattice, i.e.,

$$H \psi_{n,\mathbf{k}}(\mathbf{r}) = E_n(\mathbf{k}) \psi_{n,\mathbf{k}}(\mathbf{r}),$$

where n denotes the energy band and \mathbf{k} denotes the wave vector. The sum over spins is taken for granted. Normalized appropriately, the Bloch functions are orthonormal. The Bloch theorem implies

$$\psi_{\mathbf{k}}(\mathbf{r}) = u_{\mathbf{k}}(\mathbf{r}) e^{i\mathbf{k}\cdot\mathbf{r}}, \quad u_{\mathbf{k}}(\mathbf{r} + \boldsymbol{\ell}) = u_{\mathbf{k}}. \quad (6.93)$$

Any periodic wave function $\Psi(\mathbf{r})$ can be expanded in Bloch functions,

$$\Psi(\mathbf{r}) = \sum_{n,\mathbf{k}} c_{n,\mathbf{k}} \psi_{n,\mathbf{k}}(\mathbf{r}),$$

where

$$c_{n,\mathbf{k}} = \int d\mathbf{r} \Psi(\mathbf{r}) \psi_{n,\mathbf{k}}^*(\mathbf{r}).$$

Lattice Dynamics

The Hamiltonian that describes the oscillations of the lattice system is

$$H_{\text{ph}} = \frac{1}{2M} \sum_{\ell} p_{\ell}^i \cdot p_{\ell}^i + \frac{1}{2} \sum_{\ell} \sum_{\ell'} U_{ij}(\ell - \ell') u_{\ell}^i u_{\ell'}^j, \quad (6.94)$$

where $p_{\ell} = M\dot{u}_{\ell}$, with p_{ℓ} the conjugate momentum of u_{ℓ} and M the ion mass.

Applying the Bloch theorem to the lattice vibration u_{ℓ} , we obtain

$$u_{\ell} = e^{i\mathbf{k}\cdot\mathbf{R}_{\ell}} u_0,$$

Due to the periodicity of the lattice, the wave vector \mathbf{k} is not uniquely defined; instead, the associated Bloch functions will have the same value for two wave vectors \mathbf{k} and \mathbf{k}' , when

$$\mathbf{k}' - \mathbf{k} = \mathbf{K}_n,$$

where the length of \mathbf{K}_n is equal to n reciprocal lattice constant $1/a$. We restrict the domain of \mathbf{k} to the first Brillouin zone, within which the difference between any two wave vectors is smaller than the reciprocal lattice constant. We define N as the total number of wave vectors within the first Brillouin zone. Therefore, the Brillouin zone contains N different \mathbf{k} , and each \mathbf{k} is associated with three polarizations. In total there are $3N$ normal modes, which we denote as Q_k . We use these $3N$ normal modes to expand the lattice vibration \mathbf{u}_{ℓ} as follows:

$$\mathbf{u}_{\ell} = \frac{1}{\sqrt{NM}} \sum_{\mathbf{k}} \epsilon_k Q_k e^{i\mathbf{k}\cdot\mathbf{R}_{\ell}}, \quad (6.95)$$

where ϵ_k denotes the polarization of the wave vector \mathbf{k} . Plugging the normal mode expansion of \mathbf{u}_ℓ back into (6.94), we obtain

$$H = \frac{1}{2} \sum_{\mathbf{k}} (P_{\mathbf{k}}^* P_{\mathbf{k}} + \omega_{\mathbf{k}}^2 Q_{\mathbf{k}}^* Q_{\mathbf{k}}),$$

with

$$P_k = \dot{Q}_k^*,$$

the conjugate momentum of P_k . Canonically quantize the system, we obtain

$$[P_{\mathbf{k}}, Q_{\mathbf{k}'}] = -i\delta_{\mathbf{k},\mathbf{k}'}, \quad [P_{\mathbf{k}}, P_{\mathbf{k}'}] = [Q_{\mathbf{k}}, Q_{\mathbf{k}'}] = 0.$$

Applying the canonical transformation, we define

$$a_{\mathbf{k}} = \sqrt{\frac{\omega_{\mathbf{k}}}{2}} \left(Q_{\mathbf{k}} - \frac{P_{-\mathbf{k}}}{i\omega_{\mathbf{k}}} \right), \quad a_{\mathbf{k}}^\dagger = \sqrt{\frac{\omega_{\mathbf{k}}}{2}} \left(Q_{-\mathbf{k}} + \frac{P_{\mathbf{k}}}{i\omega_{\mathbf{k}}} \right),$$

with the commutation relation

$$[a_{\mathbf{k}}, a_{\mathbf{k}'}^\dagger] = \delta_{\mathbf{k},\mathbf{k}'}, \quad [a_{\mathbf{k}}, a_{\mathbf{k}'}] = [a_{\mathbf{k}}^\dagger, a_{\mathbf{k}'}^\dagger] = 0.$$

The Hamiltonian is

$$H = \sum_{\mathbf{k}} \omega_{\mathbf{k}} \left(a_{\mathbf{k}}^\dagger a_{\mathbf{k}} + \frac{1}{2} \right).$$

The Quantum Theory of Phonon-Electron Interaction

Let $c_{n,\mathbf{k}}$ be the annihilation operator and $c_{n,\mathbf{k}}^\dagger$ the creation operator for electrons, satisfying

$$\{c_{\mathbf{k}}, c_{\mathbf{k}'}^\dagger\} = \delta_{\mathbf{k},\mathbf{k}'}, \quad \{c_{\mathbf{k}}, c_{\mathbf{k}'}\} = \{c_{\mathbf{k}}^\dagger, c_{\mathbf{k}'}^\dagger\} = 0.$$

The interaction Hamiltonian reads

$$H_{\text{el-ph}} = - \sum_{\ell} \sum_{\mathbf{k},\mathbf{k}'} \sum_{\mathbf{q}} \frac{1}{\sqrt{2NM\omega_{\mathbf{q}}}} (a_{\mathbf{q}} + a_{-\mathbf{q}}^\dagger) c_{\mathbf{k}'}^\dagger c_{\mathbf{k}} e^{i\mathbf{q}\cdot\ell} \\ \times \epsilon_{\mathbf{q}} \cdot \int d\mathbf{r} u_{\mathbf{k}'}^*(\mathbf{k}) u_{\mathbf{k}}(\mathbf{r}) e^{i(\mathbf{k}-\mathbf{k}')\cdot\mathbf{r}} \nabla V(\mathbf{r}-\ell),$$

where $\epsilon_{\mathbf{q}}$ is the polarization vector of the phonon with momentum \mathbf{q} .

Taking the Fourier transformation of $V(\mathbf{r})$,

$$V(\mathbf{r}) = \sum_{\mathbf{p}} V_{\mathbf{p}} e^{i\mathbf{p}\cdot\mathbf{r}},$$

we obtain

$$\int d\mathbf{r} u_{\mathbf{k}'}^*(\mathbf{k}) u_{\mathbf{k}}(\mathbf{r}) e^{i(\mathbf{k}-\mathbf{k}')\cdot\mathbf{r}} \nabla V(\mathbf{r}-\ell) = i \sum_{\mathbf{p}} \mathbf{p} V_{\mathbf{p}} \delta_{\mathbf{p},\mathbf{k}-\mathbf{k}'} e^{i(\mathbf{k}-\mathbf{k}')\cdot\mathbf{r}}.$$

For a monovalent metal, the Fourier transform of (6.92) gives

$$V_{\mathbf{q}} = -4\pi e^2 \int d^3\mathbf{r} \frac{e^{-i\mathbf{q}\cdot\mathbf{r}}}{r} e^{-\lambda r} = \frac{4\pi}{q^2 + \lambda^2}. \quad (6.96)$$

Within the first Brillouin zone, $\mathbf{K}_n = 0$ and $\mathbf{k}' = \mathbf{k} + \mathbf{q}$. In this case,

$$H_{\text{el-ph}} = -i \sum_{\mathbf{k}, \mathbf{q}} \sqrt{\frac{N}{2M}} \frac{q}{\sqrt{\omega_{\mathbf{q}}}} V_{\mathbf{q}} (a_{\mathbf{q}} + a_{-\mathbf{q}}^\dagger) c_{\mathbf{k}+\mathbf{q}}^\dagger c_{\mathbf{k}}. \quad (6.97)$$

Let us define

$$g_{\mathbf{p}} \equiv -i \sqrt{\frac{N}{2M}} \frac{q}{\sqrt{\omega_{\mathbf{q}}}} V_{\mathbf{q}},$$

then

$$H_{\text{el-ph}} = \sum_{\mathbf{k}, \mathbf{q}} \left(g_{\mathbf{p}} a_{\mathbf{p}} c_{\mathbf{k}+\mathbf{q}}^\dagger c_{\mathbf{k}} + g_{\mathbf{p}}^* a_{\mathbf{p}}^\dagger c_{\mathbf{k}-\mathbf{q}}^\dagger c_{\mathbf{k}} \right). \quad (6.98)$$

6.A.2. Nakajima Transformation and Effective Four-Electron Vertex

The full Hamiltonian of the electron-phonon system is

$$H = \sum_{\mathbf{q}} \omega_{\mathbf{q}} a_{\mathbf{q}}^\dagger a_{\mathbf{q}} + \sum_{\mathbf{k}} \varepsilon_{\mathbf{k}} c_{\mathbf{k}}^\dagger c_{\mathbf{k}} + \sum_{\mathbf{q}, \mathbf{k}} \left(g_{\mathbf{q}} a_{\mathbf{q}} c_{\mathbf{k}+\mathbf{q}}^\dagger c_{\mathbf{k}} + g_{\mathbf{q}}^* a_{\mathbf{q}} c_{\mathbf{k}-\mathbf{q}}^\dagger c_{\mathbf{k}} \right).$$

In this section we integrate out the phonon and derive the effective four-electron interaction.

In the following we introduce the Nakajima transformation, which automatically takes care of the 4-electron effective vertex with an exchanged phonon. Consider a many-body system with energy eigenvalue E , such that

$$H \Psi = E \Psi.$$

Under the canonical transformation

$$\Psi_S = e^S \Psi,$$

we define

$$H_S \equiv e^{-S} H e^S, \quad (6.99)$$

such that

$$H_S \Psi_S = E \Psi_S.$$

From (6.99) we obtain

$$\begin{aligned} H_S &= \left(1 - S + \frac{1}{2} S^2 + \dots \right) H \left(1 + S + \frac{1}{2} S^2 + \dots \right) \\ &= H + [H, S] + \frac{1}{2} [[H, S], S] + \dots \end{aligned}$$

Let us then take the following notation

$$\begin{aligned} H_0 &= \sum_{\mathbf{q}} \omega_{\mathbf{q}} a_{\mathbf{q}}^{\dagger} a_{\mathbf{q}} + \sum_{\mathbf{k}} \varepsilon_{\mathbf{k}} c_{\mathbf{k}}^{\dagger} c_{\mathbf{k}}, \\ H_1 &= \sum_{\mathbf{q}, \mathbf{k}} \left(g_{\mathbf{q}} a_{\mathbf{q}} c_{\mathbf{k}+\mathbf{q}}^{\dagger} c_{\mathbf{k}} + g_{\mathbf{q}}^* a_{\mathbf{q}} c_{\mathbf{k}-\mathbf{q}}^{\dagger} c_{\mathbf{k}} \right). \end{aligned} \quad (6.100)$$

Hence,

$$H_S = H_0 + H_1 + [H_0, S] + \frac{1}{2}[H_1, S] + \frac{1}{2}[H_1 + [H_0, S], S] + \dots$$

If we choose S such that

$$H_1 + [H_0, S] = 0, \quad (6.101)$$

then

$$H_S = H_0 + \frac{1}{2}[H_1, S] + \dots$$

To implement (6.101), S must be of the same order as H_1 , and thus we can assume the form of S to be

$$S = \sum_{\mathbf{k}, \mathbf{q}} \left(M_{\mathbf{q}} a_{\mathbf{q}} c_{\mathbf{k}+\mathbf{q}}^{\dagger} c_{\mathbf{k}} + N_{\mathbf{q}} a_{\mathbf{q}}^{\dagger} c_{\mathbf{k}-\mathbf{q}}^{\dagger} c_{\mathbf{k}} \right). \quad (6.102)$$

Denote the initial and final eigenstates of H_0 as $|i\rangle$ and $|f\rangle$, respectively, then

$$-\langle f|H_1|i\rangle = \langle f|[H_0, S]|i\rangle = (E_f - E_i) \langle f|S|i\rangle.$$

Therefore,

$$\langle f|S|i\rangle = \frac{\langle f|H_1|i\rangle}{E_i - E_f}.$$

Combined with (6.100) and (6.102), we can read off

$$M_{\mathbf{q}} = \frac{g_{\mathbf{q}}}{\omega_{\mathbf{q}} - \varepsilon_{\mathbf{k}+\mathbf{q}} + \varepsilon_{\mathbf{k}}}, \quad N_{\mathbf{q}} = \frac{g_{\mathbf{q}}^*}{-\omega_{\mathbf{q}} - \varepsilon_{\mathbf{k}-\mathbf{q}} + \varepsilon_{\mathbf{k}}}.$$

Therefore,

$$S = \sum_{\mathbf{k}, \mathbf{q}} \left(\frac{g_{\mathbf{q}} a_{\mathbf{q}} c_{\mathbf{k}}^{\dagger} c_{\mathbf{k}}}{\varepsilon_{\mathbf{k}} - \varepsilon_{\mathbf{k}+\mathbf{q}} + \omega_{\mathbf{q}}} + \frac{g_{\mathbf{q}}^{\dagger} a_{\mathbf{q}}^{\dagger} c_{\mathbf{k}-\mathbf{q}}^{\dagger} c_{\mathbf{k}}}{\varepsilon_{\mathbf{k}} - \varepsilon_{\mathbf{k}-\mathbf{q}} - \omega_{\mathbf{q}}} \right).$$

Since we are only interested in the operators $c^{\dagger} c$ and $c^{\dagger} c^{\dagger} c c$, we will compute the average of the Hamiltonian over the vacuum state of the phonon $|0\rangle$, in which all other types of terms will be excluded. Namely,

$$\langle 0| \frac{1}{2} [H_1, S] |0\rangle = \frac{1}{2} \sum_{\mathbf{q}} \left(\langle 0|H_1|1_{\mathbf{q}}\rangle \langle 1_{\mathbf{q}}|S|0\rangle - \langle 0|S|1_{\mathbf{q}}\rangle \langle 1_{\mathbf{q}}|H_1|0\rangle \right),$$

where $|1_{\mathbf{q}}\rangle$ is the one-phonon state with momentum \mathbf{q} . Note that

$$\begin{aligned}\langle 0|H_1|1_{\mathbf{q}}\rangle &= g_{\mathbf{q}} c_{\mathbf{k}+\mathbf{q}}^\dagger c_{\mathbf{k}}, & \langle 1_{\mathbf{q}}|H_1|0\rangle &= \sum_{\mathbf{k}} g_{\mathbf{q}}^\dagger c_{\mathbf{k}-\mathbf{q}}^\dagger c_{\mathbf{k}}; \\ \langle 0|S|1_{\mathbf{q}}\rangle &= \sum_{\mathbf{k}} \frac{g_{\mathbf{q}} c_{\mathbf{k}+\mathbf{q}}^\dagger c_{\mathbf{k}}}{\varepsilon_{\mathbf{k}} - \varepsilon_{\mathbf{k}+\mathbf{q}} + \omega_{\mathbf{q}}}, & \langle 1_{\mathbf{q}}|S|0\rangle &= \sum_{\mathbf{k}} \frac{g_{\mathbf{q}}^\dagger c_{\mathbf{k}-\mathbf{q}}^\dagger c_{\mathbf{k}}}{\varepsilon_{\mathbf{k}} - \varepsilon_{\mathbf{k}-\mathbf{q}} - \omega_{\mathbf{q}}}.\end{aligned}$$

Therefore,

$$\langle 0|\frac{1}{2}[H_1, S]|0\rangle = \frac{1}{2} \sum_{\mathbf{k}, \mathbf{k}', \mathbf{q}} |g_{\mathbf{q}}|^2 \left(\frac{c_{\mathbf{k}+\mathbf{q}}^\dagger c_{\mathbf{k}} c_{\mathbf{k}'-\mathbf{q}}^\dagger c_{\mathbf{k}'}}{\varepsilon_{\mathbf{k}'} - \varepsilon_{\mathbf{k}'-\mathbf{q}} - \omega_{\mathbf{q}}} - \frac{c_{\mathbf{k}+\mathbf{q}}^\dagger c_{\mathbf{k}} c_{\mathbf{k}'-\mathbf{q}}^\dagger c_{\mathbf{k}'}}{\varepsilon_{\mathbf{k}} - \varepsilon_{\mathbf{k}+\mathbf{q}} + \omega_{\mathbf{q}}} \right).$$

We can then write the effective electron-electron interaction as

$$H_{\text{el-ph}} = \frac{1}{2} \sum_{\mathbf{k}, \mathbf{k}', \mathbf{q}} G_{\mathbf{k}, \mathbf{q}} c_{\mathbf{k}+\mathbf{q}}^\dagger c_{\mathbf{k}} c_{\mathbf{k}'-\mathbf{q}}^\dagger c_{\mathbf{k}'}, \quad (6.103)$$

with

$$G_{\mathbf{k}, \mathbf{q}} = \frac{2|g_{\mathbf{q}}|^2 \omega_{\mathbf{q}}}{(\varepsilon_{\mathbf{k}} - \varepsilon_{\mathbf{k}+\mathbf{q}})^2 - \omega_{\mathbf{q}}^2}.$$

This is the effective interaction from exchanging phonons between electrons.

6.A.3. BCS Superconductivity Theory

BCS Reduced Hamiltonian

The electrons interact with each other by exchanging phonons and photons, with the former described by (6.103) and latter by the Coulomb interaction. The total interaction is

$$H_{\text{int}} = \frac{1}{2} \sum_{\mathbf{q}, \mathbf{k}_1, \mathbf{k}_2} \left(G_{\mathbf{k}, \mathbf{q}} + \frac{4\pi e^2}{q^2 + \lambda^2} \right) c_{\mathbf{k}_1+\mathbf{q}}^\dagger c_{\mathbf{k}_2-\mathbf{q}}^\dagger c_{\mathbf{k}_2} c_{\mathbf{k}_1}. \quad (6.104)$$

Hence, the total potential in Fourier space is

$$\frac{4\pi e^2}{q^2 + \lambda^2} \left(1 + \frac{8\pi e^2}{M\Omega(q^2 + \lambda^2)} \frac{q^2}{\omega^2 - \omega_{\mathbf{q}}^2} \right).$$

Note that, around the Fermi surface, the phonon frequency is $\omega_{\mathbf{q}}$ is approximately the Debye frequency ω_{D} . Below this frequency, the potential results in an attractive force and above this frequency, the force will be repulsive. Therefore, Cooper pairs are obtained only when the energy of the exchanged phonons is below the Debye frequency. Note that ω_{D} tends to be of order 10^{-2} eV, which is much less than the Fermi energy ε_F , which tends to be of order 10 eV.

Assuming that the screening is very effective, we can take $\lambda \gg q$ and thus

$$\frac{4\pi e^2}{\lambda^2} \left(1 + \frac{8\pi e^2}{M\Omega\lambda^2} \frac{q^2}{\omega^2 - \omega_{\mathbf{q}}^2} \right).$$

The factor

$$c_s = \sqrt{\frac{4\pi e^2}{M\Omega\lambda^2}},$$

is interpreted as the speed of sound via analogy with the speed of sound in a chain of masses. Therefore, the effective potential is

$$U_{\text{eff}} = \frac{4\pi e^2}{\lambda^2} \left(1 + \frac{2c_s^2 q^2}{\omega^2 - \omega_{\mathbf{q}}^2} \right).$$

If the phonon dispersion is $\omega_{\mathbf{q}} = c_s q$, and the electrons lie near the Fermi surface, then in the $\omega \rightarrow 0$ (static) limit, one finds

$$U_{\text{eff}}^{(1)} = -\frac{4\pi e^2}{\lambda^2},$$

which is a constant. Then the effective potential in position space is

$$E^{(1)} = -\frac{4\pi e^2}{\lambda^2} \delta(\mathbf{r}),$$

an attractive delta function well.

If the phonon dispersions is $\omega_{\mathbf{q}} = \zeta_2 q^2$, then the effective potential becomes

$$U_{\text{eff}}^{(2)} = \frac{4\pi e^2}{\lambda^2} \left(1 - \frac{2c_s^2}{\zeta_2^2 q^2} \right),$$

which we regulate via an IR regulator μ :

$$U_{\text{eff}}^{(2)} = \frac{4\pi e^2}{\lambda^2} \left(1 - \frac{2c_s^2}{\zeta_2^2} \frac{1}{q^2 + \mu^2} \right).$$

In position space, we find

$$E^{(2)} \sim -2\mu \left(\frac{ec_s}{\lambda\zeta_2} \right)^2 \frac{e^{-\mu r}}{\mu r}.$$

Note that we have dropped the formally repulsive delta function at the origin, because the theory will inevitably flow towards the $z = 1$ fixed point in the IR

If the phonon dispersion is $\omega_{\mathbf{q}} = \zeta_3 q^3$, then the effective potential becomes, after IR regulation,

$$U_{\text{eff}}^{(3)} = \frac{4\pi e^2}{\lambda^2} \left(1 - \frac{2c_s^2}{\zeta_3^2} \frac{1}{(q^2 + \mu^2)^2} \right).$$

In position space, we find

$$E^{(3)} \sim -\frac{1}{\mu} \left(\frac{e^2 c_s}{\lambda\zeta_3} \right)^2 e^{-\mu r}.$$

The higher-order dispersion relation resolves the delta-function well at the origin into a steep exponential well. The attractive region is enlarged, further facilitating electron pairing.

For future reference, we define

$$\mathcal{G}_{\mathbf{q}} = \frac{2\pi e^2 \gamma c_s^2 q^2}{\lambda^2 \omega_{\mathbf{q}}^2}. \quad (6.105)$$

If $\omega_{\mathbf{q}} = c_s q$, we have

$$\mathcal{G}_{\mathbf{q}}^{(1)} = \frac{2\pi e^2 \gamma}{\lambda^2},$$

which is a constant; if $\omega_{\mathbf{q}} = \xi q^3$, we have

$$\mathcal{G}_{\mathbf{q}}^{(3)} = \frac{2\pi e^2 \gamma c_s^2}{\lambda^2 \xi^2} \frac{1}{q^4}.$$

Thus we can rewrite (6.104) as

$$H_{\text{int}} = \frac{1}{2} \sum_{\mathbf{q}, \mathbf{k}_1, \mathbf{k}_2} \mathcal{G}_{\mathbf{q}} c_{\mathbf{k}_1 + \mathbf{q}}^\dagger c_{\mathbf{k}_2 - \mathbf{q}}^\dagger c_{\mathbf{k}_2} c_{\mathbf{k}_1}.$$

Now we consider the interaction between of a pair of electrons with momenta \mathbf{k}_1 and \mathbf{k}_2 , respectively, which scatter into electrons with momenta $\mathbf{k}_1 + \mathbf{q}$ and $\mathbf{k}_2 + \mathbf{q}$. Define the total wave vector as

$$\mathbf{K} = \mathbf{k}_1 + \mathbf{k}_2.$$

The phase space volume of the attractive regions (i.e., when the frequency of the exchanged phonon is smaller than ω_{D}) swept out by \mathbf{k}_1 and \mathbf{k}_2 for specific total momentum \mathbf{K} is small for $\mathbf{K} \neq 0$. However, in the case of $\mathbf{K} = 0$, the pairing region is extended to be the volume between two concentric spheres with $2\omega_{\text{D}}$ energy difference, which is much larger than the phase space volume of any electron pair with $\mathbf{K} \neq 0$. Therefore, the scattering will be dominated by the $\mathbf{K} = 0$ processes, and the interaction can be thus simplified to

$$H_{\text{int}} = -\frac{1}{2} \sum_{\mathbf{k}, \mathbf{k}'} \mathcal{G}_{\mathbf{k}' - \mathbf{k}} c_{\mathbf{k}'}^\dagger c_{-\mathbf{k}'}^\dagger c_{-\mathbf{k}} c_{\mathbf{k}},$$

Moreover, the two electrons have to be physically close to each other in position space to form a Cooper pair, due to the Pauli exclusion principle, the two electrons of opposite quasi-momentum within the Cooper pair tend to have opposite spins. Therefore, the interaction term can be further simplified to

$$H_{\text{int}} = - \sum_{\mathbf{k}, \mathbf{k}', \sigma} \mathcal{G}_{\mathbf{k}' - \mathbf{k}} c_{\mathbf{k}', \sigma}^\dagger c_{-\mathbf{k}', -\sigma}^\dagger c_{-\mathbf{k}, -\sigma} c_{\mathbf{k}, \sigma}.$$

The reduced BCS Hamiltonian reads

$$\begin{aligned} \mathcal{H} &\equiv H - \mu N \\ &= \sum_{\mathbf{k}} (\varepsilon_{\mathbf{k}} - \varepsilon_F) \left(c_{\mathbf{k}, \uparrow}^\dagger c_{\mathbf{k}, \uparrow} + c_{-\mathbf{k}, \downarrow}^\dagger c_{-\mathbf{k}, \downarrow} \right) - \sum_{\mathbf{k}, \mathbf{k}'} \mathcal{G}_{\mathbf{k}' - \mathbf{k}} c_{\mathbf{k}', \uparrow}^\dagger c_{-\mathbf{k}', \downarrow}^\dagger c_{-\mathbf{k}, \downarrow} c_{\mathbf{k}, \uparrow}. \end{aligned} \quad (6.106)$$

The Cooper Pair

We consider a system with a filled Fermi sphere and a pair of additional electrons at zero temperature. Suppose that the electrons within the Fermi sphere can be considered as free electrons. We need only consider the two-body scattering of the additional electrons. In this case, the existence of the Fermi sphere prevents the additional electrons from occupying the states with $k < k_F$, and we may neglect the scattering of electrons within the Fermi sphere. We can assume that these two additional electrons carry opposite momentum and spin. Hence the pair of electrons can be represented by the state

$$c_{\mathbf{k}}^\dagger c_{-\mathbf{k}}^\dagger |0\rangle,$$

with $|0\rangle$ denoting the ground state in which the Fermi sphere is fully occupied. However, $c_{\mathbf{k}}^\dagger c_{-\mathbf{k}}^\dagger |0\rangle$ is not an eigenstate of the reduced Hamiltonian \mathcal{H} . Generically, an energy eigenstate $|\Psi\rangle$ is a linear combination of such states:

$$|\Psi\rangle = \sum_{k>k_F} \beta_{\mathbf{k}} c_{\mathbf{k}}^\dagger c_{-\mathbf{k}}^\dagger |0\rangle.$$

We should also confine the sum over \mathbf{k} to be within the pairing region, i.e., $0 < \varepsilon_{\mathbf{k}} < \omega_D$. The coefficients $\beta_{\mathbf{k}}$ are to be determined. They satisfy the normalization condition

$$\sum_{\mathbf{k}} |\beta_{\mathbf{k}}|^2 = 1. \quad (6.107)$$

Hence,

$$E = \langle \Psi | \mathcal{H} | \Psi \rangle = 2 \sum_{k>k_F} \varepsilon_{\mathbf{k}} |\beta_{\mathbf{k}}|^2 - \sum_{k,k'>k_F} \mathcal{G}_{\mathbf{k}'-\mathbf{k}} \beta_{\mathbf{k}'}^* \beta_{\mathbf{k}}.$$

To compute the ground state energy, we introduce the Lagrangian multiplier λ to impose the condition Eqn. (6.107) and minimize the expression

$$\sum_{k>k_F} [2(\varepsilon_{\mathbf{k}} - \varepsilon_F) - \lambda] |\beta_{\mathbf{k}}|^2 - \sum_{k,k'>k_F} \mathcal{G}_{\mathbf{k}'-\mathbf{k}} \beta_{\mathbf{k}'}^* \beta_{\mathbf{k}}.$$

Taking a derivative with respect to $\beta_{\mathbf{k}}^*$, we obtain the condition

$$[2(\varepsilon_{\mathbf{k}} - \varepsilon_F) - \lambda] \beta_{\mathbf{k}} = \sum_{k'>k_F} \mathcal{G}_{\mathbf{k}-\mathbf{k}'} \beta_{\mathbf{k}'}. \quad (6.108)$$

In general it is difficult to solve for $\beta_{\mathbf{k}}$. However, for $z = 1$ phonons, $\mathcal{G}_{\mathbf{q}}^{(1)}$ is constant, as in (6.105). In this case,

$$[2(\varepsilon_{\mathbf{k}} - \varepsilon_F) - \lambda] \beta_{\mathbf{k}} = \mathcal{G}^{(1)} \sum_{k'>k_F} \beta_{\mathbf{k}'} \quad \implies \quad \beta_{\mathbf{k}} = \frac{\mathcal{G}^{(1)}}{2(\varepsilon_{\mathbf{k}} - \varepsilon_F) - \lambda} \sum_{k'>k_F} \beta_{\mathbf{k}'}$$

The normalization condition implies

$$1 = \mathcal{G}^{(1)} \sum_{k>k_F} \frac{1}{2(\varepsilon_{\mathbf{k}} - \varepsilon_F) - \lambda}.$$

The sum is converted into an integral with the use of the density of states $\mathcal{D}(\varepsilon)$,

$$\sum_{k > k_F} \rightarrow \int_0^{\omega_D} d\varepsilon \mathcal{D}(\varepsilon).$$

Since the integration region is small, we can replace $\mathcal{D}(\varepsilon)$ with $\mathcal{D}(0)$, the density of states at the Fermi surface. Then,

$$1 = \mathcal{G}^{(1)} \mathcal{D}(0) \int_0^{\omega_D} d\varepsilon \frac{1}{2\varepsilon - \lambda} = \frac{\mathcal{G}^{(1)} \mathcal{D}(0)}{2} \ln \left| \frac{\lambda - 2\omega_D}{\lambda} \right|.$$

Therefore,

$$\lambda = -\frac{2\omega_D}{\exp\left(\frac{2}{\mathcal{G}^{(1)} \mathcal{D}(0)}\right) - 1}.$$

This is nothing but the ground energy, E_{ground} .

At weak coupling, $\mathcal{G}^{(1)} \mathcal{D}(0) \ll 1$,

$$E_{\text{ground}} = -2\omega_D \exp\left(-\frac{2}{\mathcal{G}^{(1)} \mathcal{D}(0)}\right). \quad (6.109)$$

Indeed, this is a bound state, the Cooper pair. Note that this is a non-perturbative expression and cannot be derived as a series expansion in small coupling.

We may estimate the size of the Cooper pair. To maintain a Cooper pair, the kinetic energy of the electrons must be lower than the depth of the potential given in E_{ground} . This constraint puts an upper bound on the momentum of the electron:

$$\delta p \sim \frac{|E|}{v_F} \sim \frac{k_F |E|}{\varepsilon_F}.$$

The uncertainty principle gives an estimate on the size:

$$\xi_c \sim \frac{1}{\delta p} \sim \frac{\varepsilon_F}{k_F |E|}.$$

Here $\varepsilon_F \sim 1$ eV, $k_F \sim 10^8$ cm⁻¹, and $|E| \sim 10^{-4}$ eV, which derives from the typical critical temperature, $T_c < 10$ K, for superconductivity. Hence, $\xi_c \sim 10^{-4}$ cm, which is about 10^4 times of the typical lattice constant. Within the size of the Cooper pair, there exist multiple electron pairs, and their motions must be correlated. Thus the correct theory of superconductivity is truly a many-body problem.

We cannot solve (6.108) easily except for constant $\mathcal{G}_{\mathbf{q}}$. Thus, we focus on linearly dispersing phonons presently.

Self-Consistent Field Approximation

In this subsection we explore the idea proposed initially by Cooper: the ground state of superconductivity (the BCS ground state), which we denote as $|0\rangle$, is composed by Cooper pairs. That is,

$$\langle 0 | c_{\mathbf{k}}^\dagger c_{-\mathbf{k}}^\dagger | 0 \rangle \neq 0, \quad \langle 0 | c_{-\mathbf{k}} c_{\mathbf{k}} | 0 \rangle \neq 0.$$

Expanding about these vev, we can rewrite the interaction term in (6.106) as

$$- \sum_{\mathbf{k}, \mathbf{k}'} \mathcal{G}_{\mathbf{k}, \mathbf{k}'} \left(c_{\mathbf{k}'}^\dagger c_{-\mathbf{k}'}^\dagger \langle 0 | c_{-\mathbf{k}} c_{\mathbf{k}} | 0 \rangle + \langle 0 | c_{\mathbf{k}'}^\dagger c_{-\mathbf{k}'}^\dagger | 0 \rangle c_{-\mathbf{k}} c_{\mathbf{k}} - \langle 0 | c_{\mathbf{k}'}^\dagger c_{-\mathbf{k}'}^\dagger | 0 \rangle \langle 0 | c_{-\mathbf{k}} c_{\mathbf{k}} | 0 \rangle \right).$$

However, the averages of the electron-pair operators are unknown, and we will need to compute the superconductivity ground state $|0\rangle$ in order to determine these averages. This is known as the *self-consistent field approximation*.

Again, the question will be much simpler if the four-electron coupling \mathcal{G} is a constant, which is the case for phonons with a linear dispersion relation. Taking $\mathcal{G}_{\mathbf{k}-\mathbf{k}'} = \mathcal{G}^{(1)}$, we then define

$$\Delta = \mathcal{G}^{(1)} \sum_{\mathbf{k}} \langle 0 | c_{-\mathbf{k}} c_{\mathbf{k}} | 0 \rangle, \quad \Delta_{\mathbf{k}}^* = \mathcal{G}^{(1)} \sum_{\mathbf{k}} \langle 0 | c_{\mathbf{k}}^\dagger c_{-\mathbf{k}}^\dagger | 0 \rangle.$$

Note that Δ is only nonzero within the pairing region. In general, Δ is complex, but for isolated uniform macroscopic samples, one may take it to be real, in which case

$$\mathcal{H} \approx \sum_{\mathbf{k}} (\varepsilon_{\mathbf{k}} - \varepsilon_F) \left(c_{\mathbf{k}}^\dagger c_{\mathbf{k}} + c_{-\mathbf{k}}^\dagger c_{-\mathbf{k}} \right) - \Delta \sum_{\mathbf{k}} \left(c_{\mathbf{k}}^\dagger c_{-\mathbf{k}}^\dagger + c_{-\mathbf{k}} c_{\mathbf{k}} \right) + \frac{\Delta^2}{\mathcal{G}^{(1)}}.$$

We apply the Bogoliubov transformation to diagonalize this Hamiltonian. Let us define

$$a_{\mathbf{k}} = u_{\mathbf{k}} c_{\mathbf{k}} - v_{\mathbf{k}} c_{-\mathbf{k}}^\dagger, \quad a_{-\mathbf{k}} = u_{\mathbf{k}} c_{-\mathbf{k}} + v_{\mathbf{k}} c_{\mathbf{k}}^\dagger,$$

with

$$u_{\mathbf{k}}^2 + v_{\mathbf{k}}^2 = 1,$$

such that

$$\{a_{\mathbf{k}}, a_{\mathbf{k}'}^\dagger\} = \delta_{\mathbf{k}, \mathbf{k}'}, \quad \{a_{\mathbf{k}}, a_{-\mathbf{k}'}^\dagger\} = 0,$$

\mathcal{H} is diagonalized if

$$\Delta (u_{\mathbf{k}}^2 - v_{\mathbf{k}}^2) = 2\varepsilon_{\mathbf{k}} u_{\mathbf{k}} v_{\mathbf{k}}. \quad (6.110)$$

Therefore,

$$u_{\mathbf{k}}^2 = \frac{1}{2} \left(1 + \frac{\varepsilon_{\mathbf{k}} - \varepsilon_F}{\sqrt{(\varepsilon_{\mathbf{k}} - \varepsilon_F)^2 + \Delta^2}} \right), \quad v_{\mathbf{k}}^2 = \frac{1}{2} \left(1 - \frac{\varepsilon_{\mathbf{k}} - \varepsilon_F}{\sqrt{(\varepsilon_{\mathbf{k}} - \varepsilon_F)^2 + \Delta^2}} \right).$$

The diagonalized Hamiltonian is

$$\mathcal{H} = \sum_{\mathbf{k}} E_{\mathbf{k}} \left(a_{\mathbf{k}}^\dagger a_{\mathbf{k}} + a_{-\mathbf{k}}^\dagger a_{-\mathbf{k}} \right) + E_0,$$

with

$$E_{\mathbf{k}} = \sqrt{(\varepsilon_{\mathbf{k}} - \varepsilon_F)^2 + \Delta^2},$$

and

$$E_0 = 2 \sum_{\mathbf{k}} \varepsilon_{\mathbf{k}} v_{\mathbf{k}}^2 - 2\Delta \sum_{\mathbf{k}} u_{\mathbf{k}} v_{\mathbf{k}} + \frac{\Delta^2}{\mathcal{G}^{(1)}}.$$

Here a^\dagger excites a quasi-particle and Δ is the energy gap to excite a quasi-particle from the Fermi surface.

At $T = 0$,

$$\Delta = \mathcal{G}^{(1)} \sum_{\mathbf{k}} \langle c_{-\mathbf{k}} c_{\mathbf{k}} \rangle = \mathcal{G}^{(1)} \sum_{\mathbf{k}} u_{\mathbf{k}} v_{\mathbf{k}} = \frac{1}{2} \mathcal{G}^{(1)} \sum_{\mathbf{k}} \frac{\Delta}{\sqrt{(\varepsilon_{\mathbf{k}} - \varepsilon_F)^2 + \Delta^2}}.$$

Hence,

$$1 = \frac{1}{2} \mathcal{G}^{(1)} [2 \mathcal{D}(0)] \int_0^{\omega_D} \frac{d\varepsilon}{\sqrt{(\varepsilon - \varepsilon_F)^2 + \Delta^2}},$$

where the factor 2 comes from the spin sum. For metallic elements, $\mathcal{G}^{(1)} \mathcal{D}(0)$ is approximately $0.18 \sim 0.39$, which is sufficiently smaller than 1. Finally, we have

$$1 = \mathcal{G}^{(1)} \mathcal{D}(0) \ln \left(\frac{\omega_D + \sqrt{\omega_D^2 + \Delta^2}}{\Delta} \right) \quad \Rightarrow \quad \Delta \approx 2\omega_D \exp \left(-\frac{1}{\mathcal{G}^{(1)} \mathcal{D}(0)} \right).$$

Moreover, $\omega_D \sim 10^{-2}$ eV, and thus $\Delta \sim 10^{-4}$ eV.

It will also be interesting to compare the superconductivity ground state energy with the Fermi sphere energy in the normal phase. Since $\Delta \sim 10^{-4}$ eV \ll $\omega_D \sim 10^{-2}$ eV, the energy difference is

$$-\frac{1}{2} \mathcal{D}(0) \Delta^2.$$

Hence, the superconductive ground state energy is lower than the energy of the normal phase, which guarantees the phase transition.

When $T > 0$, the gap Δ is

$$\Delta(T) = \mathcal{G}^{(1)} \sum_{\mathbf{k}} \langle c_{-\mathbf{k}} c_{\mathbf{k}} \rangle_T = \mathcal{G}^{(1)} \sum_{\mathbf{k}} u_{\mathbf{k}} v_{\mathbf{k}} \left\{ 1 - 2 \left[\exp \left(\frac{\sqrt{(\varepsilon_{\mathbf{k}} - \varepsilon_F)^2 + \Delta^2(T)}}{T} \right) + 1 \right]^{-1} \right\}$$

Then

$$1 = \frac{\mathcal{G}^{(1)}}{2} \sum_{\mathbf{k}} \frac{1}{E_{\mathbf{k}}} \tanh \frac{E_{\mathbf{k}}}{2T}. \quad (6.111)$$

The phase transition occurs when $\Delta(T) \rightarrow 0$, which determines the critical temperature T_c :

$$\Delta(T_c) = 0.$$

At $T = T_c$, (6.111) gives

$$1 = \mathcal{G}^{(1)} \mathcal{D}(0) \int_0^{\omega_D} \frac{d\varepsilon}{\varepsilon} \tanh \left(\frac{\varepsilon}{2T} \right) \approx \mathcal{G}^{(1)} \mathcal{D}(0) \left[\ln \left(\frac{\omega_D}{2T_c} \right) - \int_0^\infty dx \ln x \operatorname{sech}^2 x \right].$$

Hence,

$$T_c = \frac{2e^\gamma}{\pi} \omega_D \exp\left(-\frac{1}{\mathcal{G}^{(1)} \mathcal{D}(0)}\right), \quad (6.112)$$

where $\gamma \approx 0.5772$ is the Euler constant.

For phonons, the Debye frequency $\omega_D \sim M^{-\frac{1}{2}}$, with M the mass of ions in the metal. From (6.112) we can obtain the isotope equation

$$T_c M^{\frac{1}{2}} = \text{Const.}$$

6.A.4. Anisotropic Gap Function in High- T_c Superconductivity

It has been verified in oxide high- T_c superconductors that the pairing mechanism persists most strongly between electrons of opposite spin. Suppose that the effective interaction is

$$H_{\text{eff}} = \sum_{\mathbf{k}, \mathbf{k}'} \mathcal{G}_{\mathbf{k}, \mathbf{k}'} c_{\mathbf{k}', \uparrow}^\dagger c_{-\mathbf{k}', \downarrow}^\dagger c_{-\mathbf{k}, \downarrow} c_{\mathbf{k}, \uparrow},$$

where

$$\mathcal{G}_{\mathbf{k}, \mathbf{k}'} = \int d^3r e^{-i(\mathbf{k}-\mathbf{k}') \cdot \mathbf{r}} \mathcal{G}(\mathbf{r}).$$

Confined within the energy shell of the size ω_D around the Fermi surface, we have

$$\mathcal{G}_{\mathbf{k}, \mathbf{k}'} = \mathcal{G}(\hat{\mathbf{k}} \cdot \hat{\mathbf{k}}').$$

Then, in the self-consistent field theory, the reduced Hamiltonian can be written as

$$\mathcal{H} = \sum_{\mathbf{k}} \varepsilon_{\mathbf{k}} \left(c_{\mathbf{k}}^\dagger c_{\mathbf{k}} + c_{-\mathbf{k}}^\dagger c_{-\mathbf{k}} \right) - \sum_{\mathbf{k}} \left(\Delta_{\mathbf{k}} c_{\mathbf{k}}^\dagger c_{-\mathbf{k}}^\dagger + \Delta_{\mathbf{k}}^* c_{-\mathbf{k}} c_{\mathbf{k}} \right) + \sum_{\mathbf{k}} \Delta_{\mathbf{k}} \langle c_{\mathbf{k}}^\dagger c_{-\mathbf{k}}^\dagger \rangle_T,$$

with

$$\Delta_{\mathbf{k}} = - \sum_{\mathbf{k}'} \mathcal{G}_{\mathbf{k}, \mathbf{k}'} \langle c_{-\mathbf{k}'} c_{\mathbf{k}'} \rangle_T. \quad (6.113)$$

The finite temperature expectation value, denoted by $\langle \dots \rangle_T$, is obtained using the Green's function approach. This is outlined in the following subsection. For the time being, we simply quote the result:

$$\Delta_{\mathbf{k}} = -\frac{1}{2} \sum_{\mathbf{k}'} \mathcal{G}_{\mathbf{k}, \mathbf{k}'} \Delta_{\mathbf{k}'} \frac{\tanh\left(\frac{E_{\mathbf{k}'}}{2T}\right)}{E_{\mathbf{k}'}} ,$$

with

$$E_{\mathbf{k}} = \sqrt{(\varepsilon_{\mathbf{k}} - \varepsilon_F)^2 + |\Delta_{\mathbf{k}}|^2}.$$

The T dependence of Δ is implicit. In the phenomenological theory of high T_c superconductivity, we can expand $\mathcal{G}_{\mathbf{k}, \mathbf{k}'}$ in terms of Legendre polynomials and thus discuss the pairing between two fermions with arbitrary spin orientations. This is the *generalized Cooper pair*. Ignoring the coupling between different partial waves, we can focus on the simple solution

$$\Delta_{\mathbf{k}} = \Delta_a(T) \sqrt{4\pi} Y_{\ell, m}(\theta_{\mathbf{k}}, \phi_{\mathbf{k}}). \quad (6.114)$$

We introduce the factor $\sqrt{4\pi}$ so that the average over orientations is $\Delta_a^2(T)$, i.e.,

$$\int \frac{d\Omega}{4\pi} |\Delta_{\mathbf{k}}|^2 = \Delta_a^2(T).$$

In this sense, $\Delta_a(T)$ is the average over orientations of the gap on the Fermi surface. We obtain the self-consistent equation

$$1 = \frac{1}{2} |V_\ell| \sum_{\mathbf{k}'} \frac{4\pi |Y_{\ell,m}(\hat{\mathbf{k}}')|^2 \tanh\left(\frac{E_{\mathbf{k}'}}{2T}\right)}{E_{\mathbf{k}'}}.$$

with

$$E_{\mathbf{k}'} = \sqrt{(\varepsilon_{\mathbf{k}} - \varepsilon)^2 + 4\pi \Delta_a^2(T) |Y_{\ell,m}(\hat{\mathbf{k}}')|^2}.$$

6.A.5. Green's Function Method

In this subsection, we will outline the method of Green's function, which was used to derive the self-consistent equation in the previous subsection.

In the Heisenberg picture, the *double time retarded Green's Function* associated with two operators A and B is defined as

$$G_r(t, t') = -i \theta(t - t') \langle [A(t), B(t')]_{\pm} \rangle \equiv \langle \langle A(t); B(t') \rangle \rangle.$$

In the canonical ensemble, $\langle \dots \rangle$ denotes

$$\langle A \rangle = Z^{-1} \text{Tr} \left(e^{-\beta H} A \right), \quad Z = \text{Tr} \left(e^{-\beta H} \right), \quad \beta = \frac{1}{T}.$$

Note that

$$\begin{aligned} \langle A(t) B(t') \rangle &= \frac{1}{Z} \text{Tr} \left(e^{-\beta H} e^{iHt} A e^{-iHt} e^{iHt'} B e^{-iHt'} \right) = \frac{1}{Z} \text{Tr} \left(e^{-\beta H} A(t-t') B \right) \\ &= \langle A(t-t') B(0) \rangle. \end{aligned}$$

Therefore,

$$G_r(t) = -i \theta(t) \langle [A(t), B]_{\pm} \rangle,$$

and $G_r(t)$ can be interpreted as a propagator.

Singularities of $G_r(\omega)$

The Fourier transformation of $G_r(t)$ is

$$G_r(t) = \int_{-\infty}^{\infty} \frac{d\omega}{2\pi} G_r(\omega) \exp[-i(\omega + i0^+)t].$$

Its inverse transformation is

$$G_r(\omega) = \int_{-\infty}^{\infty} dt G_r(t) \exp[i(\omega + i0^+)t].$$

For $T = 0$, define $|0\rangle$ and E_n , respectively, as the eigenstate and eigenvalue of the Hamiltonian; $|0\rangle$ then denotes the ground state. Note that

$$\langle 0|A(t)|0\rangle = \langle 0|A|0\rangle \exp[-i(E_n - E_0)t].$$

Then

$$\begin{aligned} G_r(t) &= -i\theta(t) \left(\langle 0|A(t)B|0\rangle \pm \langle 0|BA(t)|0\rangle \right) \\ &= -i\theta(t) \sum_n \left(\langle 0|A|n\rangle \langle n|B|0\rangle e^{-i(E_n - E_0)t} \pm \langle 0|B|n\rangle \langle n|A|0\rangle e^{i(E_n - E_0)t} \right) \end{aligned}$$

The Fourier transform is

$$G_r(\omega) = \sum_n \left(\frac{\langle 0|A|n\rangle \langle n|B|0\rangle}{\omega - E_n + E_0 + i\eta} \pm \frac{\langle 0|B|n\rangle \langle n|A|0\rangle}{\omega + E_n - E_0 + i\eta} \right).$$

Therefore, the singularities of $G_r(\omega)$ reside in the lower half plane and $G_r(\omega)$ is analytic in the upper half plane. Furthermore, in the finite temperature case, we have

$$G_r(\omega) = \frac{1}{Z} \sum_{n,m} e^{-\beta E_n} \langle n|B|m\rangle \langle m|A|n\rangle \frac{e^{\beta(E_n - E_m)} \pm 1}{\omega - (E_n - E_m) + i\eta}.$$

Equation of Motion of the Double Time Green's Function

The total double time Green's function is defined as

$$G(t) = \frac{1}{2\pi} \int_{-\infty}^{\infty} d\omega e^{-i\omega t} G(\omega) = \begin{cases} -i\theta(t) \langle [A(t), B]_{\pm} \rangle = G_r(t), \\ i\theta(-t) \langle [A(t), B]_{\pm} \rangle = G_a(t). \end{cases}$$

Then $G(t > 0)$ is the retarded Green's function and $G(t < 0)$ is the advanced Green's function. Using the equation of motion of an operator A in the Heisenberg picture,

$$i \frac{dA(t)}{dt} = A(t)H - HA(t),$$

we can derive the equation of motion for Green's function as follows:

$$\begin{aligned} i \frac{d}{dt} \langle \langle A(t); B \rangle \rangle &= \delta(t) \langle [A(t), B]_{\pm} \rangle \mp i\theta(\pm t) \langle \langle [A(t), H], B \rangle_{\pm} \rangle \\ &= \delta(t) \langle [A, B]_{\pm} \rangle + \langle \langle [A(t), H]; B \rangle \rangle. \end{aligned} \quad (6.115)$$

The Fourier transform of the double time Green's function $\langle \langle [A(t), H]; B \rangle \rangle$ is given by

$$\langle \langle [A(t), H]; B \rangle \rangle = \frac{1}{2\pi} \int_{-\infty}^{\infty} d\omega \langle \langle [A, H]|B \rangle \rangle_{\omega} e^{-i\omega t},$$

and for $i \frac{d}{dt} \langle \langle A(t); B \rangle \rangle$ we have

$$i \frac{d}{dt} \langle \langle A(t); B \rangle \rangle = \int_{-\infty}^{\infty} \frac{d\omega}{2\pi} \omega \langle \langle A|B \rangle \rangle_{\omega} e^{-i\omega t}.$$

Then the Fourier transform of (6.115) gives

$$\omega \langle\langle A|B \rangle\rangle_\omega = \langle[A, B]_\pm\rangle + \langle\langle[A, H]|B \rangle\rangle_\omega. \quad (6.116)$$

This is the formula used to calculate the finite temperature expectation value in (6.113), by setting $A = c_{-\mathbf{k}}$ and $B = c_{\mathbf{k}}$.

6.B. Boltzmann-Bloch Transport Theory

In this appendix, we will discuss the standard theory of transport due to Boltzmann and Bloch. This discussion follows closely the texts of Ziman [97] and Landau and Lifshitz [103].

6.B.1. Variational Approach to Resistivity

The Collision Function

The electron-phonon interaction is described by

$$C(n_k) = \int \frac{d^D q}{(2\pi)^D} \frac{d^D k'}{(2\pi)^D} \left\{ w(\mathbf{k}', \mathbf{q}; \mathbf{k}) [n_{k'}(1 - n_k)N_q - n_k(1 - n_{k'})(N_q + 1)] \delta(\varepsilon_k - \varepsilon_{k'} - \omega_q) \right. \\ \left. + w(\mathbf{k}'; \mathbf{k}, \mathbf{q}) [n_{k'}(1 - n_k)(N_q + 1) - n_k(1 - n_{k'})N_q] \delta(\varepsilon_k + \omega_q - \varepsilon_{k'}) \right\}.$$

which includes the processes

- $(e, \mathbf{k}) \rightleftharpoons (e, \mathbf{k}') + (p, \mathbf{q}), \mathbf{k} = \mathbf{k}' + \mathbf{q} + \mathbf{b};$
- $(e, \mathbf{k}) + (p, \mathbf{q}) \rightleftharpoons (e, \mathbf{k}'), \mathbf{k} + \mathbf{q} = \mathbf{k}' + \mathbf{b}.$

with $\mathbf{k} = \mathbf{k}' + \mathbf{q} + \mathbf{b}$, where \mathbf{b} is the reciprocal lattice period, \mathbf{k} and \mathbf{k}' the momenta of incoming and outgoing electrons, respectively, and \mathbf{q} the quasi-momentum of the emitted or absorbed phonon. Here the factors $1 - n$ and $1 - n'$ account for the Pauli principle. Here, the transition rates are $w(\mathbf{k}', \mathbf{q}; \mathbf{k}) = w(\mathbf{k}'; \mathbf{k}, \mathbf{q}) = |g_q|^2$.

Expand the electron distribution function about equilibrium via $n(\mathbf{r}, \mathbf{k}) = n_0(\varepsilon_0) + \delta n(\mathbf{r}, \mathbf{k})$, with n_0 denoting the equilibrium distribution. If n_0 is expressed as a function of the actual quasi-particle energy ε , then

$$n_0(\varepsilon_0) = n_0(\varepsilon) - \delta\varepsilon \frac{\partial n_0}{\partial \varepsilon},$$

and

$$n(\mathbf{r}, \mathbf{k}) = n_0(\varepsilon) + \delta\tilde{n}(\mathbf{r}, \mathbf{k}),$$

with $\delta\tilde{n} = \delta n - \delta\varepsilon \frac{\partial n_0}{\partial \varepsilon}$. Similarly, also let $N = N_0(\omega) + \delta N$ for phonons. Apply the following change of variables,

$$\delta\tilde{n} = -\frac{\partial n_0}{\partial \varepsilon} \Phi = \frac{1}{T} n_0(1 - n_0) \Phi, \quad \delta N = -\frac{\partial N}{\partial \omega} \chi = \frac{1}{T} N_0(1 + N_0) \chi.$$

Also note that

$$\begin{aligned}
& n_{k'}(1 - n_k)N_k - n_k(1 - n_{k'})(1 + N_k) \\
&= (1 - n)(1 - n')(1 + N) \left[\frac{n'}{1 - n'} \frac{N}{1 + N} - \frac{n}{1 - n} \right] \\
&= (1 - n)(1 - n')(1 + N) \left[\frac{n'_0}{1 - n'_0} \left(1 + \frac{\Phi'}{T}\right) \frac{N_0}{1 + N_0} \left(1 + \frac{\chi}{T}\right) - \frac{n_0}{1 - n_0} \left(1 + \frac{\Phi}{T}\right) \right] \\
&= (1 - n)(1 - n')(1 + N) \left(e^{-\frac{\varepsilon' + \omega_q - \mu}{T}} \left(1 + \frac{\Phi' + \chi}{T}\right) - e^{-\frac{\varepsilon - \mu}{T}} \left(1 + \frac{\Phi}{T}\right) \right) \\
&= \frac{1}{T} n_0(1 - n'_0)(1 + N_0)(\Phi' - \Phi + \chi).
\end{aligned}$$

Therefore,

$$\begin{aligned}
C(n_k) = \frac{1}{T} \int \frac{d^D q}{(2\pi)^D} \frac{d^D k'}{(2\pi)^D} w n_0(1 - n'_0) [(1 + N_0)(\Phi_{k'} - \Phi_k + \chi_q) \delta(\varepsilon_k - \varepsilon_{k'} - \omega_q) \\
+ N_0(\Phi_{k'} - \Phi_k - \chi_q) \delta(\varepsilon_k - \varepsilon_{k'} + \omega_q)].
\end{aligned}$$

Due to *Bloch'sche Annahme* we can treat the phonon system as if it were in thermal equilibrium, i.e., $\chi = 0$. Then $C(n_k)$ can be interpreted as an operator acting on Φ , which we denote as $P\Phi$:

$$P\Phi \equiv -C(n_k) = \frac{1}{T} \int \frac{d^D q}{(2\pi)^D} \frac{d^D k'}{(2\pi)^D} (\Phi_k - \Phi_{k'}) \left(\mathcal{P}_k^{k',q} + \mathcal{P}_{k,q}^{k'} \right),$$

where the transition probabilities are

$$\begin{aligned}
\mathcal{P}_k^{k',q} &= 2\pi |g_q|^2 n_0(1 - n'_0)(1 + N_0) \delta(\varepsilon_k - \varepsilon_{k'} - \omega_q) \delta_{\mathbf{b}, \mathbf{k} - \mathbf{k}' - \mathbf{q}} \\
\mathcal{P}_{k,q}^{k'} &= 2\pi |g_q|^2 n_0(1 - n'_0) N_0 \delta(\varepsilon_k - \varepsilon_{k'} + \omega_q) \delta_{\mathbf{b}, \mathbf{k} - \mathbf{k}' + \mathbf{q}}
\end{aligned}$$

For convenience, we define $\mathcal{P}(k, k') \equiv \frac{1}{T} \int \frac{d^D q}{(2\pi)^D} \left(\mathcal{P}_k^{k',q} + \mathcal{P}_{k,q}^{k'} \right)$ so that

$$P\Phi = \int \frac{d^D k'}{(2\pi)^D} (\Phi_k - \Phi_{k'}) \mathcal{P}(k, k').$$

The Variational Method

In the absence of a temperature gradient, which we assume is the case, the Boltzmann transport equation reads

$$X = P\Phi,$$

where

$$X \equiv -e\mathbf{E} \cdot \mathbf{v} \frac{\partial n_0}{\partial \varepsilon} + \mathbf{v} \cdot \nabla n_0.$$

Note that the diffusion term vanishes when $\nabla T = 0$:

$$\mathbf{v} \cdot \nabla n_0 = \mathbf{v} \cdot \nabla T \frac{\partial n_0}{\partial T} = -\frac{\varepsilon - \mu}{T} \nabla T \frac{\partial n_0}{\partial \varepsilon}.$$

Furthermore,

$$\begin{aligned}
\langle \Phi, P\Psi \rangle &= \int \frac{d^D k}{(2\pi)^D} \Phi_k \int \frac{d^D k'}{(2\pi)^D} (\Psi_k - \Psi_{k'}) \mathcal{P}(k, k') \\
&= \frac{1}{2} \left(\int \frac{d^D k}{(2\pi)^D} \frac{d^D k'}{(2\pi)^D} \Phi_k (\Psi_k - \Psi_{k'}) \mathcal{P}(k, k') + (k \leftrightarrow k') \right) \\
&= \frac{1}{2} \int \frac{d^D k}{(2\pi)^D} \frac{d^D k'}{(2\pi)^D} (\Phi_k - \Phi_{k'}) (\Psi_k - \Psi_{k'}) \mathcal{P}(k, k'),
\end{aligned}$$

where use was made of the symmetry $\mathcal{P}(k, k') = \mathcal{P}(k', k)$.

The following properties directly follow:

1. P is positive definite: $\langle \Phi, P\Phi \rangle \geq 0$.
2. The solution to Boltzmann's equation maximizes $\langle \Phi, P\Phi \rangle / \langle \Phi, X \rangle^2$.

Resistivity

The background-subtracted current density is given by

$$\begin{aligned}
\mathbf{J} &= - \int \frac{d^D k}{(2\pi)^D} e \mathbf{v} \Phi_{\mathbf{k}} [n(\varepsilon) - n_0(\varepsilon)] \\
&= - \int \frac{d^D k}{(2\pi)^D} e \mathbf{v} \Phi_{\mathbf{k}} \frac{\partial n_0}{\partial \varepsilon}.
\end{aligned}$$

Note that

$$\langle \Phi, X \rangle = \int \frac{d^D k}{(2\pi)^D} \Phi_{\mathbf{k}} \left(-e \mathbf{E} \cdot \mathbf{v} \frac{\partial n_0}{\partial \varepsilon} \right) = \mathbf{E} \cdot \mathbf{J} = \rho J^2 = \rho \langle \Phi, X(E=1) \rangle^2,$$

where use was made of the definition of resistivity, $\mathbf{E} = \rho \mathbf{J}$. By $E=1$ in $X(E=1)$, we really mean $\mathbf{E} = \hat{\mathbf{v}}$, the unit vector in the direction of the velocity.

Combined with Boltzmann's equation, one obtains

$$\rho = \frac{\langle \Phi, P\Phi \rangle}{\langle \Phi, X(E=1) \rangle^2} = \frac{\frac{1}{2} \int \frac{d^D k}{(2\pi)^D} \frac{d^D k'}{(2\pi)^D} (\Phi_k - \Phi_{k'})^2 \mathcal{P}(k, k')}{\left| \int \frac{d^D k}{(2\pi)^D} e \mathbf{v} \Phi \frac{\partial n_0}{\partial \varepsilon} \right|^2}.$$

The electrical resistivity is the extremal value of the variational function at unit electric field. Here it is understood that spin sums should be taken whenever they are required.

Entropic Interpretation

The Boltzmann equation can be interpreted as the vanishing of the rate of change of the mean occupation number of quantum states, n . The two main mechanisms by which n can change are via external forces, such as an electric field or a temperature gradient, and by internal scattering. Boltzmann's equation reads $\dot{n}|_{\text{field}} + \dot{n}|_{\text{scatt}} = 0$, where

$$\langle \Phi, X \rangle = \int \frac{d^D k}{(2\pi)^D} \Phi \dot{n}|_{\text{field}}, \quad \langle \Phi, P\Phi \rangle = - \int \frac{d^D k}{(2\pi)^D} \Phi_k \dot{n}|_{\text{scatt}}.$$

n is related to the entropy as follows. The standard statistical entropy for N_j identical Fermions among G_j states is

$$\begin{aligned} S &= \log \left[\prod_j \frac{G_j!}{N_j! (G_j - N_j)!} \right] = \sum_j [G_j \log G_j - N_j \log N_j - (G_j - N_j) \log(G_j - N_j)] \\ &= - \sum_j G_j [n_j \log n_j + (1 - n_j) \log(1 - n_j)], \end{aligned}$$

where $n_j \equiv \frac{N_j}{G_j}$ is the mean occupation number of quantum states.

In the continuum limit,

$$S = - \int \frac{d^D k}{(2\pi)^D} [n \log n + (1 - n) \log(1 - n)].$$

Expanding n linearly about equilibrium as $n \approx n_0 + \frac{1}{T} n_0 (1 - n_0) \Phi$, one obtains

$$\log \frac{n}{1 - n} \approx -\frac{\varepsilon - \mu}{T} + \frac{\Phi}{T}.$$

Hence,

$$\dot{S} = - \int \frac{d^D k}{(2\pi)^D} \dot{n} \log \frac{n}{1 - n} \approx -\frac{1}{T} \int \frac{d^D k}{(2\pi)^D} \Phi \dot{n} + \frac{1}{T} \int \frac{d^D k}{(2\pi)^D} (\varepsilon - \mu) \dot{n}.$$

The second term is the contribution from the increase of the average energy in the system, which is of no interest here. This derivation assumes that the system is isolated from external forces and thus \dot{n} is purely due to scattering. Therefore, we can write

$$\dot{S} = -\frac{1}{T} \int \frac{d^D k}{(2\pi)^D} \Phi \dot{n}_{\text{scatt}} = \frac{1}{T} \langle \Phi, P\Phi \rangle.$$

From the resistivity result, one obtains

$$\dot{S} = \rho \frac{J^2}{T}.$$

6.C. Derivation of the Bloch-Grüneisen Formula

In this section we calculate the resistivity defined by

$$\rho = \frac{\frac{1}{2T} \int \frac{d^D k}{(2\pi)^D} \frac{d^D k'}{(2\pi)^D} \frac{d^D q}{(2\pi)^D} (\Phi_k - \Phi_{k'})^2 (\mathcal{P}_k^{k',q} + \mathcal{P}_{k,q}^{k'})}{\left| \int \frac{d^D k}{(2\pi)^D} e \mathbf{v} \Phi \frac{\partial n_0}{\partial \varepsilon} \right|^2},$$

with

$$\begin{aligned} \mathcal{P}_k^{k',q} &= 2\pi |g_q|^2 n_0 (1 - n'_0) (1 + N_0) \delta(\varepsilon_k - \varepsilon_{k'} - \omega_q) \delta_{\mathbf{b}, \mathbf{k} - \mathbf{k}' - \mathbf{q}} \\ \mathcal{P}_{k,q}^{k'} &= 2\pi |g_q|^2 n_0 (1 - n'_0) N_0 \delta(\varepsilon_k - \varepsilon_{k'} + \omega_q) \delta_{\mathbf{b}, \mathbf{k} - \mathbf{k}' + \mathbf{q}} \end{aligned}$$

6.C.1. An Exact Solution to the Boltzmann Equation

First we select a trial function for Φ_k . Note that there exists an exact analytic solution for the Boltzmann equation when the Fermi surface is spherical (\mathbf{v} is then parallel to \mathbf{k}) and the scattering probability only depends on the angle between \mathbf{k} and \mathbf{k}' . Then

$$\cos \chi = \int d\Omega' (\Phi(\chi, \phi) - \Phi(\chi', \phi')) f(\theta), \quad (6.117)$$

where χ is the angle between \mathbf{k} and the direction of the electric field \vec{u} and θ is the angle between the directions (χ, ϕ) and (χ', ϕ') . It can be verified that $\Phi(\chi, \phi) = \alpha \cos \chi$ is a solution: without loss of generality, take $\hat{\mathbf{k}} = (0, 0, 1)$, $\hat{\mathbf{k}}' = (\sin \theta \cos \phi, \sin \theta \sin \phi, \cos \theta)$ and $\hat{u} = (\sin \chi, 0, \cos \chi)$. Then,

$$\cos \chi' = \hat{\mathbf{k}}' \cdot \hat{u} = \sin \theta \cos \phi \sin \chi + \cos \theta \cos \chi.$$

Hence,

$$\begin{aligned} \int d\Omega' (\Phi(\chi, \phi) - \Phi(\chi', \phi')) f(\theta) &= \alpha \int_0^\pi d\theta \sin \theta \int_0^{2\pi} d\phi [(1 - \cos \theta) \cos \chi - \sin \theta \cos \phi \sin \chi] f(\theta) \\ &= 2\pi \alpha \cos \chi \int_0^\pi d\theta f(\theta) \sin \theta (1 - \cos \theta) \\ &\propto \cos \chi. \end{aligned}$$

Therefore, we can take the trial function to be $\Phi_k = \alpha \mathbf{k} \cdot \hat{\mathbf{u}}$. Note that this continues to hold for $D \geq 3$.

$D = 2$ represents a special case since

$$\cos \chi' = \cos(\chi - \theta),$$

and (6.117) now reads

$$\cos \chi = \int_0^{2\pi} d\theta \sin \theta [\Phi(\chi) - \Phi(\chi - \theta)] f(\theta). \quad (6.118)$$

Usually $f(\theta) = f(-\theta)$ and hence

$$\begin{aligned} \int_0^\infty d\theta \sin \theta f(\theta) &= 0, \\ \int_0^\infty d\theta \sin \theta \cos \theta f(\theta) &= 0. \end{aligned}$$

Equation (6.118) imposes the form

$$\Phi(\chi) - \Phi(\chi - \theta) = g(\theta) \cos \chi,$$

for some function $g(\theta)$. When θ is infinitesimal, we have

$$-\Phi'(x)\theta = g(0) + g'(0)\theta \cos \chi.$$

Therefore,

$$\Phi(\chi) \propto \sin \chi.$$

It is straightforward to verify that (6.118) is satisfied:

$$\begin{aligned} \int_0^{2\pi} d\theta \sin \theta f(\theta) [\sin \chi - \sin(\chi - \theta)] &= \int_0^{2\pi} d\theta \sin \theta f(\theta) (\sin \chi - \sin \chi \cos \theta + \cos \chi \sin \theta) \\ &= \cos \chi \int_0^{2\pi} d\theta \sin^2 \theta f(\theta) \\ &\propto \cos \chi. \end{aligned}$$

We will continue to write $\alpha \mathbf{k} \cdot \hat{\mathbf{u}}$ for the trial function. It is taken for granted that one must use the cross product instead of the dot product when $D = 2$.

6.C.2. Bloch-Grüneisen Formula

We assume $D \geq 2$ in the following calculations. Under the assumption of isotropy in the electron distribution, one can take $(\vec{A} \cdot \hat{\mathbf{u}})^2 = \frac{1}{D} A^2$ for any vector \vec{A} , with which we can evaluate the resistivity. The denominator in the variational expression of resistivity can be calculated as follows:

$$\text{den} = \left| \int \frac{2d^D k}{(2\pi)^D} e \mathbf{v} \Phi \frac{\partial n_0}{\partial \varepsilon} \right|^2 = \left| \frac{2e\alpha}{(2\pi)^D} \int dS^{D-1} \frac{d\varepsilon_k}{v_k} \frac{\partial n_0}{\partial \varepsilon} \mathbf{v} \mathbf{k} \cdot \hat{\mathbf{u}} \right|^2.$$

We now take the low temperature limit. Note that in the zeroth order approximation with respect to the small ratio T/ε_F , the function $n_0(\varepsilon)$ is a step function, $\theta(\varepsilon_F - \varepsilon)$. Then

$$\frac{\partial n_0}{\partial \varepsilon} = -\delta(\varepsilon - \varepsilon_F).$$

Therefore,

$$\text{den} = \left| \frac{2e\alpha}{(2\pi)^D} \int dS_F^{D-1} \mathbf{k} \cdot \hat{\mathbf{u}} \right|^2 = \frac{4e^2\alpha^2}{D(2\pi)^D} k_F^2 \left(S_F^{D-1} \right)^2,$$

where S_F^{D-1} is the surface area of the Fermi sphere.

Next we evaluate numerator for the process $(e, \mathbf{k}) + (p, \mathbf{q}) \rightleftharpoons (e, \mathbf{k}')$:

$$\begin{aligned} \text{num}_1 &= \int \frac{d^D k}{(2\pi)^D} \frac{d^D k'}{(2\pi)^D} \frac{d^D q}{(2\pi)^D} (\Phi_k - \Phi_{k'})^2 \mathcal{P}_{k,q}^{k'} \\ &= \frac{2\alpha^2}{(2\pi)^{3D-1}} \int d^D k d^D k' d^D q \frac{(\mathbf{k} - \mathbf{k}')^2}{D} |g_q|^2 n_0(1 - n'_0) N_0 \delta(\varepsilon_k - \varepsilon_{k'} + \omega_q) \delta_{\mathbf{b}, \mathbf{k} - \mathbf{k}' + \mathbf{q}}, \end{aligned}$$

note that we have inserted a factor of 2 for the appropriate spin sum. Note further that Umklapp processes are negligible in metals, so that \mathbf{b} can be set to zero. Therefore, in the

$T \rightarrow 0$ limit,

$$\begin{aligned}
\text{num}_1 &= \frac{2\alpha^2}{D(2\pi)^{3D-1}} \int d^D k \frac{dS_F'^{D-1}}{v_{k'}} q^2 |g_q|^2 n_0 (1 - n'_0) N_0 \\
&= \frac{2\alpha^2}{D(2\pi)^{3D-1}} \int \frac{dS_F'^{D-1}}{v_{k'}} q^2 |g_q|^2 N_0 \int \frac{dS^{D-1}}{v_k} \int_0^\infty d\varepsilon_k \frac{1}{\left(e^{\frac{\varepsilon_k - \mu}{T}} + 1\right) \left(1 + e^{-\frac{\varepsilon_k + \omega - \mu}{T}}\right)} \\
&= \frac{2\alpha^2}{D(2\pi)^{3D-1}} \int \frac{dS_F'^{D-1}}{v_{k'}} q^2 |g_q|^2 N_0 \int \frac{dS^{D-1}}{v_k} \int_{-\infty}^\infty \frac{T dx}{(e^x + 1) \left(1 + e^{-x} e^{-\frac{\omega}{T}}\right)} \\
&= \frac{2\alpha^2}{D(2\pi)^{3D-1}} \int \frac{dS_F'^{D-1}}{v_{k'}} q^2 |g_q|^2 N_0 \int \frac{dS^{D-1}}{v_k} \frac{\omega}{1 - e^{-\frac{\omega}{T}}} \\
&= \frac{2\alpha^2}{D(2\pi)^{3D-1}} \int \frac{dS_F'^{D-1}}{v_{k'}} \frac{dS^{D-1}}{v_k} \frac{q^2 |g_q|^2 \omega}{\left(e^{\frac{\omega}{T}} - 1\right) \left(1 - e^{-\frac{\omega}{T}}\right)} \\
&= \frac{\alpha^2}{2D(2\pi)^{3D-1}} \int \frac{dS_F'^{D-1}}{v_{k'}} \frac{dS_F^{D-1}}{v_k} \frac{q^2 |g_q|^2 \omega}{\sinh^2\left(\frac{\omega}{2T}\right)}
\end{aligned}$$

Now we examine how the surface integrals are defined. Assume that the phonon is sufficiently soft ($\omega_q \ll \varepsilon_k$) such that the two energy surfaces defined, respectively, by ε_k and $\varepsilon_{k'}$ lie fairly close to each other. This means that $n_0(1 - n'_0)$ is approximately $n_0(1 - n_0)$, which is

$$n_0(1 - n_0) = \frac{\partial n_0}{\partial \varepsilon} \approx -\delta(\varepsilon - \varepsilon_F)$$

for sufficiently low temperature. Therefore, both of the energy surfaces are constrained to be the Fermi surface, which we assume to be near-spherical. Moreover, for $D = 3$, since $q = 2k_F \sin \frac{\theta_1}{2}$ and thus $q^2 = 2k_F^2(1 - \cos \theta_1)$, we have $q dq = k_F^2 \sin \theta_1 d\theta_1$. Meanwhile, $\sin \theta_1 = \frac{q}{k_F} \sqrt{1 - \frac{q^2}{4k_F^2}}$, and the hyper-surface element is

$$dS^{D-1} = \prod_{j=1}^{D-1} \sin^{D-1-j} \theta_j d\theta_j.$$

Hence,

$$\int dS_F'^{D-1} d\Omega_F^{D-1} = \int dS_F'^{D-1} \int \prod_{j=2}^{D-1} \sin^{D-1-j} \theta_j d\theta_j \int_0^{2k_F} \frac{dq q}{k_F^2} \left(\frac{q}{k_F} \sqrt{1 - \frac{q^2}{4k_F^2}}\right)^{D-3}.$$

Since the integrand in num_1 is a function of q , we can insert a redundant integral over θ_1 above to recover the full surface integral, as long as we divide by the appropriate normalization factor dependent on D :

$$\frac{\Gamma\left(\frac{D}{2}\right)}{\sqrt{\pi} \Gamma\left(\frac{D-1}{2}\right)} \int dS_F'^{D-1} dS_F^{D-1} \int_0^{2k_F} \frac{dq q^{D-2}}{k_F^{D-1}} \left(1 - \frac{q^2}{4k_F^2}\right)^{\frac{D-3}{2}}.$$

Therefore,

$$\begin{aligned} \text{num}_1 &= \frac{\Gamma\left(\frac{D}{2}\right)}{\sqrt{\pi}\Gamma\left(\frac{D-1}{2}\right)} \frac{\alpha^2 \left(S_F^{D-1}\right)^2}{2D(2\pi)^{3D-1}v_F^2} \int_0^{2k_F} \frac{dq q^D |g_q|^2 \omega}{\sinh^2\left(\frac{\omega}{2T}\right)} \left(1 - \frac{q^2}{4k_F^2}\right)^{\frac{D-3}{2}} \\ &= \frac{\Gamma(D-1)}{2^{\frac{3+D}{z}-1-2D} D \pi^{2D}} \frac{e^2 \alpha^2 \left(S_F^{D-1}\right)^2}{\lambda^{2D-2} M V v_F^2} T^{\frac{D+3}{z}} \int_0^{\frac{\Theta_D}{T}} \frac{dx x^{\frac{D+3}{z}-1}}{\sinh^2(x)} \left[1 - x^{\frac{2}{z}} \left(\frac{T}{\Theta_D}\right)^{\frac{2}{z}}\right]^{\frac{D-3}{2}}. \end{aligned}$$

where $T \ll \Theta_D \ll \frac{1}{2}(2k_F)^z$ and z is the dynamical exponent ($\omega = q^z$). Analogously, for the other process,

$$\text{num}_2 = \int \frac{2d^D k}{(2\pi)^D} \frac{d^D k'}{(2\pi)^D} \frac{d^D q}{(2\pi)^D} (\Phi_k - \Phi_{k'})^2 \mathcal{P}_k^{k',q} = \text{num}_1.$$

Therefore, at low temperature,

$$\begin{aligned} \rho &= \frac{\Gamma(D-1)}{2^{\frac{3+D}{z}+1-D} \pi^D} \frac{1}{\lambda^{2D-2} M V k_F^2 v_F^2} T^{\frac{D+3}{z}-1} \int_0^\infty \frac{dx x^{\frac{D+3}{z}-1}}{\sinh^2(x)} \\ &= \frac{\Gamma(D-1)}{2^{\frac{6+2D}{z}-1-D} \pi^D} \frac{1}{\lambda^{2D-2} M V k_F^2 v_F^2} T^{\frac{D+3}{z}-1} \Gamma\left(\frac{D+3}{z}\right) \zeta\left(\frac{D+3}{z} - 1\right), \end{aligned}$$

where use was made of the formula

$$\int_0^\infty \frac{x^s}{(\sinh x)^2} = \frac{1}{2^{s-1}} \Gamma(s+1) \zeta(s).$$

Thus, we derive the temperature dependence of the resistivity,

$$\rho \propto T^{\frac{D+3}{z}-1}.$$

Chapter 7

Conclusion

The introduction of Lifshitz scaling symmetries into quantum gravity, in the form of Hořava-Lifshitz gravity, has motivated and inspired us to study Lifshitz quantum field theories in general. Since many of the fundamental and most pressing problems in physics can be represented as problems in technical naturalness, we are particularly interested in any new lessons that Lifshitz field theories might teach us about this topic.

First, we studied the phenomenon of spontaneous symmetry breaking in the Lifshitz case. We discovered that, contrary to the intuition afforded us by relativistic physics, Nambu-Goldstone modes of Type A (with a kinetic term quadratic in time derivatives) or of Type B (with a kinetic term linear in time derivatives) exhibit a hierarchy of multicritical phenomena with dynamical exponents $z > 1$. We also discovered the polynomial shift symmetry, which protects the technical naturalness of this behavior. This symmetry shifts the field component by a polynomial in the spatial coordinates.

Having established the utility of these polynomial shift symmetries as “guardians of naturalness”, we proceeded to classify the lowest-dimension operators that preserve these symmetries. We developed a new graph-theoretical technique to address this classification problem in which each factor of the field is represented by a vertex and a pair of contracted derivatives is represented by an edge joining the two vertices representing the field factors on which the derivatives act. We reproduced the known Galileon N -point invariants in the case of the linear shift symmetry and reinterpreted them as equal-weight sums over all labeled trees with N vertices. More importantly, we were able to extend the classification to higher-order polynomial shifts, without essentially having to solve the problem all over again, by constructing higher-order polynomial shift invariants out of superpositions of exact lower-order polynomial shift invariants and linear shift invariants. Since the latter are relatively easy to deal with, we drastically simplified the problem of generating and classifying polynomial shift invariants. We studied the connection and relationship of this graph-theoretical approach to the standard cohomological approach, but much remains to be understood. Some invariants appear simple in the language of graphs and yet overwhelmingly complicated in the cohomological approach. We suspect that the clarification of the relationship between these approaches will be of great interest to mathematics as well as to physics.

With explicit examples of theories with lowest-order shift-invariant interactions, we

investigated the role of infrared divergences in the patterns of renormalization group flow exhibited by Lifshitz theories. We obtained the nonrelativistic generalization of the celebrated Coleman-Hohenberg-Mermin-Wagner (CHMW) theorem, which prohibits spontaneous symmetry breaking for would-be Type A modes with dynamical exponent z , unless z is strictly less than the spatial dimension. In contrast, Type B modes can exist in any spatial dimension. However, we discovered a cascading phenomenon by which a would-be Type A (or Type B) mode may change at low energies to a Type A (or Type B) mode with a lower value of the dynamical exponent. In addition, would-be Type A modes may change into a Type B mode. This phenomenon is absent in the relativistic case; It represents a new and interesting way to avoid the “no-go” consequences of the CHMW theorem.

Furthermore, we discovered interesting subtleties in the application of the standard methods of renormalization to the Lifshitz case. We used the techniques of the Wilsonian approach, the Callan-Symanzik equation, and the $\overline{\text{MS}}$ scheme with dimensional regularization. After explicitly showing how these calculations proceed in detail in the Lifshitz case, and checking their consistency, we demonstrated that these RG flows exhibit a continuum of distinct, yet mutually consistent physical interpretations. On the one hand, we may choose to fix the scaling of time, in which case the interaction coefficient does not run, but the lightcone opens up towards the infrared, eventually driving the theory towards lower values of the dynamical exponent. Meanwhile, the lightcone closes at high energies and the theory ceases to be sensible. On the other hand, one may fix the relative coupling of the temporal- and spatial-derivative quadratic terms, which forces the dynamical exponent and the interaction coefficient to flow. The theory is strongly coupled in the UV.

Finally, as a first application, we considered what would happen to the usual BCS picture of superconductivity involving electron-phonon interactions if one allowed the phonons to be multicritical, described by a dynamical exponent $z = 3$ in $3 + 1$ dimensions. Applying the standard Boltzmann-Bloch theory of transport, we discovered that the resistivity of such a system would exhibit a technically natural linear dependence on temperature. This represents a new and fascinating way to generate this “strange metal” behavior and overcomes the fine tuning problems inevitably exhibited by theories with a unit dynamical exponent.

We might also apply these lesson to the effective field theory of inflation. There is existing work on $z = 2$ and $z = 3$ scalar inflation [87, 12, 88]. However, this work predates our work on polynomial shift symmetries, which are precisely those symmetries we use to protect the naturalness of these Lifshitz field theories. We expect that these symmetries may be used to control the non-Gaussianities as well as provide a mechanism out of the usual pitfalls of many theories of inflation, such as the technical naturalness of a small slow-roll parameter in the standard slow-roll picture [27].

Our long-term goal is to apply these lessons to quantum gravity. This would require their extension to the case of gauge theories, which, in itself, represents a significant hurdle. We hope that these lessons will inspire new ways to address naturalness problems in general and, perhaps eventually, even the big Kahuna, the cosmological constant problem. This thesis represents the beginnings of our exploration of the uncharted territories of the Landscape of Naturalness. We believe that untold riches await those who dare break this new ground.

Bibliography

- [1] B. I. Halperin and P. C. Hohenberg. Theory of dynamic critical phenomena. *Reviews of Modern Physics*, 49(3):435, (1977).
- [2] D. J. Amit and V. M. Mayor. *Field theory, the renormalization group, and critical phenomena*, volume 18. World Scientific Singapore, (1984).
- [3] M. Le Bellac. *Quantum and statistical field theory*. Clarendon Press Oxford, (1991).
- [4] J. J. Binney, N. J. Dowrick, A. J. Fisher, and M. Newman. *The theory of critical phenomena: an introduction to the renormalization group*. Oxford University Press, Inc., (1992).
- [5] J. Zinn-Justin. *Quantum Field Theory and Critical Phenomena*. Oxford University Press, Inc., 4th edition, (2002).
- [6] M. Kardar, G. Parisi, and Y.-C. Zhang. Dynamic scaling of growing interfaces. *Physical Review Letters*, 56(9):889, (1986).
- [7] B. I. Halperin, P. C. Hohenberg, and E. D. Siggia. Renormalization-group treatment of the critical dynamics of superfluid helium, the isotropic antiferromagnet, and the easy-plane ferromagnet. *Physical Review B*, 13(3):1299, (1976).
- [8] N. V. Antonov and A. N. Vasil'ev. Critical dynamics as a field theory. *Theoretical and Mathematical Physics*, 60(1):671–679, (1984).
- [9] V. Dohm. Dynamical spin-spin correlation function of an isotropic ferromagnet at T_c ; in $6 - \epsilon$ dimensions. *Solid State Communications*, 20(7):657–660, (1976).
- [10] P. Hořava. Membranes at quantum criticality. *Journal of High Energy Physics*, 2009(03):020, (2009).
- [11] P. Hořava. Quantum gravity at a Lifshitz point. *Physical Review D*, 79(8):084008, (2009).
- [12] S. Mukohyama. Hořava–Lifshitz cosmology: a review. *Classical and Quantum Gravity*, 27(22):223101, (2010).
- [13] J. Ambjørn, A. Görlich, S. Jordan, J. Jurkiewicz, and R. Loll. CDT meets Hořava–Lifshitz gravity. *Physics Letters B*, 690(4):413–419, (2010).

- [14] P. Hořava. General covariance in gravity at a Lifshitz point. *Classical and Quantum Gravity*, 28(11):114012, (2011).
- [15] C. Anderson, S.J. Carlip, J.H. Cooperman, P. Hořava, R.K. Kommu, and P.R. Zulkowski. Quantizing Hořava-Lifshitz gravity via causal dynamical triangulations. *Physical Review D*, 85(4):044027, (2012).
- [16] S. Janiszewski and A. Karch. String theory embeddings of nonrelativistic field theories and their holographic Hořava gravity duals. *Physical Review Letters*, 110(8):081601, (2013).
- [17] S. Janiszewski and A. Karch. Non-relativistic holography from Hořava gravity. *Journal of High Energy Physics*, 2013(2):1–35, (2013).
- [18] T. Griffin, P. Hořava, and C. M. Melby-Thompson. Lifshitz gravity for Lifshitz holography. *Physical Review Letters*, 110(8):081602, (2013).
- [19] A. Contillo, S. Rechenberger, and F. Saueressig. Renormalization group flow of Hořava-Lifshitz gravity at low energies. *Journal of High Energy Physics*, 2013(12):1–42, (2013).
- [20] D. Benedetti and F. Guarneri. One-loop renormalization in a toy model of Hořava-Lifshitz gravity. *Journal of High Energy Physics*, 2014(3):1–17, (2014).
- [21] T. Griffin, K. T. Grosvenor, P. Hořava, and Z. Yan. Multicritical Symmetry Breaking and Naturalness of Slow Nambu-Goldstone Bosons. *Phys. Rev.*, D88:101701, (2013).
- [22] T. Griffin, K. T. Grosvenor, P. Hořava, and Z. Yan. Scalar Field Theories with Polynomial Shift Symmetries. to appear in *Commun. Math. Phys.*, (2015).
- [23] T. Griffin, K. T. Grosvenor, P. Hořava, and Z. Yan. Cascading multicriticality in nonrelativistic spontaneous symmetry breaking. 07 (2015).
- [24] K. T. Grosvenor, P. Hořava, C. J. Mogni, and Z. Yan. Nonrelativistic Renormalization of Scalar Fields. to appear.
- [25] T. Griffin, K. T. Grosvenor, P. Hořava, and Z. Yan. Multicritical phonons and electron-phonon interactions in metals. to appear.
- [26] G. 't Hooft. Naturalness, chiral symmetry, and spontaneous chiral symmetry breaking. *NATO Adv. Study Inst. Ser. B Phys.*, 59(PRINT-80-0083 (UTRECHT)):135, (1979).
- [27] K. T. Grosvenor, P. Hořava, C. J. Mogni, and Z. Yan. Polynomial shift symmetries and the effective field theory of inflation. to appear.
- [28] Y. Nambu. Dynamical model of elementary particles based on an analogy with superconductivity. I. *Physical Review*, 122(1):345–358, (1961).
- [29] Y. Nambu. Quasi-particles and gauge invariance in the theory of superconductivity. *Physical Review*, 117(3):648–663, (1960).

- [30] J. Goldstone. Field theories with superconductor solutions. *Il Nuovo Cimento*, 19(1):154–164, (1961).
- [31] J. Goldstone. Broken symmetries. *Physical Review*, 127(3):965–970, (1962).
- [32] T. Brauner. Spontaneous symmetry breaking and Nambu-Goldstone bosons in quantum many-body systems. *Symmetry*, 2, 01 (2010).
- [33] G. E. Volovik and M. A. Zubkov. Higgs bosons in particle physics and in condensed matter. *arXiv:1305.7219*, (2013).
- [34] S. Weinberg. *The quantum theory of fields. Vol. 2: Modern applications*. Cambridge University Press, (1996).
- [35] A. M. Schakel. *Boulevard of broken symmetries: Effective field theories of condensed matter*. World Scientific, (2008).
- [36] C. P. Burgess. Goldstone and pseudo-Goldstone bosons in nuclear, particle and condensed-matter physics. *Physics Reports*, 330:193, (2000).
- [37] H. B. Nielsen and S. Chadha. On how to count Goldstone bosons. *Nuclear Physics*, B105:445, (1976).
- [38] V. A. Miransky and I. Shovkovy. Spontaneous symmetry breaking with abnormal number of Nambu-Goldstone bosons and kaon condensate. *Physical Review Letters*, 88(11), (2002).
- [39] Y. Nambu. Spontaneous breaking of Lie and current algebras. *J. Stat. Phys.*, 115:7, (2004).
- [40] S. Weinberg. The cosmological constant problem. *Reviews of Modern Physics*, 61(1):1–23, (1989).
- [41] S. Weinberg. The cosmological constant problems (talk given at Dark Matter 2000, february, 2000). *arXiv:astro-ph/0005265*, (2000).
- [42] S. Carroll. The cosmological constant. *Living Rev. Rel.*, 4:1, (2001).
- [43] G. F. Giudice. Naturally speaking: The naturalness criterion and physics at the LHC. *arXiv:0801.2562*, (2008).
- [44] L. Álvarez-Gaumé and M. A. Vázquez-Mozo. *An invitation to quantum field theory, Ch. 12*. Lect. Notes Phys. **839**. Springer, (2012).
- [45] P. Binétruy. *Supersymmetry: Theory, experiment and cosmology, Ch. 1*. Oxford University Press, (2006).
- [46] R. K. Kaul. Naturalness and electro-weak symmetry breaking. *arXiv:0803.0381*, (2008).
- [47] G. F. Giudice. Naturalness after LHC8. *arXiv:1307.7879*, (2013).

- [48] P. Hořava and C. M. Melby-Thompson. Anisotropic conformal infinity. *Gen. Rel. Grav.*, 43:1391–1400, (2011).
- [49] S. Kachru, X. Liu, and M. Mulligan. Gravity duals of Lifshitz-like fixed points. *Phys.Rev.*, D78:106005, (2008).
- [50] H. Watanabe and H. Murayama. Unified description of Nambu-Goldstone bosons without Lorentz invariance. *Physical Review Letters*, 108(25):251602, (2012).
- [51] H. Watanabe. Redundancies in Nambu-Goldstone bosons. *Physical Review Letters*, 110(18), (2013).
- [52] A. Michelson. Phase diagrams near the Lifshitz point. I. Uniaxial magnetization. *Physical Review B*, 16(1):577–584, (1977).
- [53] A. Michelson. Phase diagrams near the Lifshitz point. II. Systems with cylindrical, hexagonal, and rhombohedral symmetry having an easy plane of magnetization. *Physical Review B*, 16(1):585–592, (1977).
- [54] A. Michelson. Phase diagrams near the Lifshitz point. III. Tetragonal crystals with an easy plane of magnetization. *Physical Review B*, 16(11):5121–5124, (1977).
- [55] R. Iengo, J. G. Russo, and M. Serone. Renormalization group in Lifshitz-type theories. *Journal of High Energy Physics*, 0911:020, (2009).
- [56] K. Anagnostopoulos, K. Farakos, P. Pasipoularides, and A. Tsapalis. Non-Linear Sigma Model and asymptotic freedom at the Lifshitz point. *arxiv:1007.0355*, 07 (2010).
- [57] M. Visser. Lorentz symmetry breaking as a quantum field theory regulator. *Physical Review D*, 80(2), (2009).
- [58] P. R. S. Gomes, P. Bienzobaz, and M. Gomes. Competing interactions and the Lifshitz-type Nonlinear Sigma Model. *Physical Review D*, 88:025050, (2013).
- [59] M. E. Peskin and D. V. Schroeder. *An introduction to quantum field theory*. Addison-Wesley, (1995).
- [60] A. Nicolis, R. Rattazzi, and E. Trincherini. Galileon as a local modification of gravity. *Physical Review D*, 79(6):064036, (2009).
- [61] S. R. Coleman. There are no Goldstone bosons in two dimensions. *Communications in Mathematical Physics*, 31(259), (1973).
- [62] P.C. Hohenberg. Existence of Long-Range Order in One and Two Dimensions. *Phys.Rev.*, 158:383–386, (1967).
- [63] N. D. Mermin and H. Wagner. Absence of ferromagnetism or antiferromagnetism in one- or two-dimensional isotropic Heisenberg models. *Physical Review Letters*, 17(22):1133–1136, (1966).

- [64] S. Sachdev. *Quantum Phase Transitions*. Cambridge University Press, (2001).
- [65] K. Hinterbichler and A. Joyce. Goldstones with Extended Shift Symmetries. *Int. J. Mod. Phys.*, D23:1443001, (2014).
- [66] J. A. Bondy and U. S. R. Murty. Graph theory (graduate texts in mathematics), Springer, 2008.
- [67] S. R. Coleman, J. Wess, and B. Zumino. Structure of phenomenological Lagrangians. 1. *Phys.Rev.*, 177:2239–2247, (1969).
- [68] Jr. Callan, C. G., S. R. Coleman, J. Wess, and B. Zumino. Structure of phenomenological Lagrangians. 2. *Phys.Rev.*, 177:2247–2250, (1969).
- [69] D. V. Volkov. Phenomenological lagrangians. *Fiz.Elem.Chast.Atom.Yadra*, 4:3–41, (1973).
- [70] V.I. Ogievetsky. Nonlinear realizations of internal and space-time symmetries. *Proc. of X-th Winter School of Theoretical Physics in Karpacz*, 1, (1974).
- [71] G. Goon, K. Hinterbichler, A. Joyce, and M. Trodden. Galileons as Wess-Zumino terms. *JHEP*, 1206:004, (2012).
- [72] J. A. de Azcárraga and J. M. Izquierdo. *Lie groups, Lie algebras, cohomology and some applications in physics*. Cambridge University Press, (1998).
- [73] E. A. Ivanov and V. I. Ogievetskii. Inverse Higgs effect in nonlinear realizations. *Theor. Math. Phys.*, 25(2):1050, (1975).
- [74] T. Brauner and H. Watanabe. Spontaneous breaking of spacetime symmetries and the inverse Higgs effect. *Phys.Rev.*, D89:085004, (2014).
- [75] H. B. Nielsen and S. Chadha. On how to count Goldstone bosons. *Nucl. Phys.*, B105:445, (1976).
- [76] C.P. Burgess. Goldstone and pseudo-Goldstone bosons in nuclear, particle and condensed matter physics. *Phys. Rept.*, 330:193–261, (2000).
- [77] Y. Nambu. Spontaneous breaking of Lie and current algebras. *J. Stat. Phys.*, 115(1/2):7–17, (2004).
- [78] T. Brauner. Spontaneous Symmetry Breaking and Nambu-Goldstone Bosons in Quantum Many-Body Systems. *Symmetry*, 2:609–657, (2010).
- [79] H. Watanabe and H. Murayama. Effective Lagrangian for Nonrelativistic Systems. *Phys. Rev.*, X4(3):031057, (2014).
- [80] H. Watanabe and H. Murayama. Effective lagrangian for nonrelativistic systems. *Physical Review X*, 4(3):031057, (2014).

- [81] G. Grinstein. Spin-Wave Theory for the Biaxial ($m = 2$) Lifshitz Point Problem in Three Dimensions. *J. Phys. A: Math. Gen.*, 13:L201, (1980).
- [82] P. M. Chaikin and T. C. Lubensky. *Principles of Condensed Matter Physics*. Cambridge U.P., (1995).
- [83] A. Kapustin. Remarks on nonrelativistic Goldstone bosons. (2012).
- [84] C. Cheung, P. Creminelli, A. Liam Fitzpatrick, J. Kaplan, and L. Senatore. The Effective Field Theory of Inflation. *JHEP*, 03:014, (2008).
- [85] S. Weinberg. Effective Field Theory for Inflation. *Phys. Rev.*, D77:123541, (2008).
- [86] D. Baumann and L. McAllister. *Inflation and String Theory*. Cambridge University Press, (2015).
- [87] N. Arkani-Hamed, P. Creminelli, S. Mukohyama, and M. Zaldarriaga. Ghost inflation. *JCAP*, 0404:001, (2004).
- [88] S. Mukohyama. Scale-invariant cosmological perturbations from Hořava-Lifshitz gravity without inflation. *JCAP*, 0906:001, (2009).
- [89] K. G. Wilson and M. E. Fisher. Critical exponents in 3.99 dimensions. *Physical Review Letters*, 28(4):240, (1972).
- [90] M. A. Vasiliev. Higher spin gauge theories: Star product and ads space. *arXiv preprint hep-th/9910096*, pages 123–253, 2000.
- [91] I. R. Klebanov and A. M. Polyakov. AdS dual of the critical O(N) vector model. *Physics Letters B*, 550(3):213–219, 2002.
- [92] Marika Taylor. Non-relativistic holography. *arXiv preprint arXiv:0812.0530*, 2008.
- [93] J. Polchinski. Effective field theory and the fermi surface. *arXiv:hep-th/9210046*, (1992).
- [94] L. D. Landau, E. M. Lifshitz, and L. P. Pitaevskii. Statistical physics. part 2, theory of the condensed state (course of theoretical physics), (1980).
- [95] A. A. Abrikosov, L. P. Gorkov, and I. E. Dzyaloshinski. *Methods of quantum field theory in statistical physics*. Courier Corporation, (1975).
- [96] H. Haken. *Quantum Field Theory of Solids, an Introduction*. North-Holland Physics Publishing, (1983).
- [97] J. M. Ziman. *Electrons and phonons: the theory of transport phenomena in solids*. Oxford University Press, (1960).
- [98] D. Coffey and C. J. Pethick. Finite-temperature contributions to the specific heat of the electron-phonon system. *Physical Review B*, 37(1):442, (1988).

- [99] F. Piazza, W. Zwerger, and P. Strack. Fflo strange metal and quantum criticality in two dimensions: theory and experimental evidence in organic superconductors. *arXiv preprint arXiv:1506.08819*, (2015).
- [100] A. B. Migdal. Interaction between electrons and lattice vibrations in a normal meta. *Sov. Phys. JETP*, 7(6):996–1001, (1958).
- [101] R. D. Mattuck. *A guide to Feynman diagrams in the many-body problem*. Courier Corporation, (2012).
- [102] Zheng-Zhong Li. *Solid State Theory*. Higher Education Press, Beijing, China, 2nd edition, (2002).
- [103] L. D. Landau and E. M. Lifshitz. Physical kinetics, vol. 10. *Course of Theoretical Physics*, (1981).
- [104] K. T. Grosvenor, P. Hořava, and C. M. Melby-Thompson. Phases of gravity with anisotropic scaling. to appear.